ELECTRONIC EXCITATION IN ATOM/MOLECULE COLLISIONS

DAVID PROVEN SUTTON

Ph.D
UNIVERSITY of EDINBURGH
1980

ABSTRACT OF THESIS (Regulation 6.9)

Name of Candidate David Proven SUTTON

Address [redacted]

Degree Doctor of Philosophy *Date* April 1980

Title of Thesis Electronic Excitation in Atom/Molecule Collisions

A time of flight crossed beams technique has been used to study the narrow angle scattering of a fast beam of potassium atoms by various alkyl halide like systems. The primary beam is produced by charge exchange of a focussed, pulsed beam of K^+ ions. Results are reported for laboratory collision energies of 100 and 200 eV with target beams of HI, CH_3I, CH_3Cl, CF_3I and C_3H_7I.

The data show a number of peaks in the scattered time of flight spectra indicating inelastic processes taking place with energy transfers between 0.7 and 14 eV. The excitations are interpreted in terms of K atom electronic excitation, $n \rightarrow \sigma^*$ transitions in the carbon-halide bond, excitation of various s Rydberg states of the target molecules and $\sigma \rightarrow \sigma^*$ transitions in the C-H bonds. Some of these processes are accompanied by vibrational excitation due to the involvement of intermediate potential surfaces with equilibrium geometries different from the ground state.

Potassium excitation is explained using a harpooning model involving electron donation into the σ^* (C-X) orbital, well established as the mechanism for reaction at lower collision energies. Excitation of the other electronic states involves electron donation into high lying vacant orbitals being followed by recapture of an electron from a lower normally filled orbital. Assignments are made to each of the observed transitions and reasonable agreement is found between observation and the predicted energy losses.

The possibility of adapting the equipment to perform photon-particle coincidence experiments is considered and a feasibility calculation is presented in the last Chapter.

DECLARATION

I Hereby Declare that this Thesis has been composed by myself and that I made a substantial contribution to the results reported whilst working in the Molecular Beams Group. All members of the Group participated in data collection. I analysed all the data presented in this Thesis, wrote the modelling program (Appendix C) and carried out maintenance and updating of the data collection and analysis software. The interpretation of the results, presented in Chapter 5, was developed in discussions with my Supervisors, M.A.D. Fluendy and K.P. Lawley.

[redacted]

DAVID P. SUTTON
April 1980

CONTENTS

CONTENTS (contd)

CHAPTER 1

INTRODUCTION

Much of physical chemistry is concerned with the understanding of the bulk properties of matter in terms of the basic laws of physics. Particle scattering has been of major importance in physics since Rutherford yet, despite the fundamental role collisions play in chemistry, it is only in the last twenty years that a concerted study of inter-molecular dynamics has been started by chemists. Chemical and thermal equilibrium are both maintained by collisions and rates of reaction and energy transfer are governed by the rate and dynamics of molecular collisions.

Chemical experiments, usually performed on a bulk sample of matter in thermal equilibrium with its surroundings, assume a Boltzmann distribution of molecules amongst the available states and, if the measured property is a function of the quantum state of the molecule, only an ensemble average can be obtained. A statistical theory of the state of the matter as well as one of the quantum mechanics of the isolated process is involved in the full interpretation of the measurements. The use of molecular beam scattering techniques enables the selection of a single quantum state or range of states for measurement and the exploration of the dynamics of the molecular collision and the angular and energy dependence of the associated scattering. Thus direct molecular information can be obtained without the need to use theories relating molecular to non-equilibrium properties. The realisation that the application of scattering methods to chemical problems provides an insight into intermolecular dynamics that can not

be obtained in any other way has led to the development of new experimental techniques (see FLU 73) for use in a number of different fields of chemical interest.

The first chemical applications of beam techniques were in the fields of bimolecular reactions (BUL 54, TAY 55) and elastic scattering (BUC 75). The early experiments were performed with alkali metals. The results from reactive scattering studies led to the recognition of different limiting models for reaction and their link with product angular scattering pattern, whilst elastic scattering resulted in the first unambiguous measurement of intermolecular potentials. Subsequent to those earlier experiments investigations have been performed on non-alkali systems in both reactive (LEE 69, LEE 68 and Grice's review (GRI 75)) and elastic (AQU 72, SCH 72) scattering.

Initially beam studies were confined to systems in which the collision dynamics were governed by a single potential surface. Improvements in beam sources and detection techniques in about 1968 gave impetus for scattering studies in the energy range 1-100 eV, where new areas of the potential surface are explored and electronic states come much closer or may even cross. In this energy regime the fields of chemistry and physics truly merge (HAS 64).

If the ground state surface of the colliding pair comes close to an ionic one then the system may exit in the ionic channel. The special interest in charge transfer lies in its close relationship to chemical reaction kinetics and its suitability to provide information about diabatic behaviour at the crossing of potential surfaces. A large number of papers have appeared in the literature (see, for example, AUE 73, HUB 75 and

BAE 75 for a review), primarily reporting results for alkali beams crossed with halogens (BAE 69, MOU 71) or small inorganic molecules (BAE 71, LAC 70). These measurements have enabled the Landau-Zener approximation (ZEN 32) to be tested and it has been shown to describe the behaviour of the total cross section with collision energy quite well. This has led to the determination of a number of non-diagonal matrix elements, H_{12}, for the systems.

Differential cross section measurements, giving the angular distribution of the ions produced, potentially provide more information about the dynamics of the collision and total cross section measurements were soon followed by experiments intended to determine the differential cross sections (e.g. DEL 72). Data obtained from these experiments are compared with simplified classical calculations or trajectory calculations (DUR 73), in which the three-body character of the collision is taken into account.

(More generally, the development of "fast" digital computers has enabled the powerful technique of classical trajectory calculations (WAL 58, BLA 63) to be applied to chemical areas of interest. Earlier trajectory calculations on the single lowest adiabatic surface (e.g. BLA 69) have been followed by calculations involving more than one surface (TUL 71).)

Non-adiabatic collisions have also been investigated by observation of electrons or photon emitted following collisional excitation. A number of possible non-adiabatic transitions can take place during a collision (see Table I, KEM 75) and the information yielded from total cross section, $Q(E,\Delta E)$, measurements depends on the experimental technique adopted (see Table III, KEM 75).

Measurement of $\sigma(\theta, E, \Delta E)$, the differential cross section as a function of scattering angle θ, collision energy E, and energy loss ΔE contains a similar wealth of information and the experimental work reported in this Thesis was carried out on a crossed beams time of flight machine in which $\sigma(\theta, E, \Delta E)$ is determined by measuring the time of flight spectrum of the projectile beam as a function of scattering angle. Suitable analysis of the data provides information on the relative probabilities for population of excited states, crossing radii, coupling matrix elements and details of excitation mechanisms.

Chapter 2 describes, in some detail, the apparatus used in this work. The primary beam is produced by ion beam neutralization, one of the oldest methods of producing high energy neutral beams. The sole disadvantage of this technique is the decrease in beam intensities at lower energies due to space charge effects.

Chapter 3 deals with K/Ar differential cross sections which have already been reported in the literature (KER 75, FLU 75a) but because of conflicting results reported by other groups have since been checked. Oscillatory structure is observed in these differential cross sections which can not be interpreted in terms of any of the standard phenomena giving rise to such features in differential cross sections.

The time of flight data collected over the period of the Thesis is reported in Chapter 4. The results are presented as time of flight profiles at a range of scattering angles and as differential cross sections obtained from them for the inelastic processes taking place. The systems which have undergone investigation are HI, CH_3I, CH_3Cl, CF_3I and C_3H_7I. These molecules have received considerable attention

in the literature and the reaction $K + CH_3I \longrightarrow KI + CH_3$ follows a classic harpooning mechanism. The electron affinities of the methyl halides have also been studied (MOU 74).

A discussion of the results presented in Chapter 4 is given in Chapter 5. The energy losses in the potassium electronic excitation are compared with a simple model in which the differential cross section is calculated from the small angle formulae (FLU 73) and the Landau-Zener approximation. It is found that stretching of the target molecule bond during the collision plays a key role in determining the energy loss (see MOU 79 and LOS 79 re bond stretching in alkali/halide experiments) and, not surprisingly, (BRO 66) the collision dynamics are highly orientation dependent. The model parameters are listed for CH_3I. The close link between the excitation mechanism and that for reaction is obvious. Higher energy transfer processes are reported though no quantitative modelling has been carried out.

The possibility of conducting an experiment in which the observation of a photon emitted from an excited particle is accompanied by detection of the associated scattered particle was considered and is presented in the final Chapter.

CHAPTER 2

APPARATUS

The apparatus used to obtain the results reported in this thesis has been designed to measure the differential cross sections of alkali metal atoms at energies up to 1000 eV scattered from various target molecules. The fast alkali beam can be pulse modulated so that any electronic or vibrational excitation taking place in the course of the collision can be recorded by measurement of the time of flight of the scattered atom, allowing the post-collision states of the colliding partners to be inferred. The observations are confined to a narrow angular region about the main beam line because of the low beam intensities, however by varying the incident beam energy it is possible to probe different regions of the potentials involved. The initial construction of the equipment has been described by Duchart (DUC 71) and subsequent alterations by Kerr (KER 75) and Reddington (RED 73). A relatively brief description of the apparatus shall be given here as no major modifications have been made to it in the course of the present work.

2.1 GENERAL DESCRIPTION

A charge exchange mechanism is used to produce the fast main beam of potassium atoms. Produced initially as ions, the fast beam is focussed and modulated by a series of electrostatic lenses before being neutralised. The neutral beam is collimated and intersected by a target beam at right angles. The scattered potassium atoms are ionised on a cool tungsten wire and detected

via a scintillator and photomultiplier. The detector is scanned in a plane at right angles to the plane defined by the two beams. Atoms arriving at the detector stop a 50 MHz clock running in synchronism with the pulse modulation so that the flight time can be recorded. A schematic diagram of the apparatus is given in figure 2.1.

2.2 VACUUM SYSTEM

The various sections of the experiment are contained within a vacuum system composed of four differentially pumped chambers. These contain the main beam source, the cross beam source, the intersection region and the detection system. The first three chambers are pumped by oil diffusion pumps with liquid nitrogen cryo baffles. The diffusion pumps are backed by two rotary pumps on a common roughing line. The detector is connected to the collision chamber by flexible bellows and the only aperture into the detection region is a narrow slit permitting atoms scattered from the collision zone to reach the filament. The detector chamber is initially pumped out through this slit and an ion pump and a titanium sublimation pump used to bring it down to a high vacuum. This system allows pressures of around 10^{-6} torr to be obtained in the main beam source chamber during an experiment, with the cross beam source and collision chambers at 5×10^{-5} and 2×10^{-5} torr respectively. The detector chamber maintains a pressure of around 5×10^{-8} torr.

2.3 MAIN BEAM SOURCE

Potassium ions are produced by surface ionisation on a porous tungsten disk heated to about 1500K by a radiation heater.

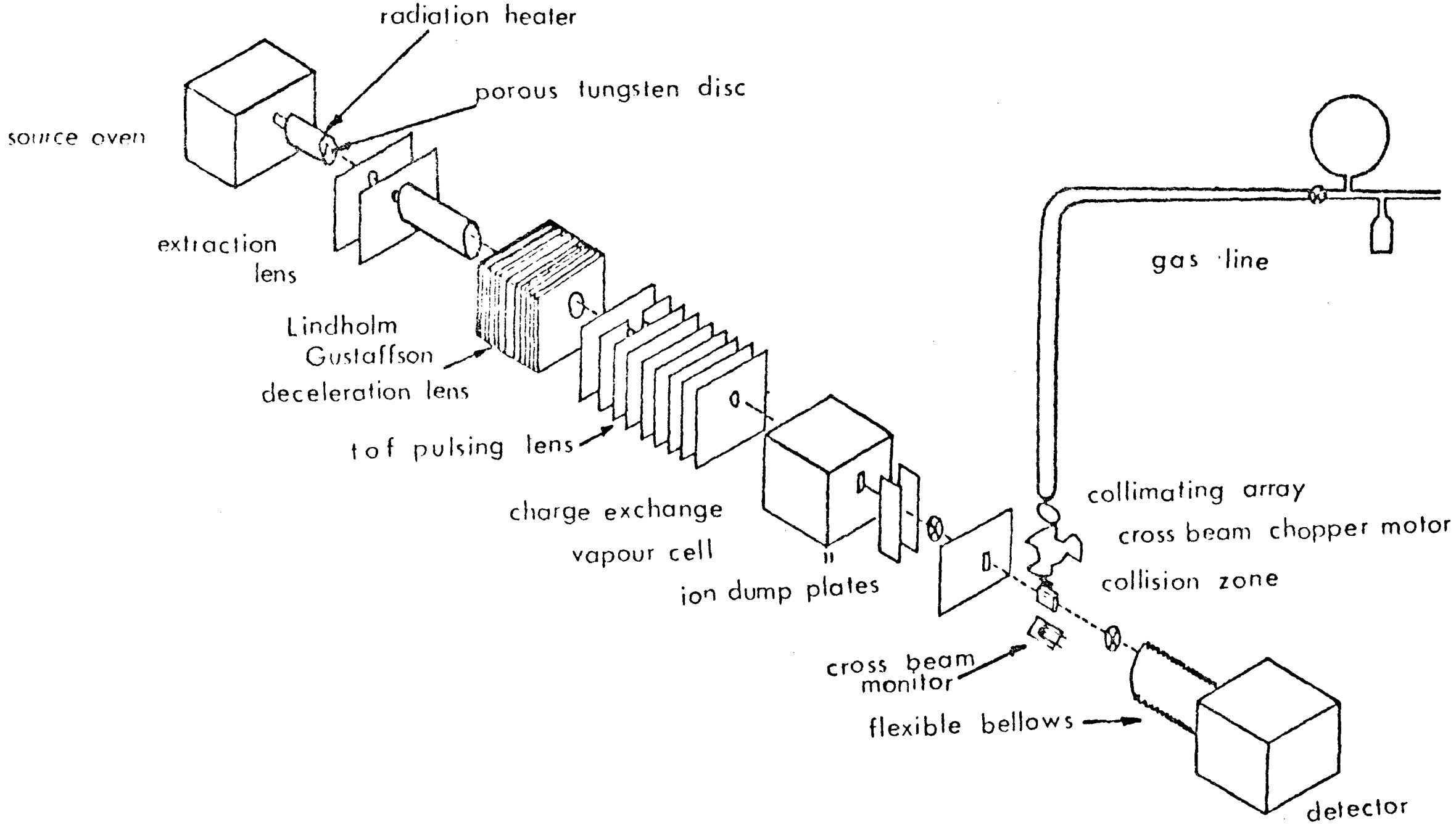
radiation heater
porous tungsten disc
source oven
extraction lens
Lindholm Gustaffson deceleration lens
tof pulsing lens
charge exchange vapour cell
ion dump plates
gas line
collimating array
cross beam chopper motor
collision zone
cross beam monitor
flexible bellows
detector

Figure 2.1

The potassium vapour diffuses to the ionising surface from the rear of the disk which is bathed in potassium vapour from an oven maintained at a temperature of about 250°C. The ion source is kept at a positive voltage corresponding to the desired final beam energy. A simple two element electrostatic lens system serves to focus the ions into the Lindholm Gustaffson lens. the function of this lens is to focus and steer the ion beam and its modification to suit this apparatus is fully described in Reddington's thesis. Several of the lens elements in this are split to allow the operator to compensate for slight misalignments of the ion lenses by the application of suitable steering voltages.

Exiting from the Lindholm Gustaffson lens the ion beam enters the pulsing lens. Beam modulation is accomplished by the application of a pulsed voltage across the beam path. After a suitable delay a voltage is applied down the beam line such that those ions at the rear of the beam pulse experience a greater acceleration than those at the front of the pulse. This has the effect of compressing the original beam pulse, which has a half width of about 1.3 μs, into a much narrower pulse with a half width of 60-80 ns. For a beam with a laboratory energy of 200 eV this corresponds to a width of about 1.5 eV. A more complete description of the velocity compression is given elsewhere (MCC 78).

The pulsed ion beam is now neutralised by passing it through the charge exchange chamber which contains potassium vapour at 150°C. This temperature is required to give the optimum

intensity in the neutral beam. For lower temperatures the number density of the vapour is too low to neutralise adequate numbers of the ions. Conversely, if the vapour pressure is too large, the beam intensity is reduced by multiple collisions within the chamber.

Any ions remaining in the main beam are deflected by the dump plates which have a voltage across them of 100V. The pulsed neutral beam passes through the collimating slits into the scattering chamber.

2.4 CROSS BEAM PRODUCTION

The main beam has been designed to run for periods of up to 120 hours and in this time it may be desirable to perform experiments with a number of different target beams. It was therefore important to design the cross beam source with this in mind. In the present apparatus a gas line is used for cross beam production. The primary advantage of such a system is that any problems arising in this area can be rectified externally without disrupting the main beam source and collision chambers. Similarly by isolating the gas line from the collision chamber it is possible to replenish or replace the cross beam material. Figure 2.2 shows a typical gas line and illustrates how both gases and liquids at room temperature can be handled.

The cross beam is introduced from the gas line into the cross beam source chamber via tap 1. The cross beam source chamber and the collision chamber are differentially pumped to reduce

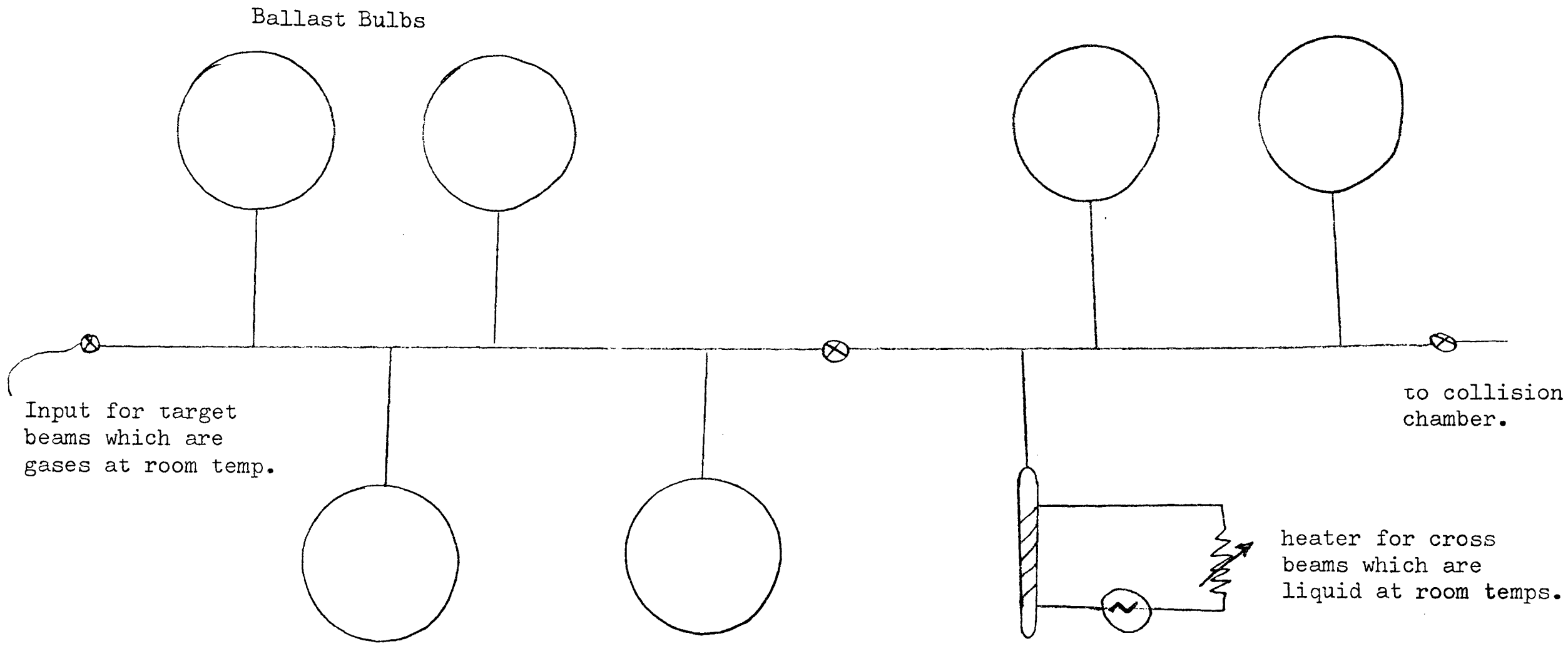

Figure 2.2: Gas line for Cross Beam Production

the pressure in the latter. The cross beam is produced by effusion through a capillary array and is chopped by a mechanical chopper to enable Signal + Noise (S + N) and Noise (N) to be differentiated. Light from a bulb falling on a photocell is also chopped, the light being off when the cross beam is off. The output from the photocell is monitored and each arrival at the detector is labelled according to whether the target beam was on or off when the potassium atom passed through the collision zone. The target beam intensity is continuously monitored by a differential ion guage placed immediately underneath the collision zone.

2.5 THE DETECTOR

The detector can be varied in angle with a precision of +/- 0.002 degrees and is based on the ion detector described by Daly (DAL 60). Scattered potassium atoms entering the detector chamber are ionised on a cool tungsten wire. The ions produced are focussed on to an aluminised surface and the secondary electrons emitted are accelerated on to the scintillator. The voltages used in the detector to focus the ions and accelerate the electrons are in the range 10-20 kV. The exact running voltage is determined by the need to balance the increased efficiency at higher voltages with the increased noise rate which is obtained as the voltages are increased. The photons produced by the electron burst impinging on the scintillator are detected by a photomultiplier and the output pulse passed through an amplifier and discriminator. The detection of a pulse stops a 50MHz clock counting into a 10 bit scalar and thus the time of arrival of the scattered potassium atom at

the detector is recorded. A schematic diagram of the detector is shown in Figure 2.3.

2.6 ALIGNMENT

Obviously when dealing with such a complex experimental system as that described here there are many components which can break down and lead to an experiment being aborted. It is therefore essential to thoroughly check all parts prior to starting a run and to minimise the problems caused by poor or careless assembly of the equipment. One of the main causes of trouble in this area is in the alignment of the ion lenses. Poor alignment leads to poor time of flight profiles and losses in the beam intensity. The present technique for alignment of the lenses uses a Helium/Neon laser with a fine copper mesh in front of the beam. The diffraction pattern produced can be used to ensure that the apertures in the lens elements are all centred on the main beam line. This has proved to be a most satisfactory method of alignment as it is both accurate and quick to perform.

2.7 DATA COLLECTION SYSTEM

The collection of data and control of the experiment is carried out by an on line DEC PDP11/45 (FLU 75). A listing of the data collection software is given in Appendix A and Figure 2.4 shows the signal collection and experimental control arrangements schematically.

Experiments can run for times of up to 120 hours and data collection at the wider angles can take 12 hours so it is highly desirable to have the data collection and monitoring of important

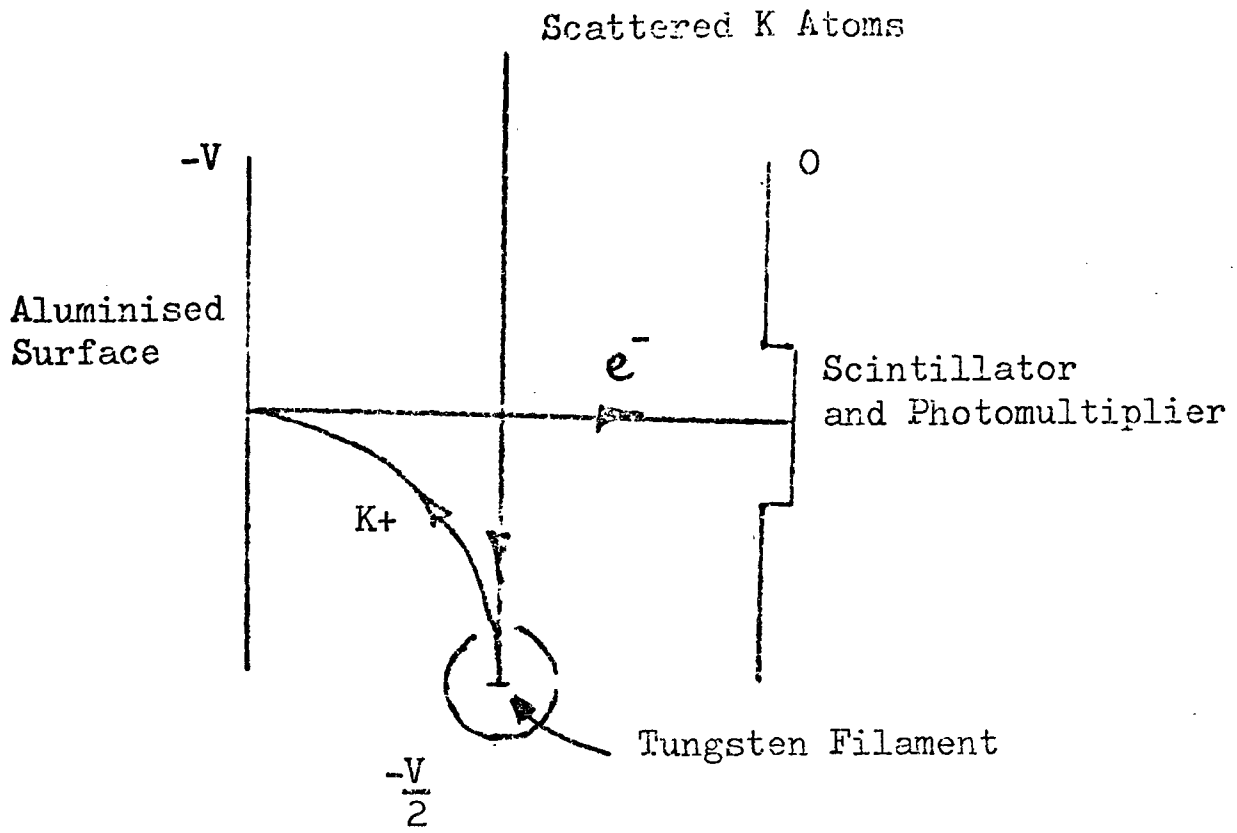

Figure 2.3 : SCHEMATIC OF THE DETECTOR

The diagram above shows the Detector used to collect the results presented in this Thesis. In an attempt to improve detection efficiency, reduce noise levels and decrease the pulse FWHH an improved ion focussing system was designed along the lines shown below. Although this was not installed in the equipment prior to completion of this work, tests since have shown an improvement in energy resolution and S/N ratios.

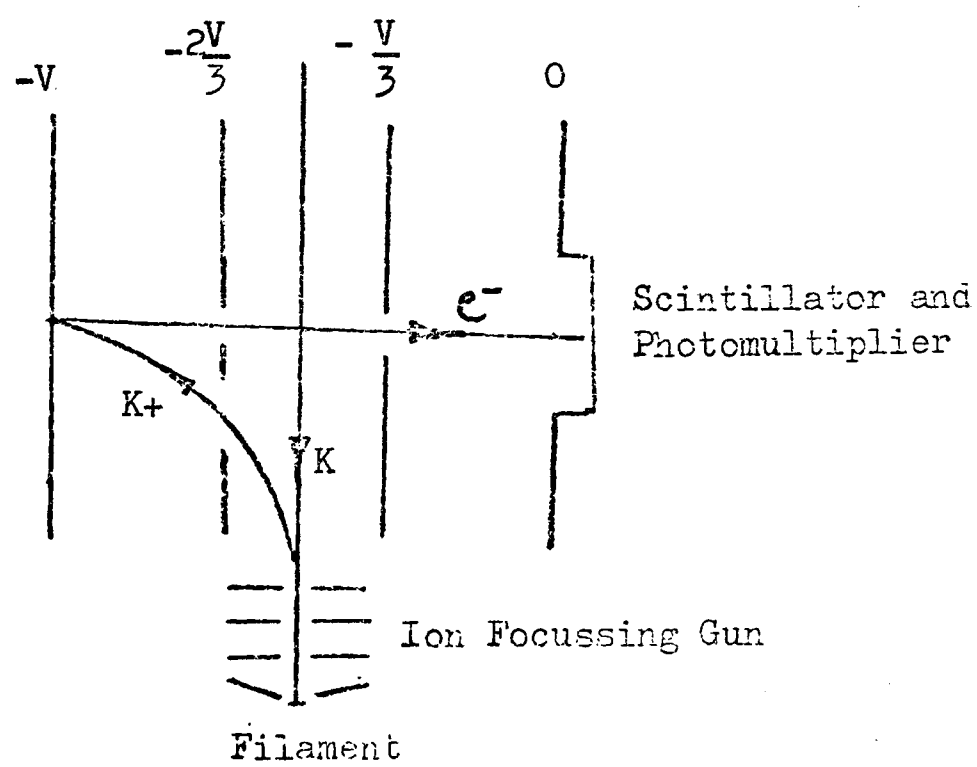

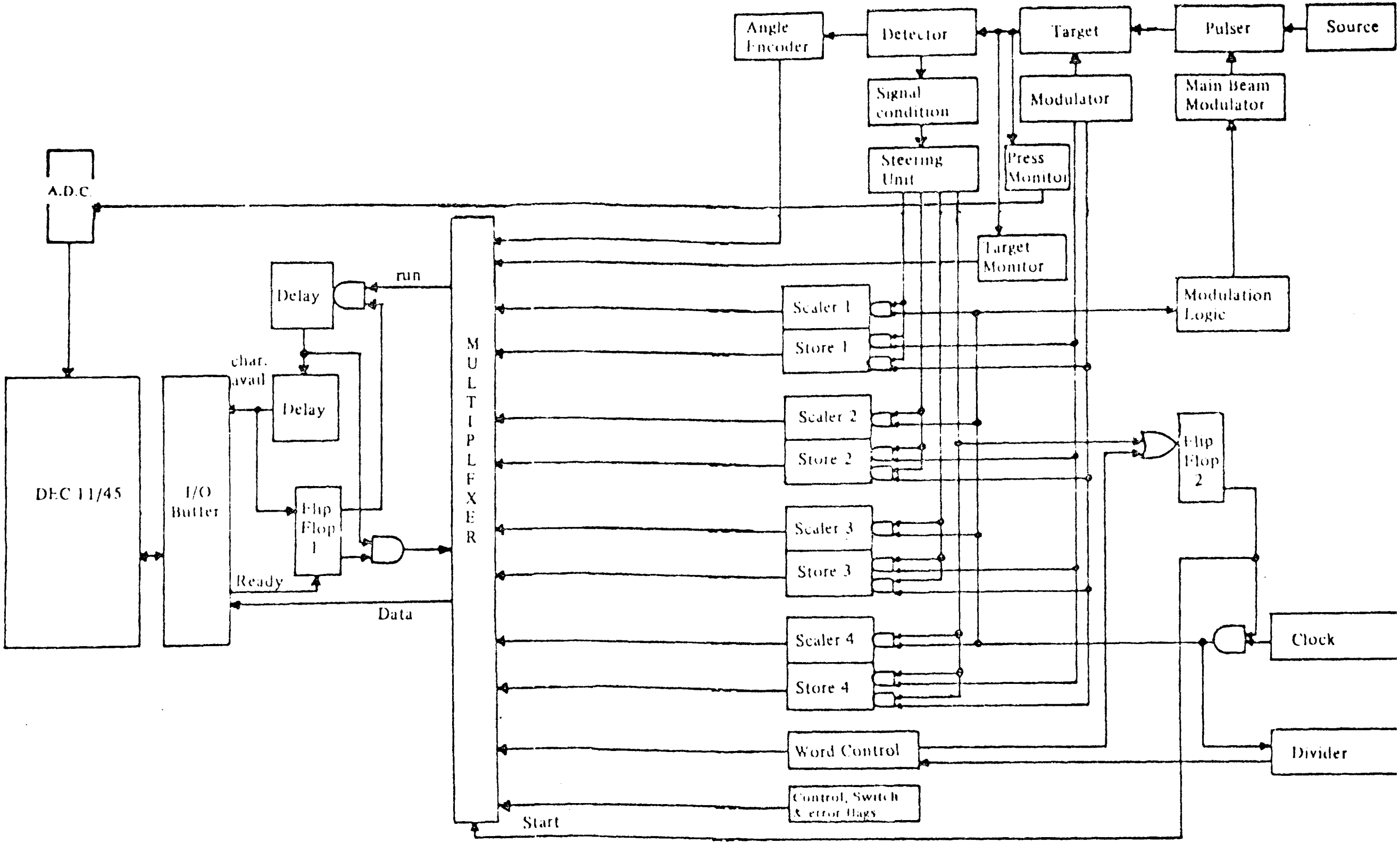
Angle Encoder
Detector
Target
Pulser
Source
Signal condition
Modulator
Main Beam Modulator
Steering Unit
Press Monitor
A.D.C.
Target Monitor
Delay
run
Scaler 1
Store 1
Modulation Logic
M U L T I P L E X E R
char. avail
Delay
Scaler 2
Store 2
Flip Flop 2
DEC 11/45
I/O Buffer
Flip Flop 1
Scaler 3
Store 3
Ready
Data
Scaler 4
Store 4
Clock
Word Control
Divider
Control, Switch & error flags
Start

Figure 2.4

experimental variables as automated as possible. Also, in order to optimise the efficiency of an experimental run, it is important to keep the operator well informed about the current experiment, allowing him to change the course of the experiment as appropriate.

The initial development of the control software was carried out by Kerr and the requirements of the program are fully described in his thesis. Various refinements have been added since then but neither these nor the introduction of beam modulation have radically altered the structure of the program.

As described above, each arrival at the detector stops a 50MHz clock counting into a 10 bit scalar. There are four separate scalars and every fourth arrival at the detector triggers an interrupt to the computer and the scalar readings, the total experimental time since the last transfer and the cross beam on/off flag are transferred to the PDP11/45. At the same time output from the cross beam monitor, an ion guage to monitor chamber pressures, the detector's angular position and the condition of the experimental control flags are passed to the data collection program. The operator interacts with the software via the control flags which take the form of three push buttons, coded in binary as an integer in the range 0 to 7. Different combinations of the buttons produce different responses from the computer.

The program reads in thirty-two experimental variables at the start of a run and these define the nature of the experiment and

the way in which it is to be carried out. The data passed from the experiment to the computer is given in Table 2.1 and the thirty-two experimental variables in Table 2.2.

Changes in the beam intensities or pressure in the collision chamber will lead to the operator being notified and data collection may be suspended to avoid corruption of data already written to disk. Data is written to disk every ten minutes. More frequent writing to disk would leave less computer time for the actual collection of data, whereas less frequent writing could lead to the loss of more data in the event of the computer breaking down.

The Signal to Noise ratio is estimated every two minutes as is the rate of counting into the peak in the spectrum. Feedback to the operator is provided automatically every fifteen minutes giving information about average peak growth rates, current peak growth rates, estimated Signal/Noise ratios and the beam intensities. Additional feedbacks may be obtained at any time by pressing the appropriate experimental control buttons.

Recently the cross beam intensity control has been automated. If the signal from the cross beam monitor indicates a decrease in intensity the computer notifies the operator and switches a relay, thereby increasing the current to the heating coils on the cross beam reservoir. If the intensity is persistently high or low the operator is advised, via the teletype, to adjust the rheostat accordingly. This modification has proved to be

TABLE 2.1 : 32 EXPERIMENTAL VARIABLES

1	Date
2	Main Beam Energy
3	Main Beam Mass
4	Target Beam Temp
5	Target Beam Mass
6	Main Beam Centre Position
7	Output File Number
8	C.E.C. Slit Size
9	Post C.E.C. Slit Size
10	Pre-scattering Centre Slit Size
11	Target Beam Width
12	Detector Width
13	Detector Height
14	Beam Height at Scattering Centre
15	Clock Period
16	= 0 : Spectrum = S + N - N
	= 1 : Spectrum = S + N + N
17	Angle for Measurement of Reference Profile
18	Unused
19	Minimum Angle
20	Maximum Angle
21	Step Size for Angle Scan
22	= 0 : Manual Angle Selection
	= 1 : Stepwise Angle Scan
	= 2 : Pseudo-random Angle Scan
23	Number of Main Beam Pulses per 1024 Clock Pulses
24	Required Counts in Peak Before Angle Change
25	= 0 : Manual Control of Cross Beam
	= 1 : Automatic Control of Cross Beam
26	Minimum Acceptable Peak Counting Rate
27,28	Angle Table Entry Points
29	Frequency of Reference Profile Collection
30	Time Between Main Beam Intensity Checks
31	= 0 : No Main Beam Monitoring
	= 1 : Monitor Main Beam and Notify Operator of any Changes
	= 2 : Monitor Main Beam and Suspend Data Collection if it Changes by More Than 10%.
32	As 31, but for Cross Beam Monitoring.

TABLE 2.2 : FORMAT FOR DATA TRANSFER TO THE PDP 11

	0	1	2	3	4	5	6	7	8
0	START CODE								
1	SCALER 1								
2	SCALER 1	STORE 1						SPARE	
3	SCALER 2								
4	SCALER 2	STORE 2						SPARE	
5	CROSS BEAM MONITOR								
6	MODE	MANUAL FLAGS				CROSS BEAM MONITOR			
7	ANGLE								
8	ANGLE								
9	SCALER 3								
10	SCALER 3	STORE 3					FAULT	SPARE	
11	SCALER 4								
12	SCALER 4	STORE 4					TEST	SPARE	
13	WORD COUNTER								
14	WORD COUNTER								
15	END CODE								

successful and provides the experimenter with a more stable cross beam.

Further programs exist on the PDP 11 allowing the operator to inspect the time of flight spectra on the Tektronix VDU and to perform simple statistical measurements on the data.

2.8 RUNNING AN EXPERIMENT

The final section in this Chapter is intended to give, in some detail, an account of the communications to and from the data collection program (DCP5) and the accompanying operator actions. Having produced the two beams (see Table 2.3 for normal running conditions) the 32 experimental variables should be initialised to their appropriate values and the data collection program run.

The first action of the software is to "flash" the detector filament for two minutes. A relay is used to switch off the detector EHT supply and simultaneously doubling the current through the detector filament. This has the effect of decontaminating the tungsten wire, thereby reducing the noise level and is repeated periodically throughout an experimental run.

This completed, the 32 variables are read in and the operator is prompted "Ideal Cross Beam:" The correct response is the signal which the PDP11 should receive from the ADC, connected to the cross beam monitor, corresponding to the chosen attenuation.

TABLE 2.3 : NORMAL OPERATING CONDITIONS

All ion beam currents, neutral beam intensities and voltages are for a 200 eV beam.

Source oven temperature	250°C
Grid Voltage	~ +100V
Accelator Voltage	~ -900V
Ion current on 1st plate of deceleration lens	5×10^{-6}A
Pulsing lens : Z Pulse	19.8V
Pulsing lens : clear pulse	30V
C.E.C. temperature	150°C
Ion pump plate voltage	110V
Current on Dump Plates	$\sim 5 \times 10^{-10}$A
Pressure in Chambers 1 and 2	$\sim 10^{-6}$TORR
Pressure in cross beam source chamber	$\sim 5 \times 10^{-5}$TORR
Pressure in collision chamber	$\sim 2 \times 10^{-5}$TORR
Main beam attenuation	10%
Detector pressure	$\sim 5 \times 10^{-8}$TORR
Neutral atom count rate (pulsed)	~ 300kHz
Detector EHT voltage	~ 12kV
Detector noise rate	< 40Hz

The main beam intensity is then measured, a scattering angle in the range specified by the operator selected, and the detector driven to that angle to commence data collection.

Assuming that no problems arise, the program will now collect a number of time of flight spectra, automatically changing angle when a pre-selected number of arrivals (typically $\sim$1200) have been counted into the peak in the spectrum. Cross beam intensity, detector angular position, chamber pressure and experimental control flags are constantly monitored through two ADCs and the interface communications. The main beam is monitored, references taken and the filament flashed at time intervals specified by the operator. Under such conditions the experiment is fully automated and the operator's tasks are reduced to reading the quarter-hourly feedback and topping up the cold traps with liquid nitrogen.

Unfortunately, such an idyllic situation is not always achieved and a number of situations can arise requiring operator intervention. Some of the more common of these are described below with the associated computer message and suitable operator response.

i) Pressure Problems:

The PDP11 monitors the collision chamber pressure and if this changes the message "Pressure changed from ␣ to ␣ " is printed. No further action is taken by the software. However, if this is because of a decrease in the target beam intensity (due possibly to the cross beam reservoir running out) this, too,

shall be detected and data collection suspended pending operator intervention. A rise in the pressure can be due to pump failure or a leak but is more commonly associated with cold traps warming up. A consequence of increased pressure in the collision chamber is an increase in the noise level and a decrease in the signal rate. This is detected by the software, which measures the count rate every two minutes and the message "Count rate very low; Data collection stopped" is output on the TT. Thus corruption of existing data is avoided and, having remedied the fault, the operator may restart data collection where it was abandoned.

ii) Cross Beam Problems:

The cross beam intensity is constantly monitored. The program attempts to correct for any changes in this by switching a rheostat and also informs the operator of its action. If it is unable to control the beam, data collection is halted and the operator is required to find and fix the problem before restarting it.

iii) Main Beam Problems:

The main beam intensity is measured fairly infrequently since it is found, once established, to be fairly stable. Main beam failure would give rise to "low count rate" messages and would also be obvious from the calculate signal/noise ratios given in the feedback every 15 minutes. No action, other than alerting the operator, is taken for changes in the beam intensity less than 10%. This prevents small drifts in the beam intensity disrupting data collection. For changes larger than this, data collection is suspended and the operator informed.

Changes in the neutral flux can arise for a number of reasons. These include blockage of the CEC slits, contamination of ion lenses by diffusion pump oil and warming of cold traps in the main beam source traps.

The software also checks the angular position of the detector and halts data collection if this changes. In all cases, data collection is restarted by pressing the appropriate coding on the 3 communication flags on the interface. These are constantly monitored by the program and its response to each of the 8 possible codes is as follows:-

000 No action.

001 Read new values for one or more of the 32 experimental variables.

010 Give a "feedback" immediately.

011 Write all data to disk and stop program.

100 Go to TT for instruction. Valid responses are:-

F : Flash filament for 60 seconds;

L : List values for 32 experimental variables;

R : Measure reference spectrum;

X : Read in new value for ideal cross beam.

101 Halt data collection;

110 Restart data collection.

111 Write data to disk, select new angle, drive to it and continue data collection.

CHAPTER 3

K/Ar DIFFERENTIAL CROSS SECTIONS

This chapter is concerned with differential cross sections collected for the collision system potassium/argon. This system has been extensively studied over the years (KEM 74), (BUC 68) and the experimental results discussed in this chapter have been previously published (KER 75), (FLU 75a). The reasons for the current analysis are twofold. Firstly, to check the potentials obtained from these experimental results in view of the conflicting results reported by other workers (MAL 70), (PAS 74), and to determine whether the oscillatory structure observed in the cross sections is the result of noise or evidence of some process taking place in the course of the collision.

3.1 DATA COLLECTION AND ANALYSIS

The data takes the form of a series of scattering intensities measured at scattering angles from 0 to 5 degrees in the lab frame of reference and at collision energies between 100 and 400 eV lab. These were collected on the crossed molecular beams apparatus described in the previous chapter, prior to the development of the time of flight technique. The data collection took place under program control by the PDP11/45. For each set of data the angle scan was completed in a pseudo-random manner to prevent any systematic noise effects creeping into the data. The detector was returned to the main beam centre at periods of about six minutes to monitor the main beam intensity. Relative, rather than absolute, intensities have been gathered but they are inter angle normalised. The data are fully presented in Kerr's thesis and are shown here in figures 3.1 to 3.7.

Figure 3.1

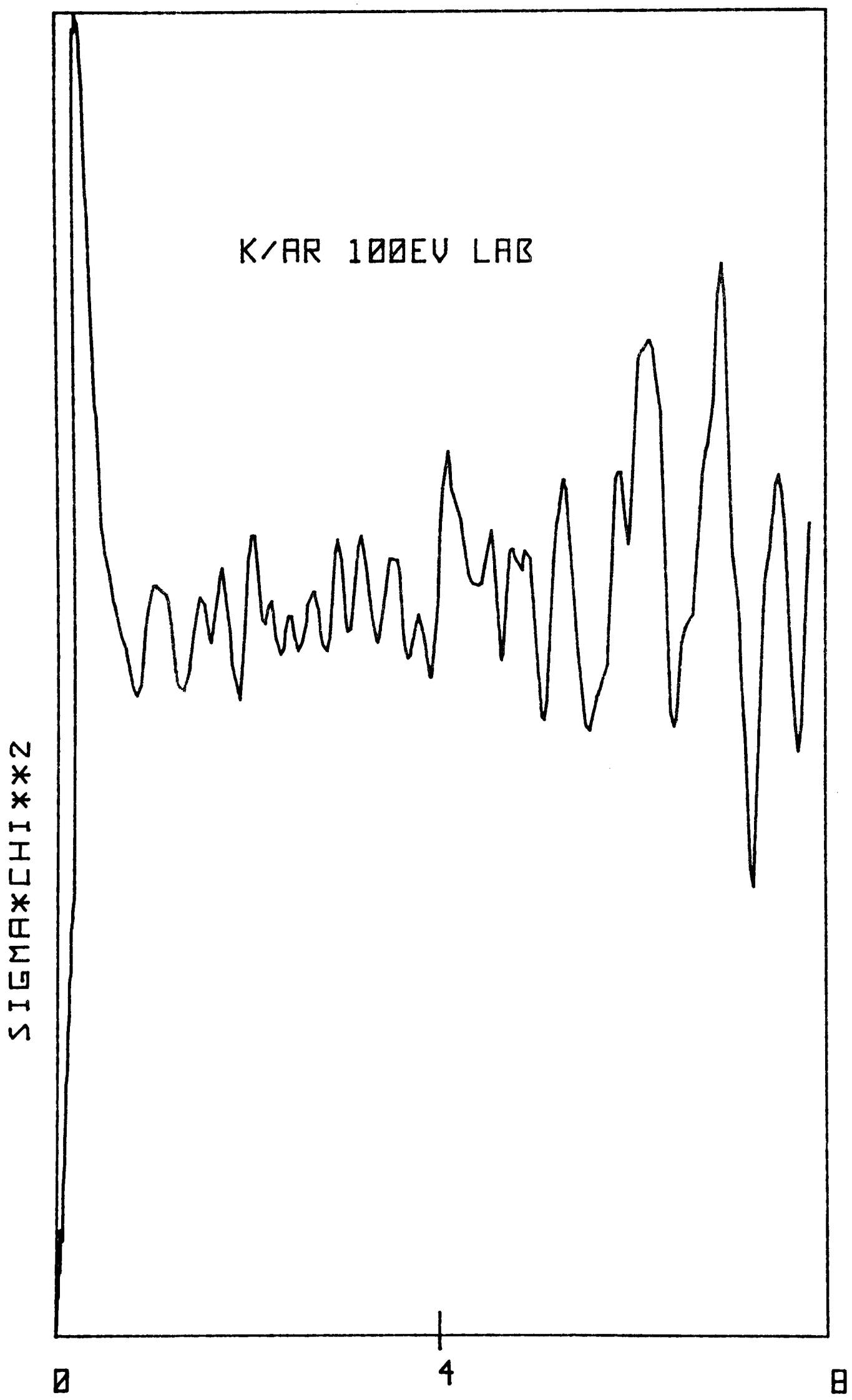

Figure 3.2

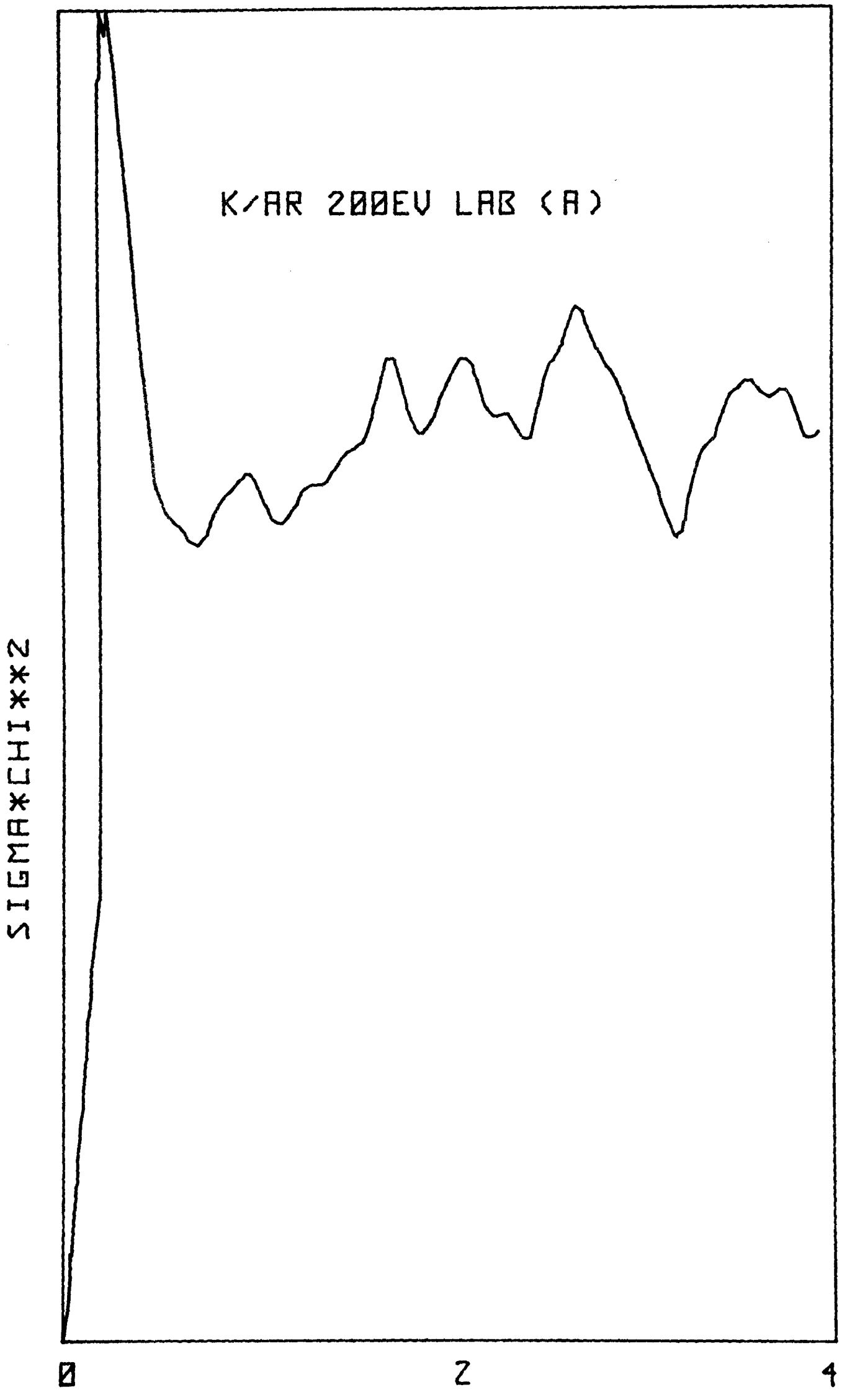

Figure 3.3

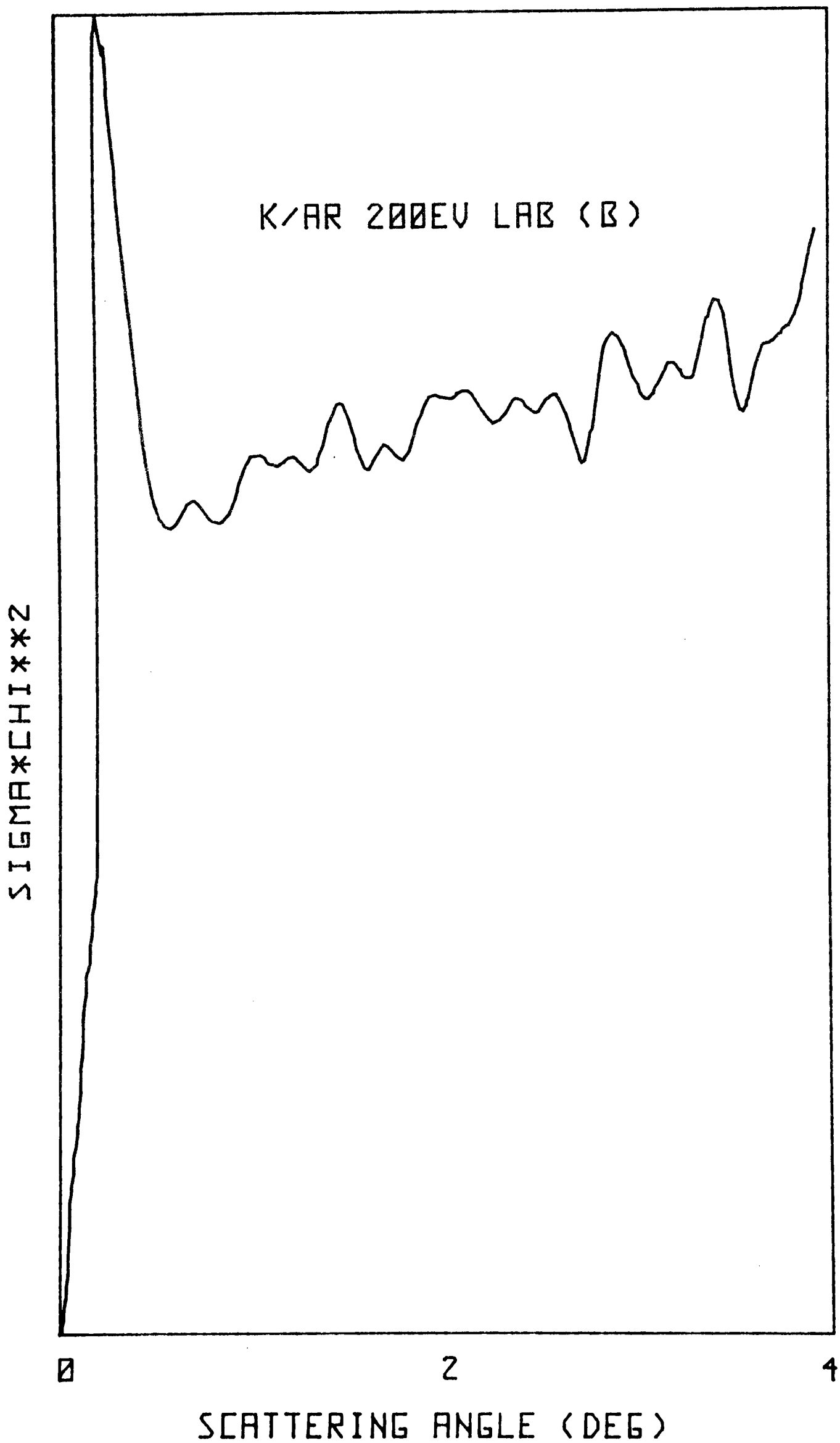

Figure 3.4

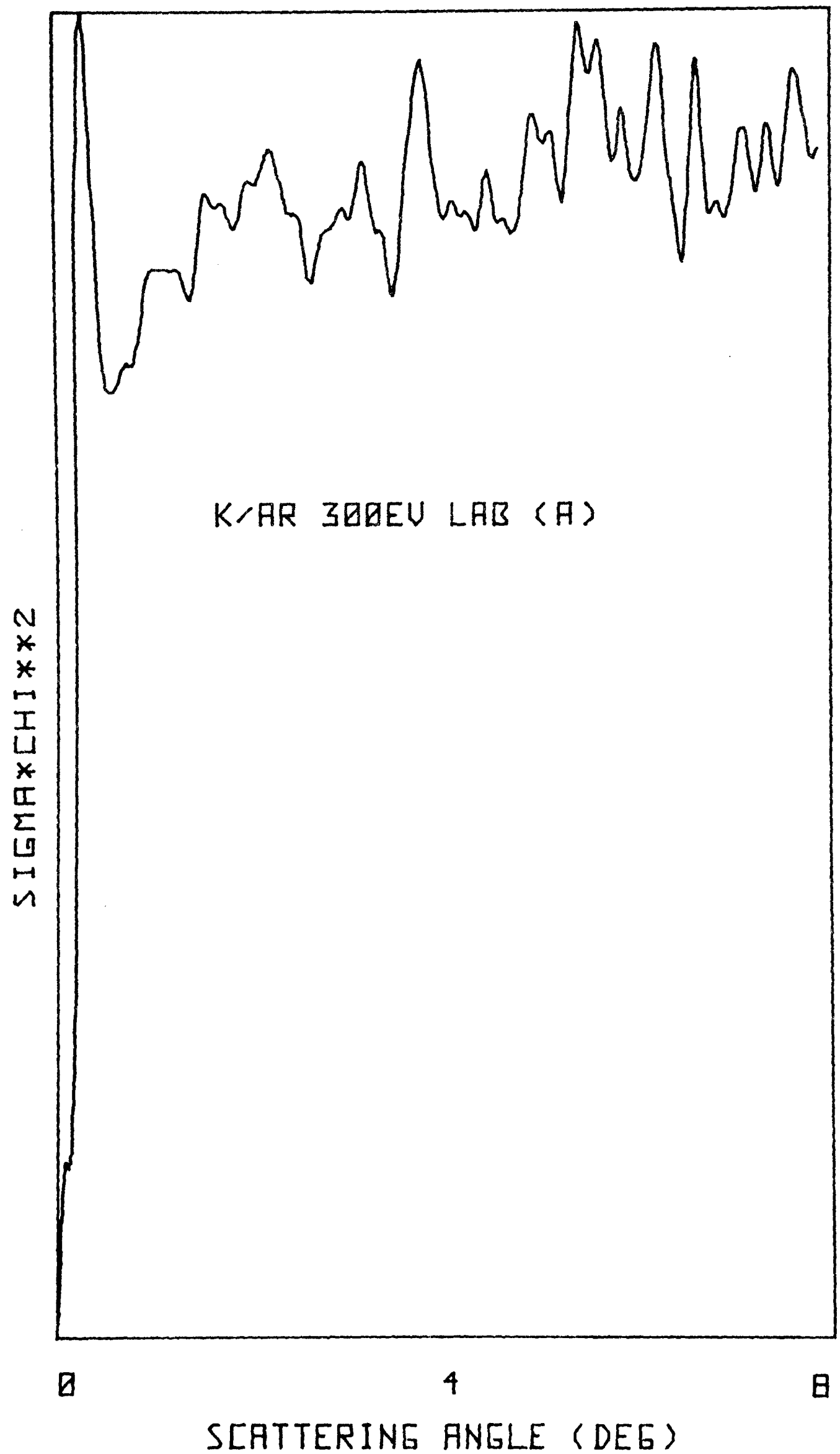

Figure 3.5

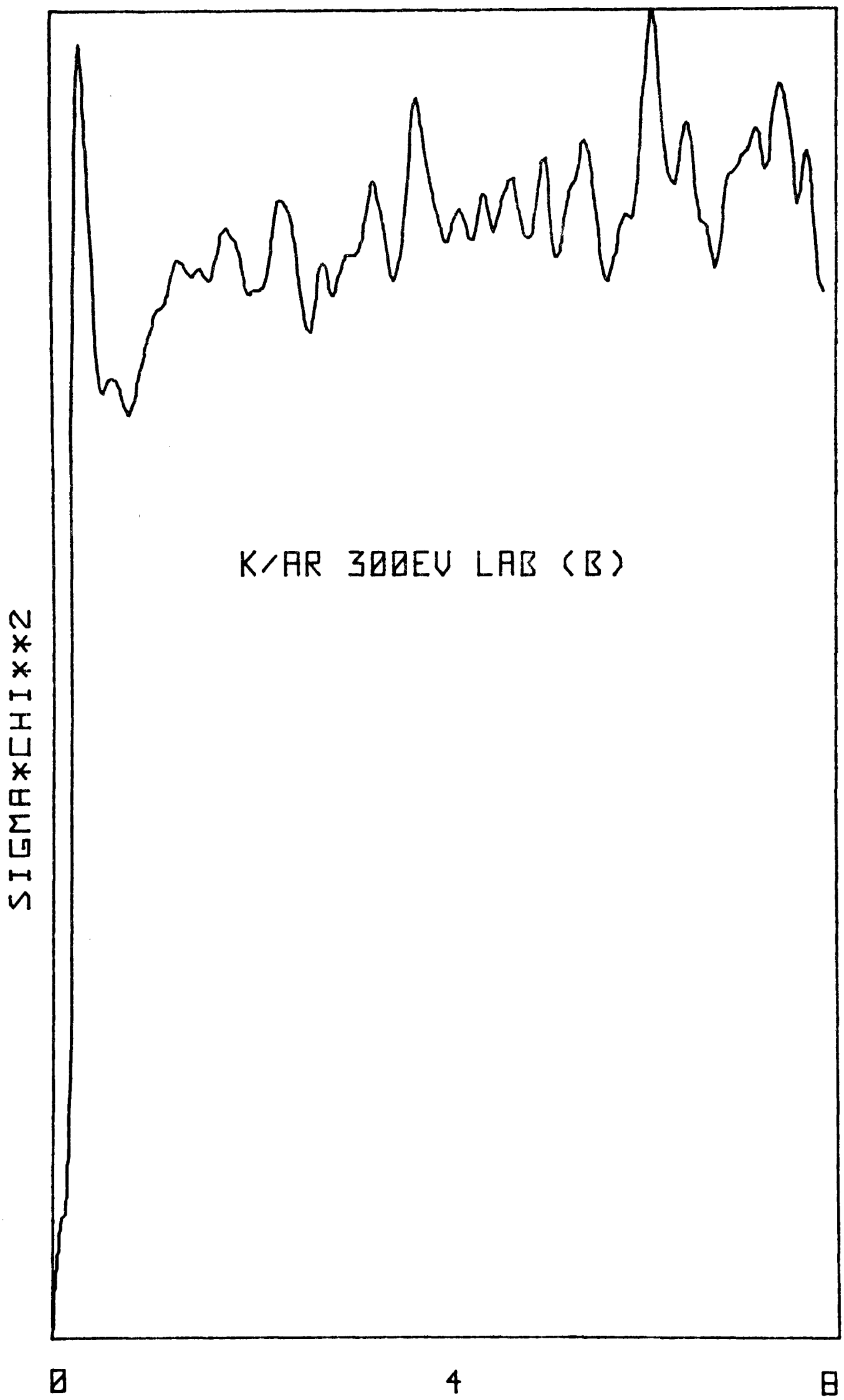

Figure 3.6

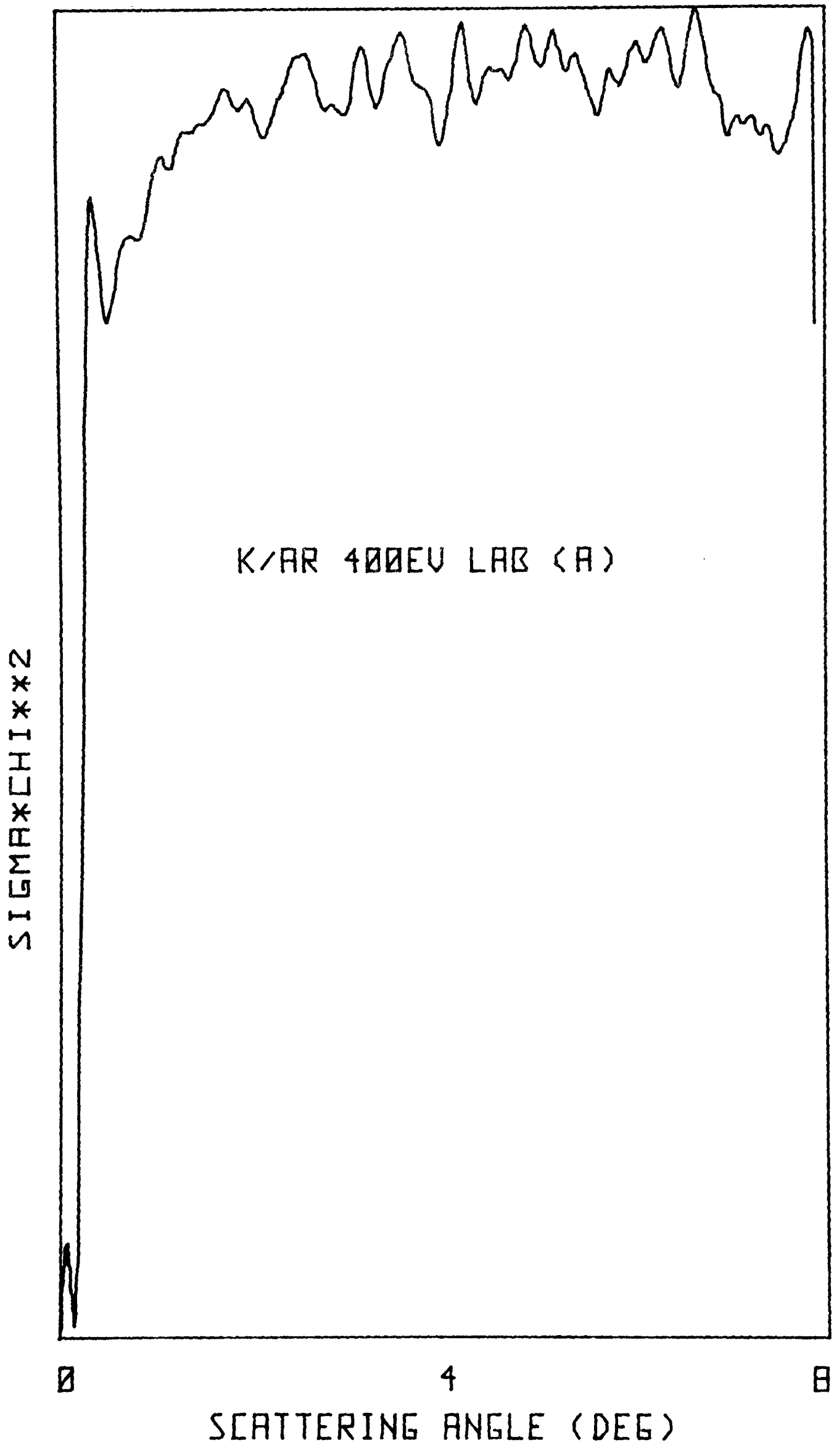

Figure 3.7

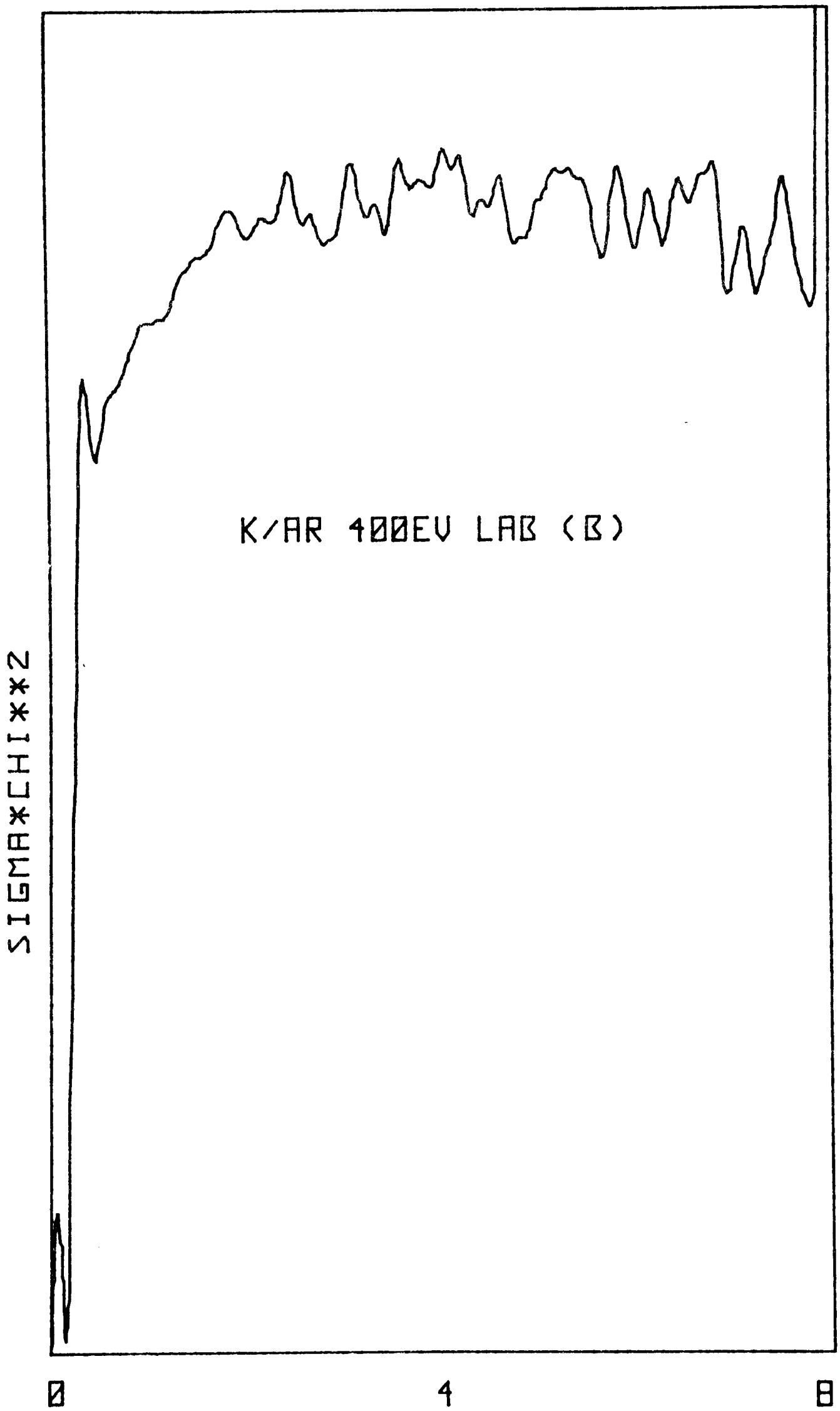

The first step in the analysis of the data is the transformation to the centre of mass frame and the application of the resolution correction calculated for the apparatus (RED 73). The method of obtaining the potentials, due to Firsov (FIR 53), relied on the manipulation of the classical deflection function given by equation 3.1.

$$\chi(b) = \pi - \int_{R_c}^{\infty} \frac{2b\,dR}{R^2 \left(1 - \frac{V(R)}{E} - b^2/R^2\right)^{\frac{1}{2}}} \qquad 3.1$$

where
- b = impact parameter
- χ = scattering angle
- R = particle separation
- $V(R)$ = inter particle potential at R
- E = collision energy
- R_c = point of closest approach of particles

The potential can then be obtained by numerically evaluating the relations 3.2 and 3.3.

$$V(R) = E\,(1 - b^2/R^2) \qquad 3.2$$

$$R = b \exp\left\{\frac{1}{\pi} \int_{b}^{\infty} \frac{\chi(b')\,db'}{(b'^2 - b^2)^{\frac{1}{2}}}\right\} \qquad 3.3$$

The problem, therefore, is one of evaluating the deflection function, $\chi(b)$, from the observed scattering data. The classical scattering intensity, $I(\chi)$, is given by equation 3.4 .

$$I(\chi) = \frac{b}{\text{Sin}\,\chi \left|\frac{d\chi}{db}\right|} \qquad 3.4$$

Re-arrangement of this gives:-

$$b^2(\chi) = 2\int_{k}^{\pi} I(\chi)\,\text{Sin}\,\chi\,d\,\chi \qquad 3.5$$

It is not possible to calculate $b(\chi)$ directly from the present data as it does not extend to π radians. In addition the fact that the data consists of relative, rather than absolute, differential cross sections means that there is a constant in front of the integral. The method of normalisation involves choosing some previously evaluated potential for the K/Ar system and computing $\sigma(\chi)$ and $b(\chi)$ for that potential at the appropriate energy at the normalising angle χ_n. The values thus obtained are assumed to agree with the experimental results and the deflection function is calculated using equation 3.6.

$$b(\chi) = (b^2(\chi_n) - 2\int_{\chi_n}^{\chi} \sigma(\chi')\,\text{Sin}\,\chi'\,d\,\chi')^{\frac{1}{2}} \qquad 3.6$$

This is equivalent to equating both $\chi(b)$ and $\frac{d}{db}\chi(b)$ of the data and the normalising potential at the normalisation angle, χ_n.

It can be seen that this technique is only valid if the experimental results are in good agreement with the normalising potential as it forces the deflection function on to that of the normalising potential. The results using this technique

to normalise the data under discussion to the potential obtained by Kempter's group (KNE 76) are shown in figure 3.8.

For narrow angle scattering from potentials of the form $V(R) = {}^{C}/_{R^S}$ the following relations hold:-

$$\sigma(\chi) = \frac{1}{S}\left\{S\pi^{\frac{1}{2}}\frac{\Gamma(\frac{S+1}{2})\ C}{\Gamma(\frac{S}{2}+1)\ E}\right\}^{2/S}\chi^{-(2+2/S)} \qquad 3.7$$

$$b^S(\chi) = \left\{SC\pi^{\frac{1}{2}}\Gamma\frac{(S+1)}{(2)}\Big/\Gamma\left(\frac{S}{(2}+1\right)\right\}\Big/2E\chi \qquad 3.8$$

All variables have the previously given definitions.

From equation 3.7 it can be seen that the cross section, σ, is proportional to $\chi^{-(2+2/S)}$. Hence a plot of log $(\sigma\chi^2)$ against log (χ) will have slope $-2/S$ and will therefore give an estimate of the R dependence of the potential. This has been carried out for the data shown in figures 3.1 to 3.7 and the potential is estimated to be:-

$$V(R) = {}^{C}/_{R}{}^{15 \pm 3}$$

The potential shown in figure 3.8 has a much softer R dependence than this - a result of forcing the deflection function on to that of Kempter's potential.

Equations 3.7 and 3.8 can be re-arranged to give:-

$$C = \frac{E\Gamma(\frac{S}{2}+1)}{S\pi^{\frac{1}{2}}\Gamma\frac{S+1}{2}}\left[S\sigma\chi^{(2+2/S)}\right]^{S/2} \qquad 3.9$$

$$C = 2E\chi b^S(\chi)\ \frac{\Gamma(\frac{S}{2}+1)}{S\pi^{\frac{1}{2}}\Gamma\frac{(S+1)}{2}} \qquad 3.10$$

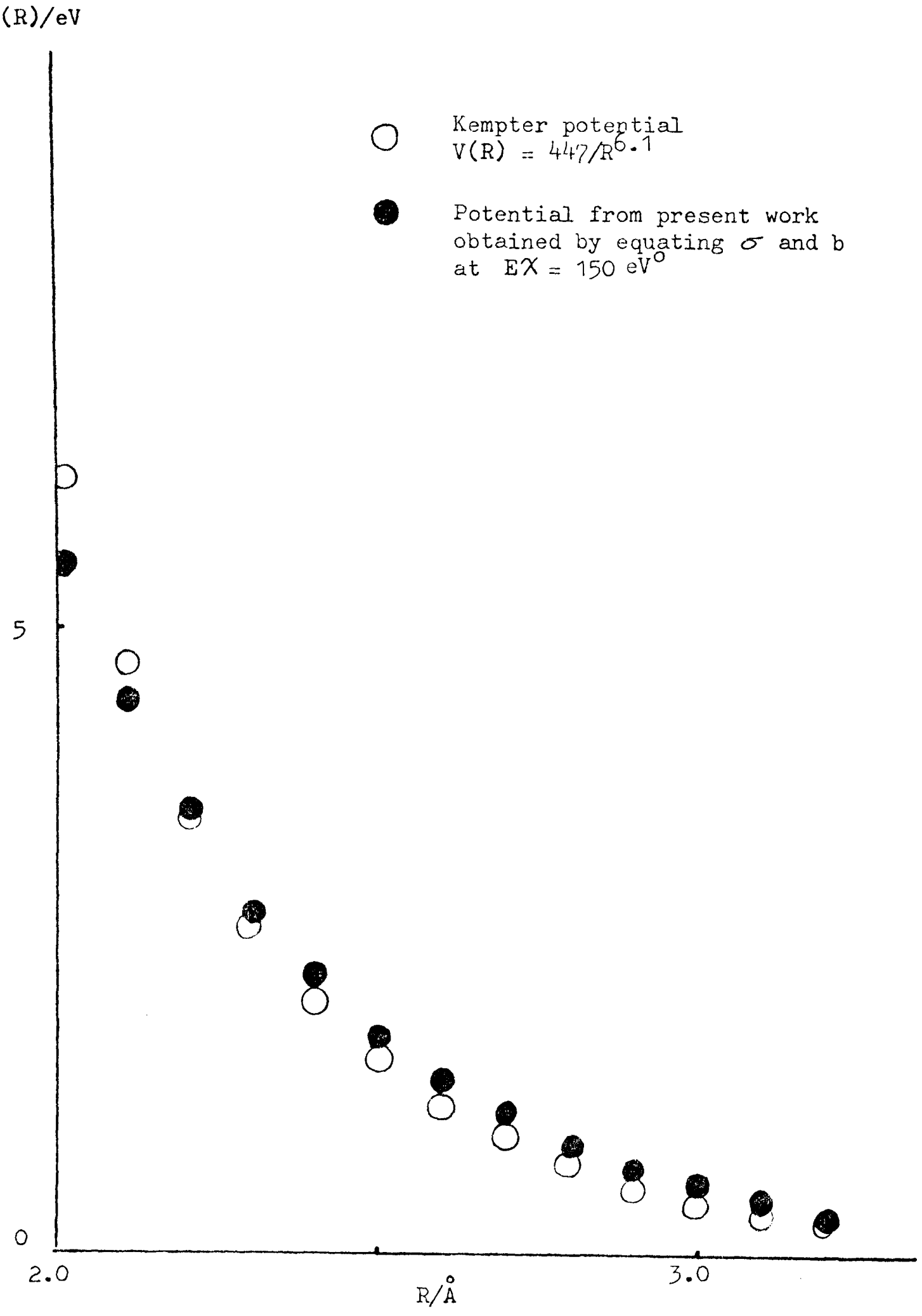

Figure 3.8 : K/Ar potentials

If a value of S is obtained from a plot of log $(\sigma\chi^2)$ against log (χ) and $\sigma(\chi_n)$ is used to normalise the data then equation 3.9 can be used to obtain a value for C. Equation 3.8 is then used to calculate $b(\chi_n)$ from the estimated potential. In terms of the deflection function this is equivalent to equating the value of $b/\frac{d\chi}{db}$ for the normalising potential with $\frac{b}{\frac{d\chi}{db}}$ for the experimental results.

Similarly it is possible to equate $b(\chi)$ at χ_n for the data and potential and to use equation 3.10 to obtain a value for C. It is then possible to calculate $\sigma(\chi)$ at any angle using equation 3.7 and thus normalise the intensity. This method of normalisation corresponds to equating b but not $\frac{d\chi}{db}$ at χ_n.

All three normalisation procedures are completely equivalent if the experimental results are in agreement with the normalising potential. This is not the case with the results discussed here and the normalising potentials of Cross and Malerich and Kempter. This is shown in figures 3.9 and 3.10.

In order to verify the accuracy of each of the three potentials obtained from the inversions a forward calculation was carried out in each case. This simply involved evaluating the differential cross sections predicted by each of the three parameterised potentials. The results of this calculation indicated that the best agreement was produced by equating $b(\chi)$ at the normalising angle χ_n.

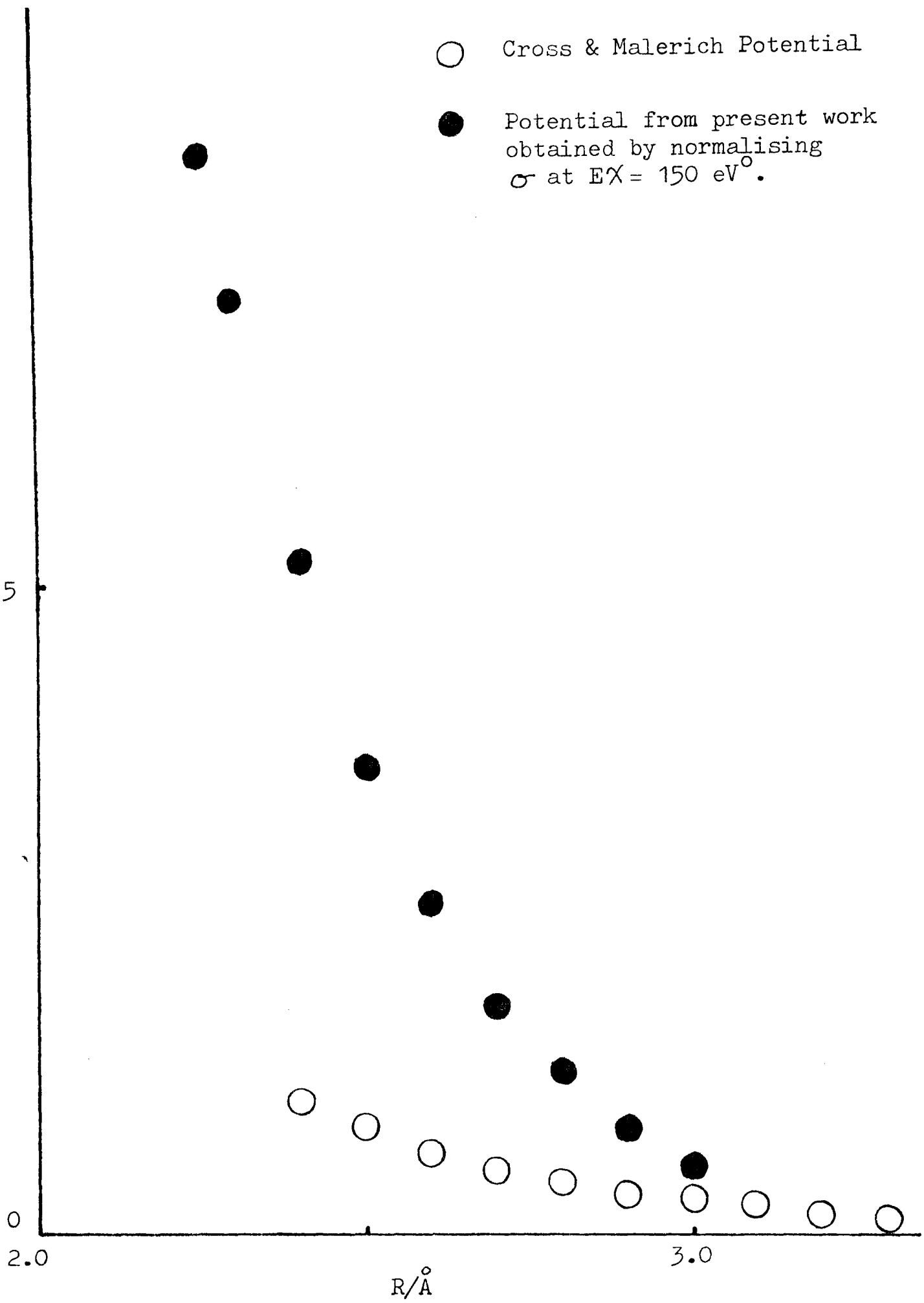

Figure 3.9 : K/Ar Potentials

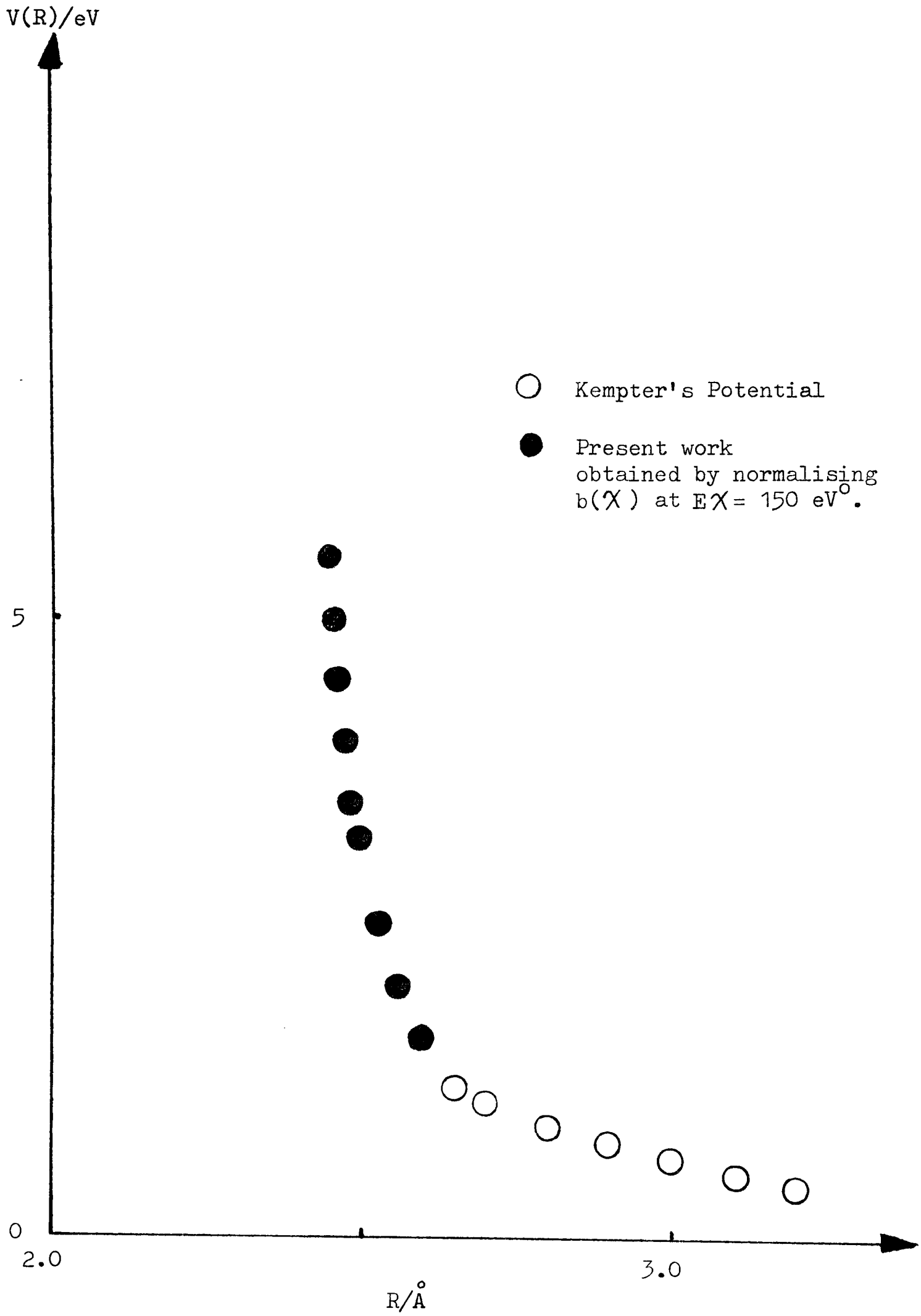

Figure 3.10 : K/Ar Potentials

The potential obtained from this work on the K/Ar differential cross sections has the form -

$$V(R) = \frac{5.8 \times 10^7}{R^{18.2}}$$

and is valid in the region $2.45 < R < 2.6$ Å and $1.6 < V(R) < 5$ eV.

In view of the discrepancy between this result and other work a more recent experiment has been carried out with K/Ar in collision at 200 eV lab collision energy. The results of this work were in agreement with the earlier work carried out by Kerr.

3.2 OSCILLATIONS IN THE K/Ar DATA

As was mentioned in the introduction to this chapter, the Potassium/Argon differential cross sections exhibit an oscillatory structure and this can be readily observed in figures 3.1 to 3.7. The magnitude of these oscillations is comparable with the size of the error bars, which have been omitted in these diagrams for clarity.

It was felt worthwhile to carry out further investigation into the oscillations to determine if they were purely due to noise or if they were evidence for some underlying process occurring during the course of the collision. Each data set consisted of about 500-600 observations at different angles throughout the range and the pseudo random angular scan should have avoided any systematic errors from entering the results due to important experimental variables drifting over an extended period of time.

The maxima and minima appeared to illustrate a fairly regular angular spacing for each data set and in order to check this the angular positions of the extrema were located and the extrema were indexed sequentially. Thus, if the peaks are at uniform angular separation, a plot of index number against angular position will produce a straight line.

Peaks which were both very small and close to their neighbours were thought to be noise and discounted. Similarly, extrema which were very far apart with a point of inflection between them had their index number increased as it was felt that the inflection probably corresponded to a peak in the data which had been masked by noise.

Plots were made of index number against angle for each of the sets of data and three of them are shown in figures 3.11 to 3.13. These can be seen to be linear with increasing angle and the slope decreasing as the collision energy is increased. Data sets at the same collision energy are found to be in good agreement with each other. It is also noted that the angular spacing of the extrema, $\Delta\theta$, increases in a regular way with collision energy such that $\Delta\theta/E^{\frac{1}{2}}$ remains constant.

A number of different phenomena can lead to the appearance of oscillatory structure in the differential cross section. Oscillations always occur when more than one classical trajectory leads to the same deflection angle. These can arise as a result of a potential well in the scattering surface giving supernumerary

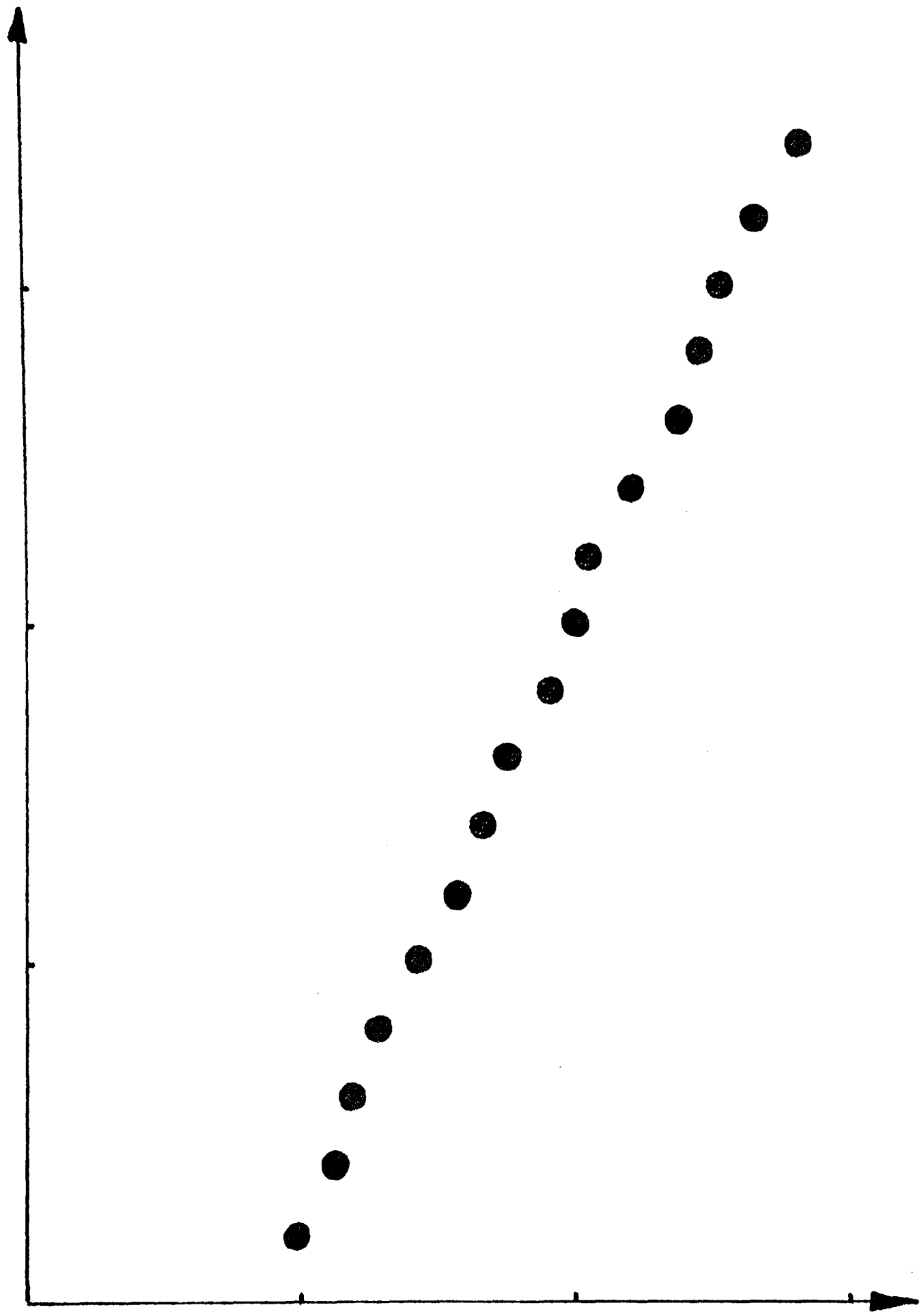

Figure 3.11 : K/Ar positions of extrema in the differential Cross Section

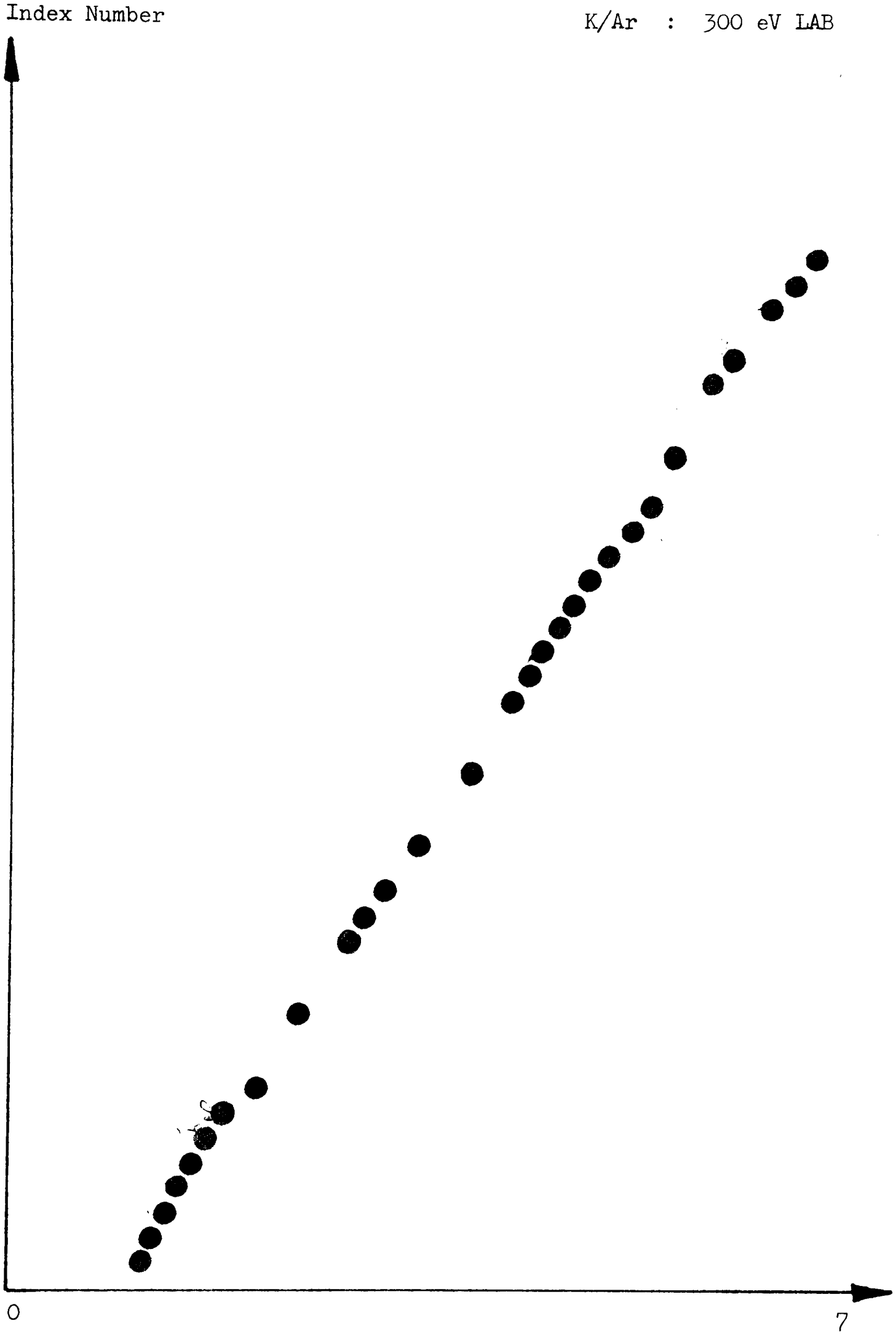

Figure 3.12 : K/Ar positions of the extrema in the differential cross sections

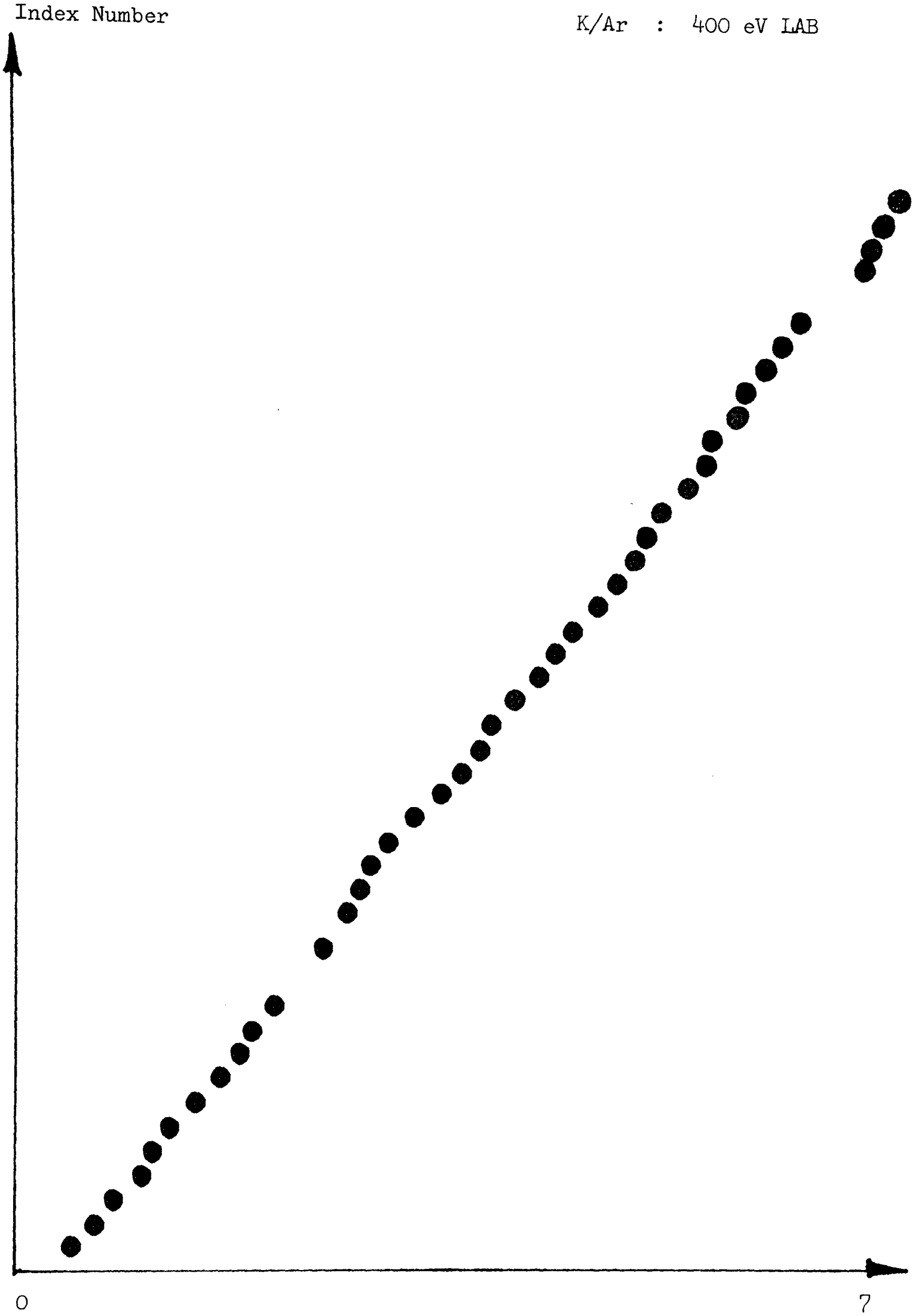

Figure 3.13 : K/Ar positions of extrema in the differential cross sections

rainbows (widely spaced oscillations) and rapid oscillations. For angles greater than the rainbow angle, scattering on a single surface leads to a monotonic differential cross section as there is only one contribution to the classical path. This is the case with the range of the potential probed here. A revue of the features of elastic scattering is given in BUC 75.

For collisions in which a potential crossing can take place the possibility of interference in the elastic cross section arises. There are two trajectories in the elastic channel, one corresponding to scattering on the ground state potential and the other coming from a crossing to the excited state potential on the inward passage followed by a transition to the ground state on the outward passage. The interference pattern is seen as a perturbation on the elastic scattering and was first reported by Stueckelberg in 1932 (STU 32).

The observed structure can not be Stueckelberg oscillations for a number of reasons. In the K/Ar data reported here the angular spacing of the extrema in the differential cross sections varies such that $\Delta\theta/E^{\frac{1}{2}}$ remains constant whereas for Stueckelberg oscillations $\Delta\theta$ varies such that $\Delta\theta E^{\frac{1}{2}}$ is constant. In fact it does not seem likely that electronic excitation or access to any excited state potential surfaces is possible for the range of the potential probed by this experiment. Kempter et al (KEM 74) showed the threshold energy for excitation of the potassium to the $4^2P_{\frac{1}{2}}$ state to be about 19 eV - much further up the repulsive wall of the potential than the current measurements.

Subsequent to the collection of these differential cross sections time of flight data has been obtained for the K + Ar collision system and the analysis of the results shows that the system is at least 98% elastic under the experimental collision conditions. These were at 105.9 eV centre of mass collision energy and out to a scattering angle of 12.14 degrees C.M.

CONCLUSIONS

The need for further work on the collision system K + Ar is apparent. Though perhaps less appealing to the experimentalist than systems in which substantial electronic excitation can be expected to take place, there are clearly two outstanding problems.

The strongly repulsive potential obtained from this work is very much out of step with that reported by other workers. It should be remembered that the values obtained for the potentials often have different ranges of validity. Nevertheless it is important to be convinced that the measurements taken and potentials obtained for this, one of the simplest systems, are correct. It may be worthwhile checking the resolution correction calculated for the apparatus though it is difficult to believe that this can radically alter the results because it is only important for the scattering at angles of less than about 0.5 degrees.

It would be worthwhile carrying out further experiments to investigate the apparent oscillatory structure. Data obtained at other collision energy would provide further evidence for the existence of the oscillations as well as testing the relationship between $\Delta\theta$ and the collision velocity.

CHAPTER 4

The bulk of the experimental work carried out for this thesis involved the investigation of inelastic collision processes using the time of flight crossed beam apparatus described in Chapter 2. The fast potassium beam was intercepted by alkyl halide type beams and time of flight profiles were collected for K + HI, CH_3Cl, CH_3I, C_3H_7I and CF_3I. The experimental results are presented in this chapter and the discussion follows in Chapter 5.

4.1 SYSTEMS STUDIED

Time of flight data has been collected for potassium/alkyl halide like collision systems. A full list of the systems studied is given in Table 4.1. These systems make suitable and interesting targets because of the large number of exit channels open to them. These include:-

$K + RX \longrightarrow K + RX\ (K + RX^X)$	elastic (vibration)	(a)
$K + RX \longrightarrow KX + R$	Reaction	(b)
$K + RX \longrightarrow K^+ + RX^-$	Chemi-ionisation	(c)
$K + RX \longrightarrow K^{\Phi} + RX$)) $K + RX \longrightarrow K + RX^{\Phi}$)	Electronic excitation	(d)
$K + RX \longrightarrow K + R + X$	Dissociation	(e)

Processes (a) and (b) have been investigated at thermal collision energies (KIN 72), (GER 72) and are well known examples of the electronic harpooning mechanism. The chemi-ionisation channel has been explored (BAE 75) and provides direct evidence for non-adiabatic behaviour at the covalent/ionic surface crossing.

SYSTEM	LAB COLLISION ENERGY
HI	200EV
CH3CL	200EV
CH3I	100EV
CH3I	200EV
CF3I	100EV
CF3I	200EV
C3H7I	200EV

TABLE 4.1 SYSTEMS STUDIED

The involvement of the ionic surface in coupling the ground and excited electronic states of the atom is confirmed by collision induced fluorescence studies (KEM 75).

In the present work the reaction channel is closed by working at high relative collision energies. By working at scattering angles of less than 7 degrees the potassium atom trajectories can be considered as rectilinear and of constant velocity. Nevertheless interesting regions inside the harpooning radius can be probed and electronic excitation of up to 14 eV is observed.

4.2 DATA COLLECTION AND ANALYSIS

As stated in Chapter 2, time of flight profiles are collected at a number of angles in the range 0 - 7 degrees laboratory scattering angle. Periodically a reference profile is taken showing the scattering spectrum at 0 degrees. The data is transferred from the DEC PDP11/45 to the Edinburgh Regional Computing Centre's ICL 4/75 and it is on this that the bulk of data analysis takes place. The data is transformed to the centre of mass frame (C.M.) and a five-point polynomial filter applied to each spectrum. The scattering data are then deconvoluted with the reference spectra using the H.P. Van Crittert method (JAN 70). A listing of the deconvolution program, FILTER 7, is given in Appendix B. The thus obtained deconvoluted spectra are output into a file along with the various parameters required for further analysis of the data.

The data presented here were collected over a period of about three years and in this time the location of the apparatus was changed. As a result of this and modification of the ion lens optics the position of the primary beam pulse varied by as much as 70ns between different experiments. The spectra were therefore adjusted in time so as to be relative to the unscattered beam arrival as measured in each experiment. It is this that has given rise to most of the noise seen in the results rather than counting statistics.

Spectra gathered at a number of angles for each target compound can be combined to produce a contour map showing the scattered flux as a function of scattering angle and post-collision velocity. Figure 4.1 shows such a plot for potassium/methyl iodide scattering at 164 eV C.M. Whilst this contour map clearly indicates that there is a lot of inelastic scattering taking place, the complexity of the surface represented tends to obscure the information contained in it.

As an aid to the interpretation of the data it is useful to take cuts across this scattering surface and sum all the arrivals within a certain narrow angular range. This gives rise to a series of angle averaged time of flight profiles for each system studied and the deconvolution process can be taken further on these, using once again the profile at 0 degrees scattering as a reference. At both this and the earlier deconvolution it was checked that each peak on the deconvoluted spectra was accompanied by at least a hint of a peak on the undeconvoluted data. This was to ensure that

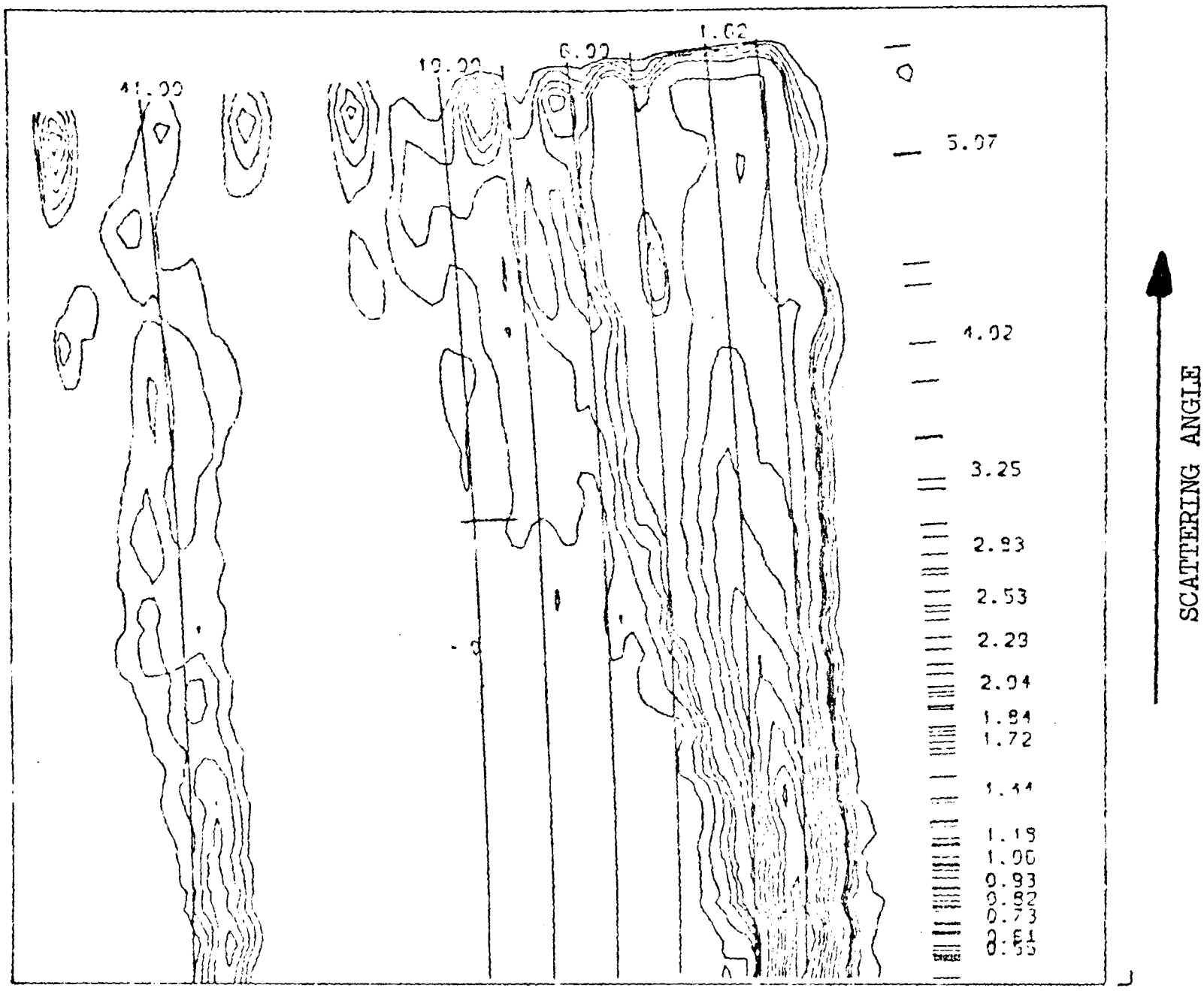

Figure 4.1 : CONTOUR MAP OF 164 eV CM K/CH_3I

This diagram shows the scattered potassium flux as a function of post-collision velocity and scattering angle. The labelled lines show the velocities corresponding to energy losses of 0, 1.62, 4, 6, 8 and 10 eV. The isotope can be seen at the left of the figure labelled 41.00. At narrow angles the scattering is almost purely elastic and the contours of highest intensity are centred on the zero energy loss line. In contrast, at larger scattering angles the scattered flux extends over a greater velocity range indicating that a substantial number of the encounters are resulting in vibrational and/or electronic excitation of one or both of the partners.

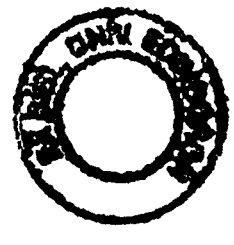

the deconvolution was not gathering noise together under a peak but was merely sharpening peaks that were already there.

The majority of the data is therefore presented as time of flight spectra and the energy losses corresponding to the positions of the peaks in the arrival spectra are shown. A table summarising the peaks in the arrival spectra at each scattering angle accompanies each set of data. Some of the spectra also show the undeconvoluted data.

Having established the energy losses it is possible to evaluate the differential cross sections for the relevant exit channels and to attempt a tentative assignment of the states involved and the mechanism by which they are populated. Some of the differential cross sections are presented in this chapter and a full discussion of the assignments and mechanisms involved follows in the next.

4.3 K/CH_3I DATA

Tables 4.2 and 4.3 list the peaks reported in the time of flight spectra for potassium/methyl iodide collisions at 81 eV and 164 eV (C.M.). All the energy losses listed in any one column are believed to be due to the same process. It will be noticed that there is a "jitter" in the values at which the maxima appear. This is presumably due to the change in the location of the equipment and the length of time over which the data were collected as the other data sets, which were mainly collected over only two or three runs each, do not exhibit this problem to the same extent.

Figure 4.2

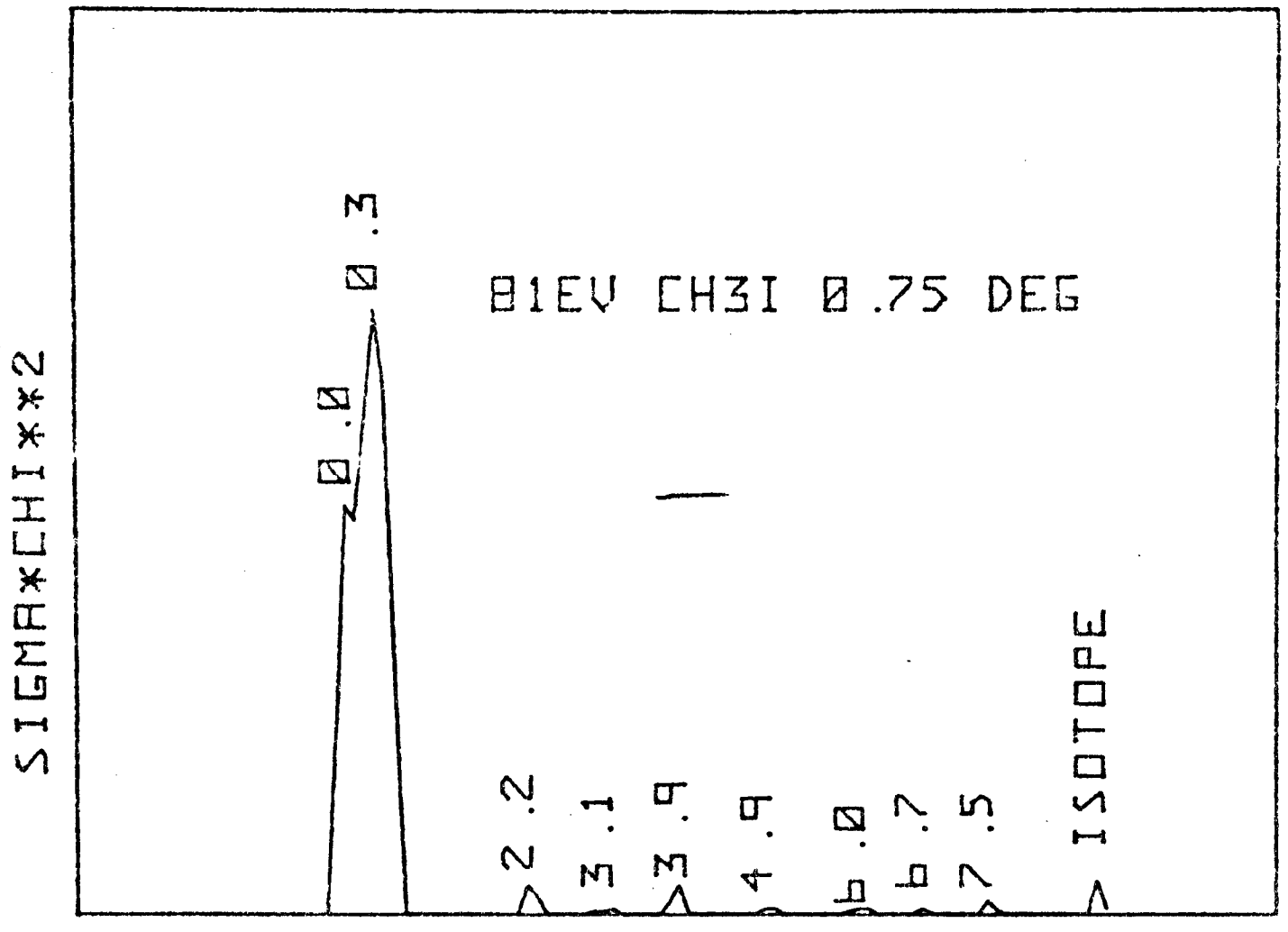

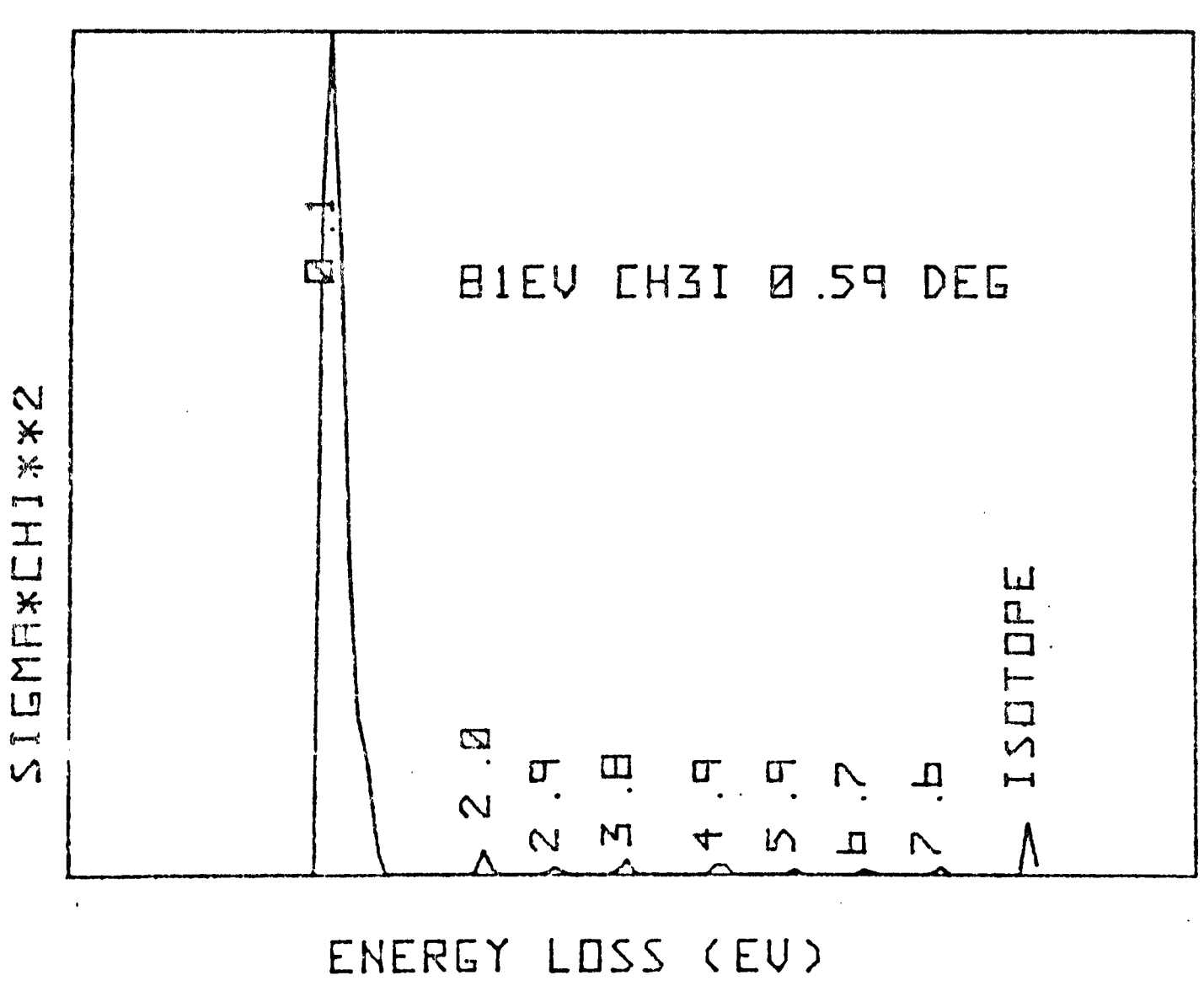

Figure 4.3

Figure 4.4

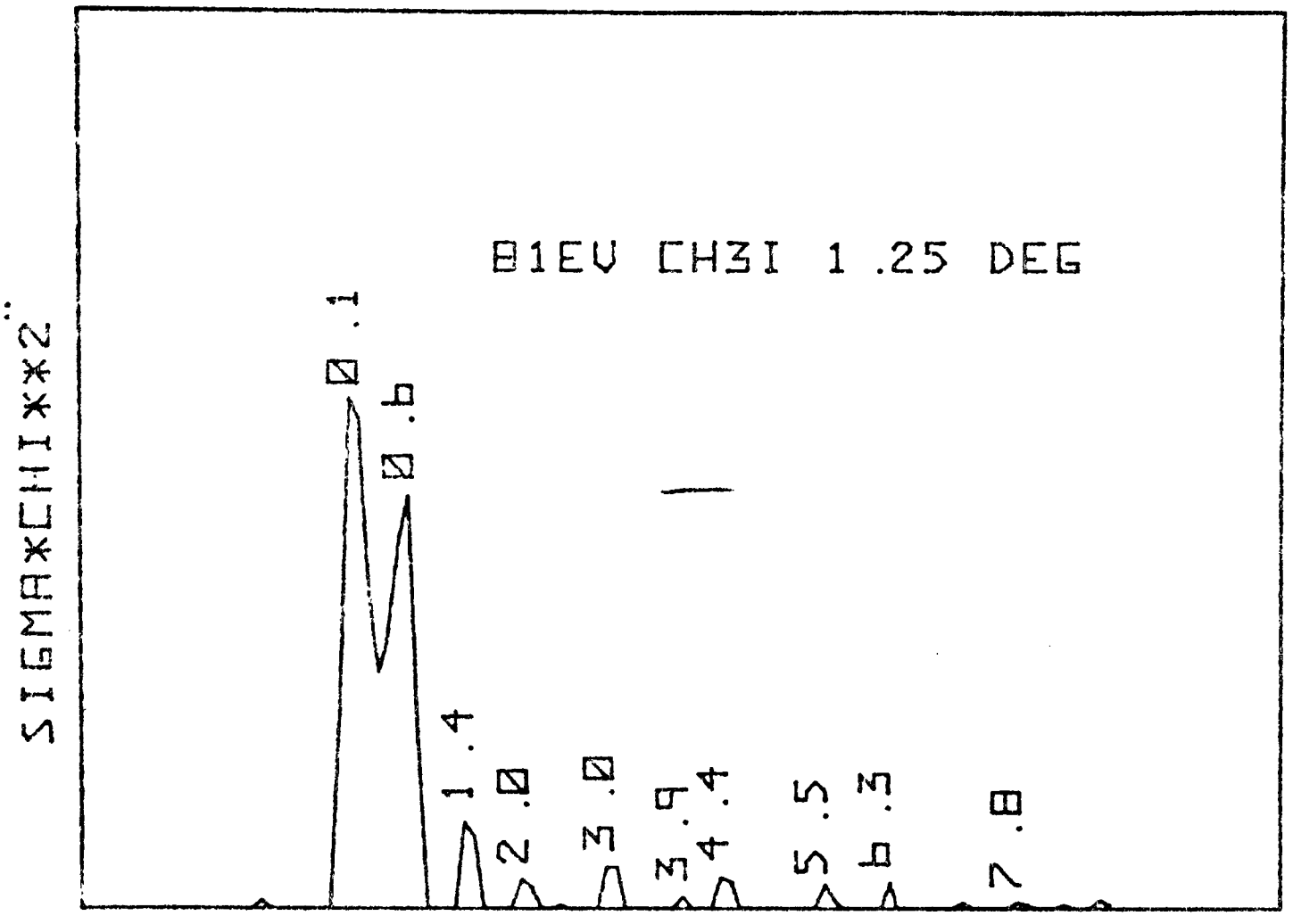

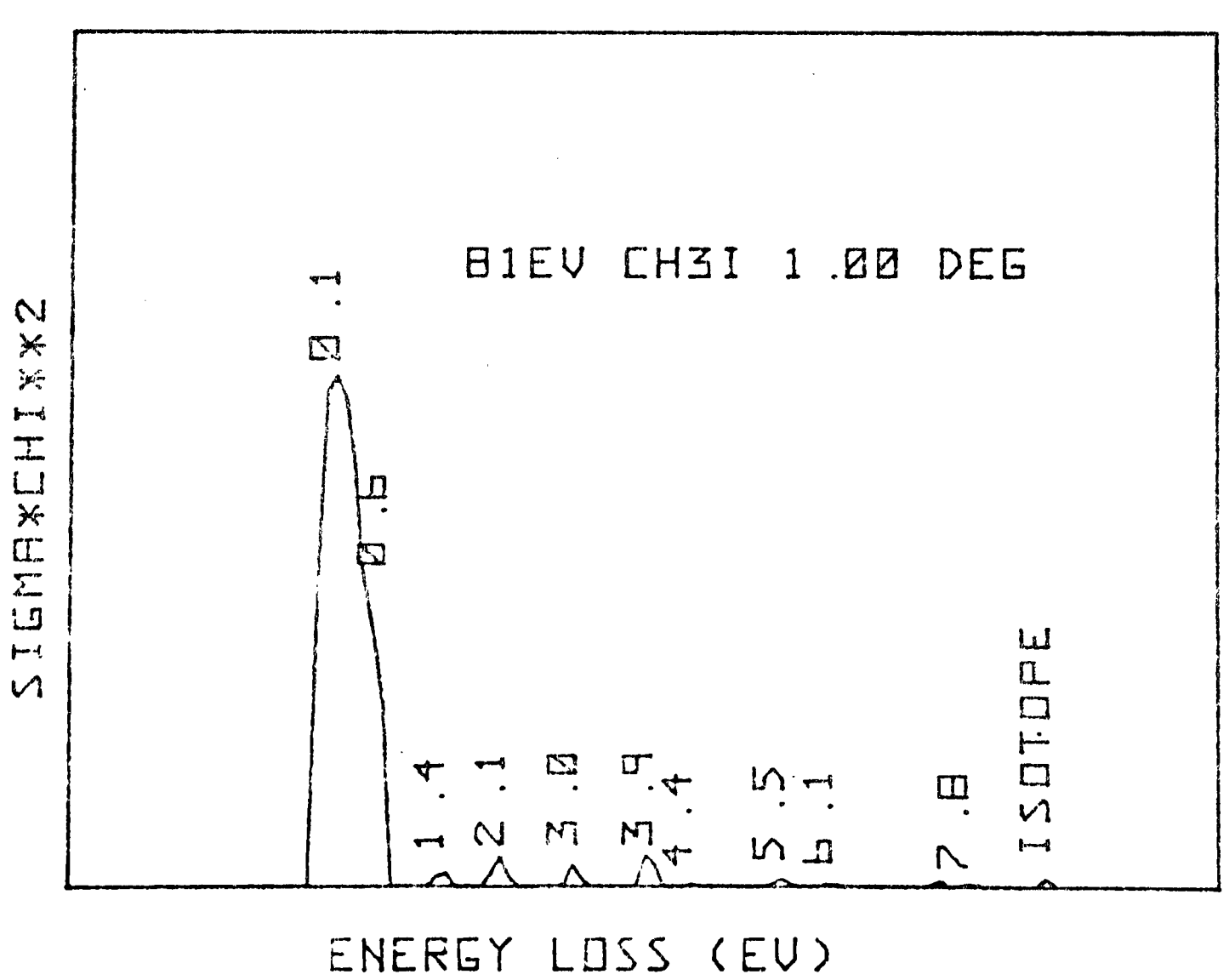

Figure 4.5

Figure 4.6

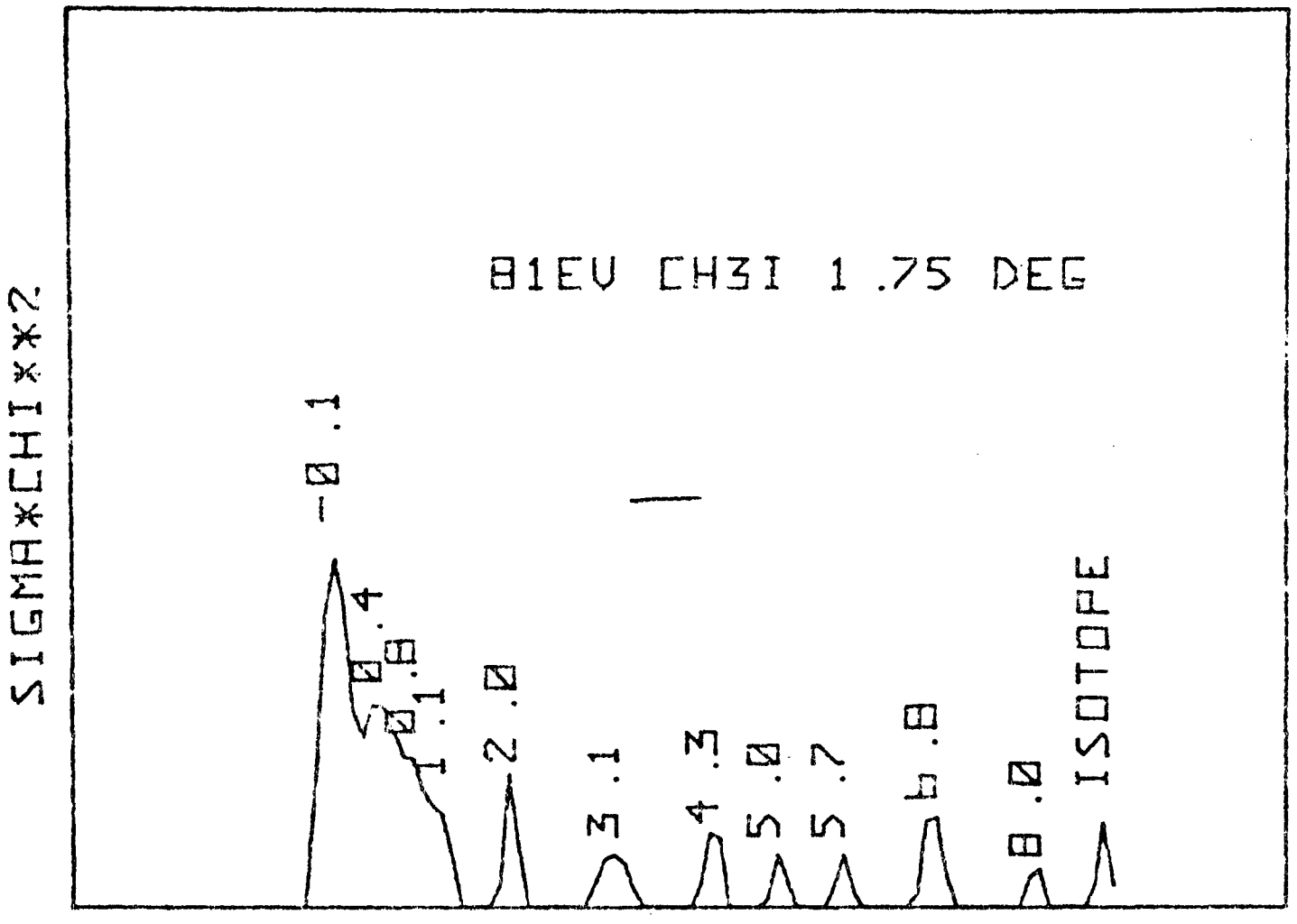

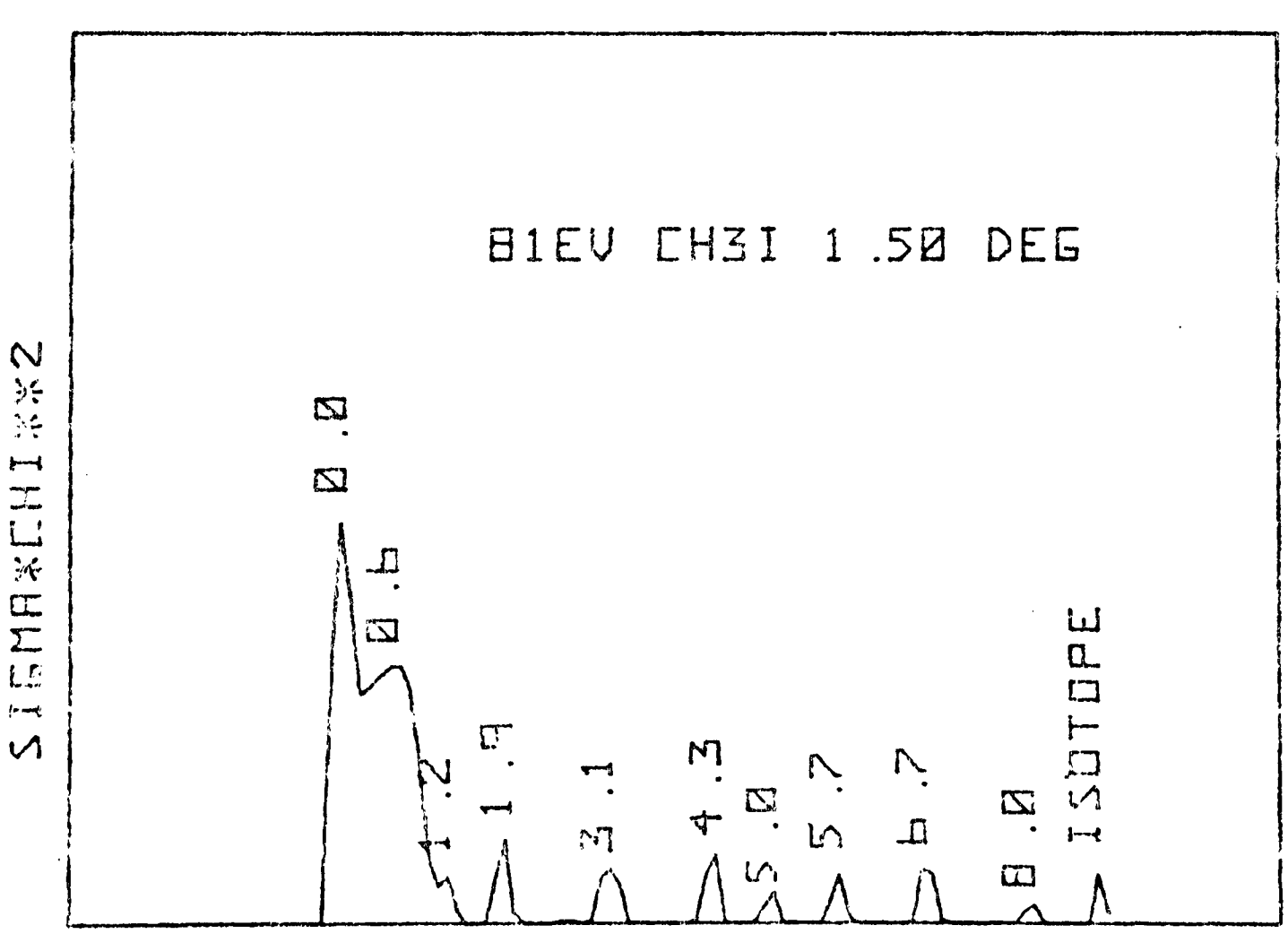

Figure 4.7

Figure 4.8

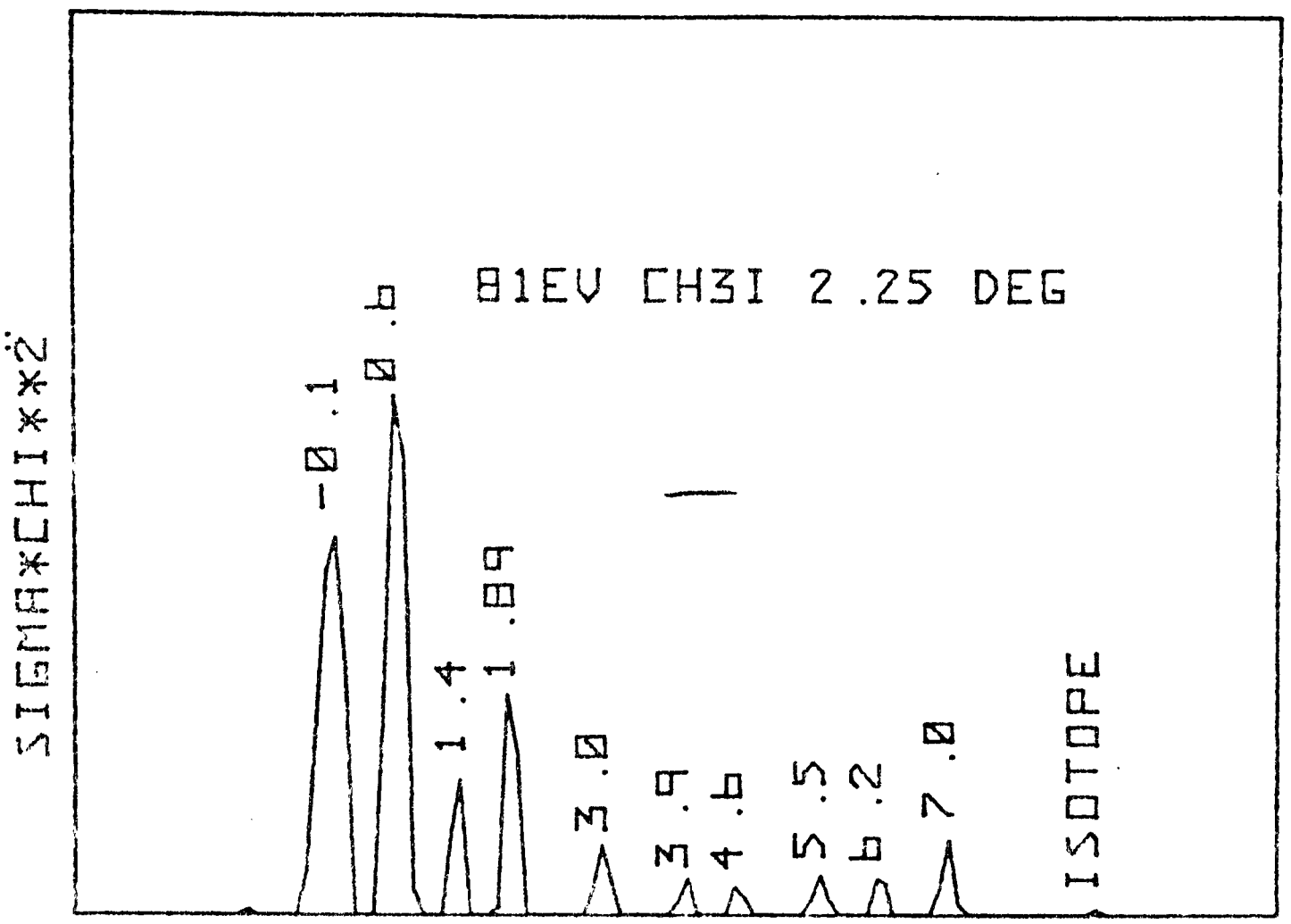

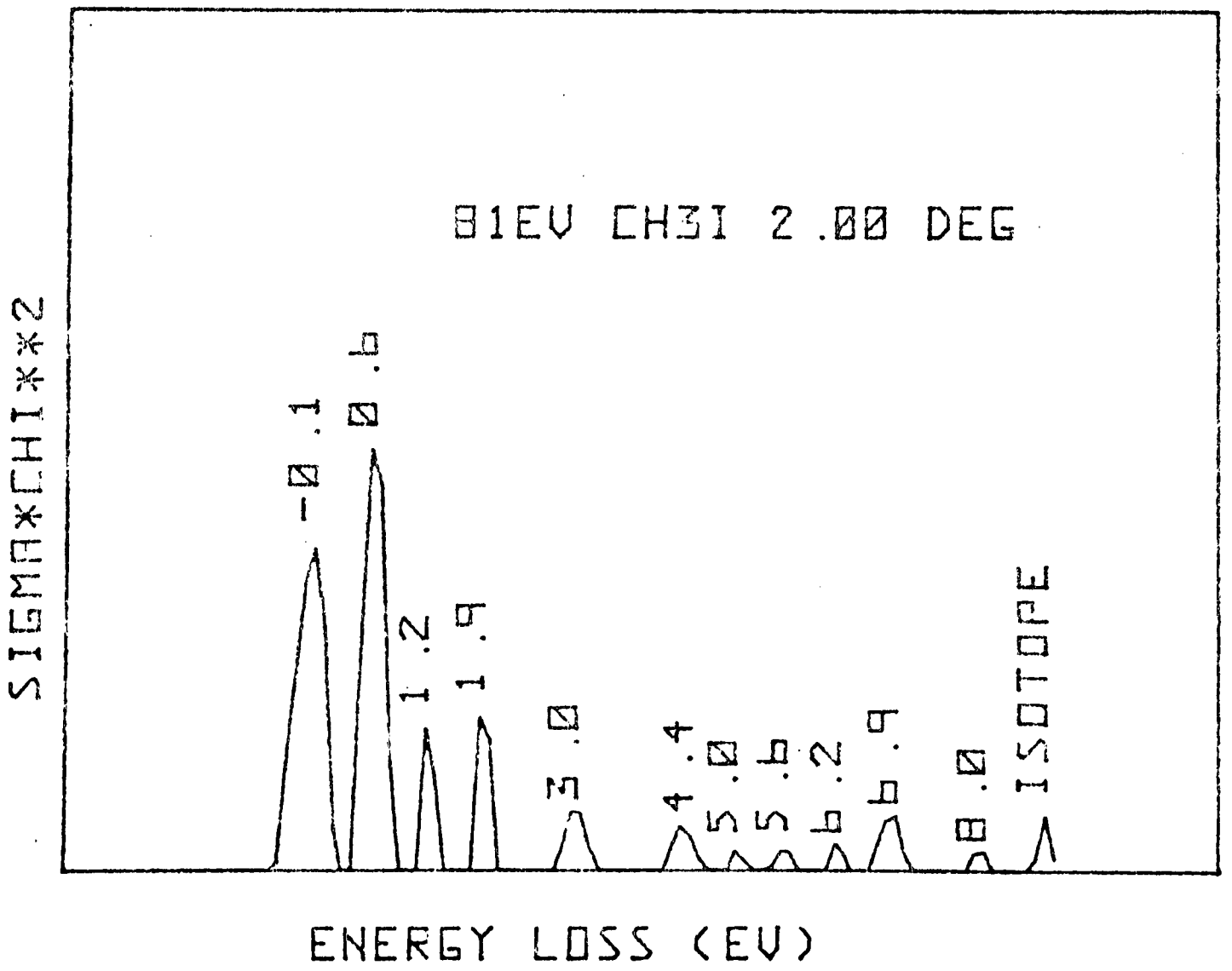

Figure 4.9

Figure 4.10

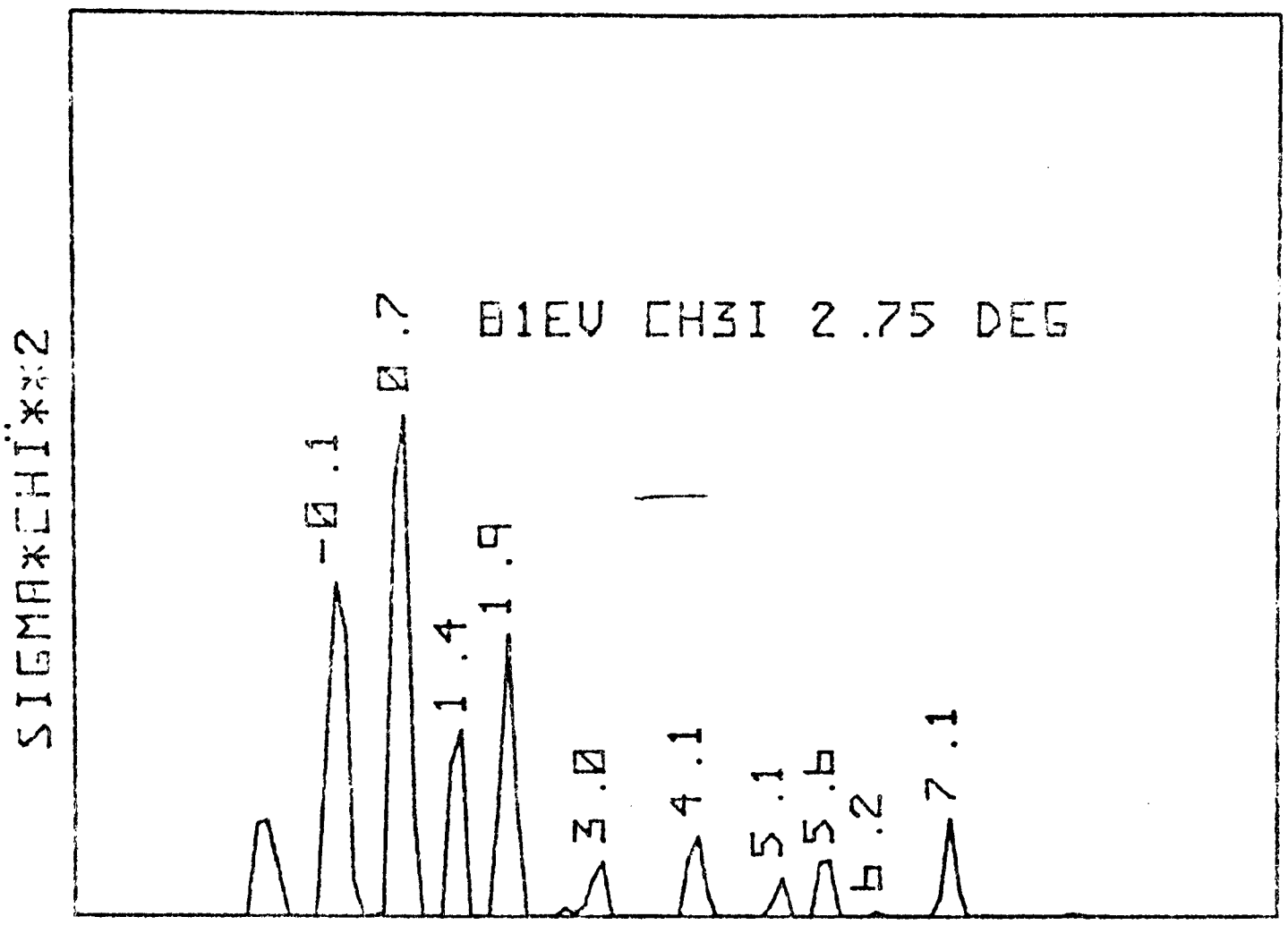

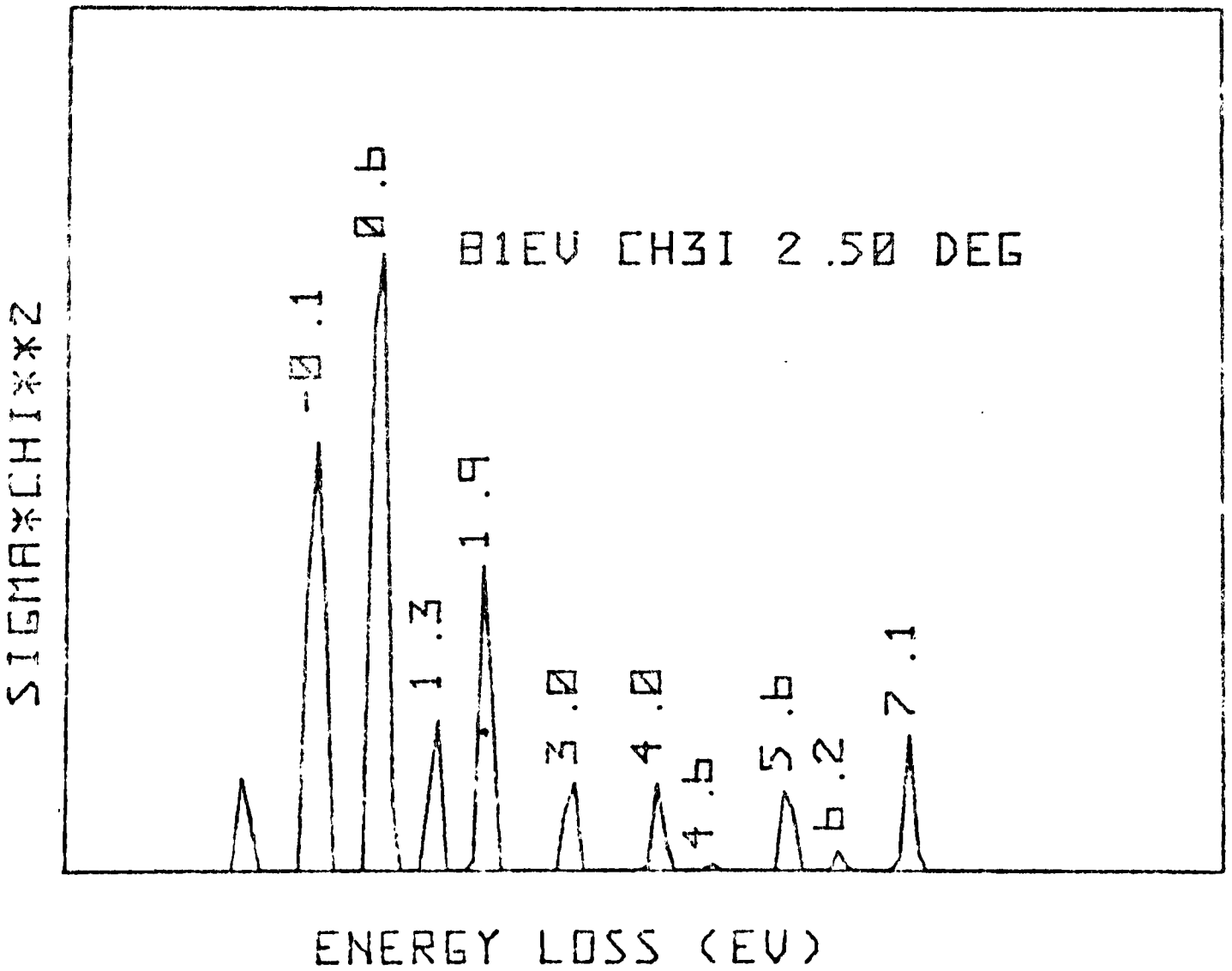

Figure 4.11

TABLE 4.2 : PEAKS IN K/CH_3I (81 eV C.M.) SPECTRA

Angle	Energy Loss 1	2	3	4	5	6	7	8	9	10	11	12	13
0.59	0.1			2.0	2.9	3.8		4.9			5.9	6.7	7.6
0.75	0.0	0.3		2.2	3.1	3.9		4.9			6.0	6.7	7.5
1.00	0.1	0.6	1.4	2.1	3.0	3.9	4.4		5.5		6.1		7.8
1.25	0.0	0.6	1.4	2.0	3.0	3.9	4.4		5.5		6.3		7.8
1.50	0.0	0.6	1.2	1.9	3.1		4.3	5.0	5.7		6.7		8.0
1.75	-0.1	0.6	1.1	2.0	3.1		4.3	5.0	5.7		6.8		8.0
2.00	-0.1	0.6	1.2	1.9	3.0		4.4	5.0	5.6	6.2	6.9		8.0
2.25	-0.1	0.6	1.4	1.9	3.0	3.9	4.6		5.5	6.2	7.0		
2.50	-0.1	0.6	1.3	1.9	3.0	4.0	4.6		5.6	6.2	7.1		
2.75	-0.1	0.7	1.4	1.9	3.0	4.1		5.1	5.6	6.2	7.1		

Figure 4.12

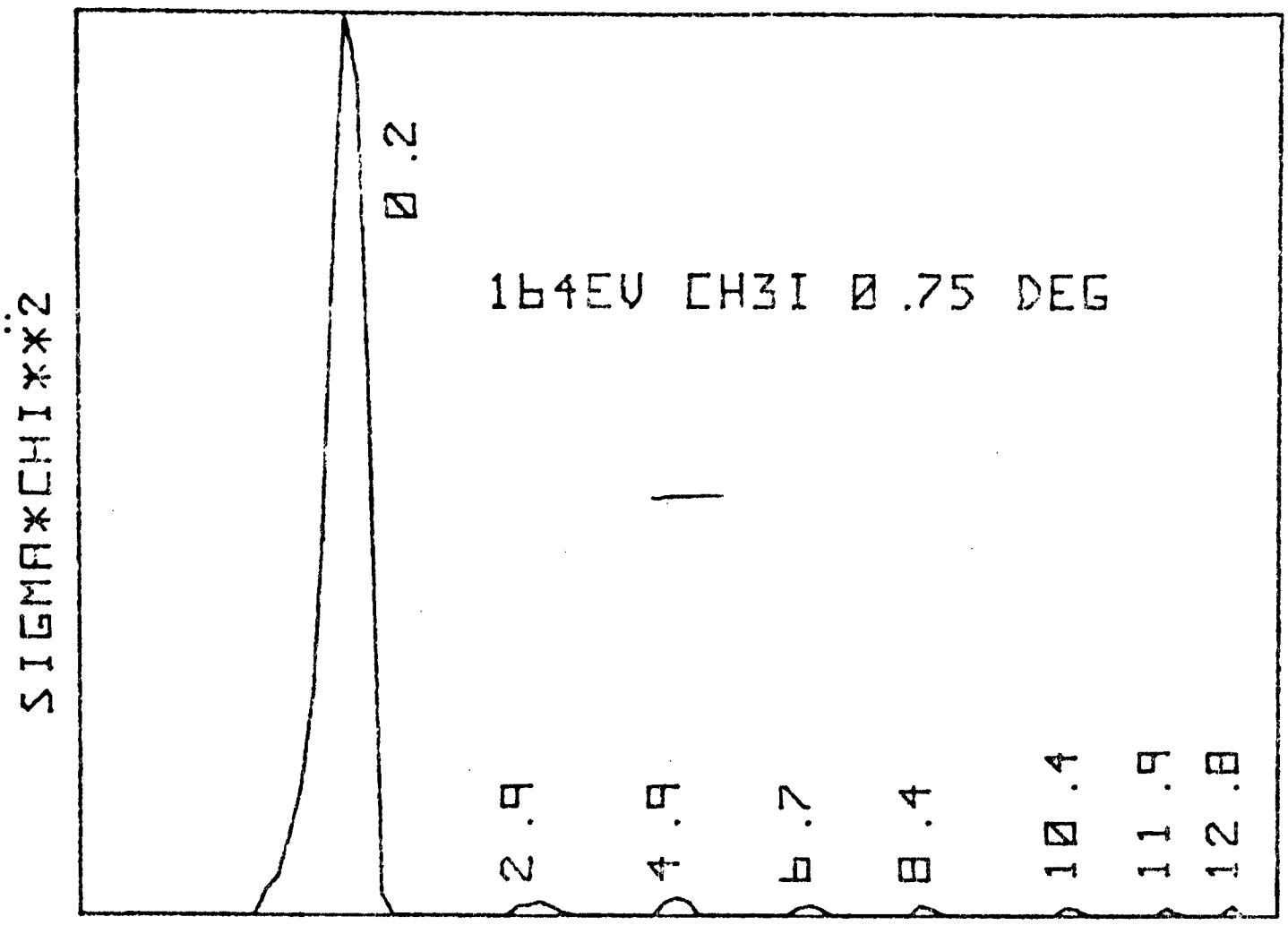

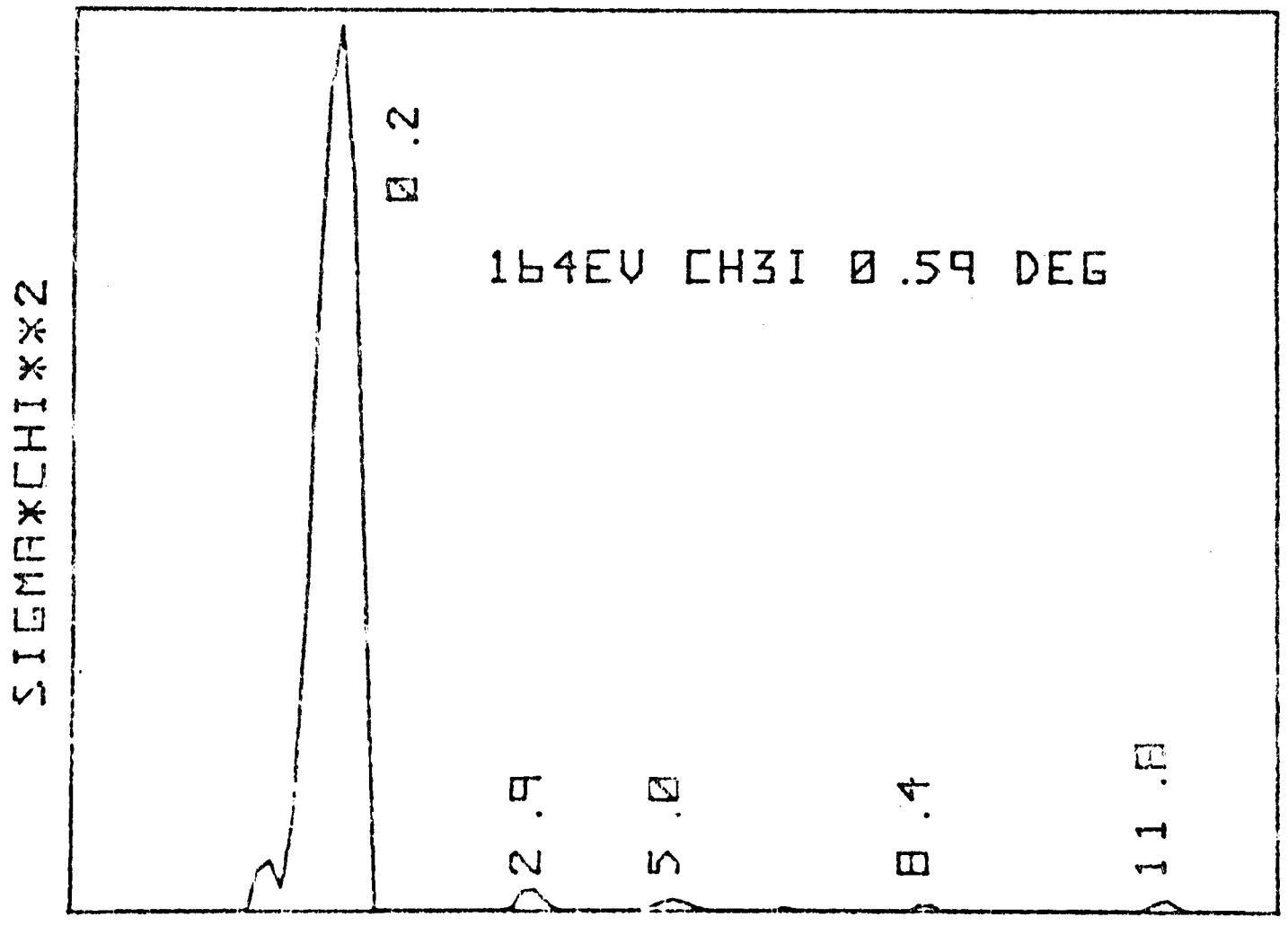

Figure 4.13

Figure 4.14

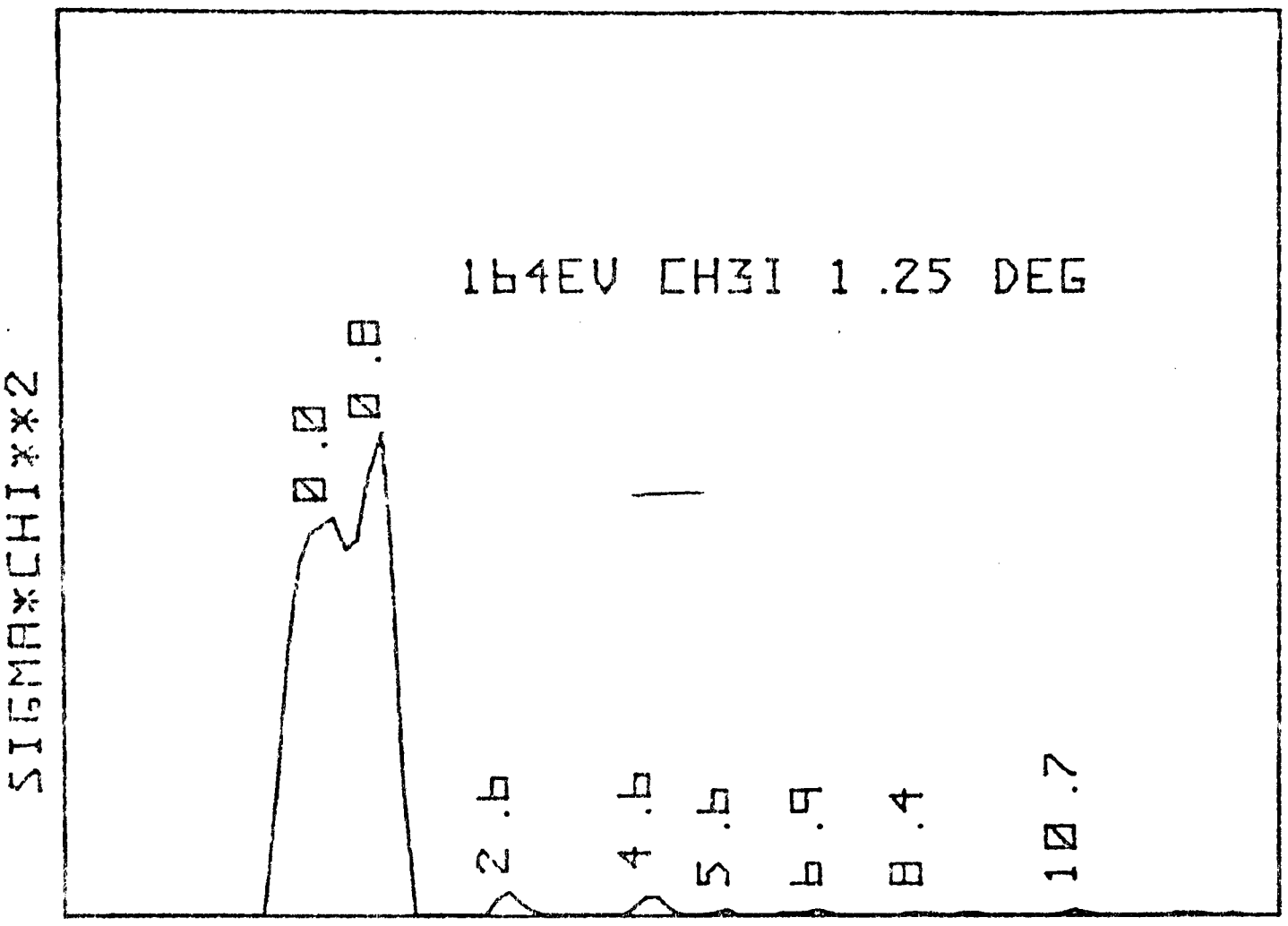

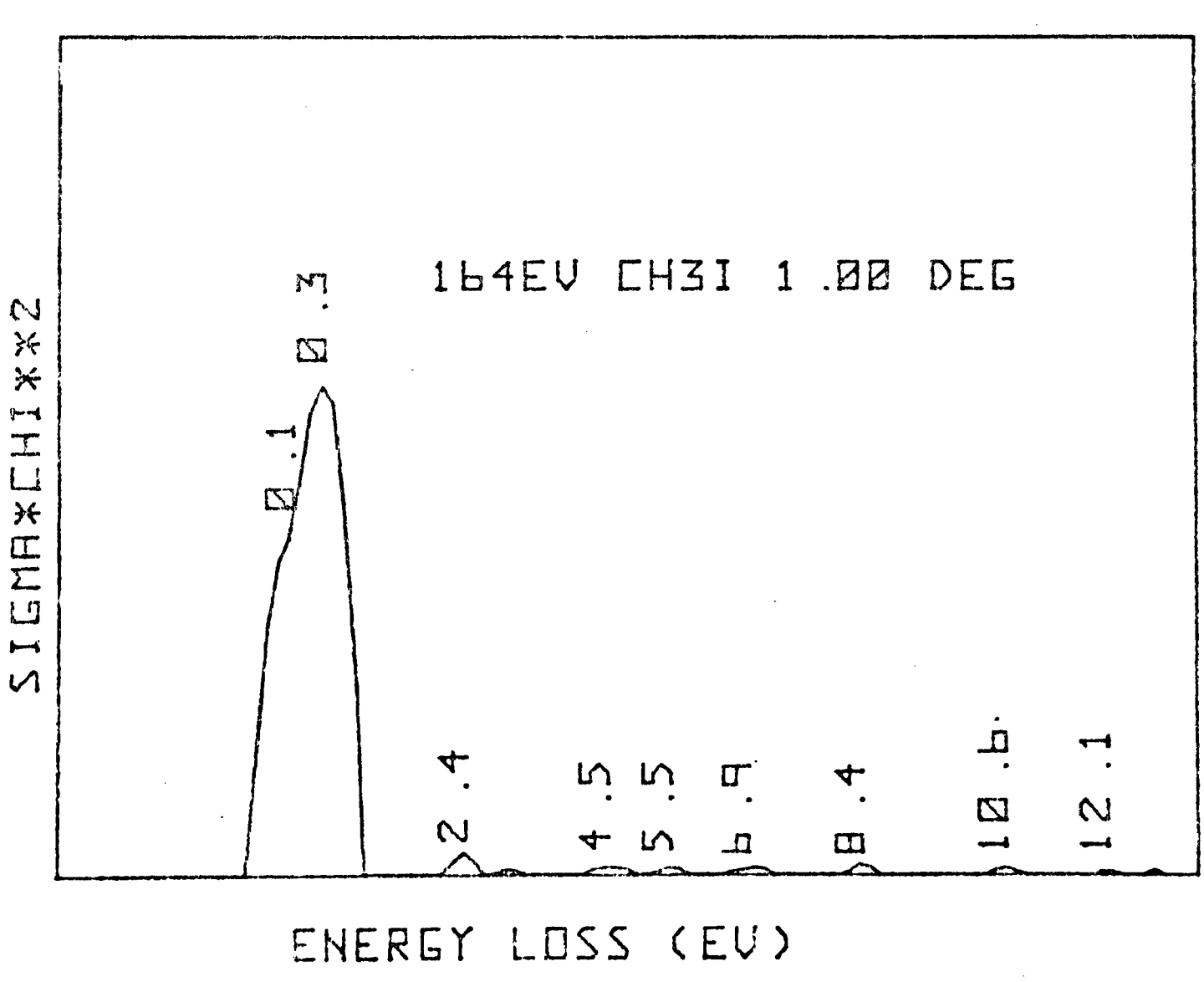

Figure 4.15

Figure 4.16

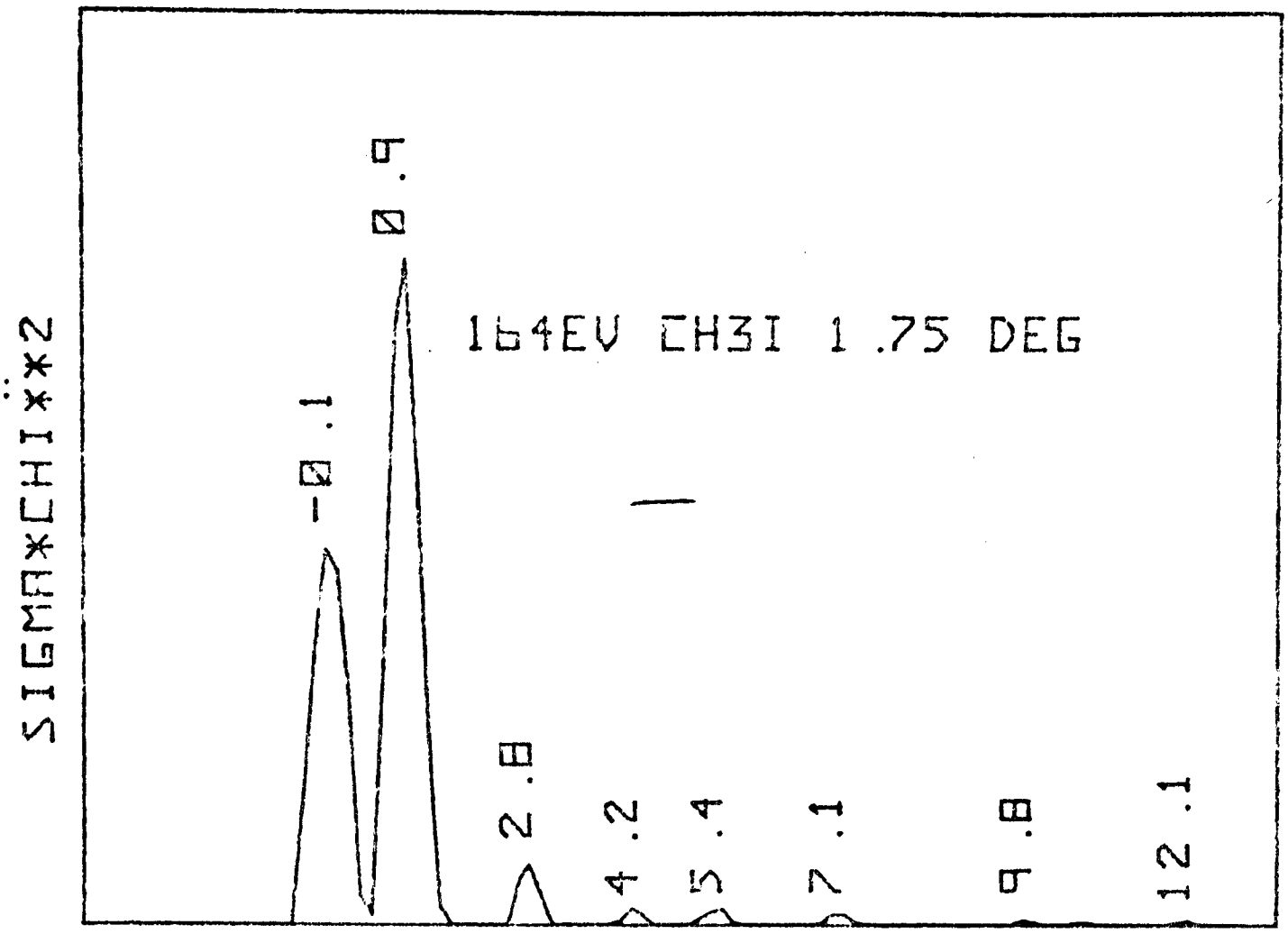

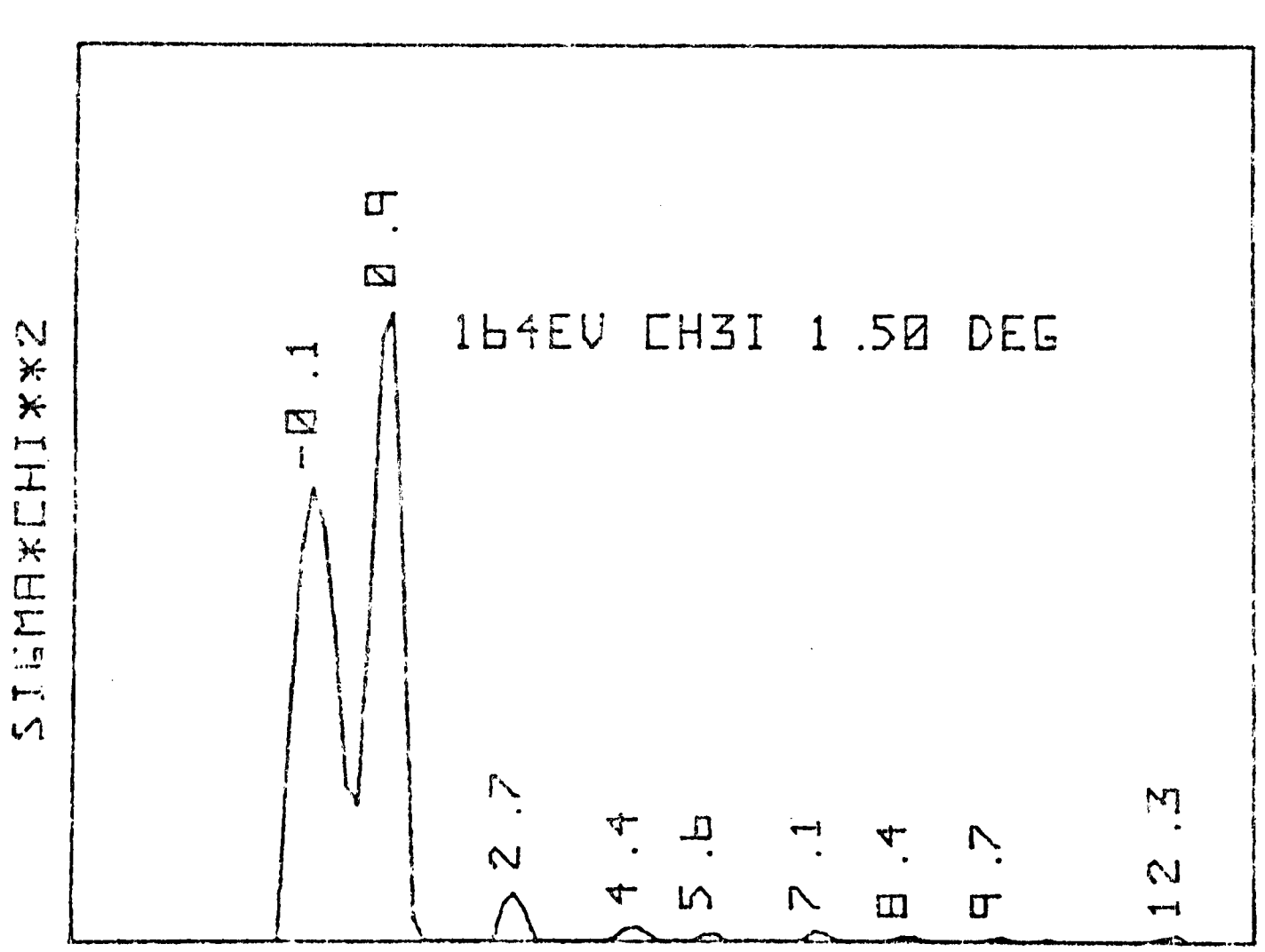

Figure 4.17

Figure 4.18

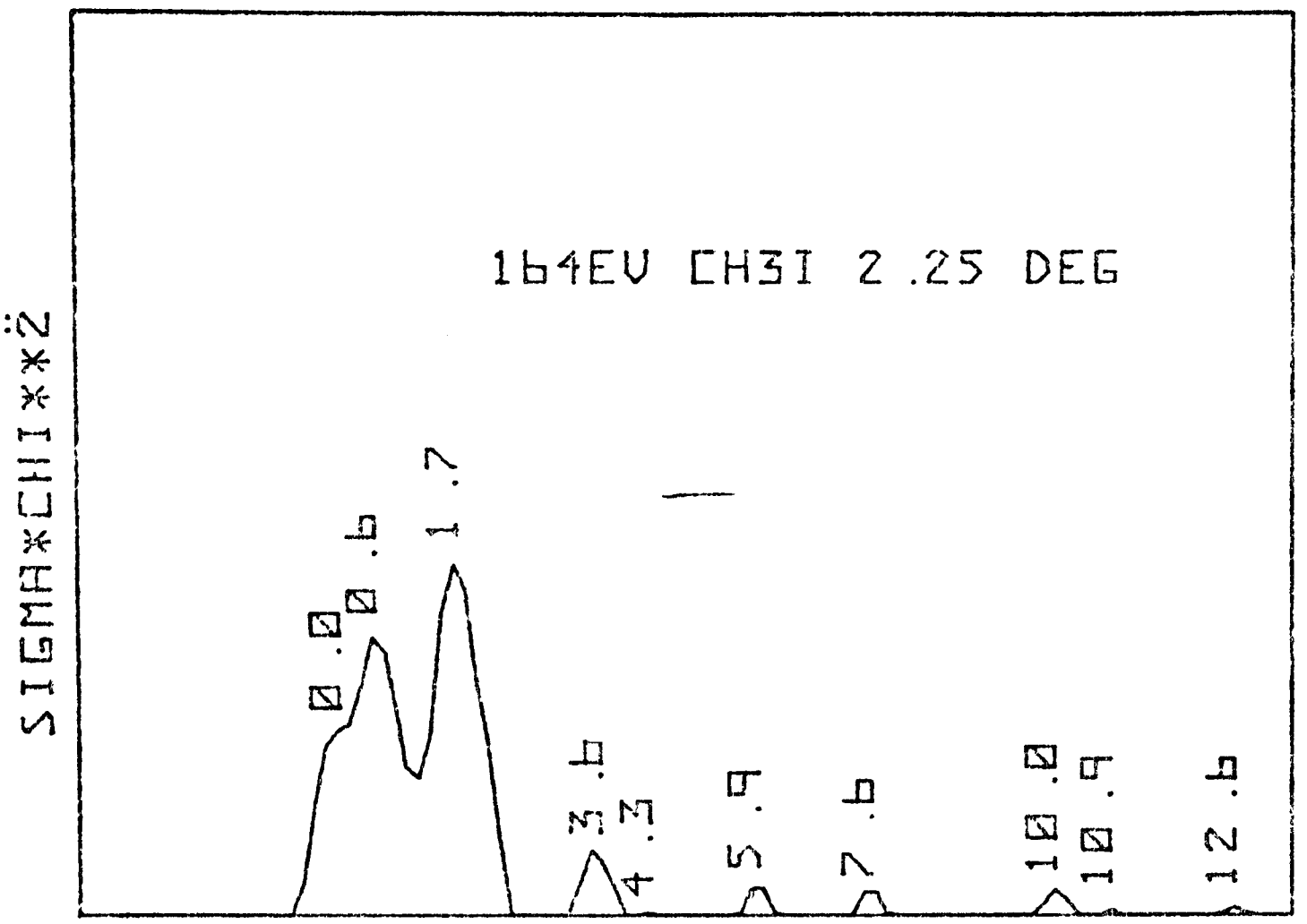

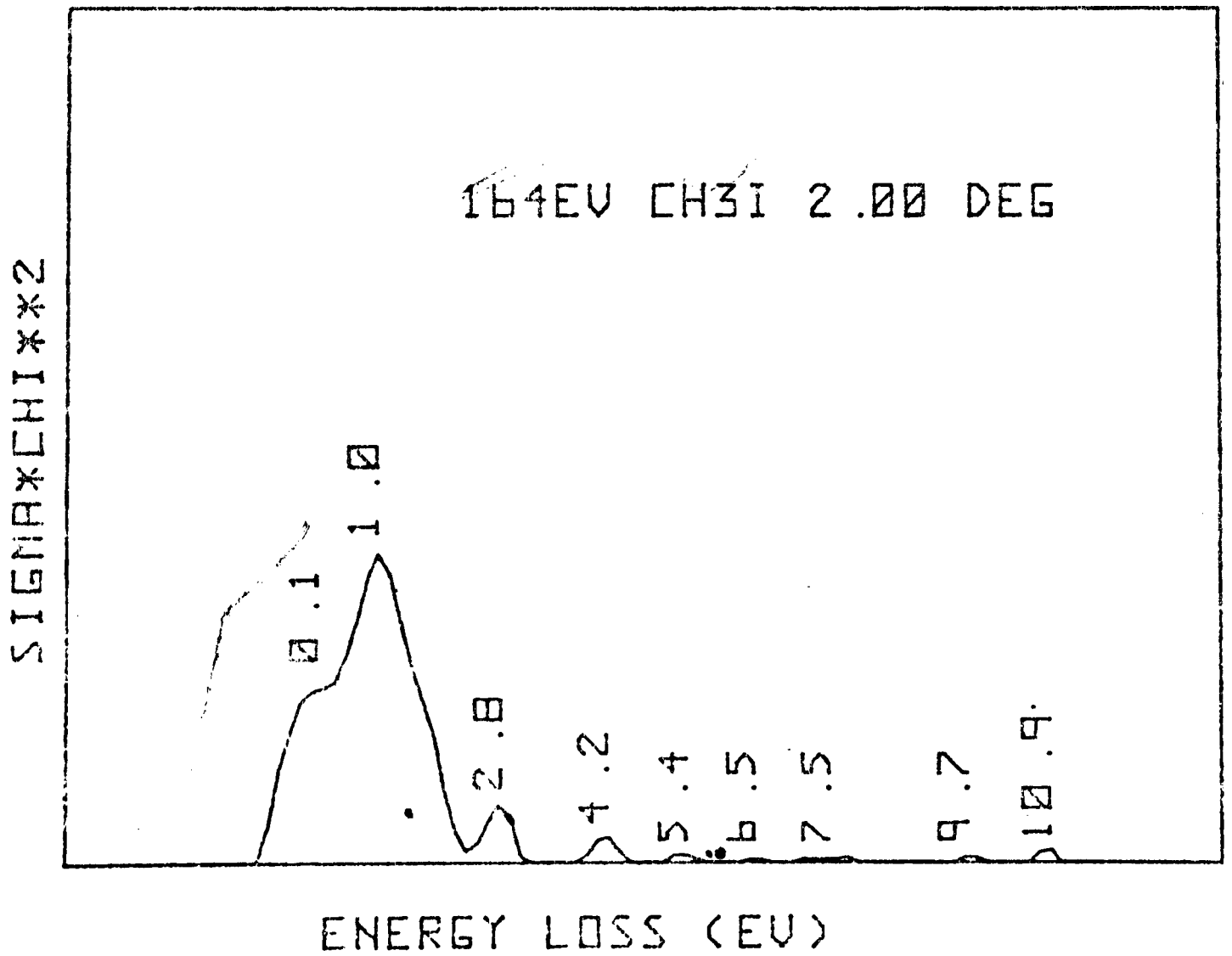

Figure 4.19

Figure 4.20

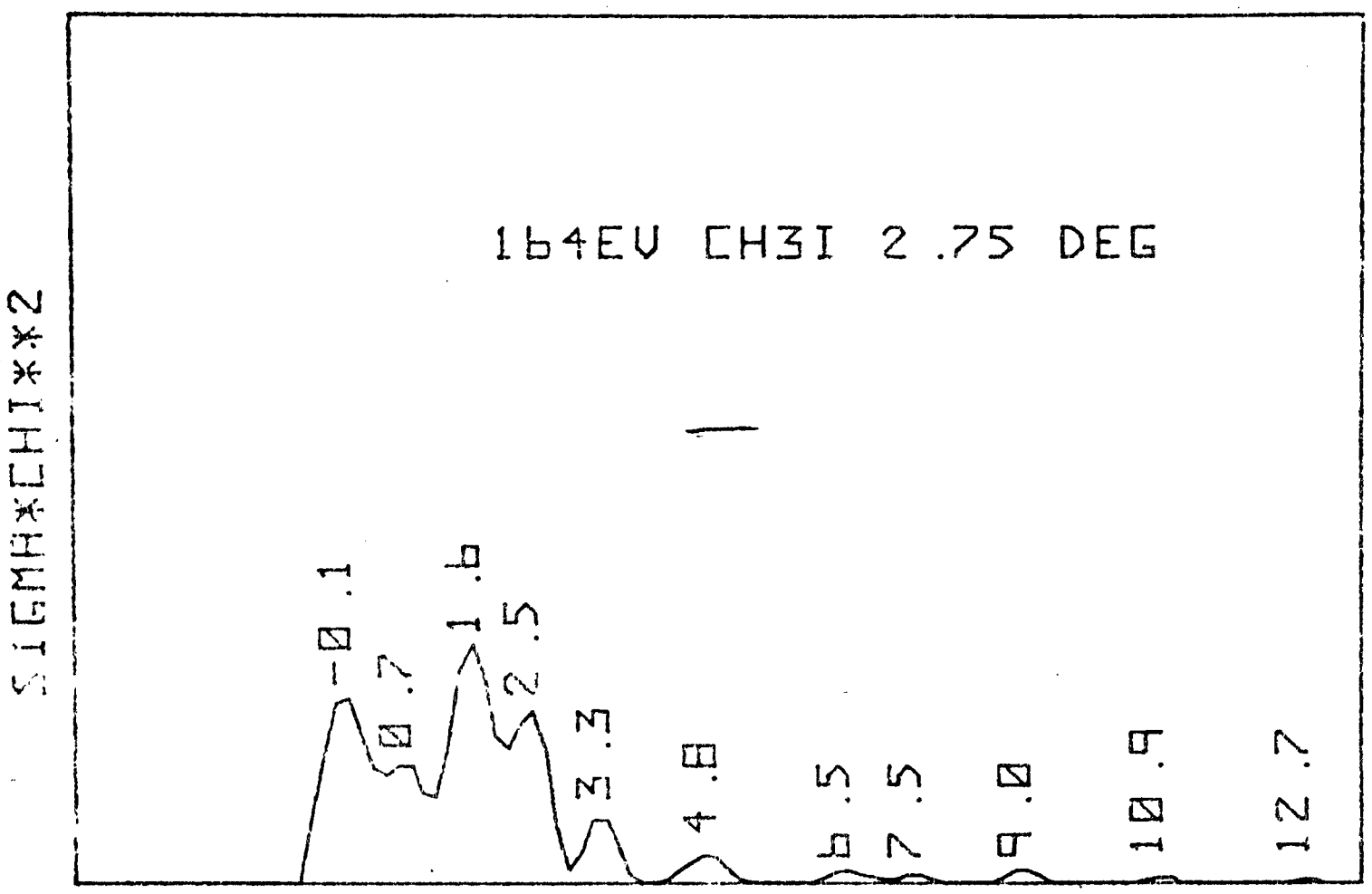

Figure 4.21

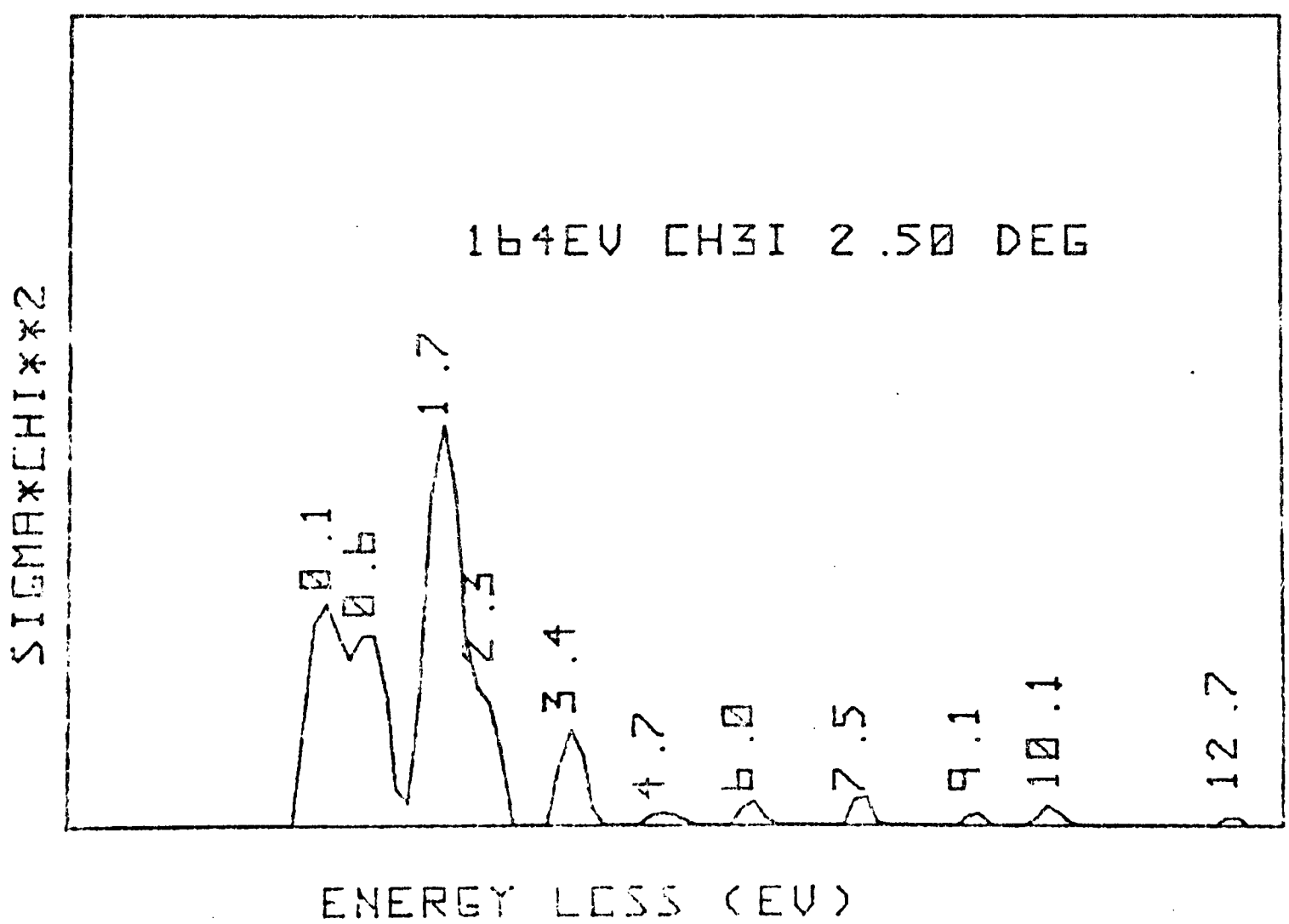

Figure 4.22

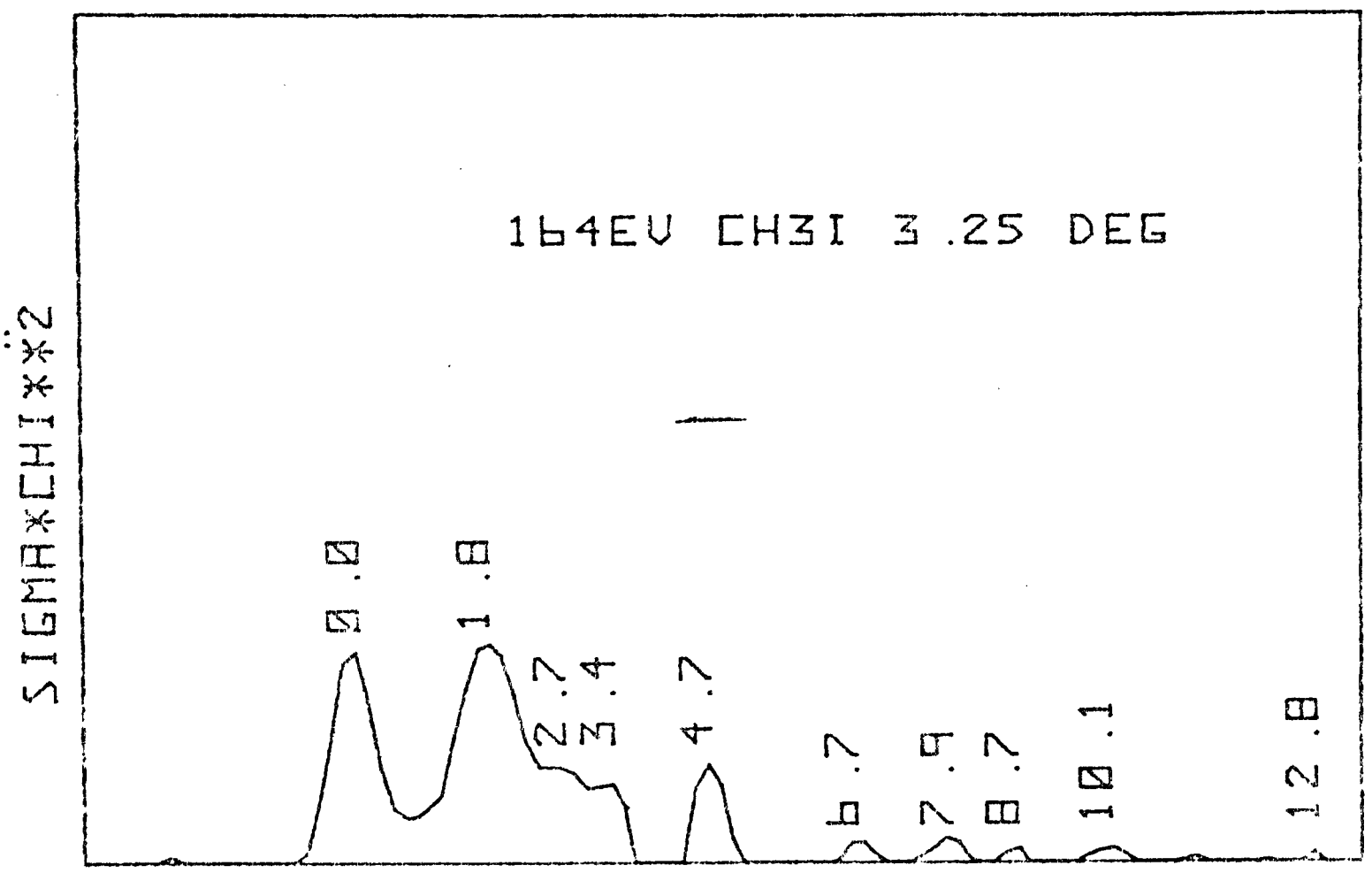

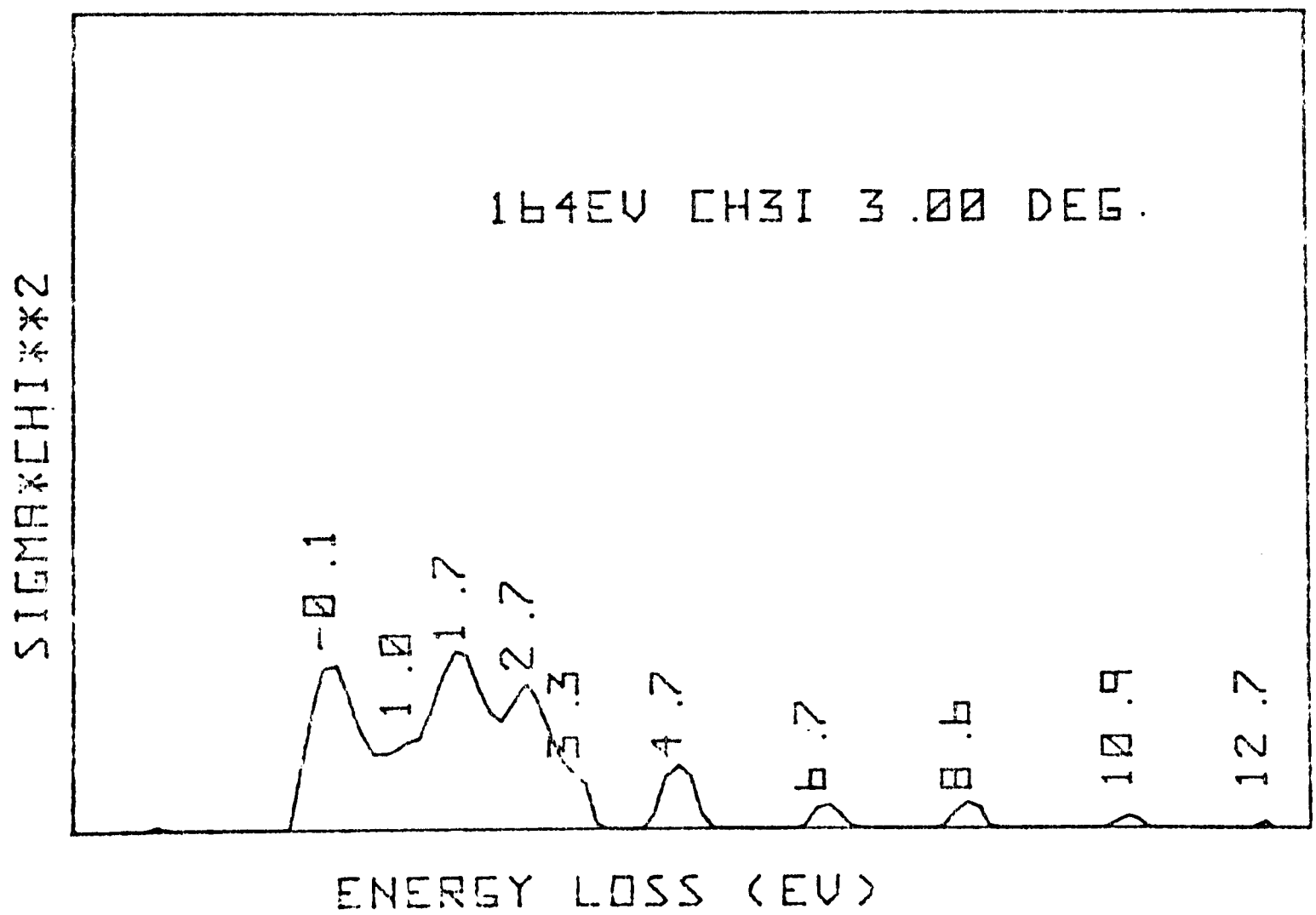

Figure 4.23

Figure 4.24

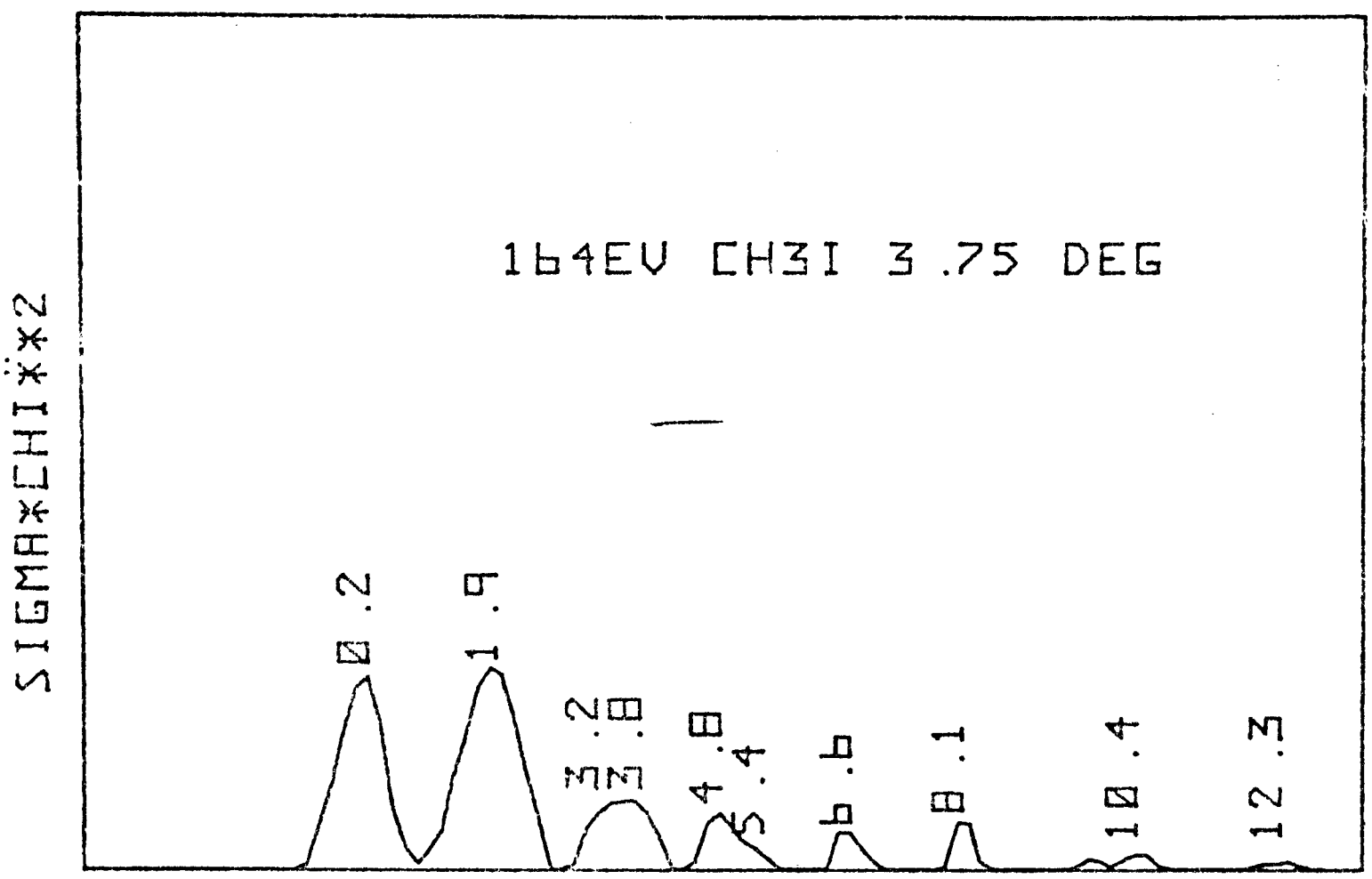

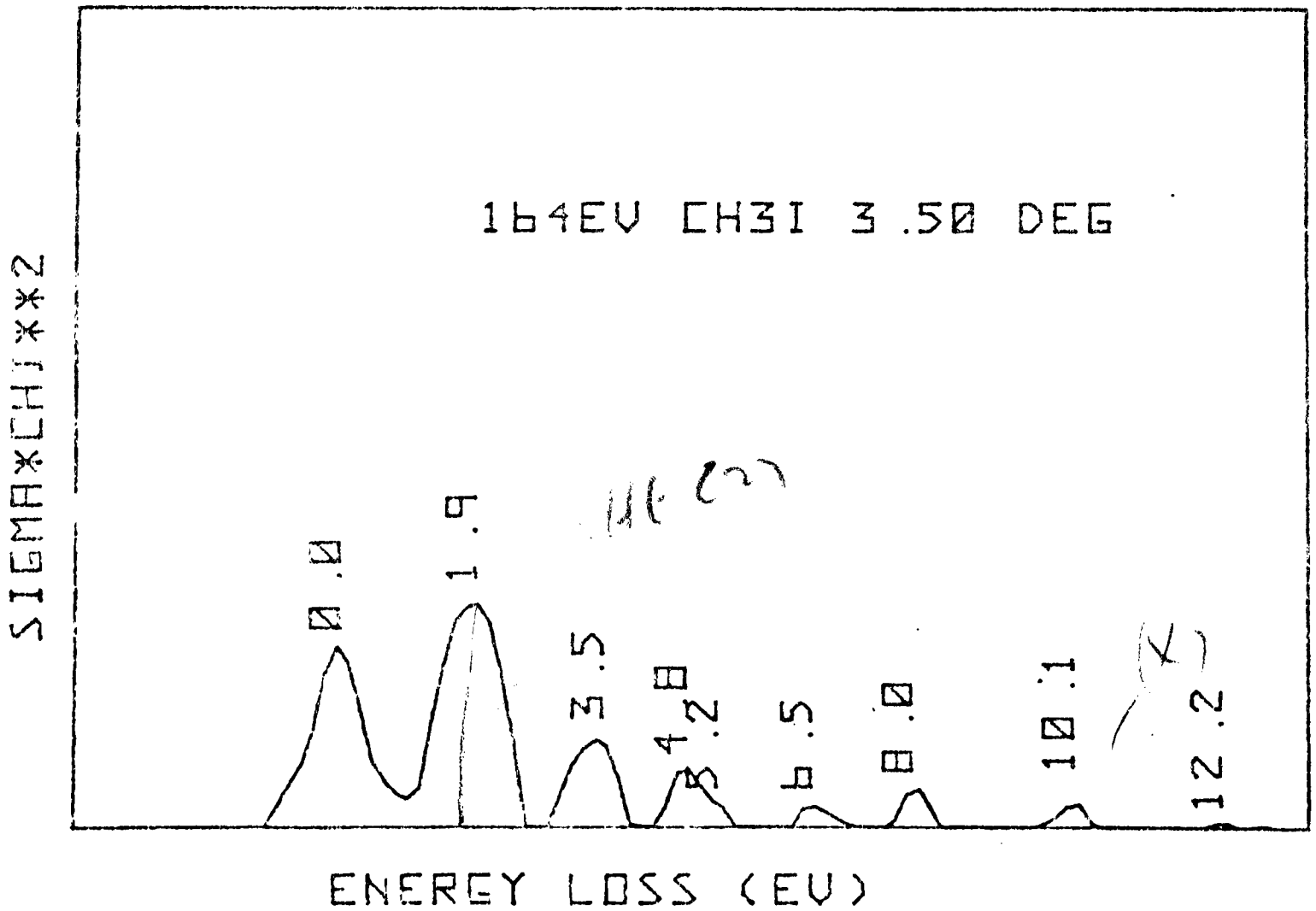

Figure 4.25

Figure 4.26

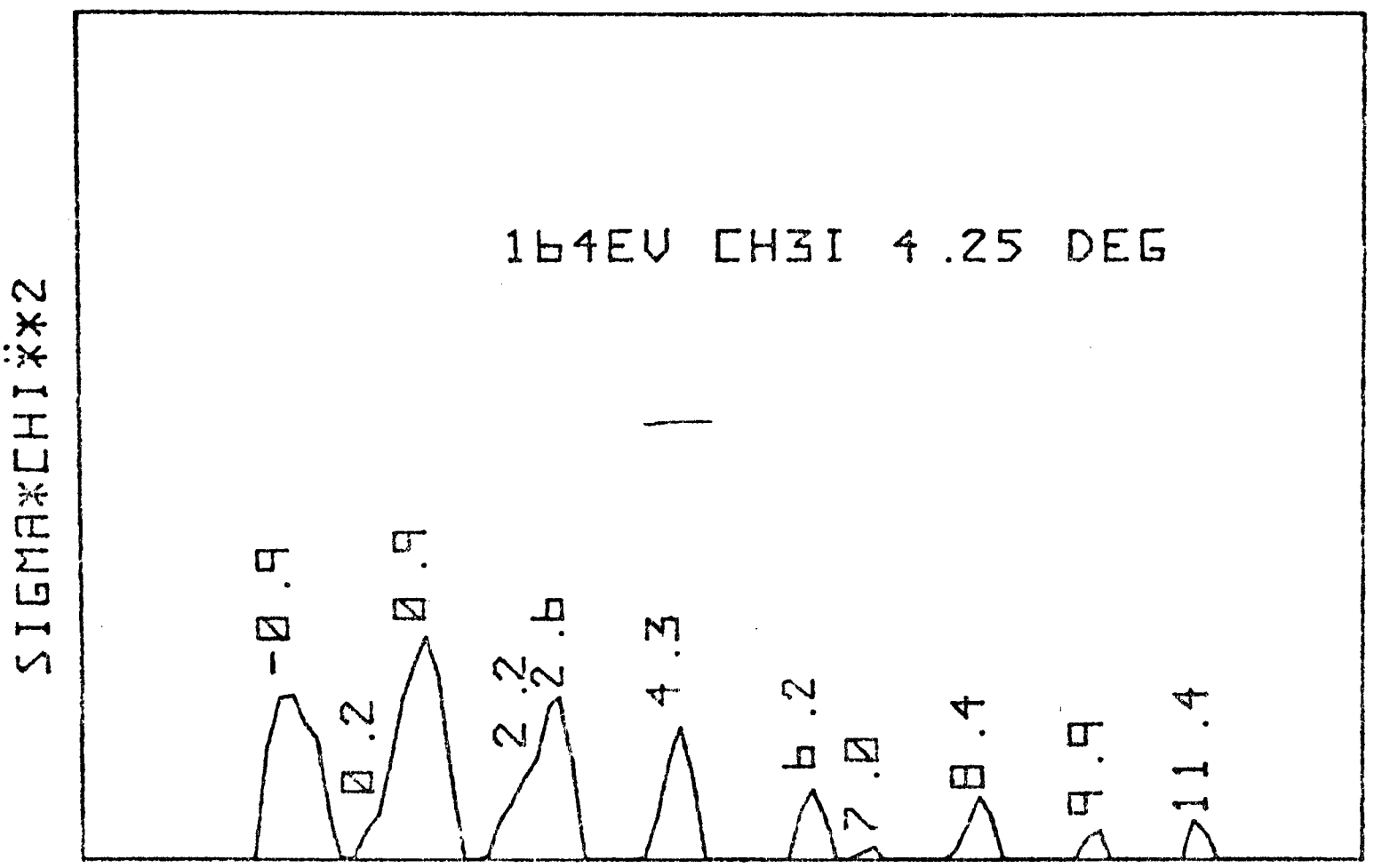

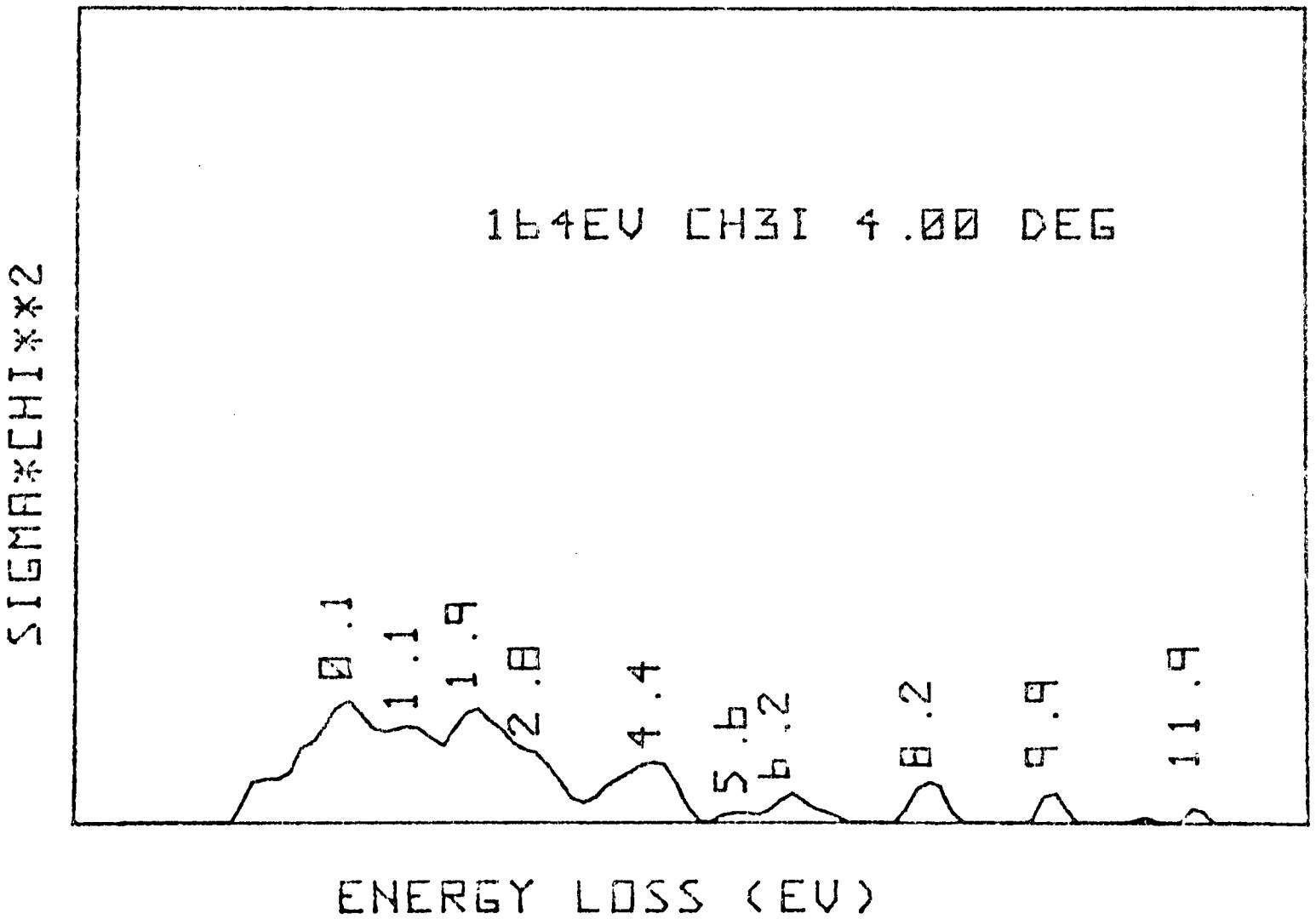

Figure 4.27

Figure 4.28

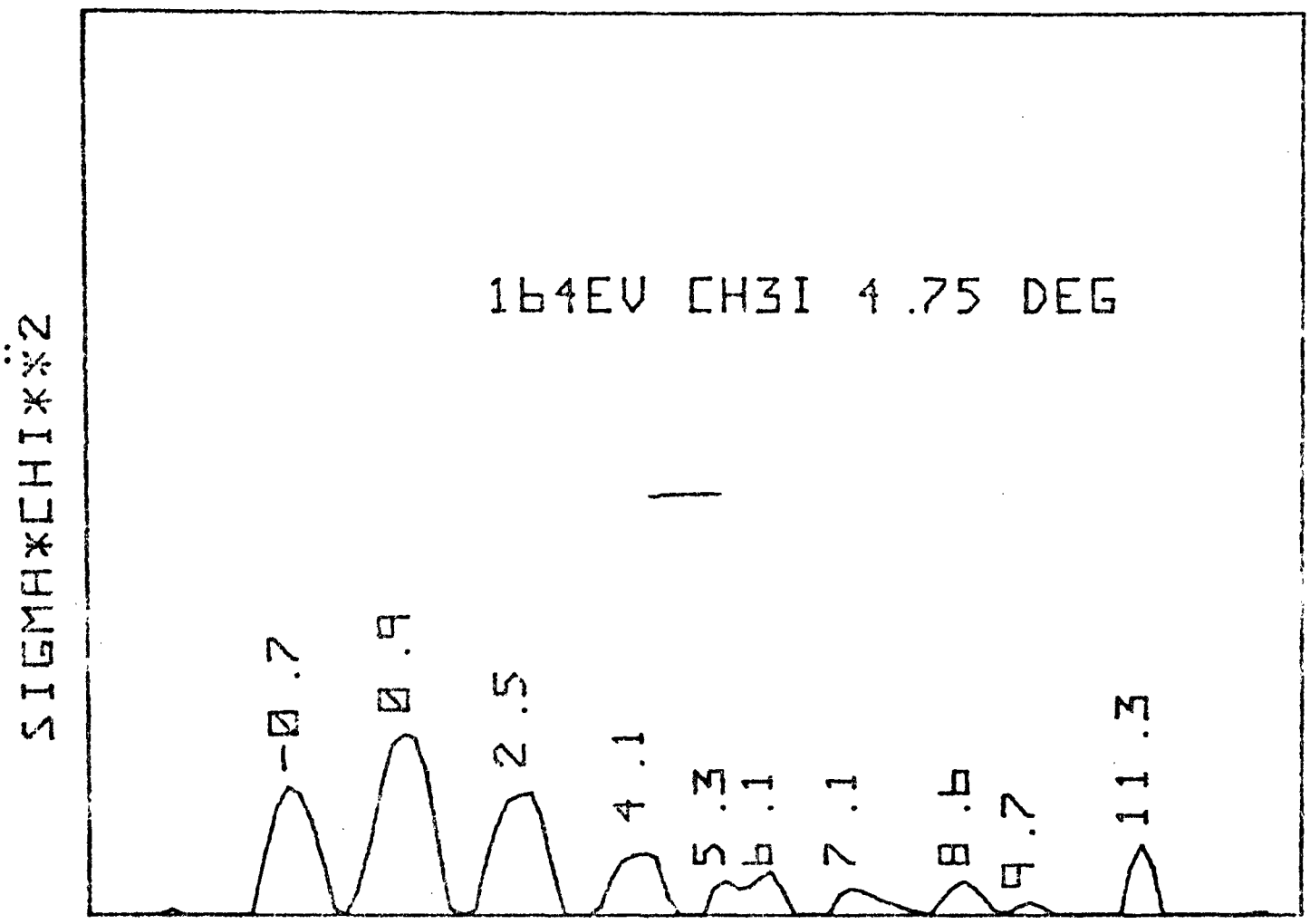

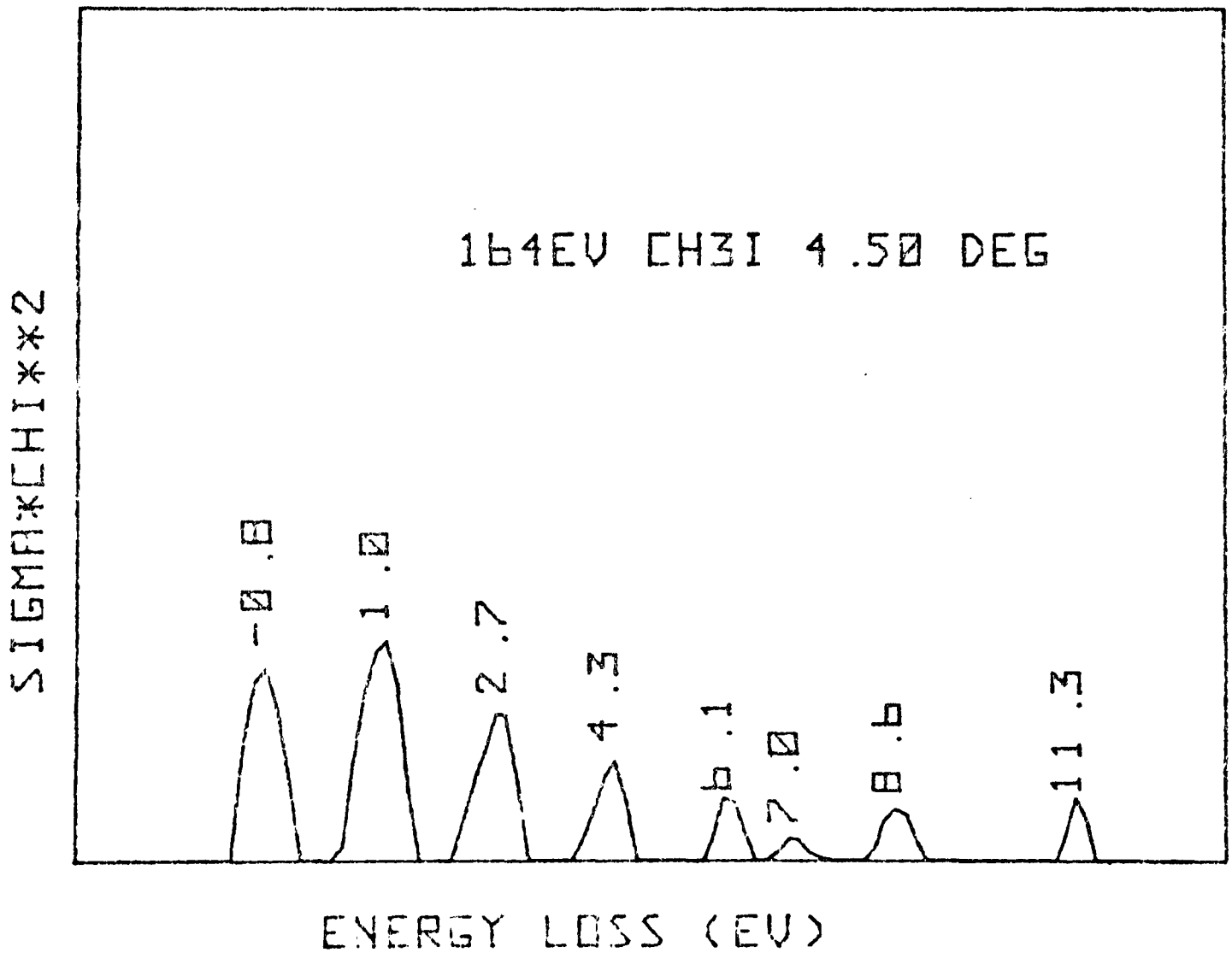

Figure 4.29

Figure 4.30

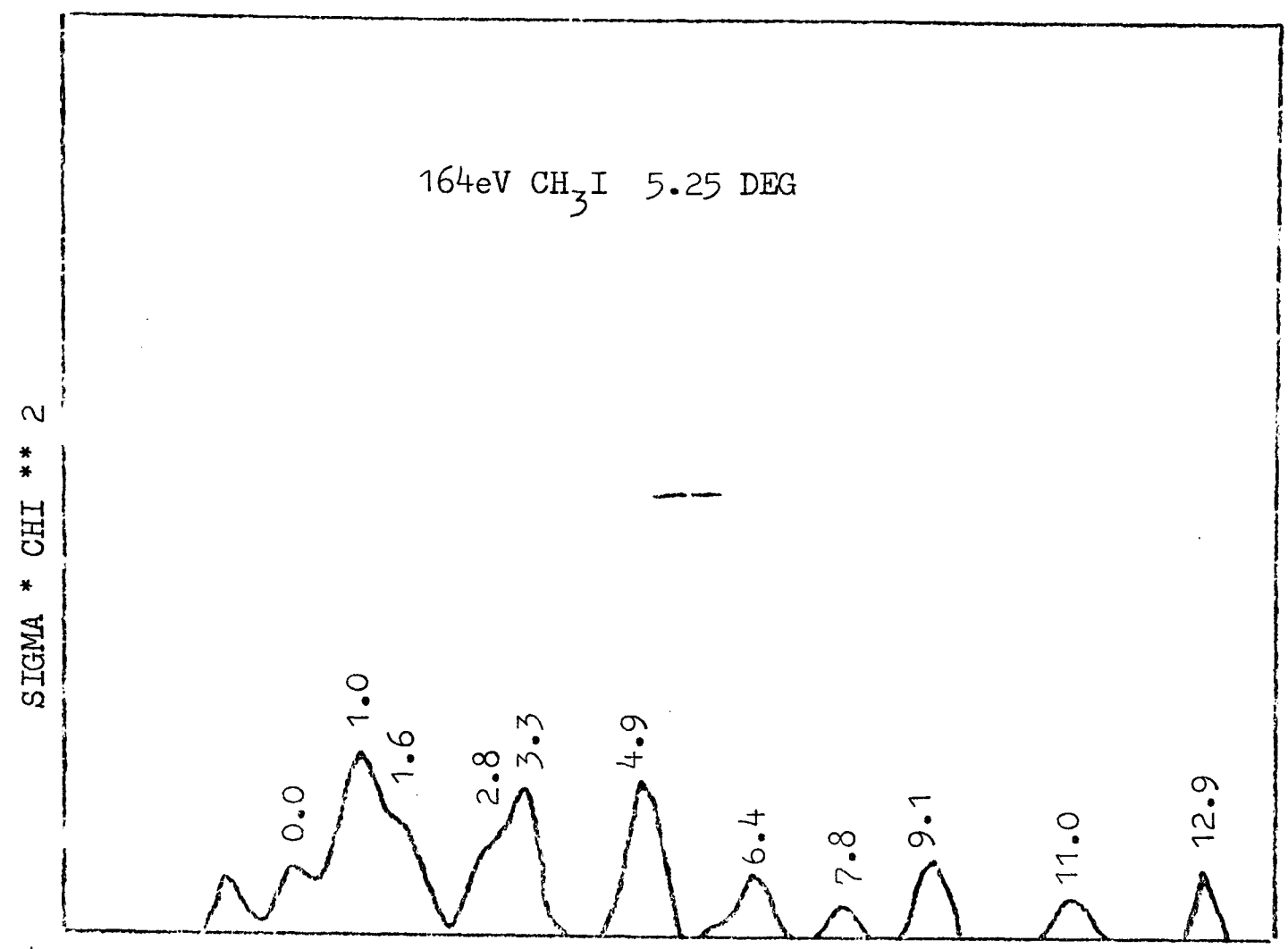

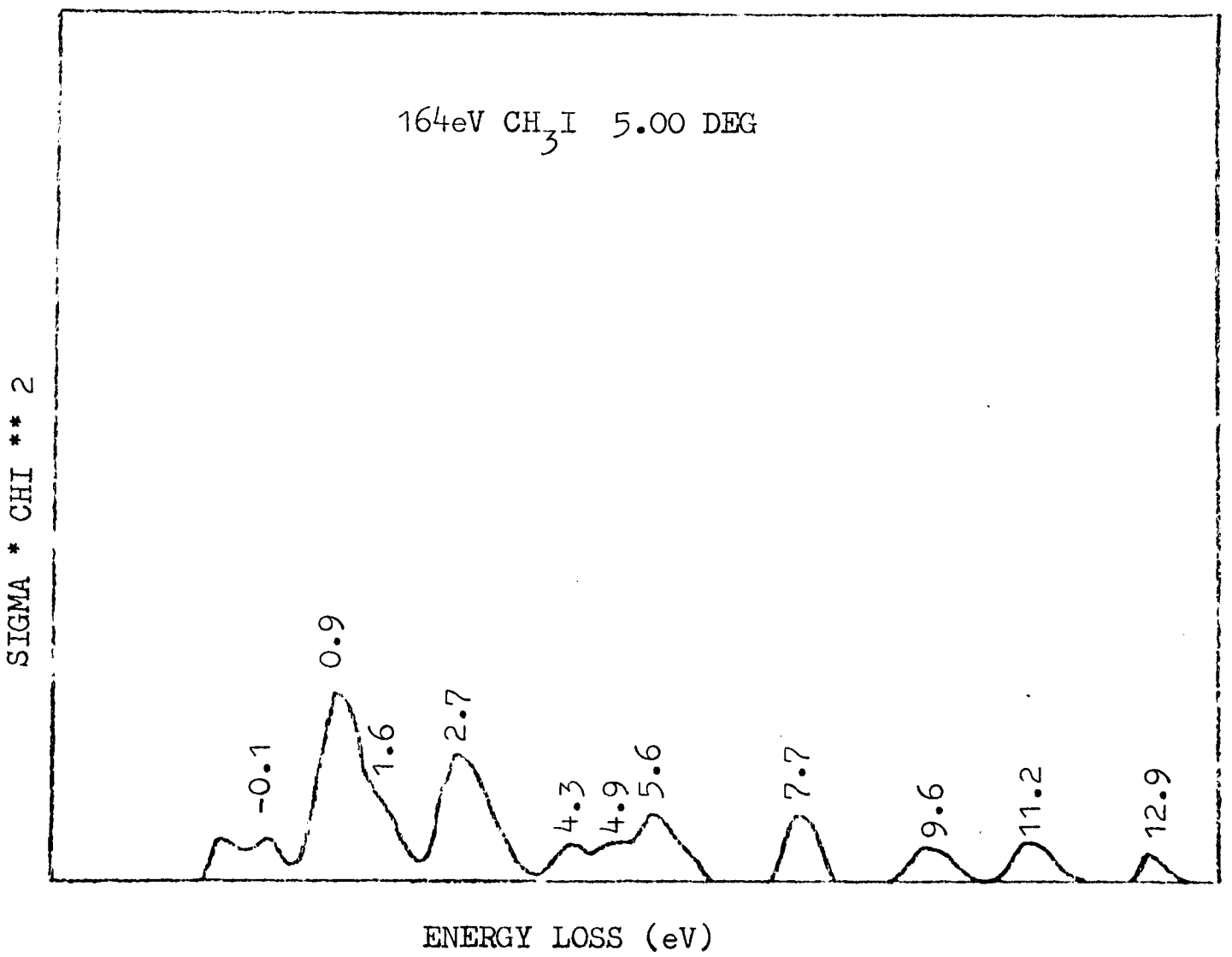

Figure 4.31

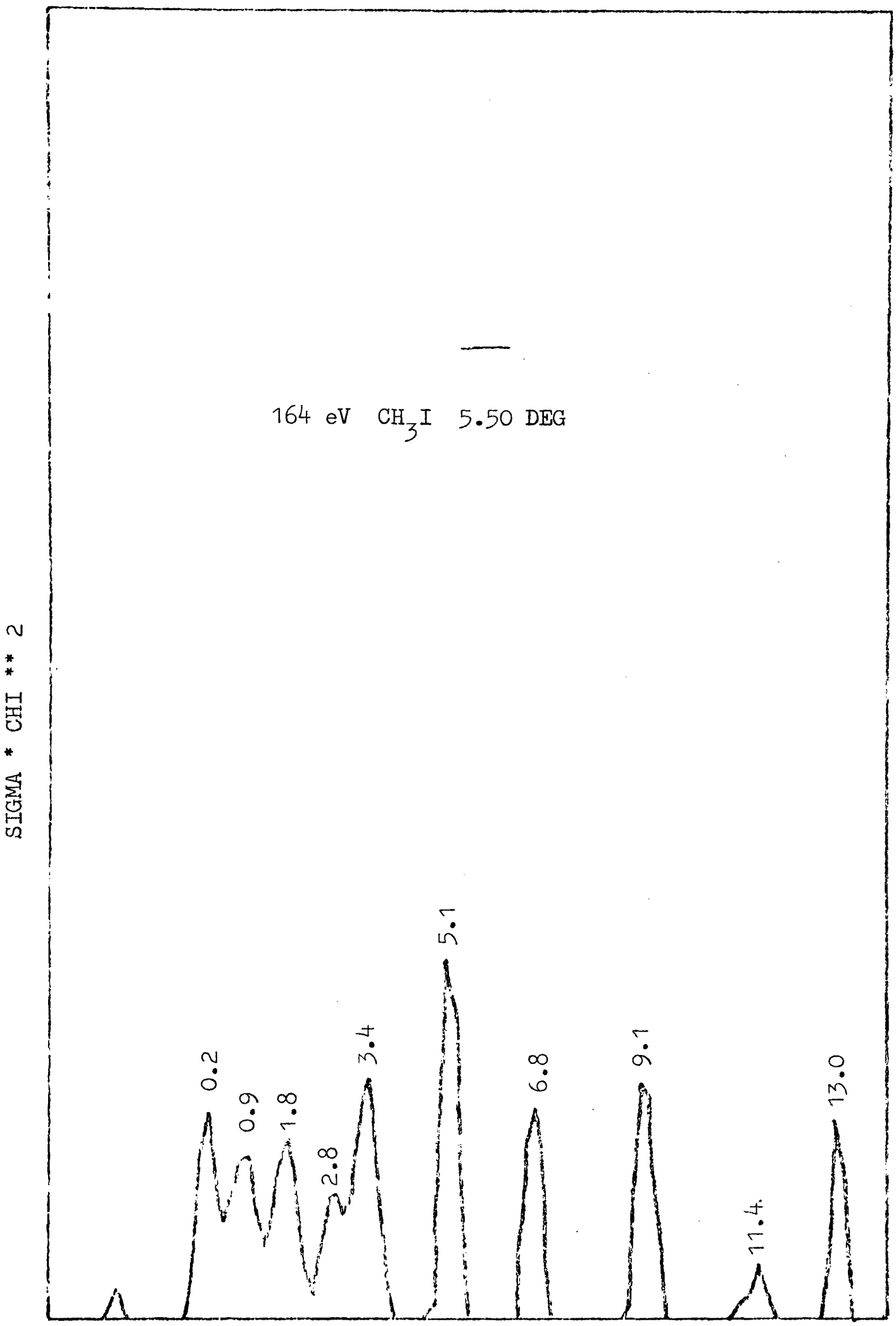
164 eV CH3I 5.50 DEG
SIGMA * CHI ** 2
0.2
0.9
1.8
2.8
3.4
5.1
6.8
9.1
11.4
13.0
ENERGY LOSS (eV)

Figure 4.32

TABLE 4.3 : 164 eV (C.M.) K/CH_3I COLLISIONS

	Energy Loss											
Angle	1	2	3	4	5	6	7	8	9	10	11	12
0.59	0.2			2.9		5.0				8.4		11.8
0.75	0.2			2.9		4.9			6.7	8.4	10.4	11.9/12.8
1.00	0.1	0.3		2.4		4.5	5.5		6.9	8.4	10.6	12.1
1.25	0.0	0.8		2.6		4.6	5.6		6.9	8.4	10.7	
1.50	-0.1	0.9		2.7		4.4	5.6		7.1	8.4	9.7	12.3
1.75	-0.1	0.9		2.8		4.2	5.4		7.1		9.8	12.1
2.00	0.1	1.0		2.8		4.2	5.4	6.5	7.5		9.7/10.9	
2.25	0.0	0.6	1.6		3.6	4.3		5.9	7.5		10.0/10.9	12.6
2.50	0.1	0.6	1.7	2.3	3.4	4.7		6.0	7.5		10.1	12.7
2.75	-0.1	0.7	1.6	2.5	3.3	4.8		6.5	7.5		10.9	12.7
3.00	-0.1	1.0	1.7	2.7	3.3	4.7		6.7		8.6	10.9	12.7
3.25	0.0		1.8	2.7	3.4	4.7		6.7	7.9	8.7	10.1	12.8
3.50	0.0		1.9		3.5	4.8	5.2	6.5	8.0		10.1	12.2
3.75	0.2		1.9	3.2	3.8	4.8	5.4	6.6	8.1		10.4	12.3
4.00	0.1	1.1	1.9	2.8		4.4	5.6	6.2	8.2		9.9	11.9
4.25	0.2	0.9	2.2	2.6		4.3		6.2	8.4		9.9	11.4
4.50	-0.8	1.0		2.7		4.3	5.3	6.1	8.6		9.7	11.3
4.75	-0.7	0.9		2.5		4.1	5.3	6.1	8.6			11.3
5.00	-0.1	0.9	1.6	2.7		4.3	5.0	5.7	9.6	7.8		13.0
5.25	0.0	1.0	1.6	2.8	3.3		5.0	6.5	9.1	7.9		13.0
5.50	0.2	0.9	1.8	2.8	3.4		5.1	6.8	9.2			12.9

However the essential features of the data are apparent. There are a large number of discrete processes taking place, the scattered potassium atoms exhibiting energy losses in the range 0 - 13 eV. Allowing for the already mentioned jitter in the location of the maxima in the arrival spectra the majority of the processes are observed to occur with an energy loss which does not vary with scattering angle. Surprisingly large energy losses of up to 12 eV are detected at the narrowest angles of observation, indicating the involvement of strongly attractive potentials in coupling the ground state to these highly excited states. It should be noted that there are differences between the data at the two different collision energies. This suggests the involvement of a potential surface on which the equilibrium geometry of the target molecule is not identical with that of the ground state and that some molecular geometrical re-arrangement takes place during the course of the collision. On exit from the collision the target molecule may be vibrationally excited. The extent of the excitation will depend on the time spent on the intermediate surface and hence on the collision energy.

In addition to the time of flight profiles, figures 4.33 to 4.38 show the differential cross sections obtained for the various exit channels. At this point in the analysis it is not possible to assign absolute values to the intensities though all the cross sections are drawn to the same scale.

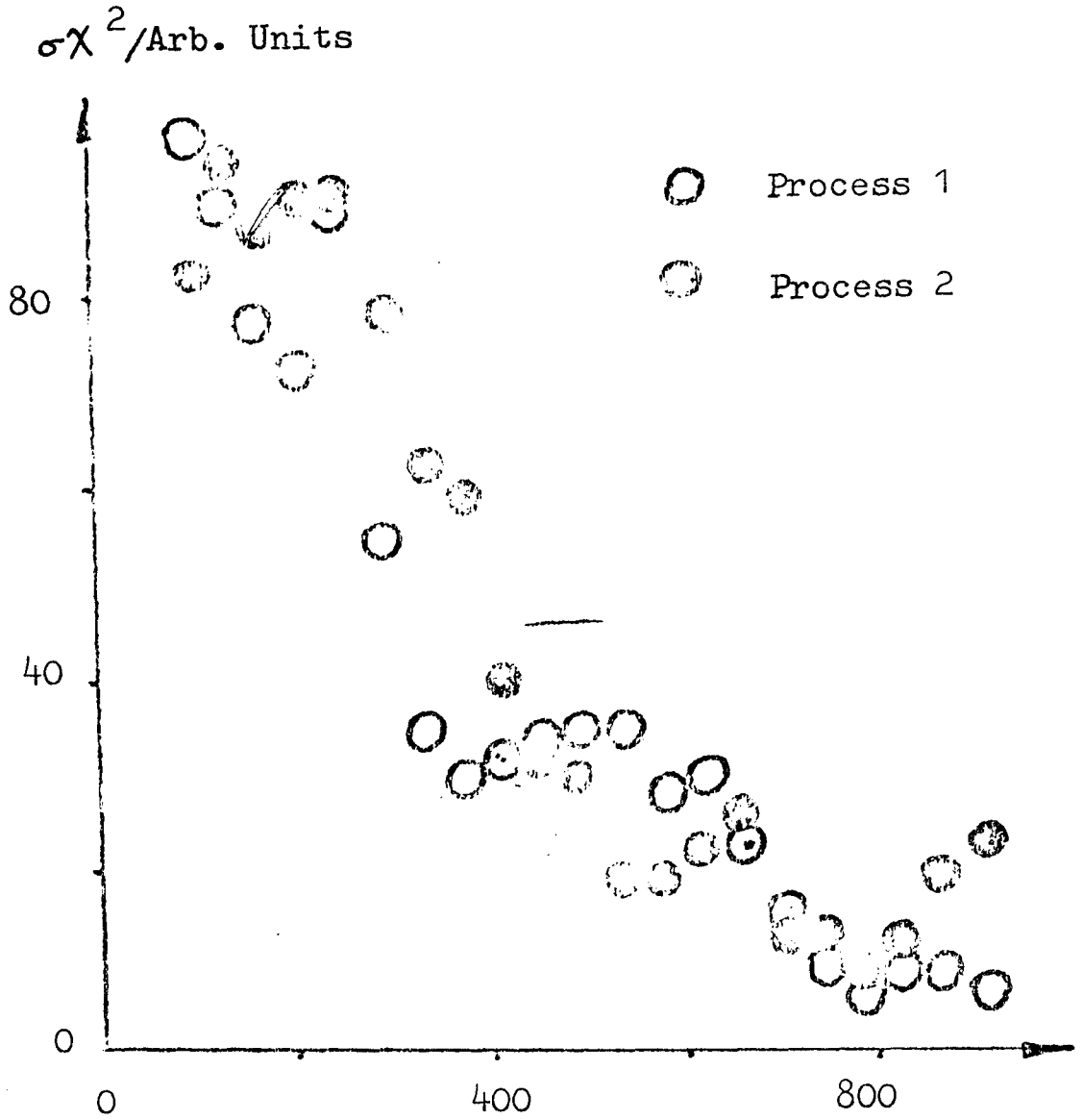

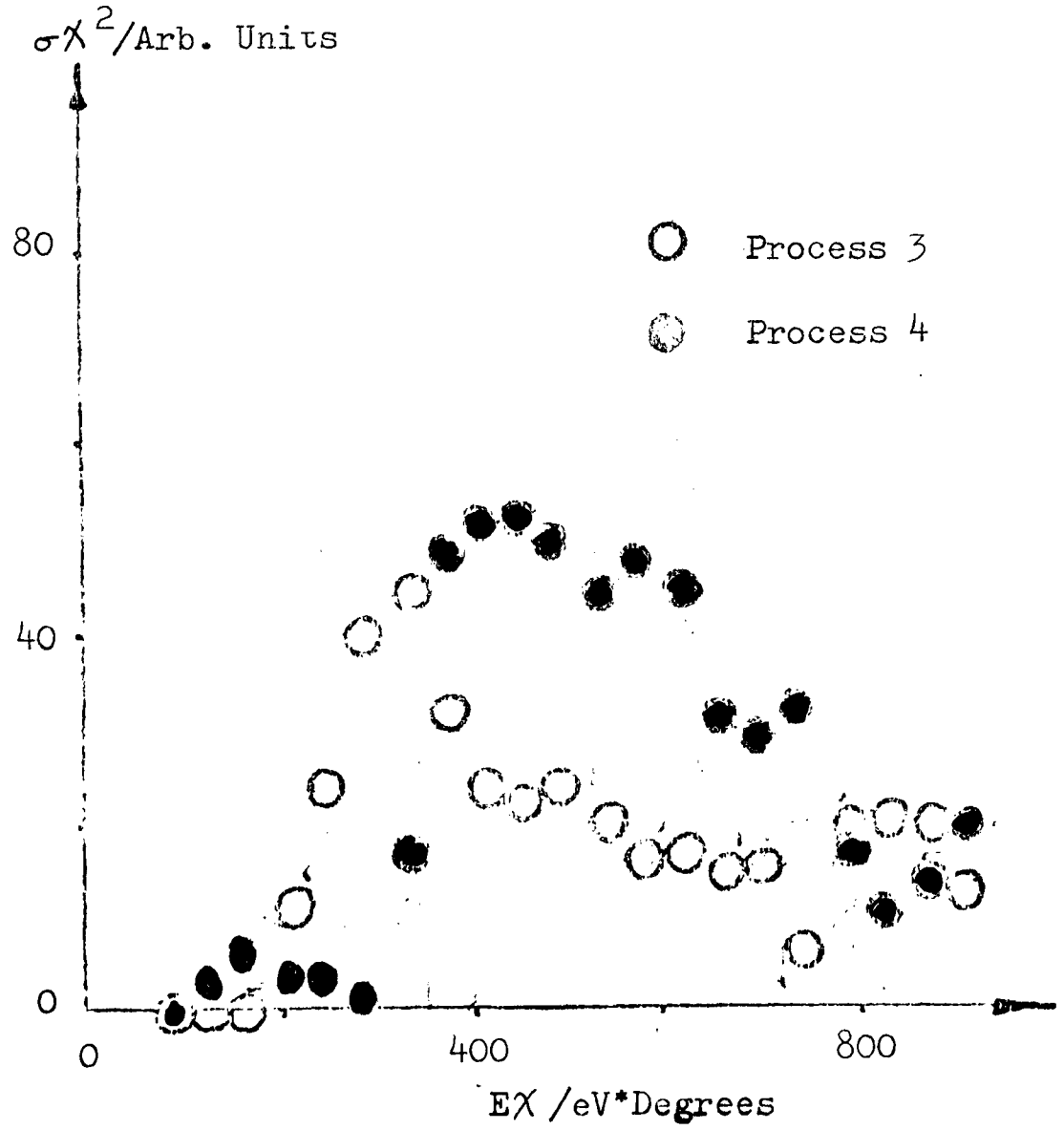

Figure 4.33 : K/CH_3I Differential Cross Sections 164eV C.M.

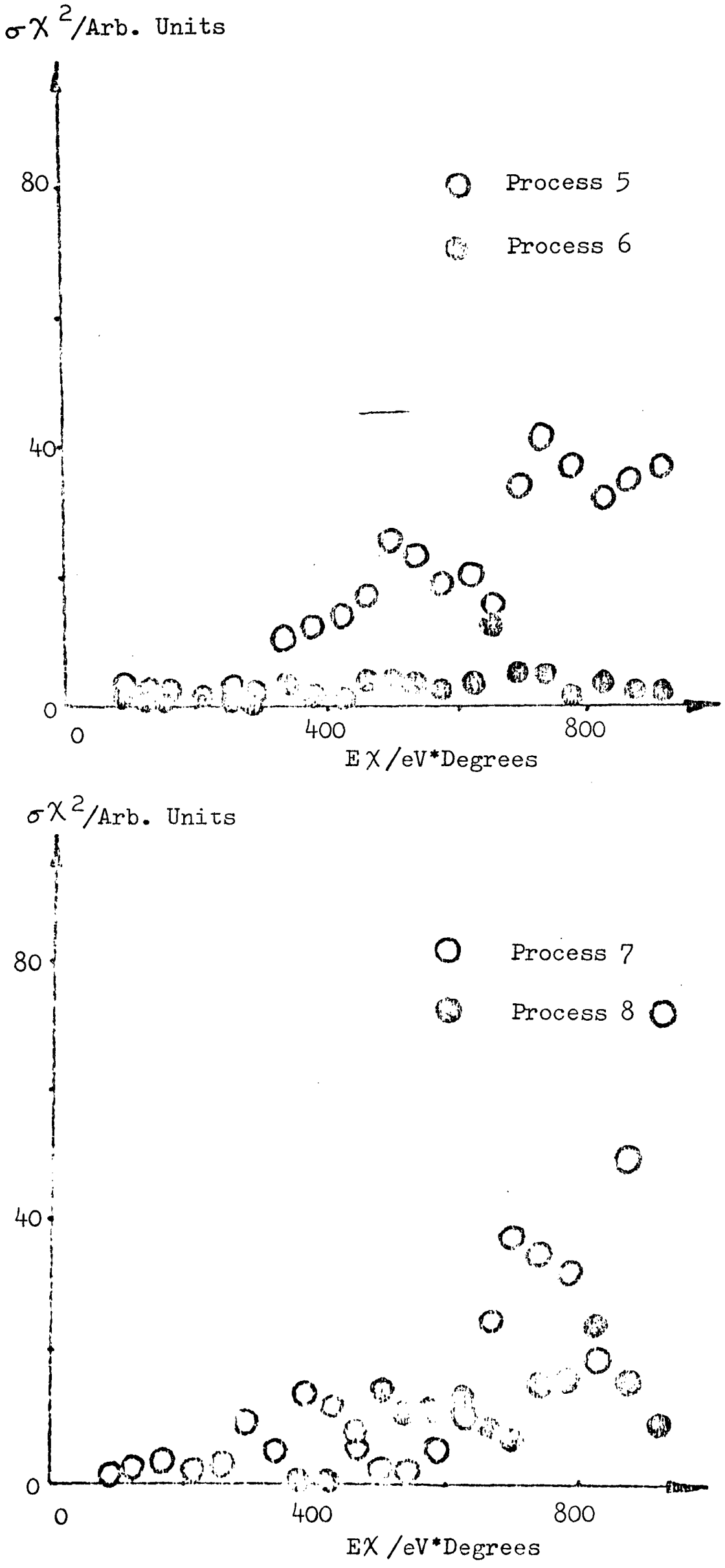

Figure 4.34 : K/CH_3I Differential Cross Sections 164eV C.M.

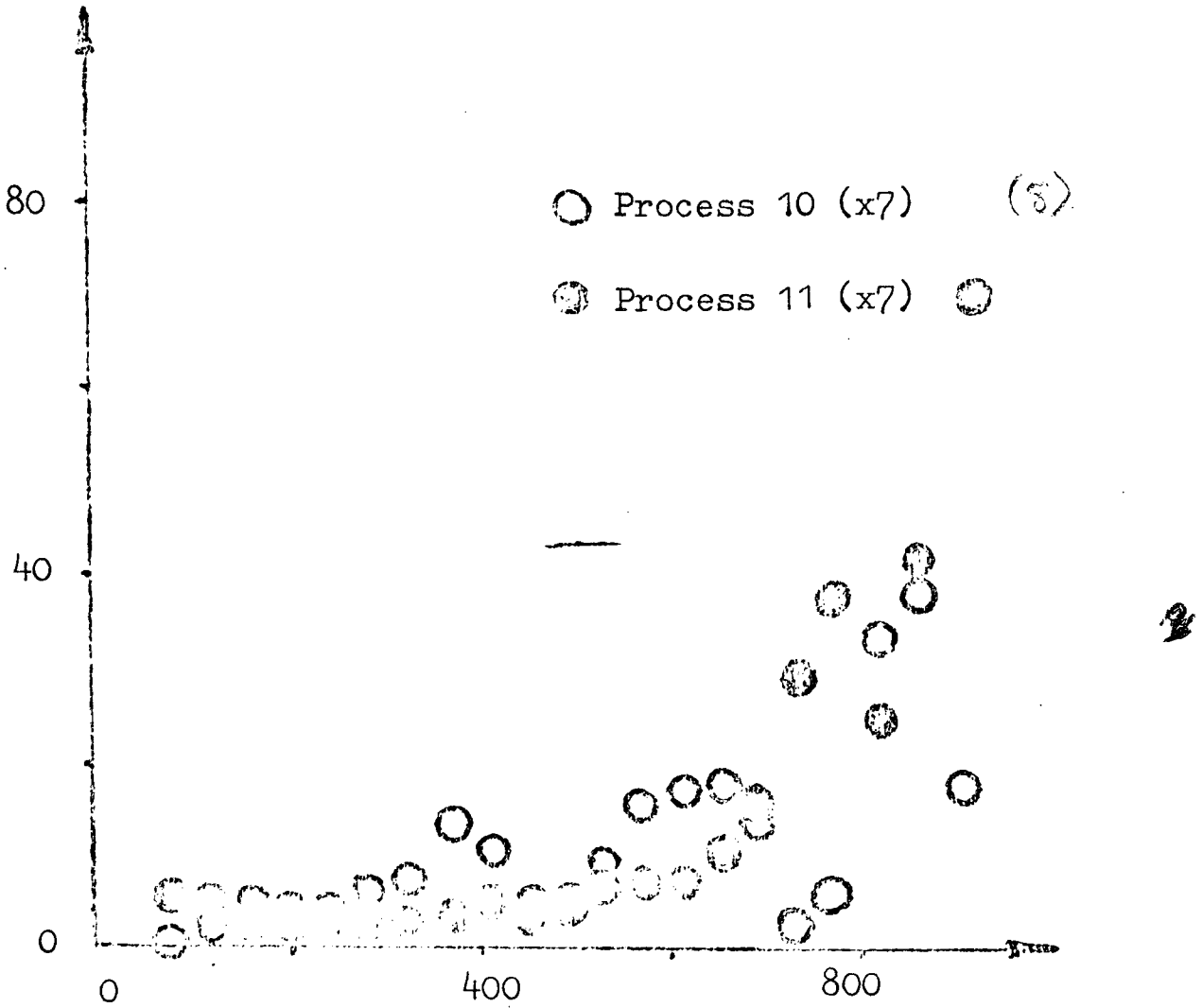

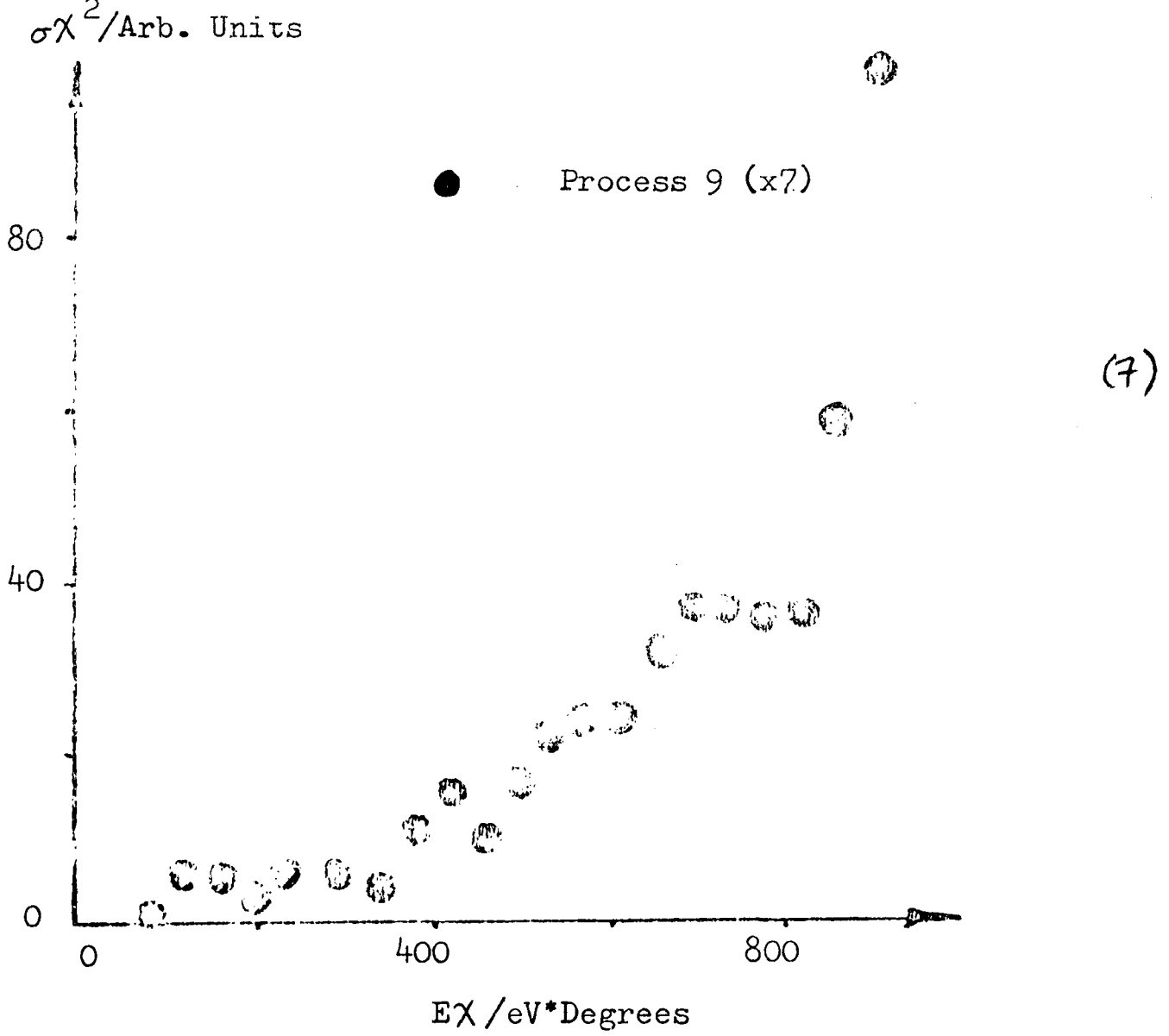

Figure 4.35 : K/CH_3I Differential Cross Sections 164eV C.M.

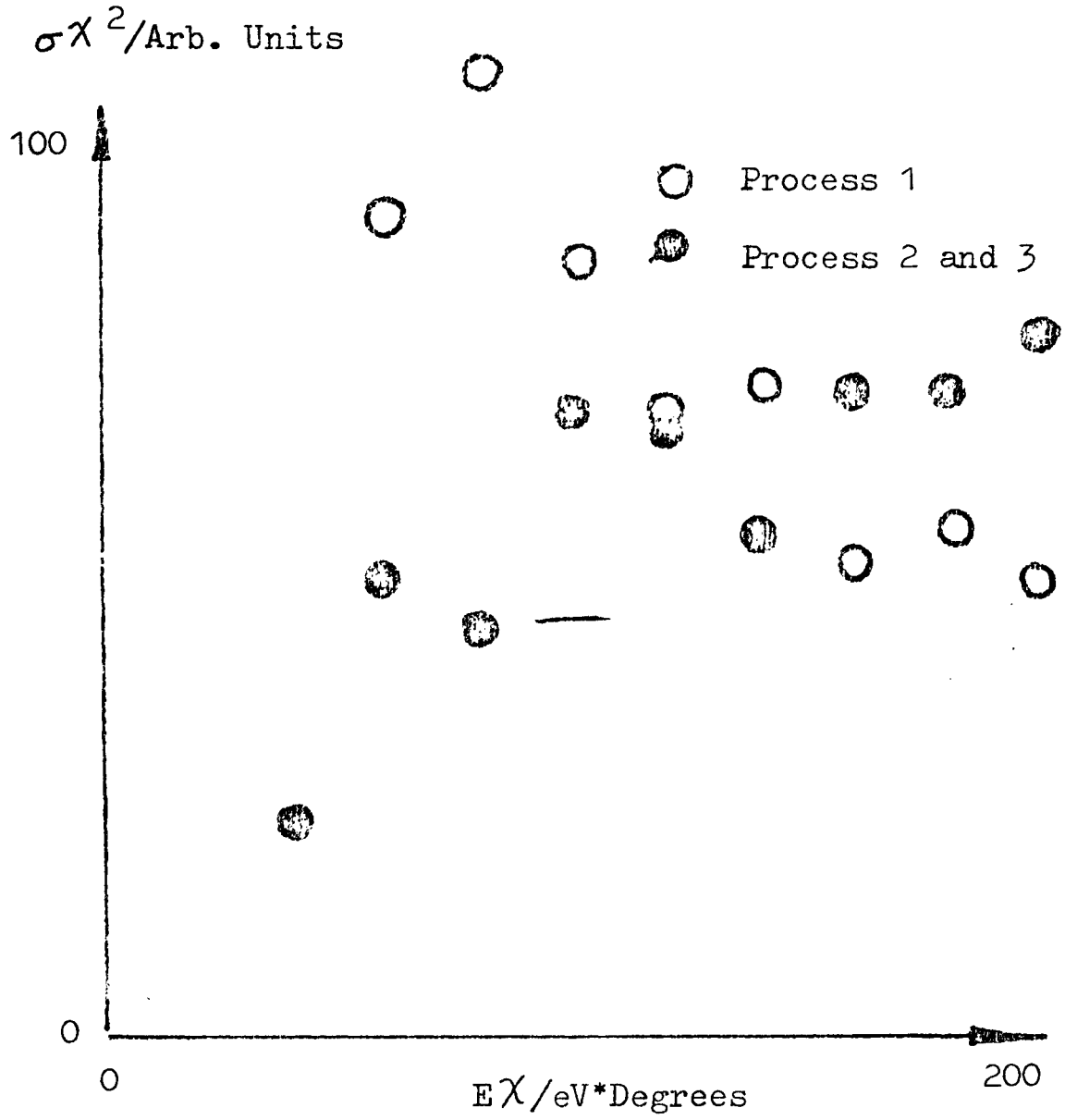

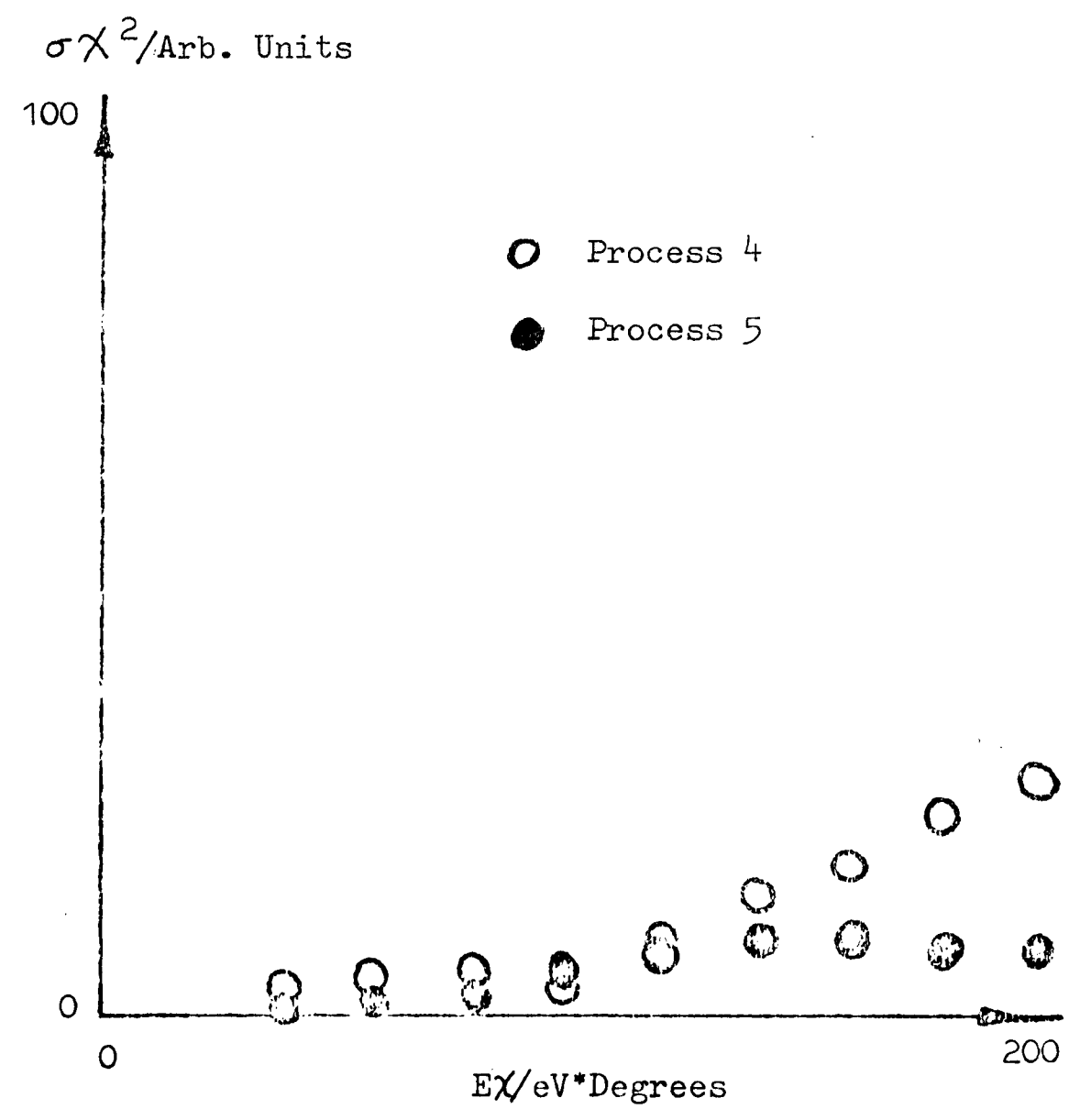

Figure 4.36 K/CH_3I Differential Cross Sections 81eV C.M.

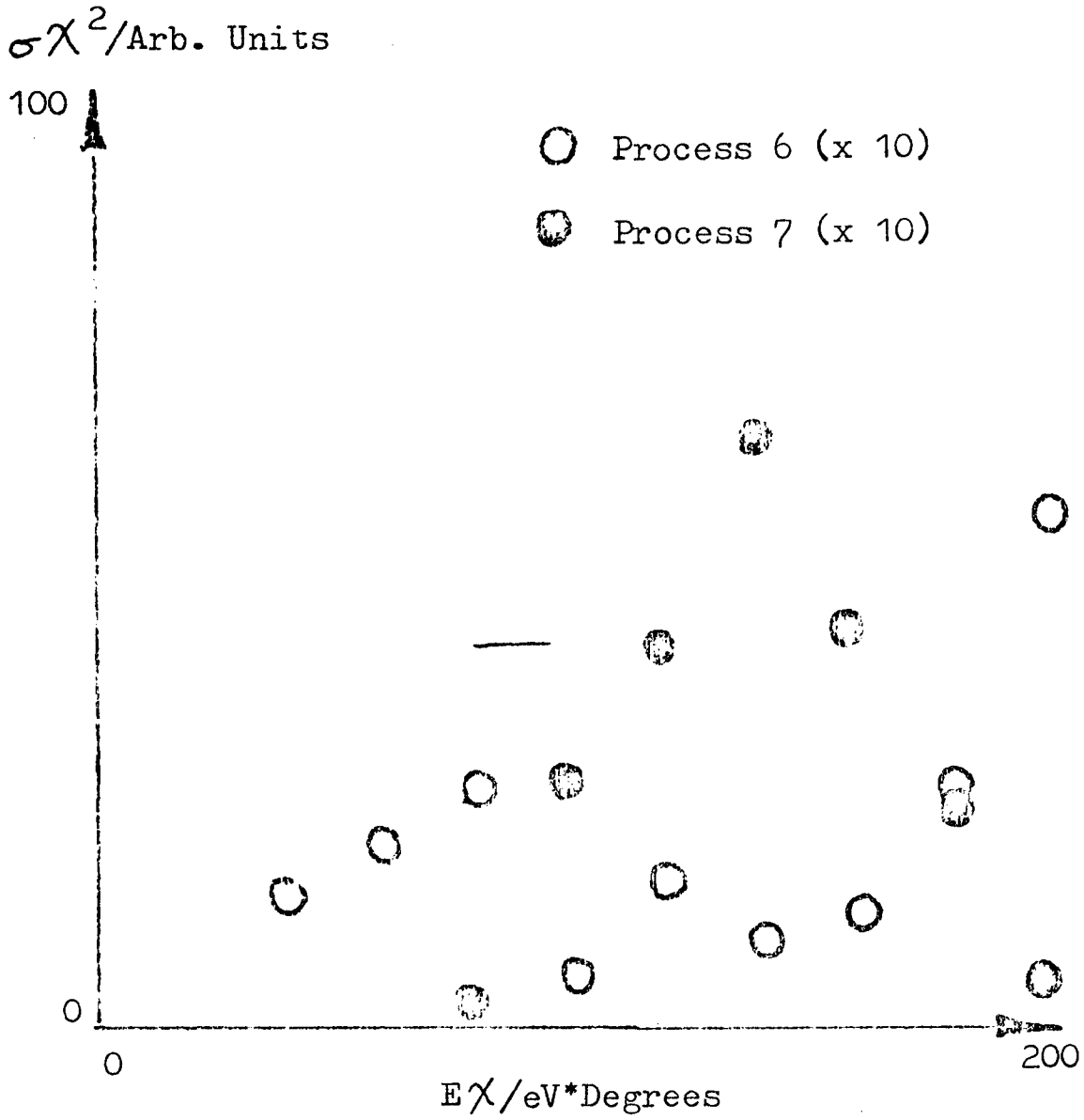

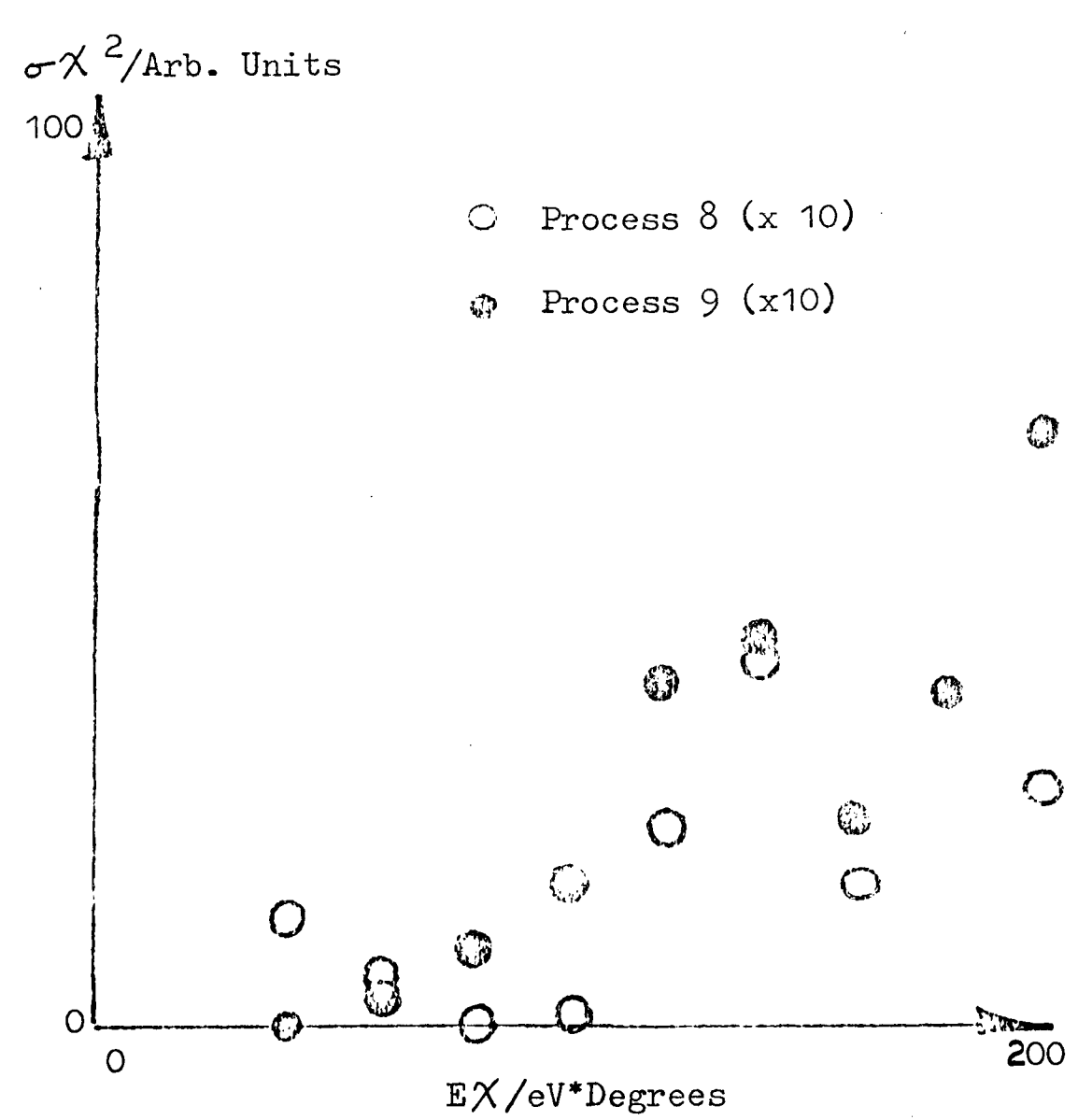

Figures 4.37 : Differential Cross Sections 81eV C.M.

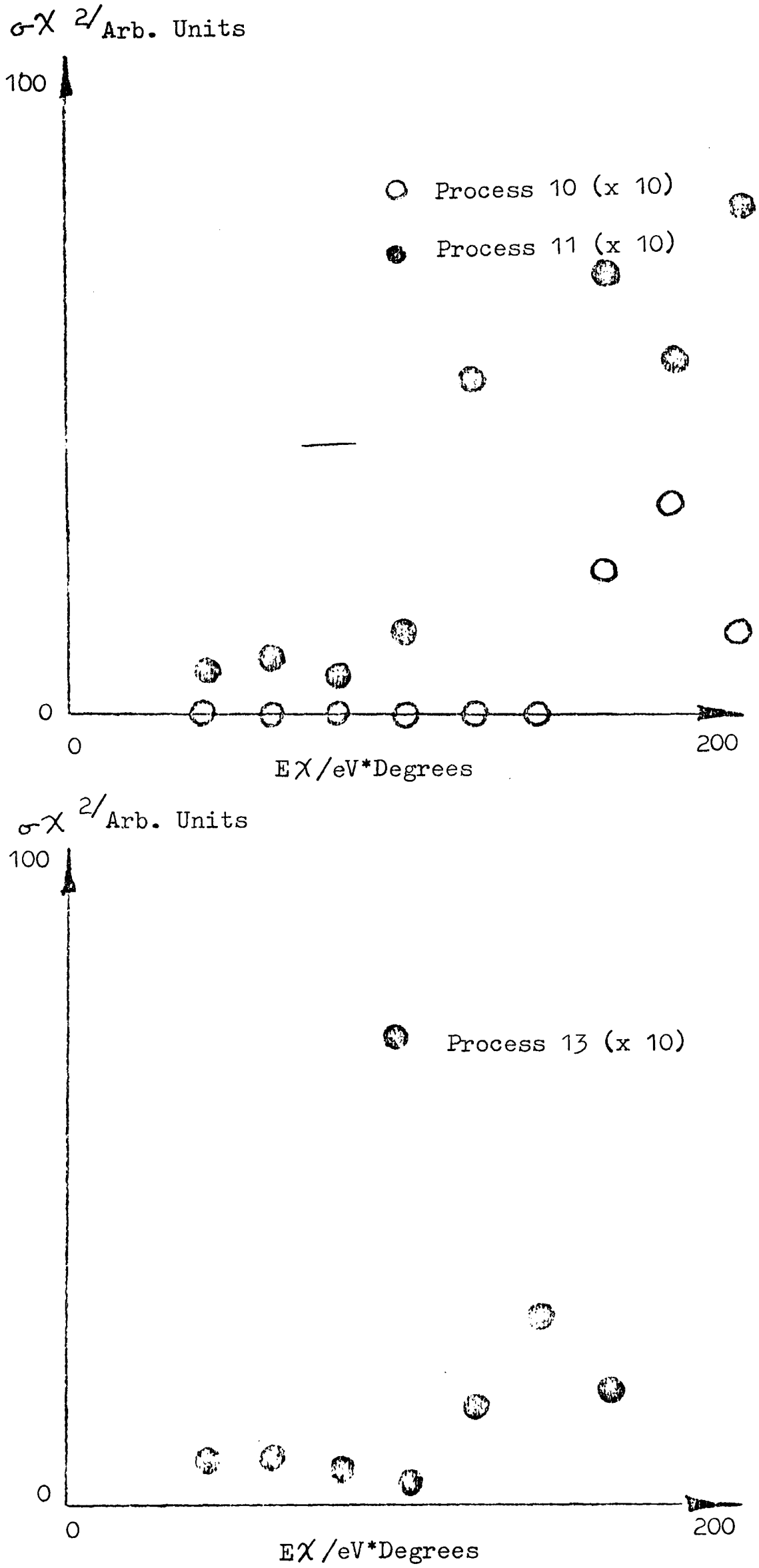

Figures 4.38 : K/CH_3I Differential Cross Sections 81eV C.M.

4.4 K/CH_3Cl DATA

Not surprisingly the methyl chloride data (shown in figures 4.39 to 4.51) is similar in many respects to the methyl iodide data. The substitution of the lighter halide atom in the alkyl halide would not be expected to alter the overall features of the spectra. Once again a large number of discrete peaks in the data can be seen, with most of the observed energy losses constant with increasing scattering angle. Similarly, processes involving an energy transfer of up to 11 eV are present and onset at the narrowest angles of observation. Table 4.4 summarises the energy losses observed.

Figures 4.52 to 4.54 show the differential cross sections for these processes.

4.5 K/CF_3I DATA

An obvious experiment to perform after changing the halide atom is to investigate the effects of changing the methyl group. Beam experiments in which a potassium atom beam is intersected by an orientated beam of CH_3I molecules show that the iodine end is much more reactive than the methyl end and that a direct collision between the potassium and iodine is probably necessary for reaction (BRO 66). In contrast, experiments on potassium in collision with orientated trifluoromethyl iodide molecules show that there is no steric hinderance to the reaction (BRO 73) and that there is a higher probability of forming potassium iodide if the K atom impinges on the CF_3 "end" of the molecule.

Figure 4.39

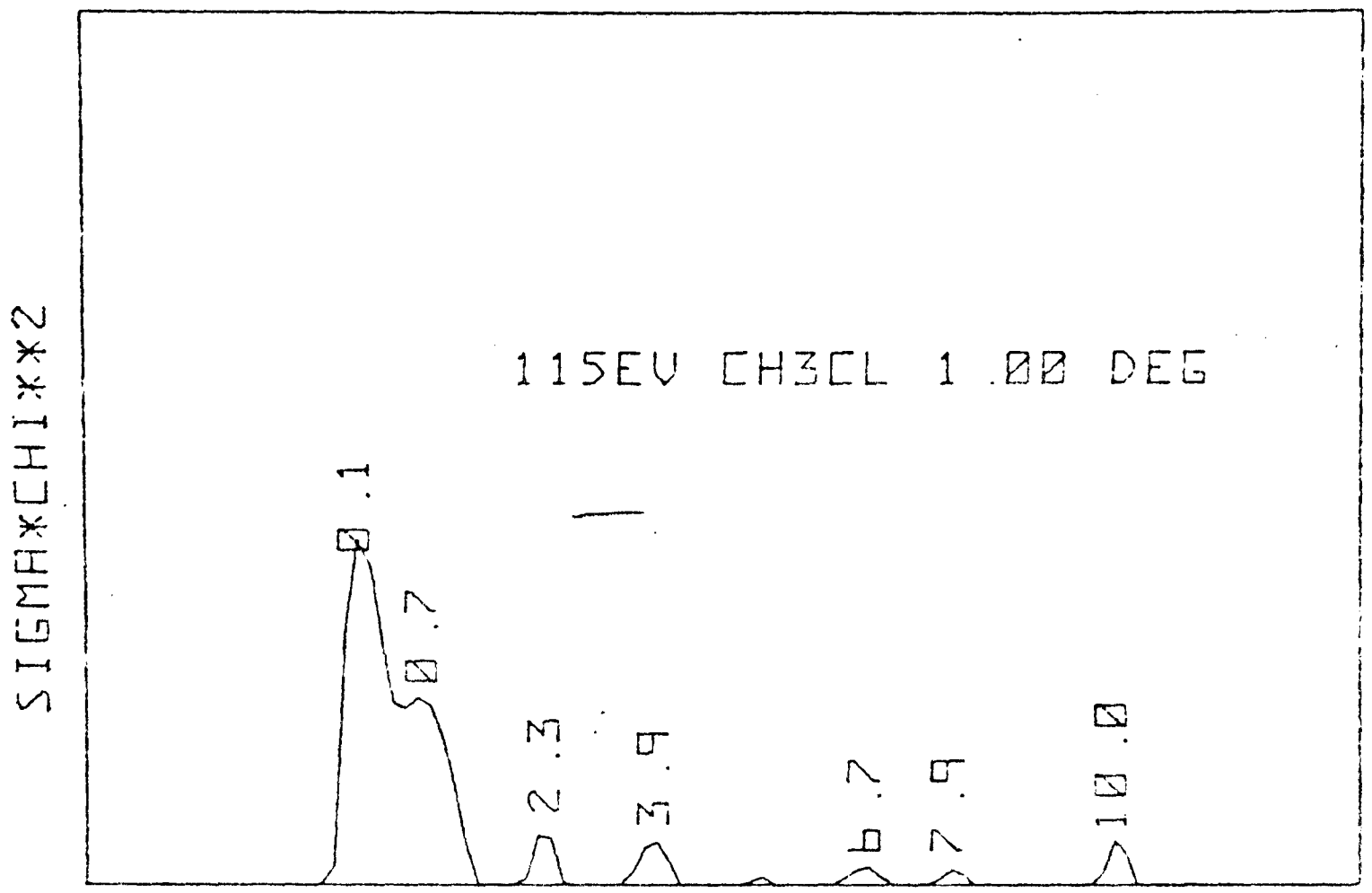

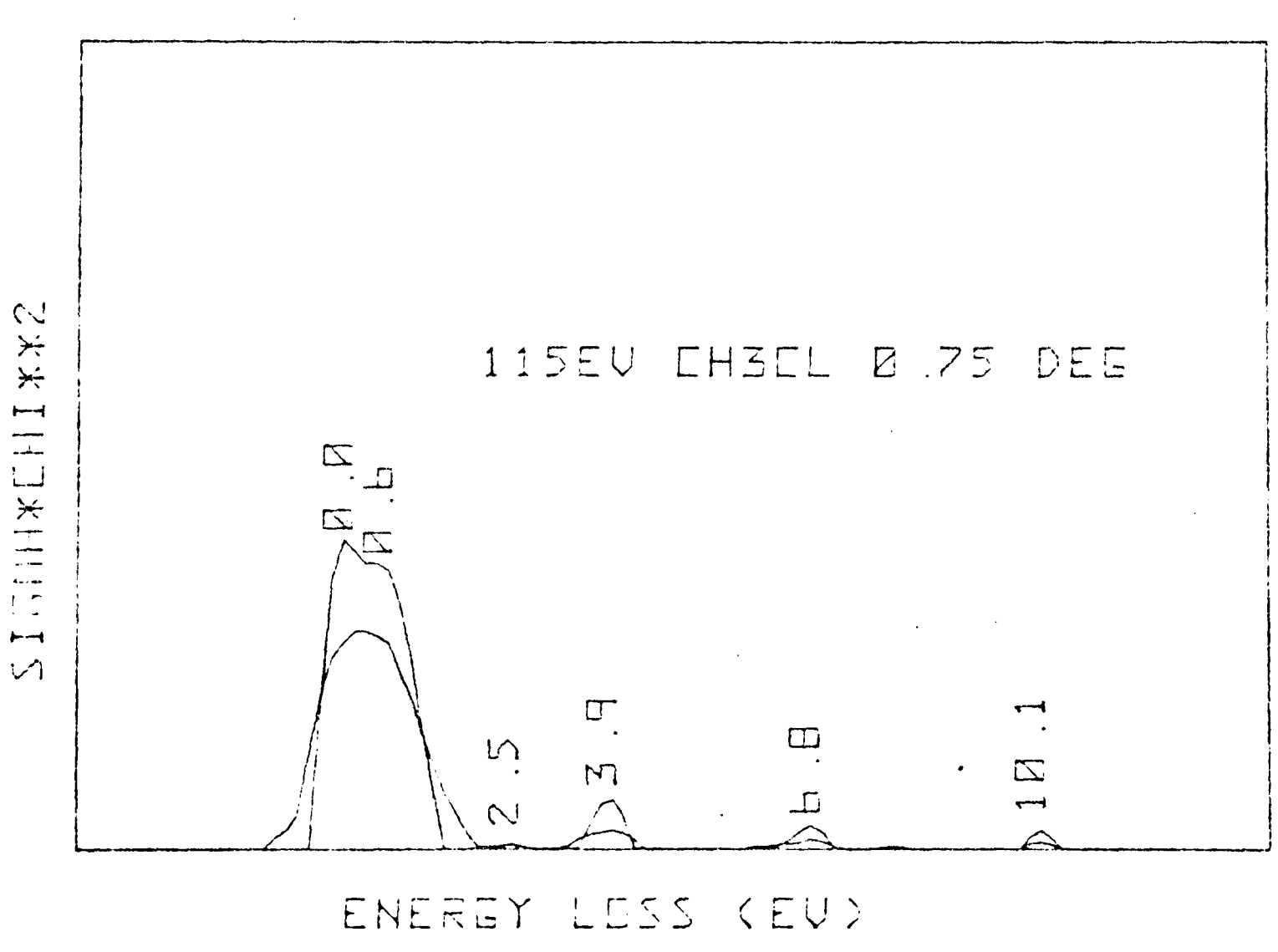

Figure 4.40

Figure 4.41

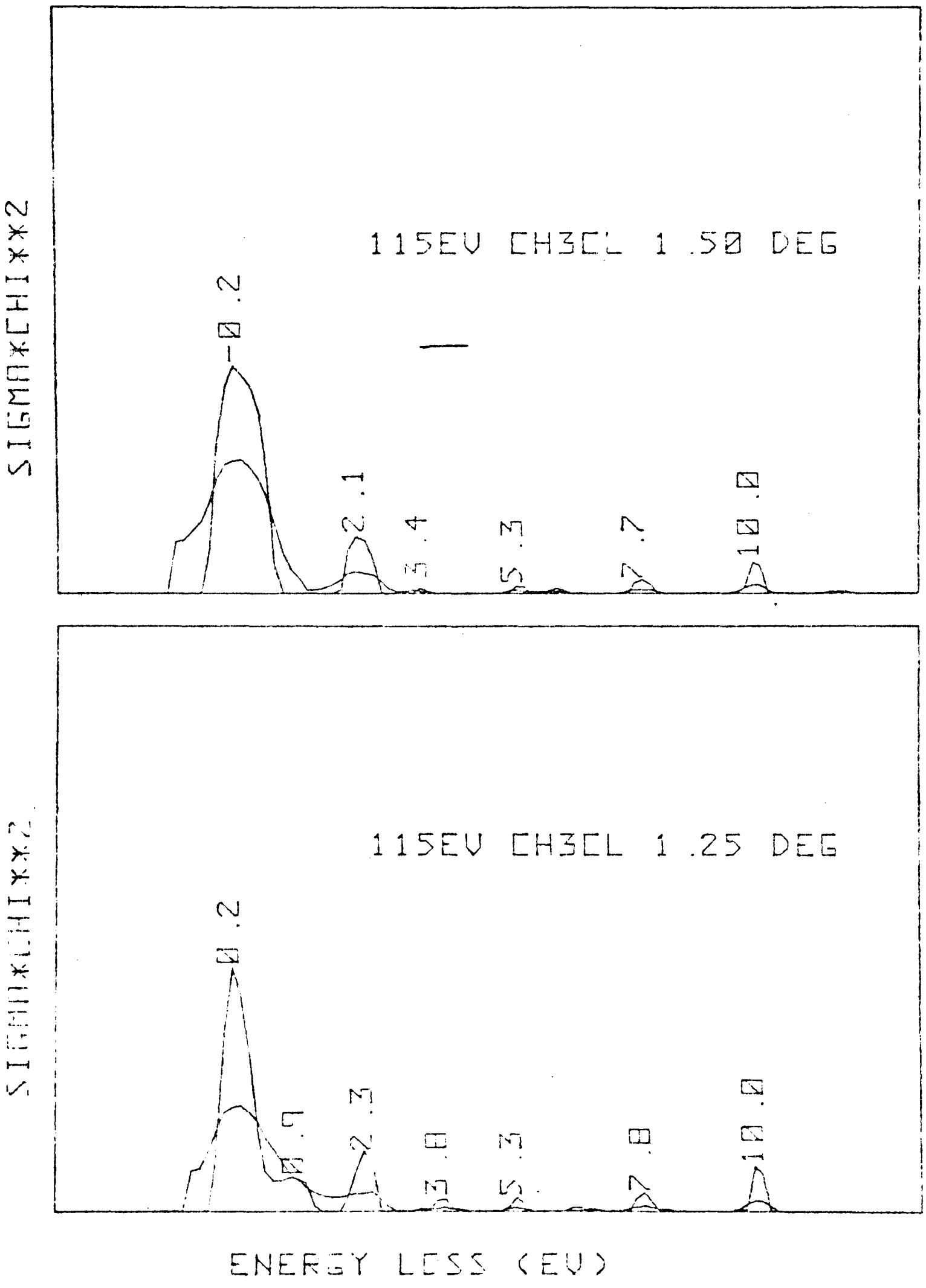

Figure 4.42

Figure 4.43

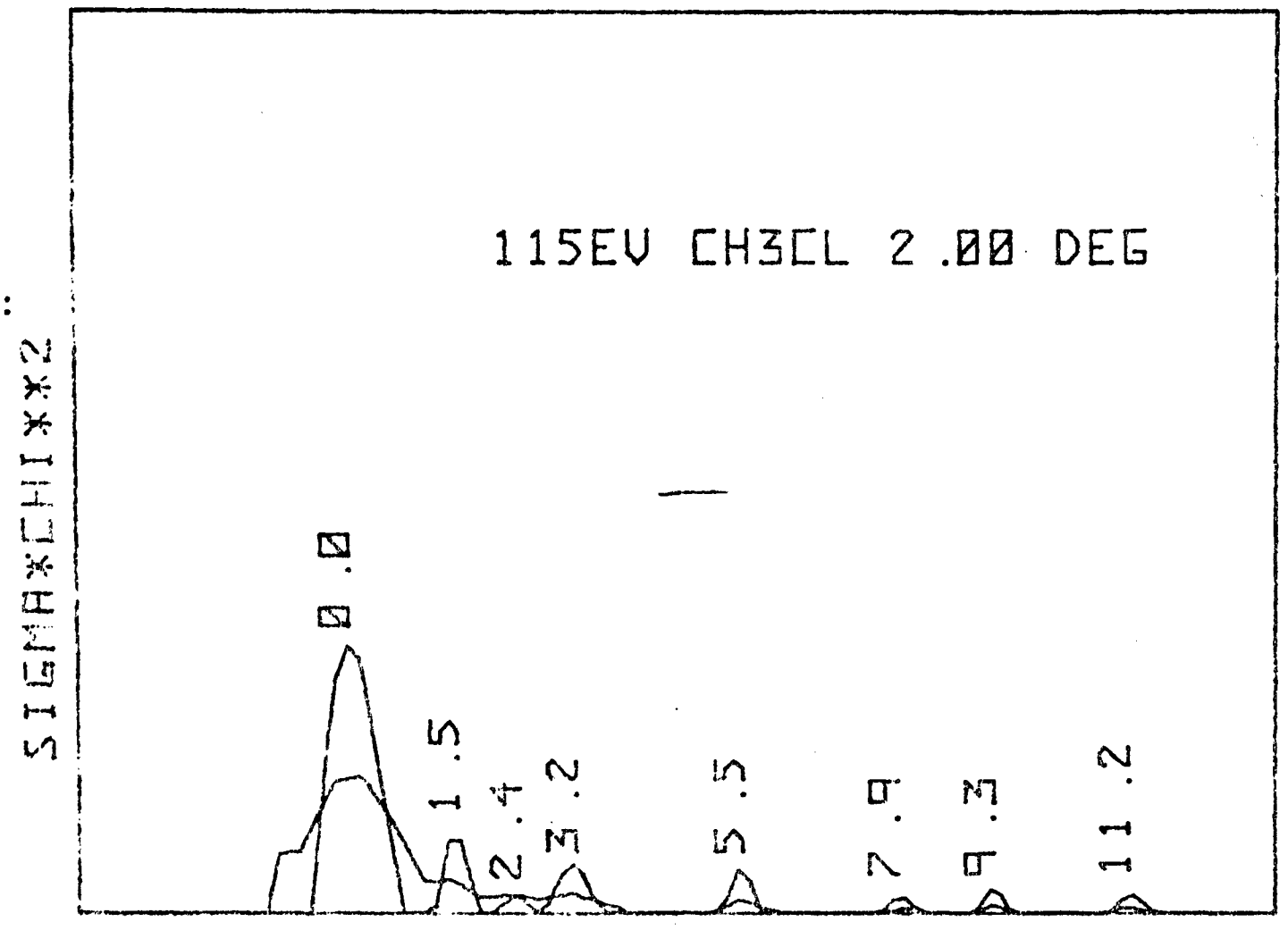

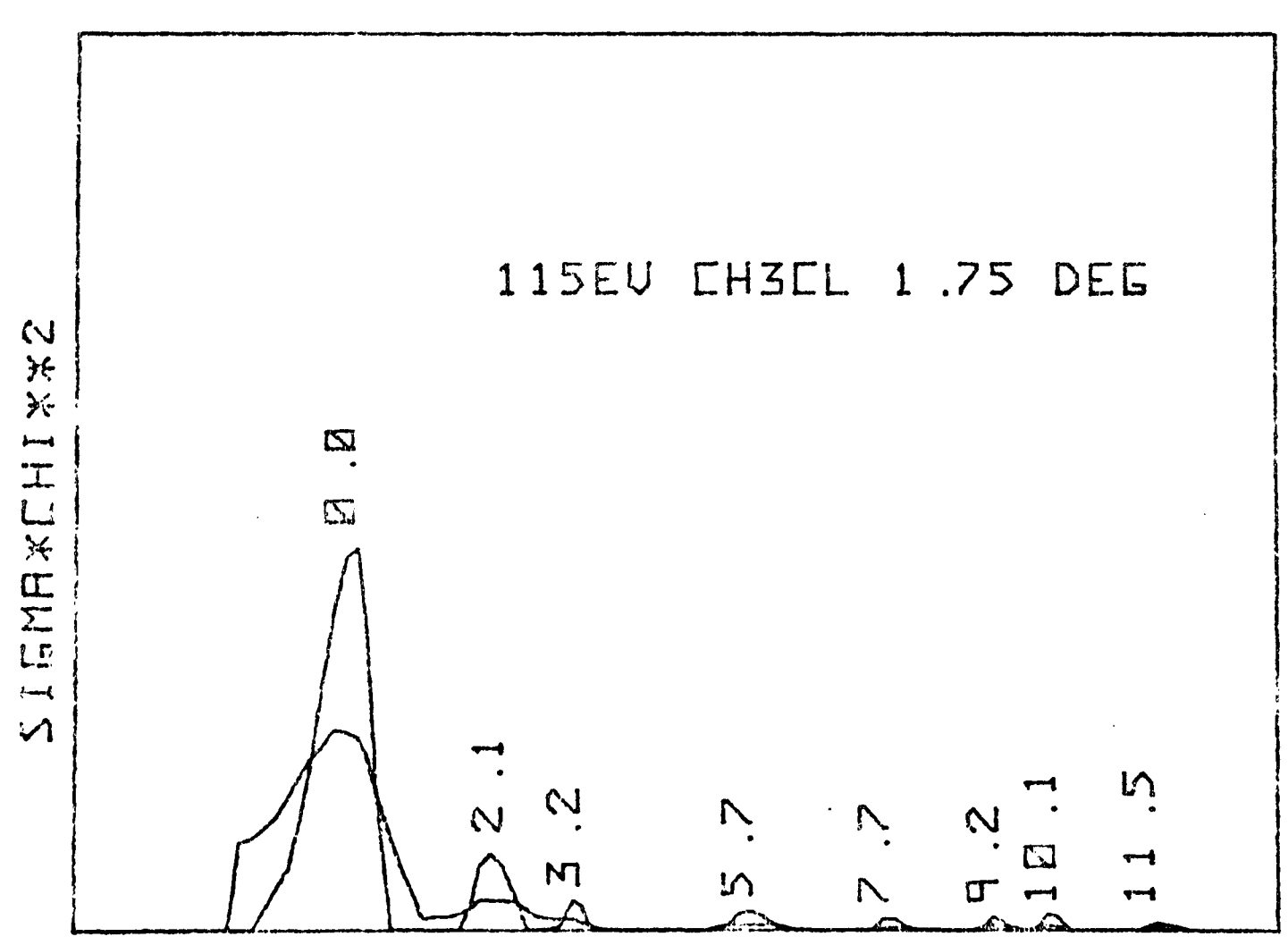

Figure 4.44

Figure 4.45

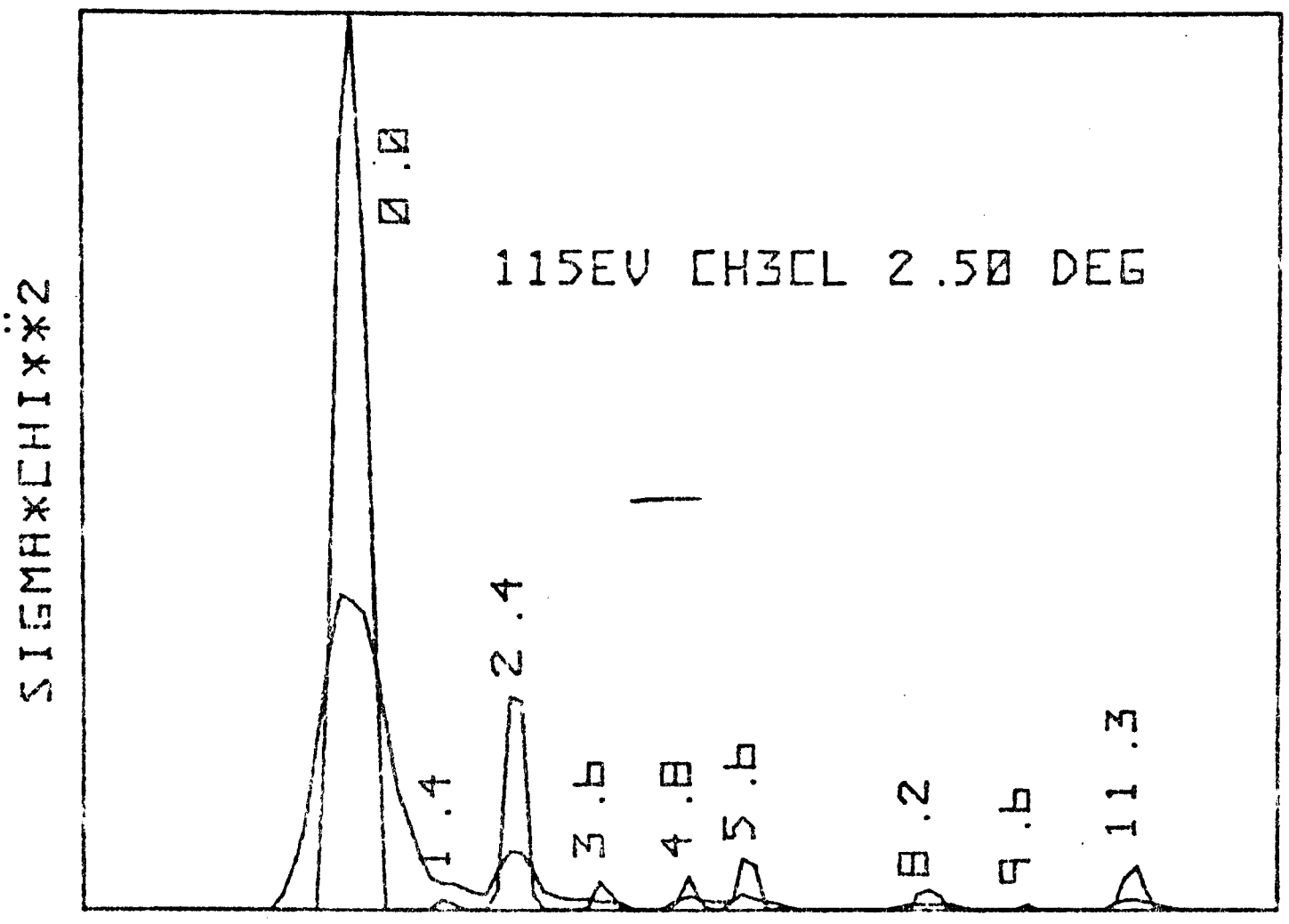

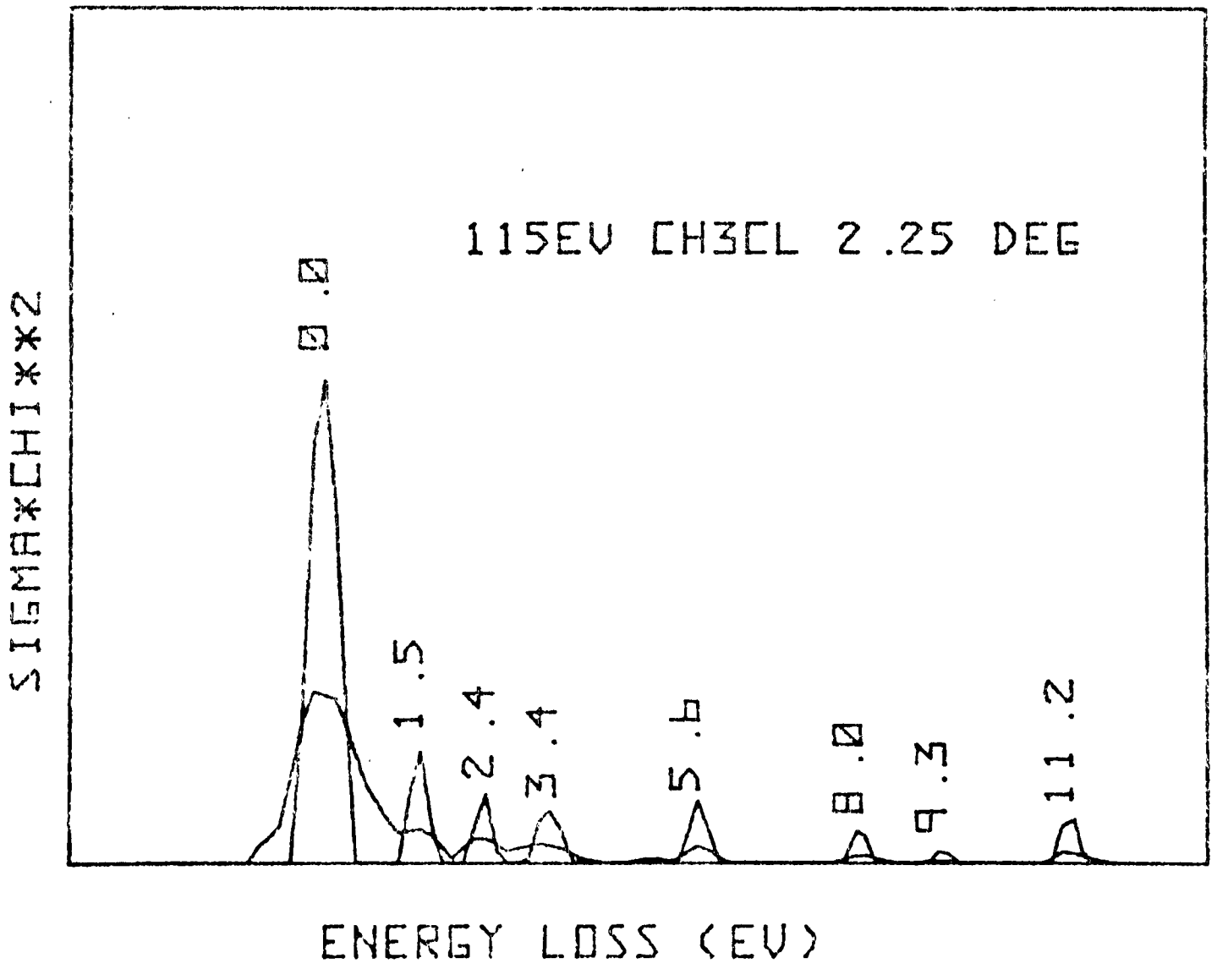

Figure 4.46

Figure 4.47

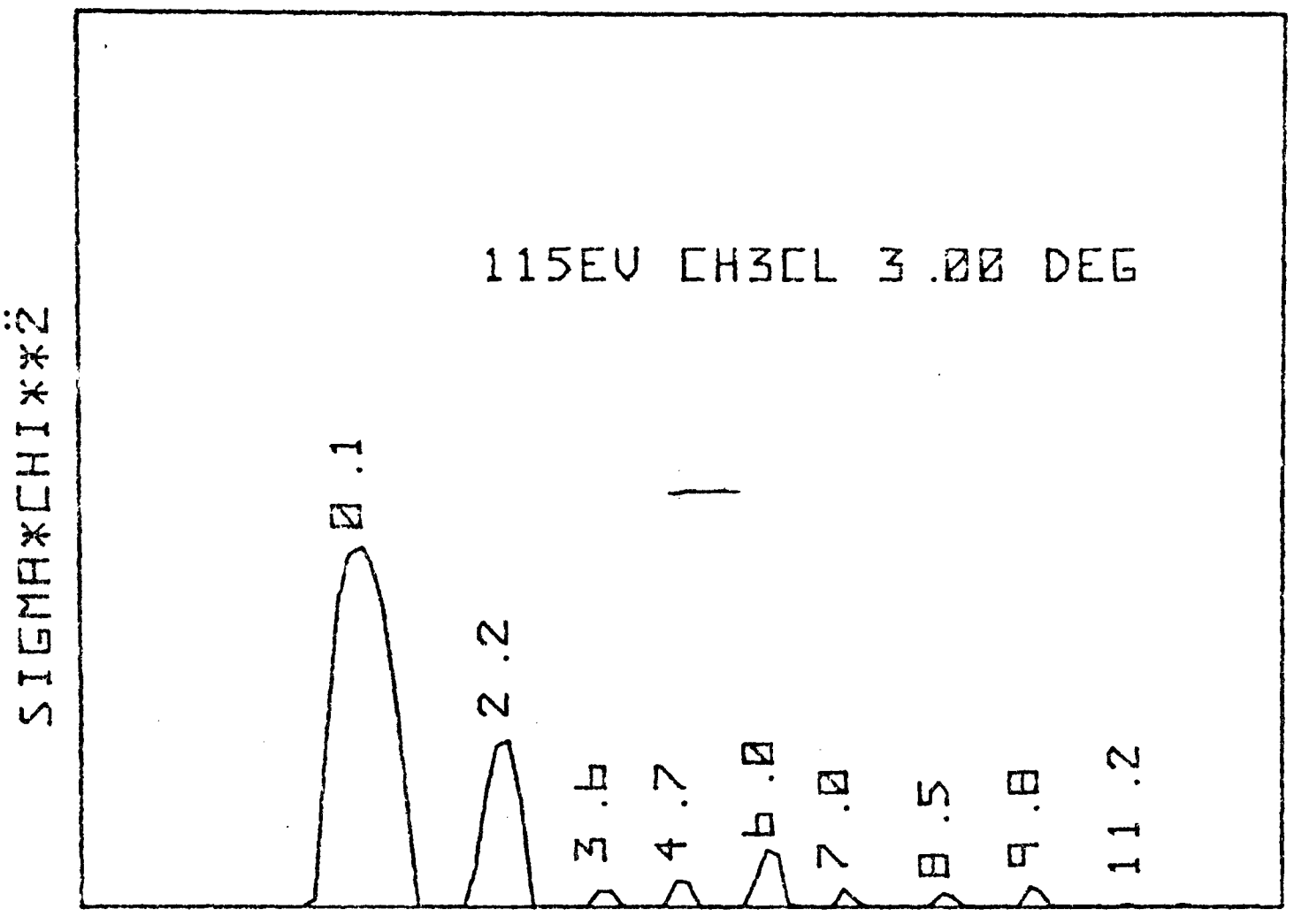

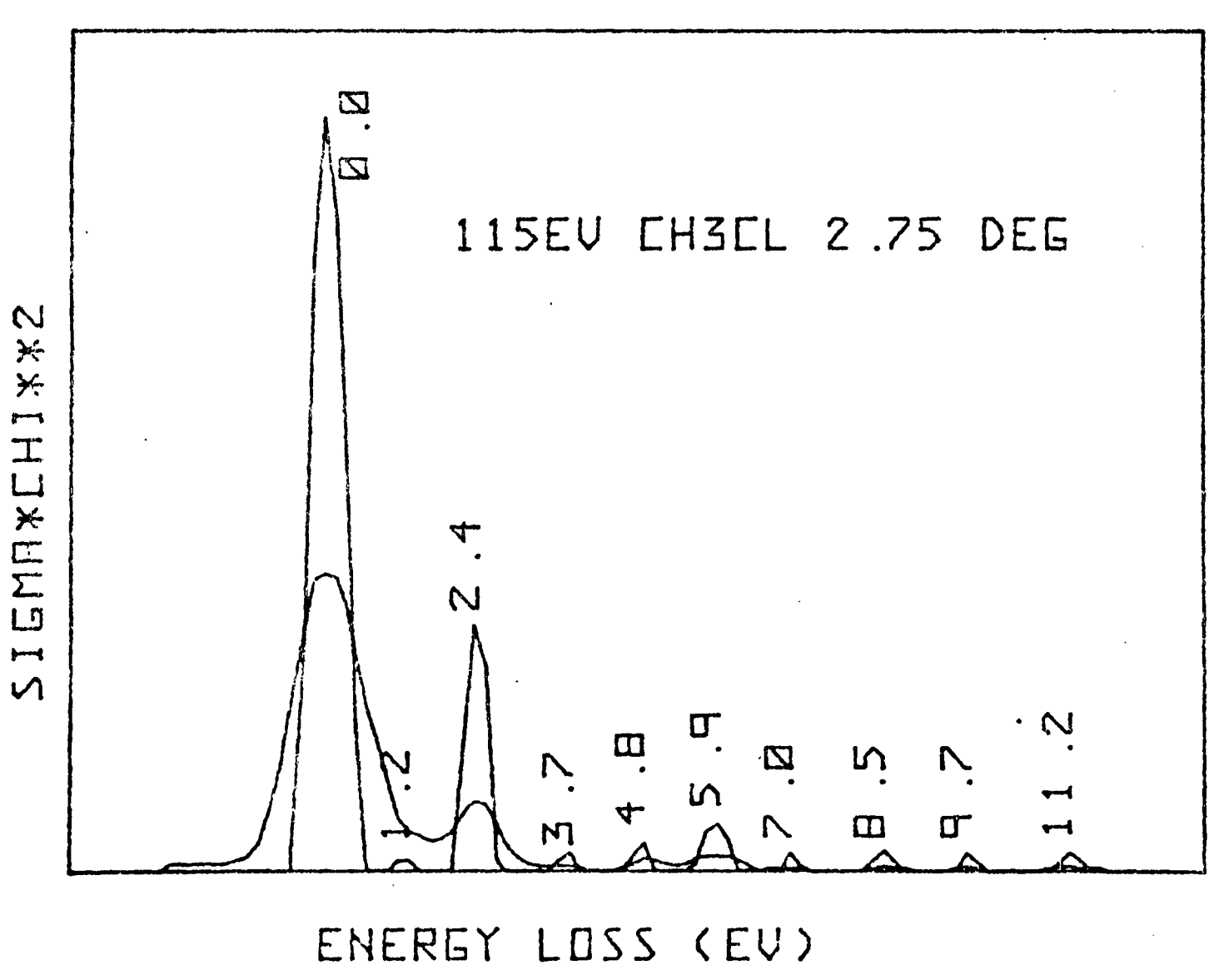

Figure 4.48

Figure 4.49

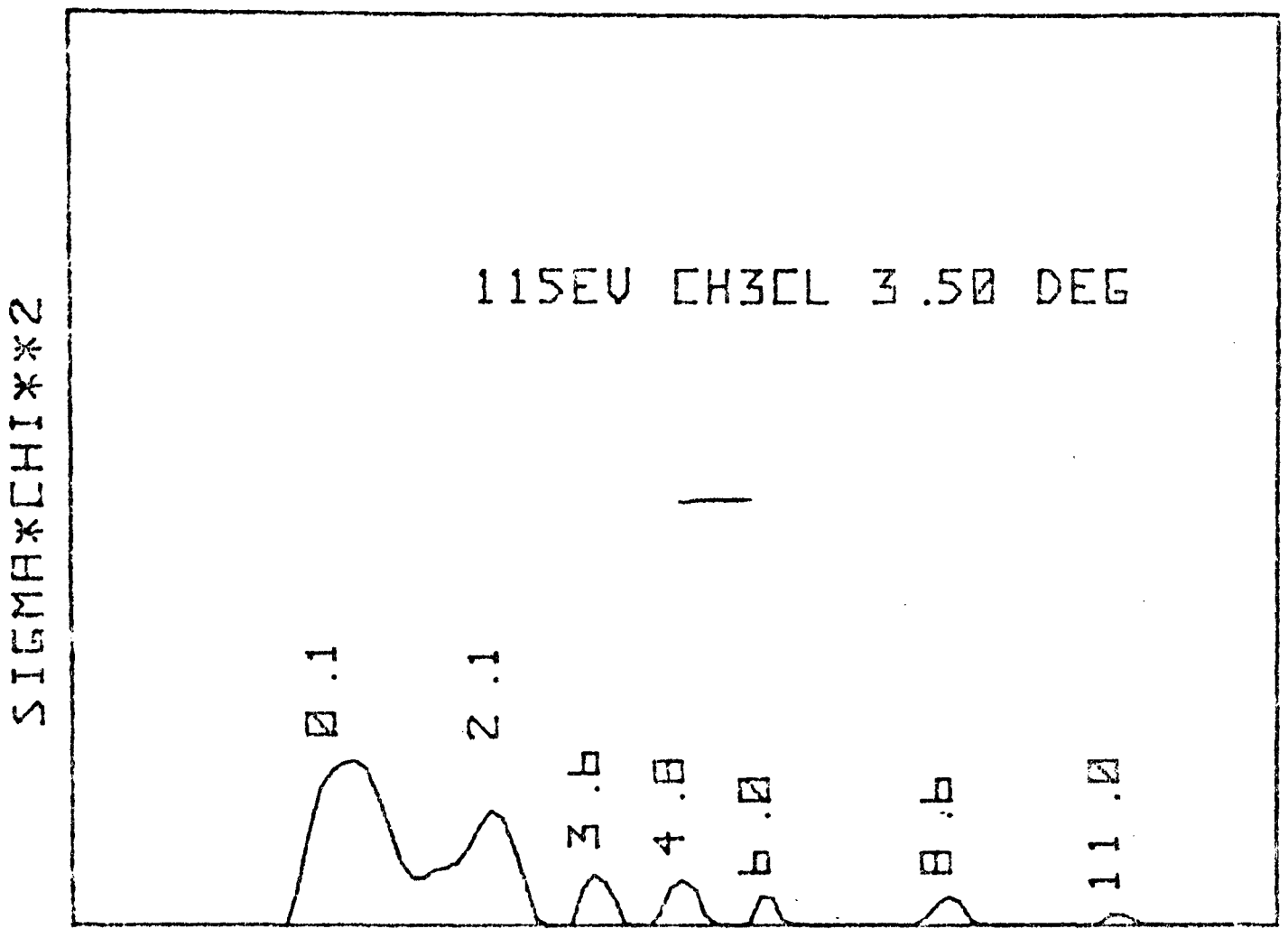

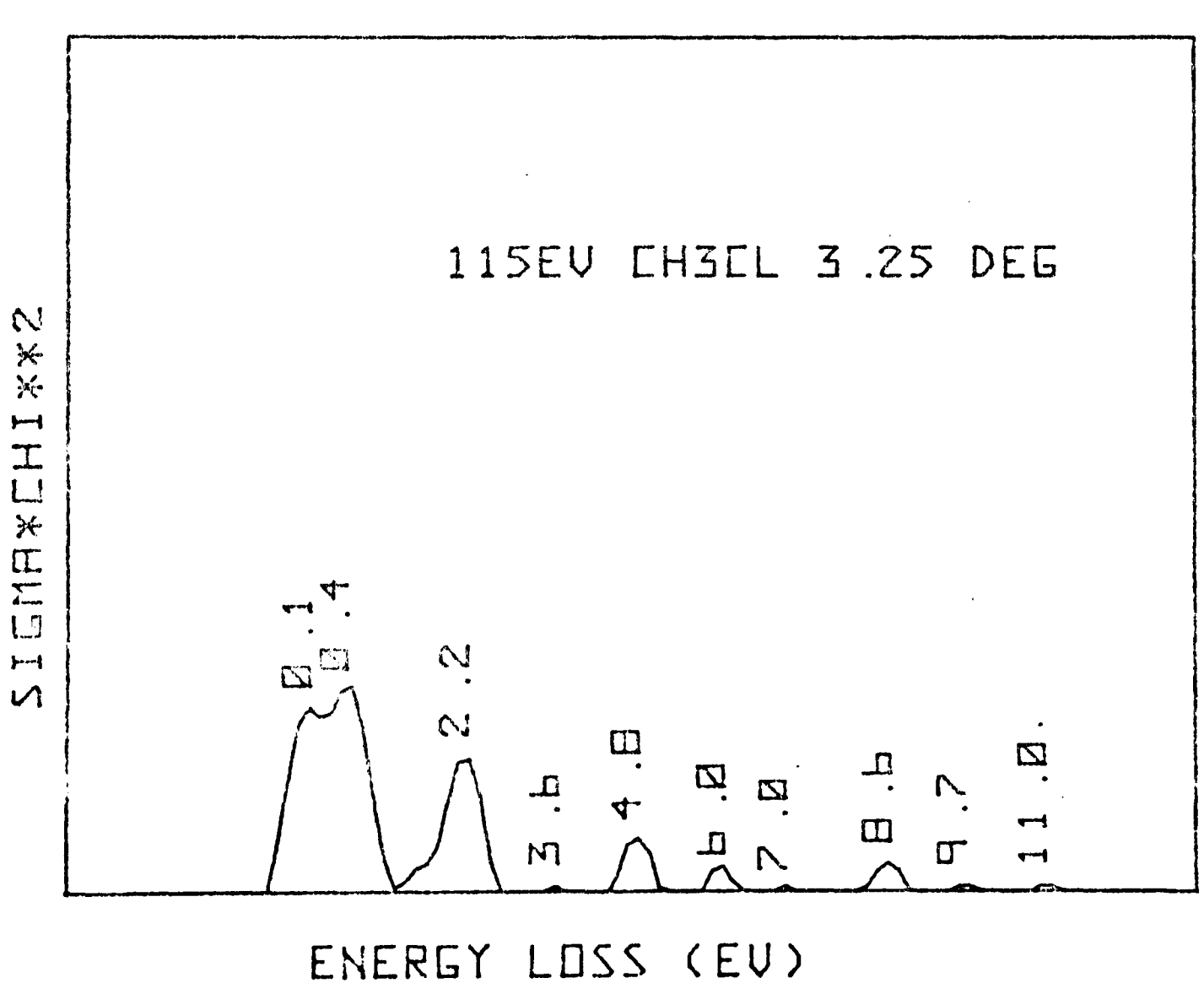

Figure 4.50

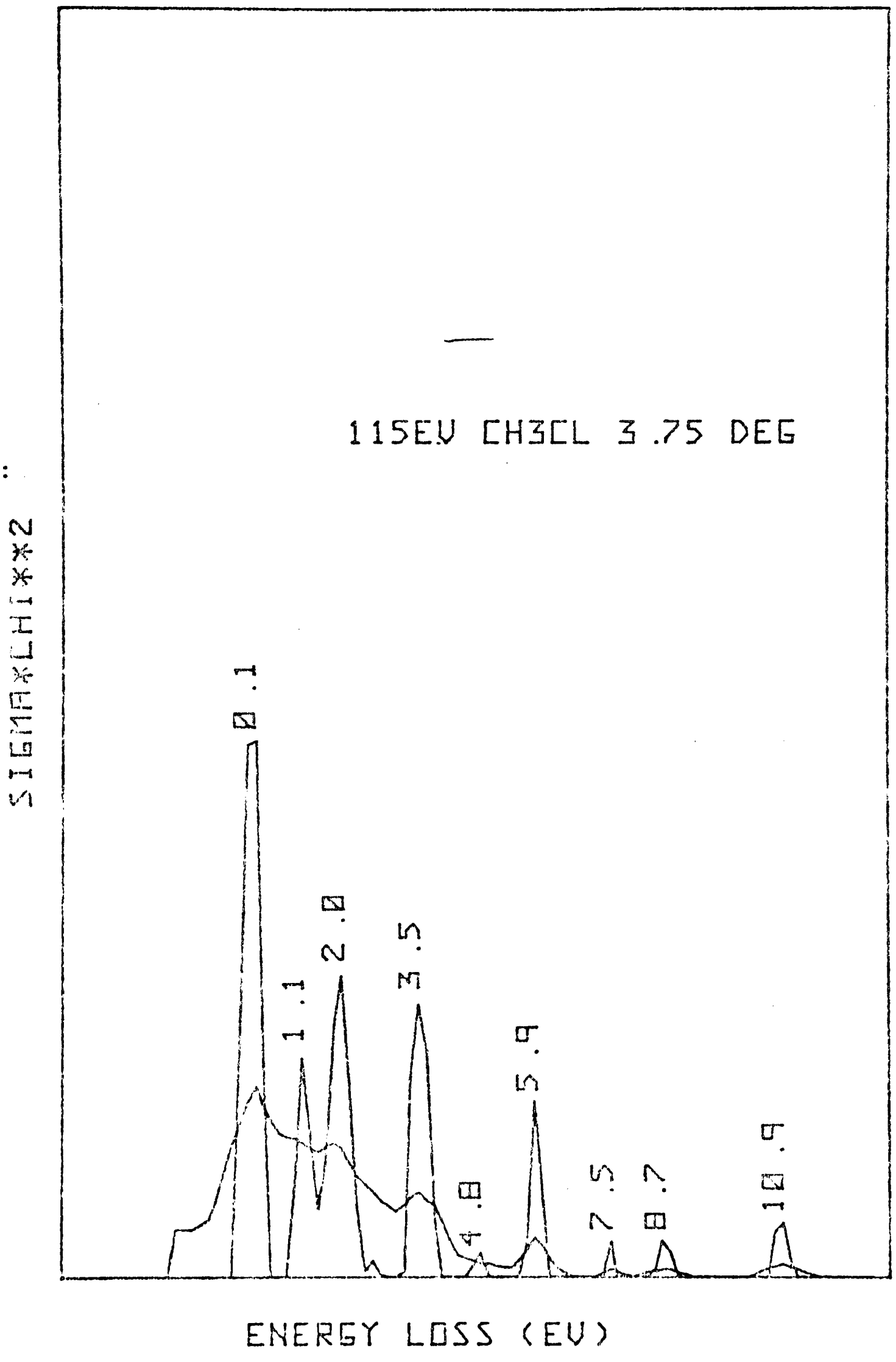
115EV CH3CL 3.75 DEG
SIGMA*LHI**2
0.1
1.1
2.0
3.5
4.8
5.9
7.5
8.7
10.9
ENERGY LOSS (EV)

Figure 4.51

TABLE 4.4 : K/CH_3Cl DATA 115 eV C.M.

Scattering Angle	Process Number 1	2	3	4	5	6	7	8	9	10	11
0.75	0.0	0.6	2.5	3.9					10.1		6.8
1.00	0.1	0.7	2.3	3.9			7.9		10.0		6.7
1.25	0.2	0.9	2.3	3.8		5.3	7.8		10.0		
1.50	-0.2		2.1	3.4		5.3	7.7		10.1		
1.75	0.0		2.1	3.2		5.7	7.7	9.2		11.5	
2.00	0.0	1.5	2.4	3.2		5.5	7.9	9.3		11.2	
2.25	0.0	1.5	2.4	3.4		5.6	8.0	9.3		11.2	
2.50	0.0	1.4	2.4	3.6	4.8	5.6	8.2	9.6		11.3	
2.75	0.0	1.2	2.4	3.7	4.8	5.9	8.5	9.7		11.2	7.0
3.00	0.1		2.2	3.6	4.7	6.0	8.5	9.8		11.2	7.0
3.25	0.1	0.4	2.2	3.6	4.8	6.0	8.6	9.7		11.0	7.0
3.50	0.1		2.1	3.6	4.8	6.0	8.6			11.0	
3.75	0.1	1.1	2.0	3.5	4.8	5.9	8.7			10.9	7.5

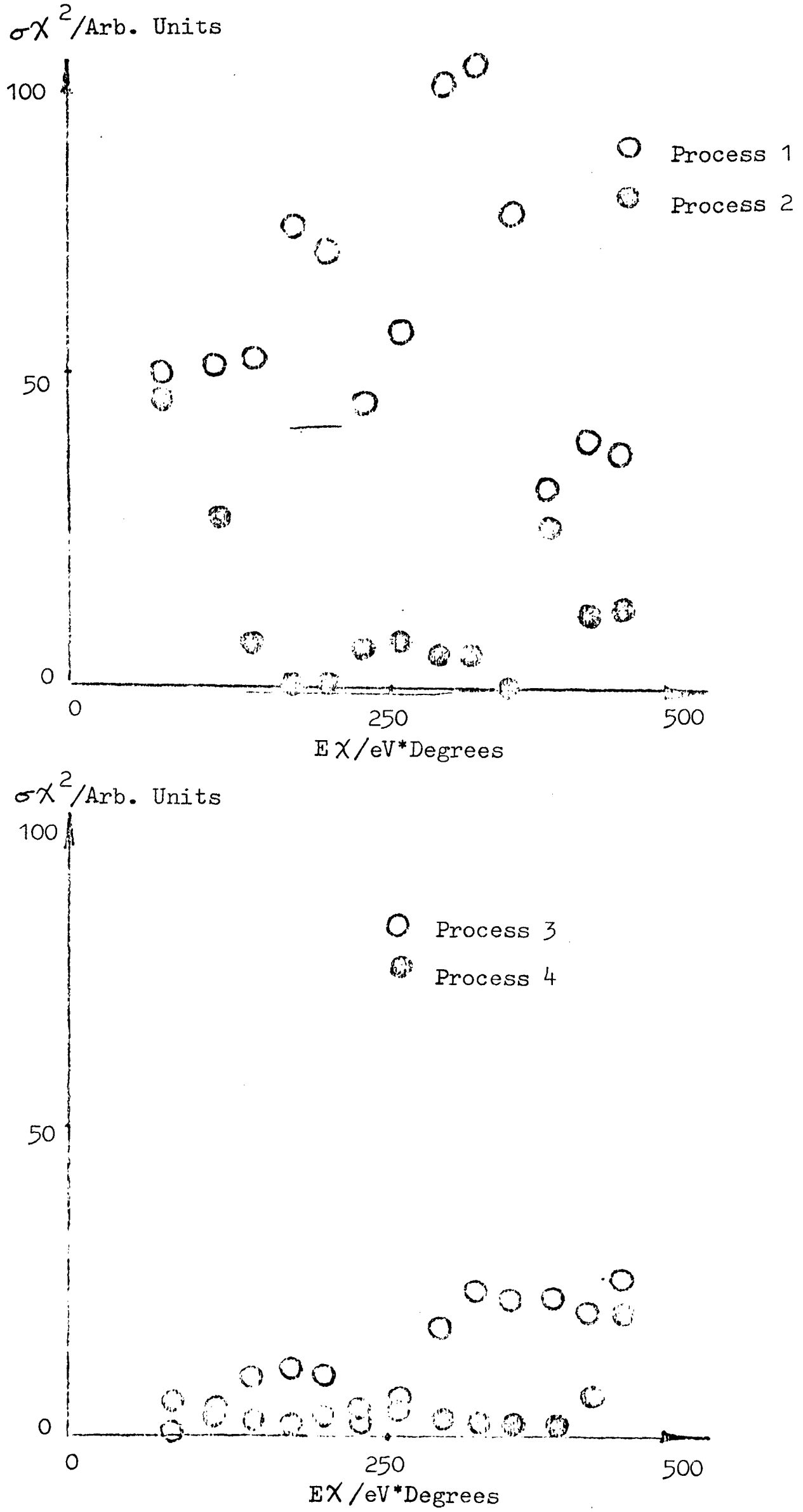

Figure 4.52 : K/CH_3Cl Differential Cross Sections 115 eV C.M.

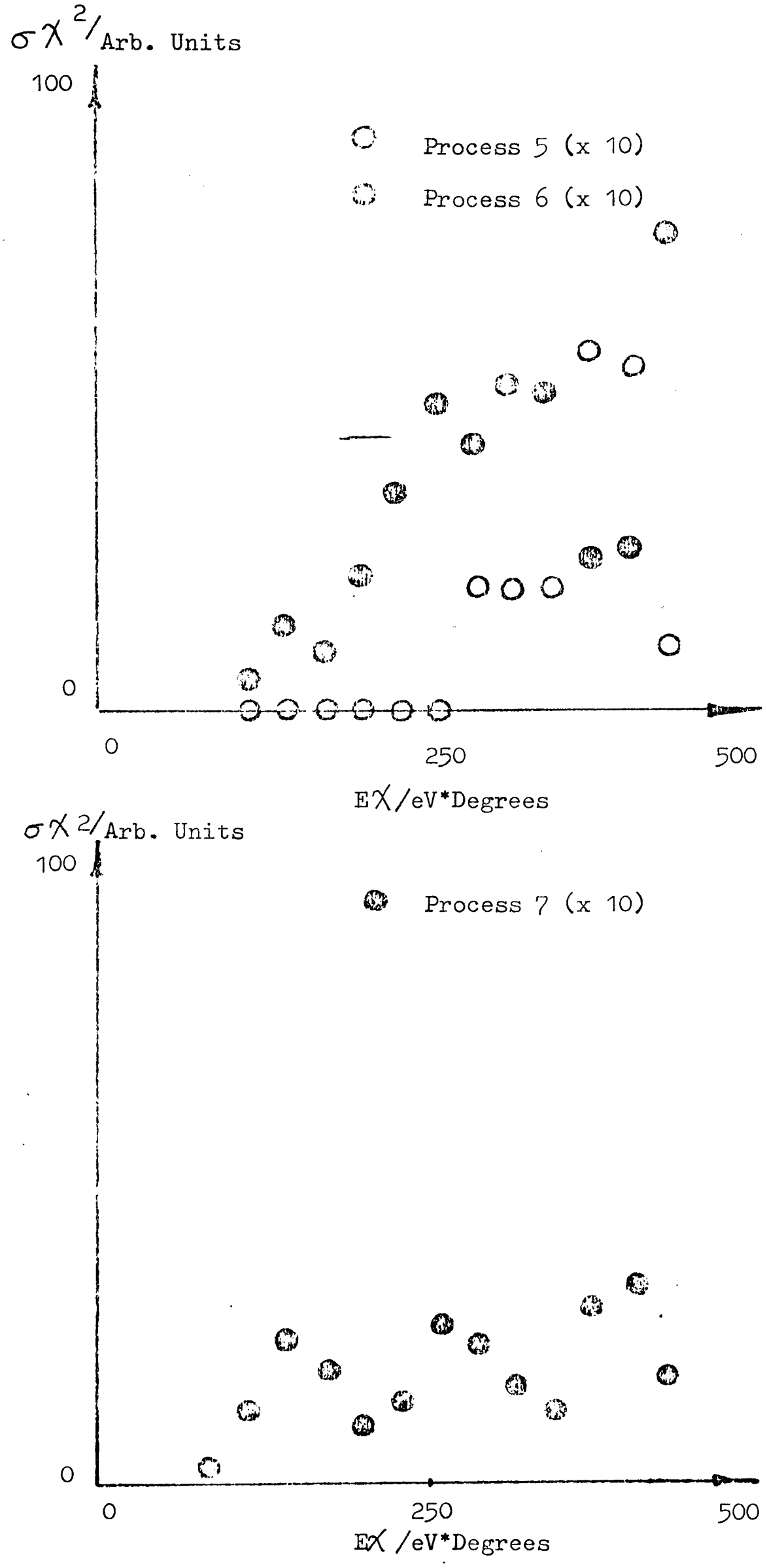

Figure 4.53 : K/CH_3Cl Differential Cross Sections 115 eV C.M.

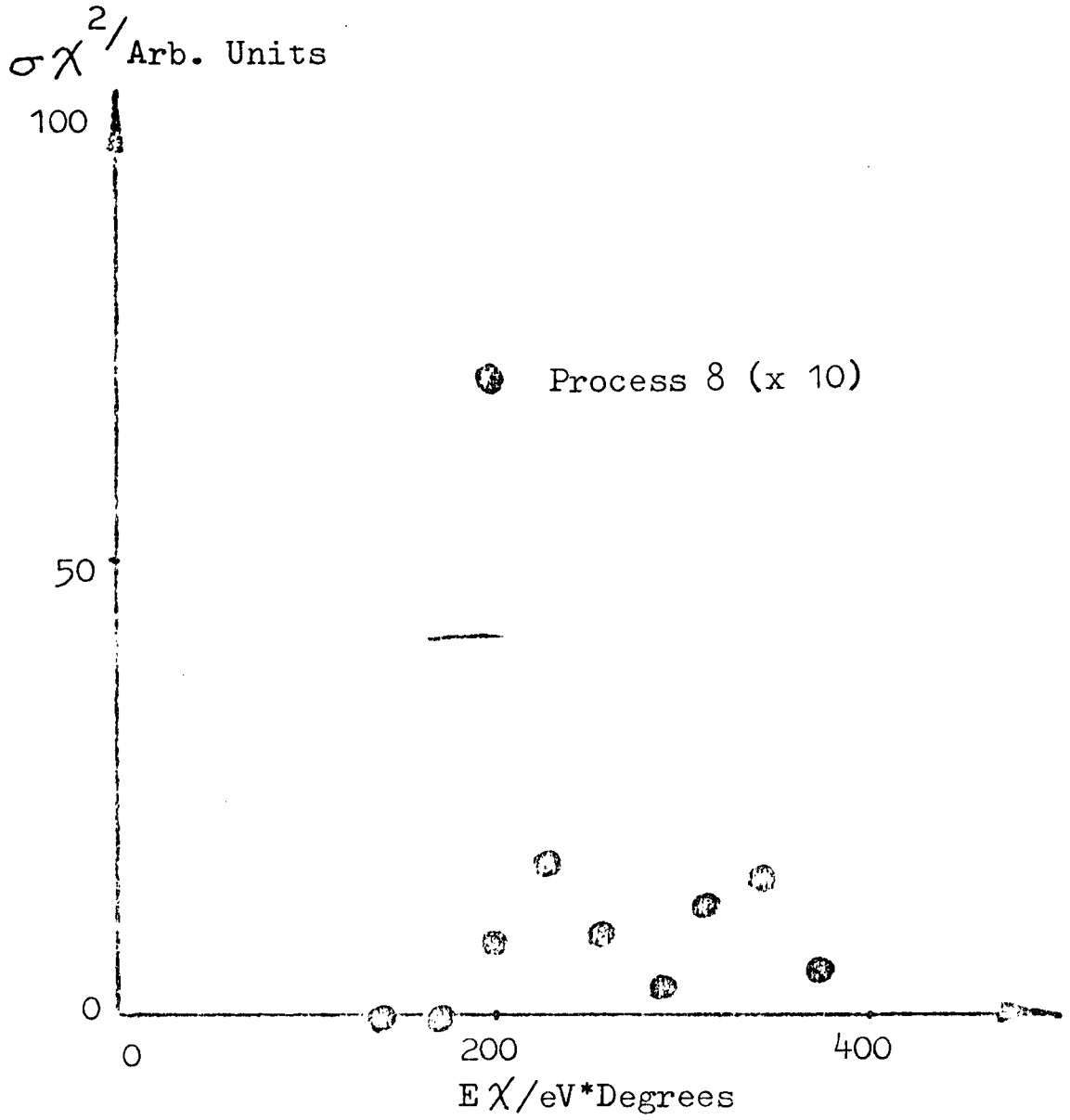

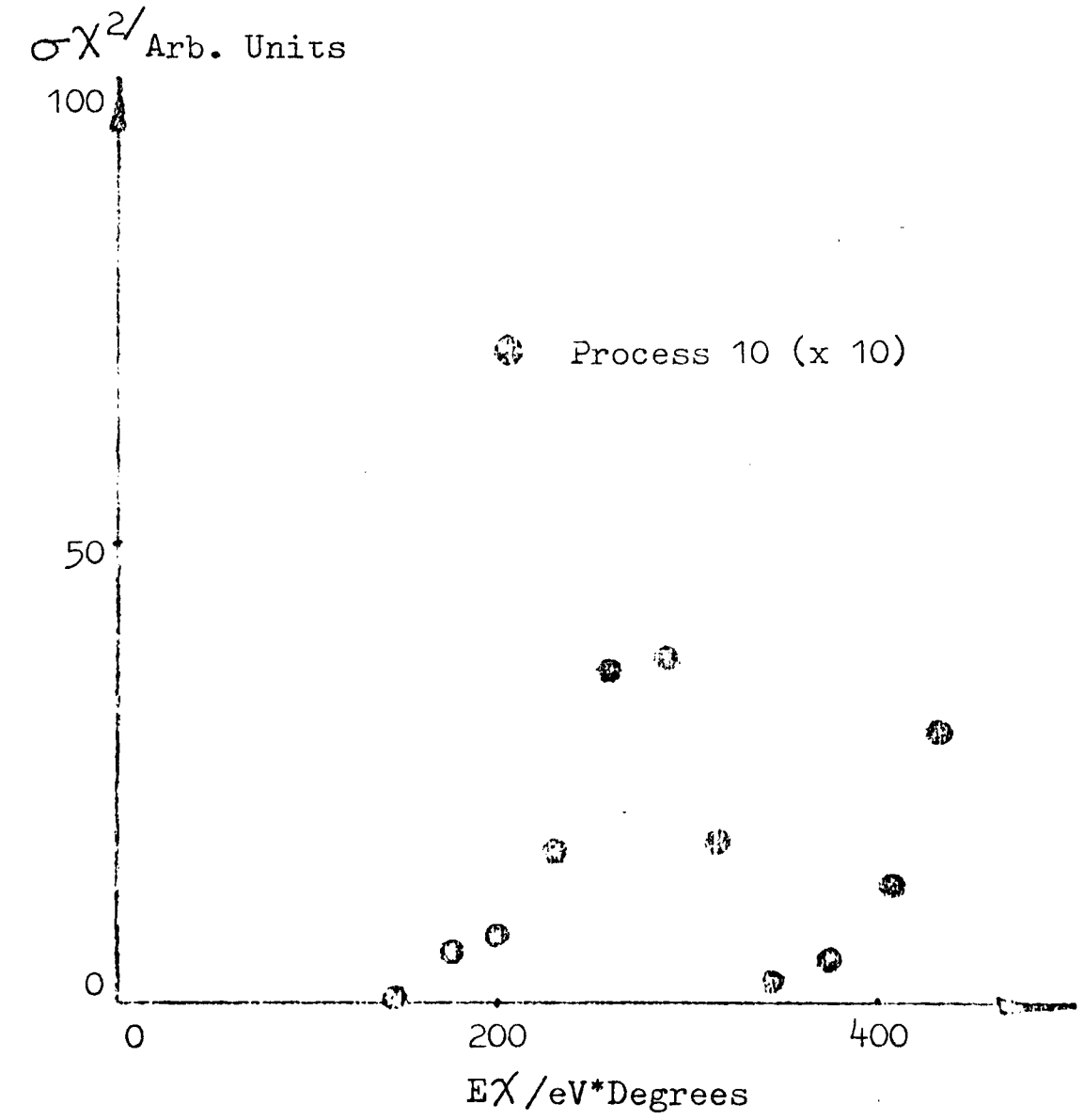

Figure 4.54 : K/CH_3Cl Differential Cross Sections 115 eV C.M.

This is explained by the fact that the CF_3 molecule has a greater electron affinity than the iodine atom and since the reaction $K + CF_3I \rightarrow KI + CF_3$ proceeds via an harpooning mechanism the CF_3 accepts the donated electron more readily than the iodine atom.

Figures 4.55 to 4.58 show the time of flight profiles for K/CF_3I at 170 eV C.M. collision energy. Table 4.5 lists the energy losses observed and shows strong similarities to the methyl halide data given in Tables 4.3 and 4.4: a number of discrete features with large energy losses detected for very narrow angular scattering. As in the CH_3I data the results for collisions at 86 eV C.M. and 170 eV C.M. differ. The cross sections obtained for the K/CF_3I are shown in figures 4.59 to 4.61.

The 86 eV C.M. K/CF_3I data is presented as a contour map (Figure 4.62) as the quality and quantity of the data is such that a contour map is fairly readily understood. Main beam intensities decrease as the lab beam energy is reduced due to increased space charge effects and the apparent increased sensitivity of the beam to the ion lens voltages and this has limited the number of experiments carried out at lower collision energies. It can be seen that the energy resolution of the equipment is improved at this energy and the different exit channels are clearly separated. The observations are summarised in Table 4.6.

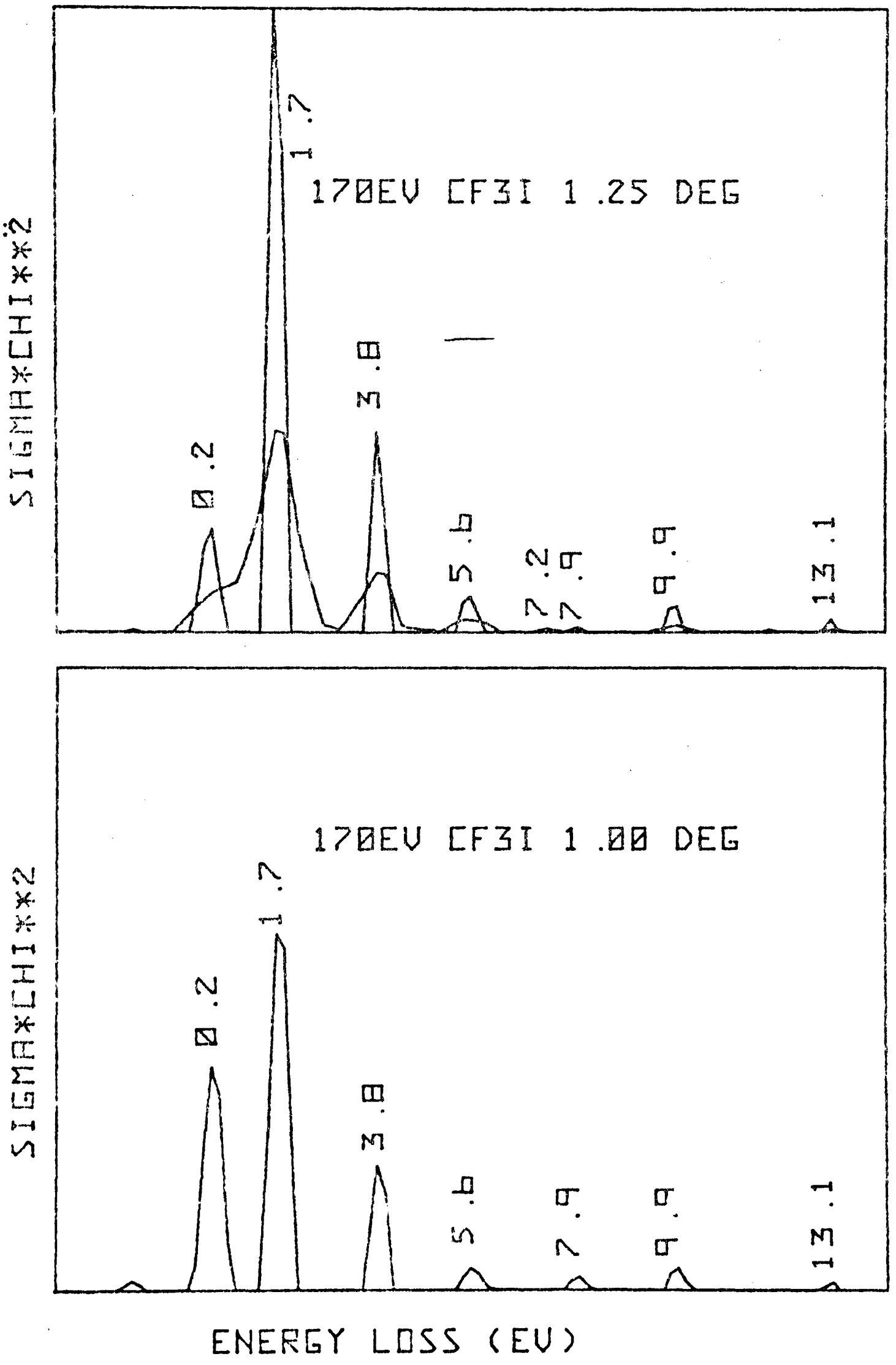
170EV CF3I 1.25 DEG
170EV CF3I 1.00 DEG
SIGMA*CHI**2
0.2
1.7
3.8
5.4
7.2
9.9
13.1
ENERGY LOSS (EV)

Figure 4.55

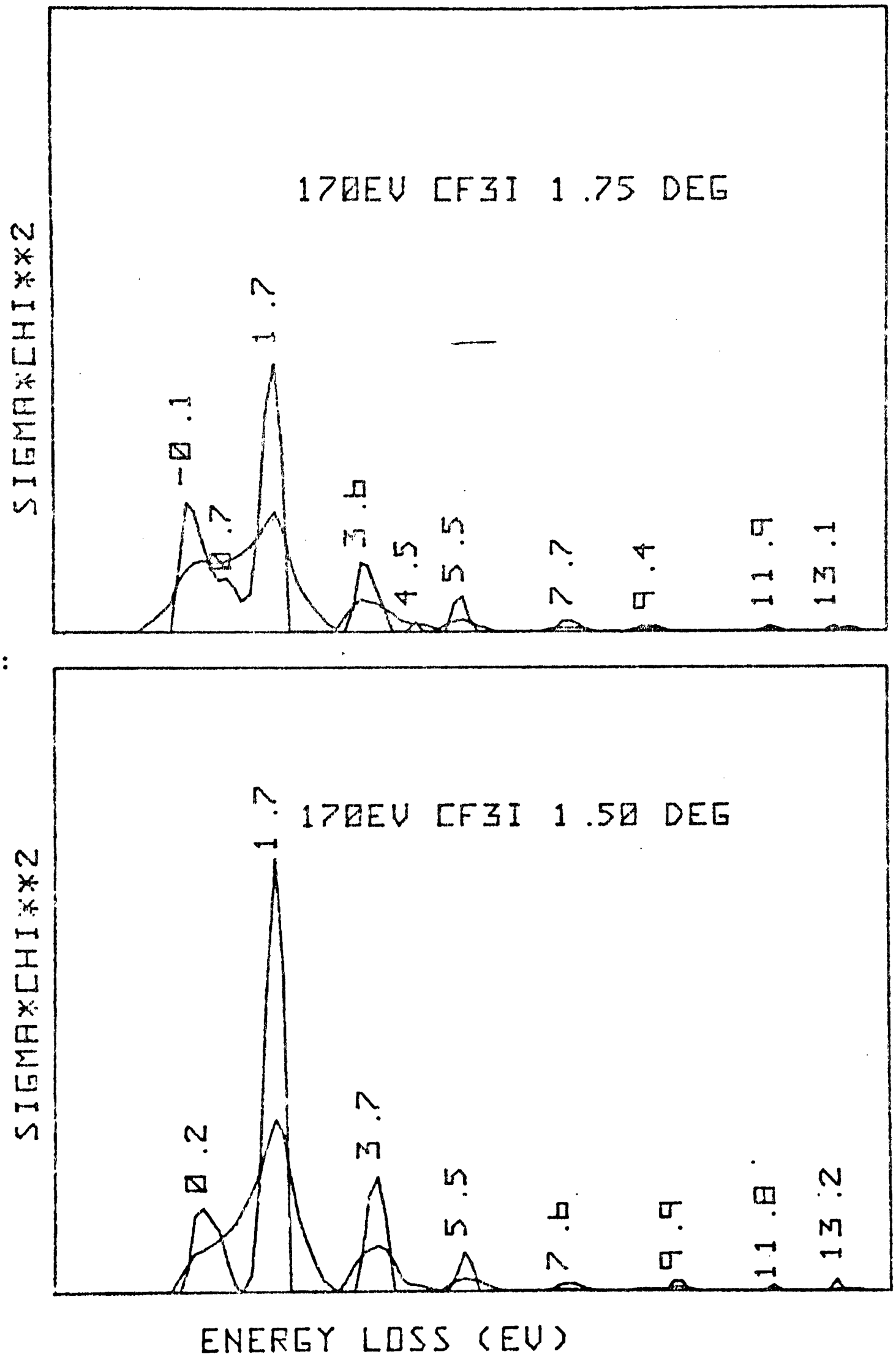
170EV CF3I 1.75 DEG
SIGMA*CHI**2
-0.1
0.7
1.7
3.6
4.5
5.5
7.7
9.4
11.9
13.1
170EV CF3I 1.50 DEG
SIGMA*CHI**2
0.2
1.7
3.7
5.5
7.6
9.9
11.8
13.2
ENERGY LOSS (EV)

Figure 4.56

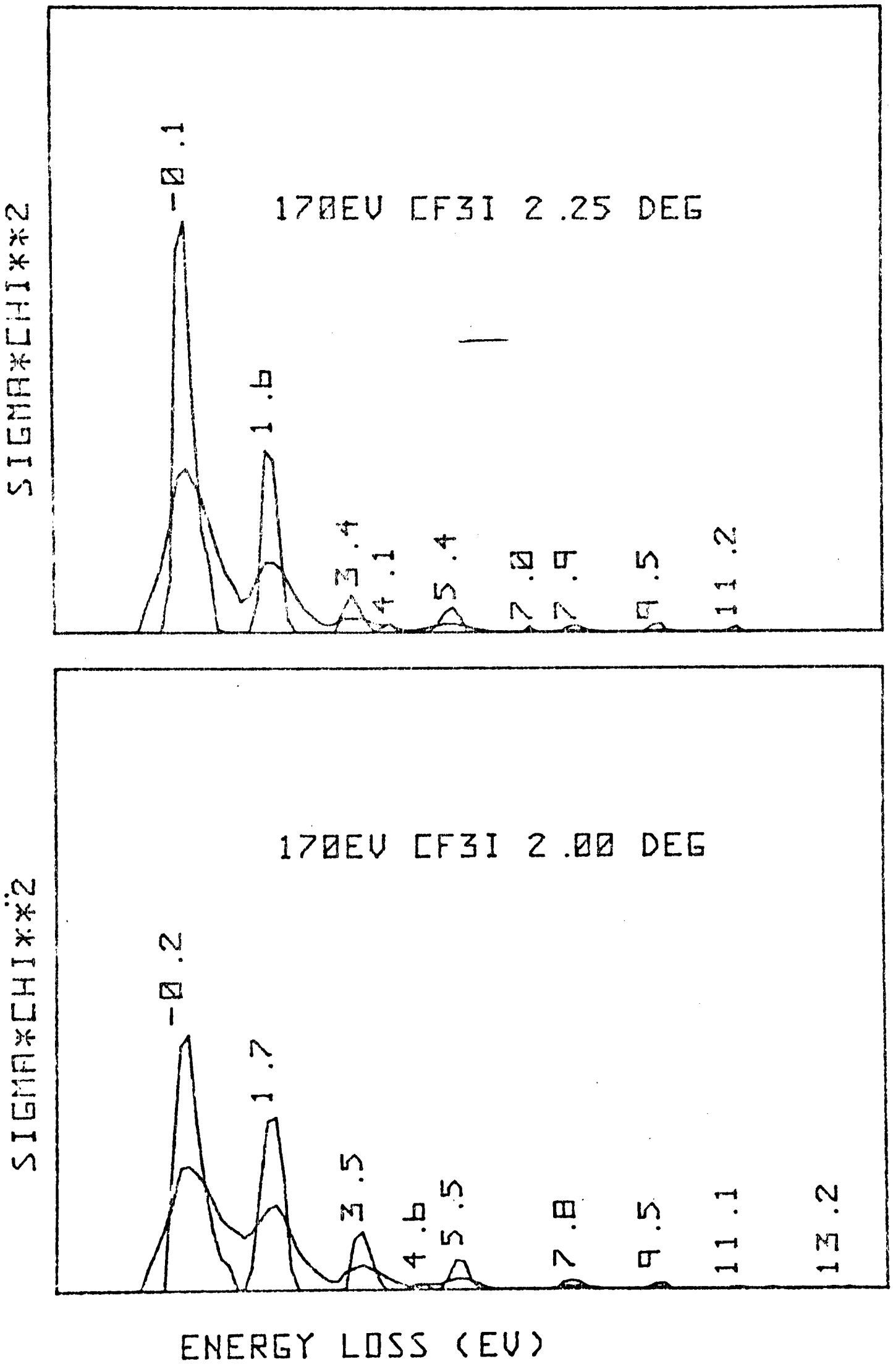
170EV CF3I 2.25 DEG
SIGMA*CHI**2
-0.1
1.6
3.4
4.1
5.4
9.0
9.5
11.2
170EV CF3I 2.00 DEG
SIGMA*CHI**2
-0.2
1.7
3.5
4.6
5.5
7.8
9.5
11.1
13.2
ENERGY LOSS (EV)

Figure 4.57

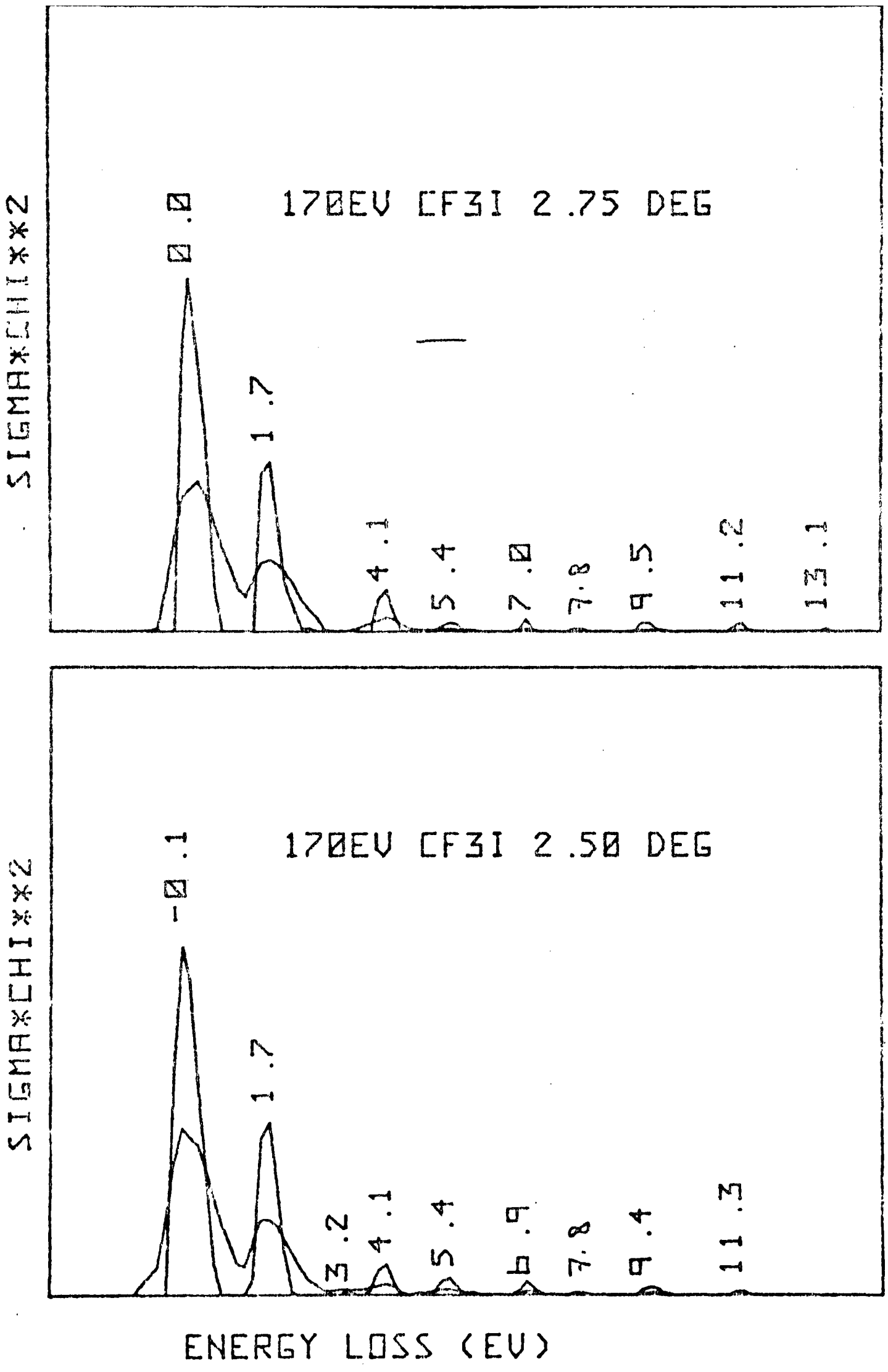
170EV CF3I 2.75 DEG
0.0
1.7
4.1
5.4
7.8
9.5
11.2
13.1
SIGMA*CHI**2
170EV CF3I 2.50 DEG
-0.1
1.7
3.2
4.1
5.4
7.8
9.4
11.3
SIGMA*CHI**2
ENERGY LOSS (EV)

Figure 4.58

TABLE 4.5

170 eV K/CF_3I ENERGY LOSSES

Angle	Process Number and Energy Loss								
	1	2	3	4	5	6	7	8	9
1.00	0.2	1.7	3.8		5.6	7.9	9.9		13.1
1.25	0.2	1.7	3.8		5.6	7.9	9.9		13.1
1.50	0.2	1.7	3.7		5.5	7.9	9.9	11.8	13.1
1.75	-0.1	1.7	3.6	4.5	5.5	7.7	9.4	11.9	13.2
2.00	-0.2	1.7	3.5	4.6	5.5	7.8	9.5	11.1	13.2
2.25	-0.1	1.7	3.4	4.1	5.4	7.9	9.5	11.2	
2.50	-0.1	1.6	3.2	4.1	5.4	7.8	9.4	11.3	
2.75	0.0	1.7			5.4	7.8	9.5	11.2	13.1

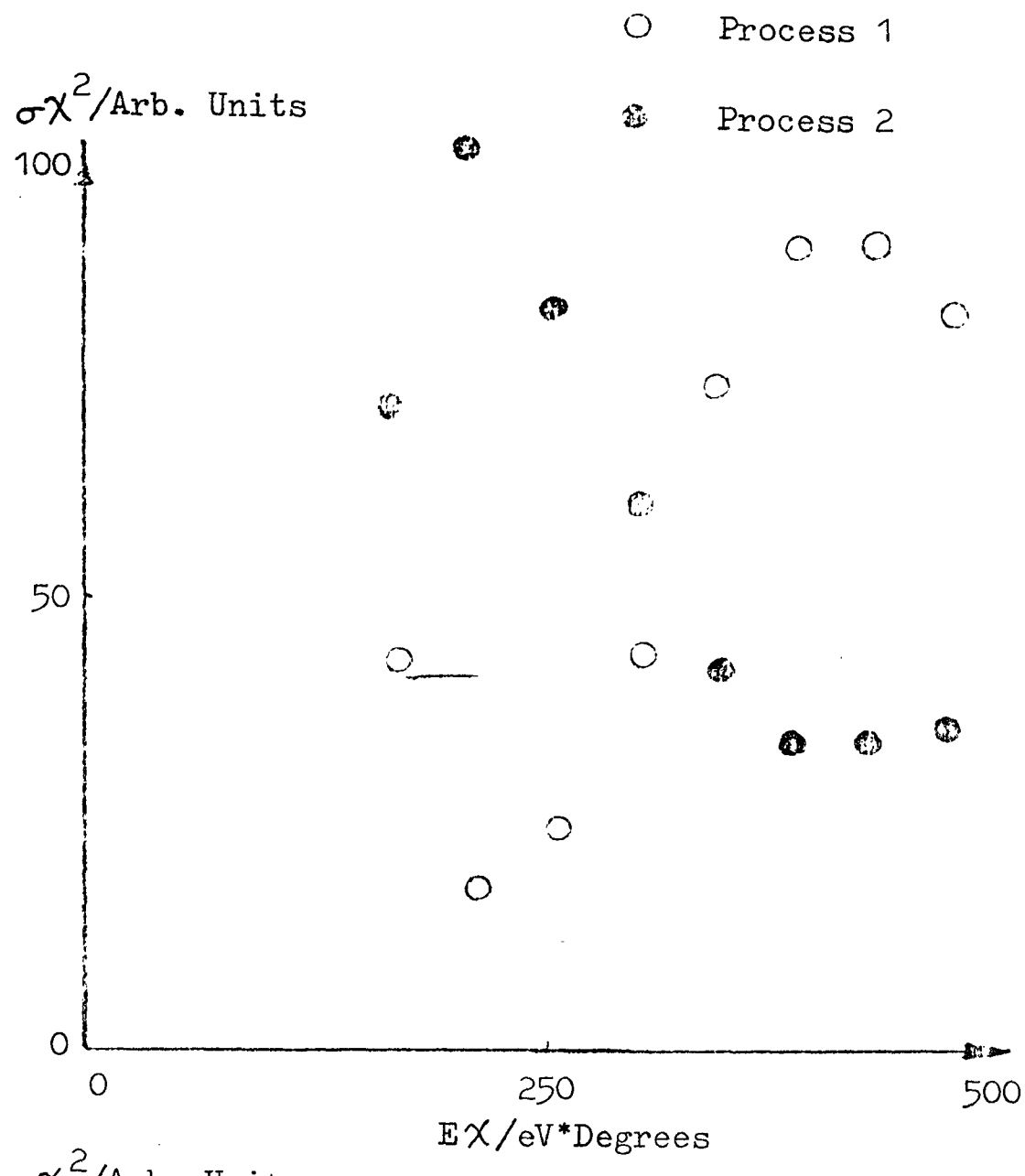

Figure 4.59 : K/CF_3I Differential Cross Sections 170 eV C.M.

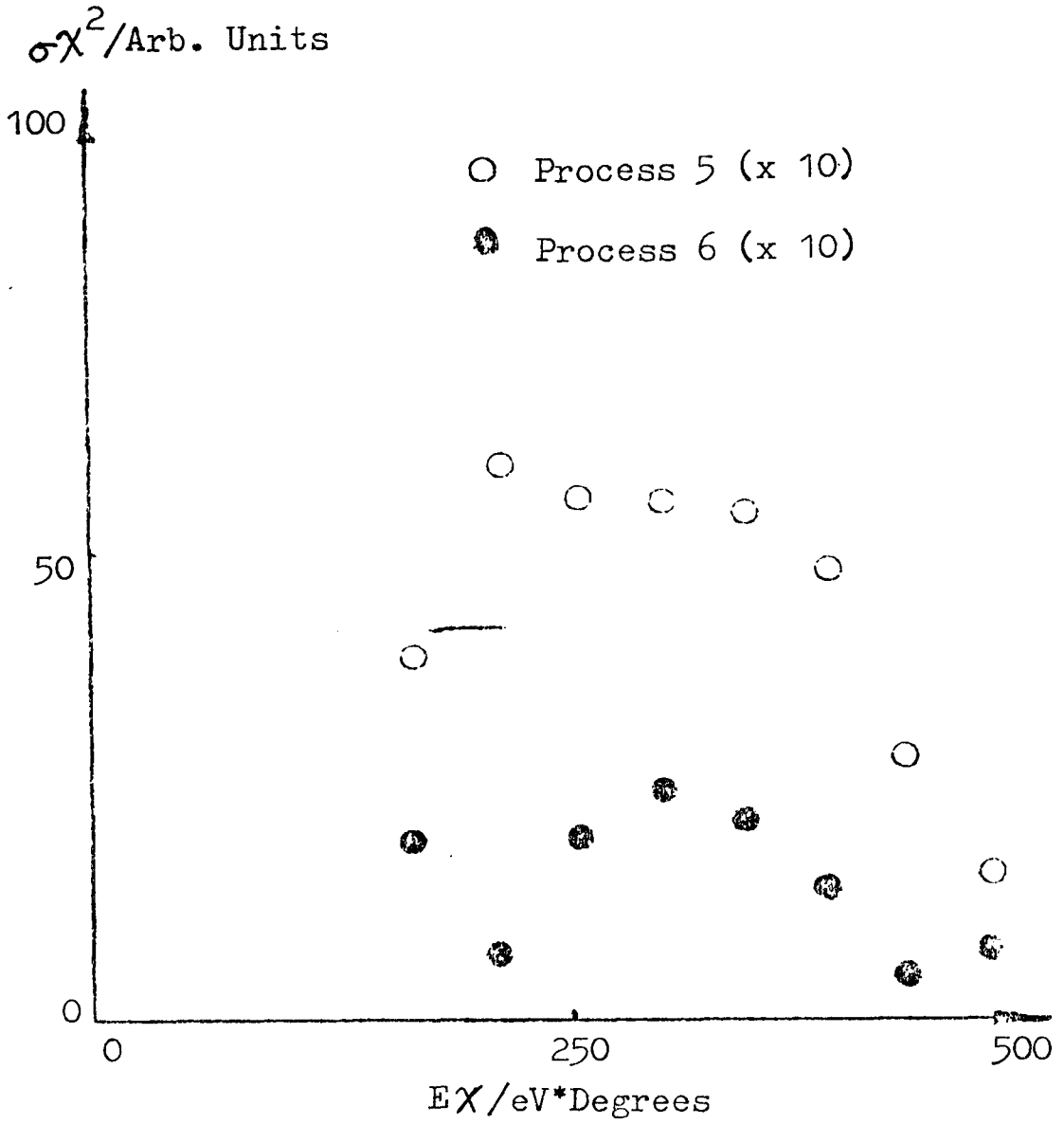

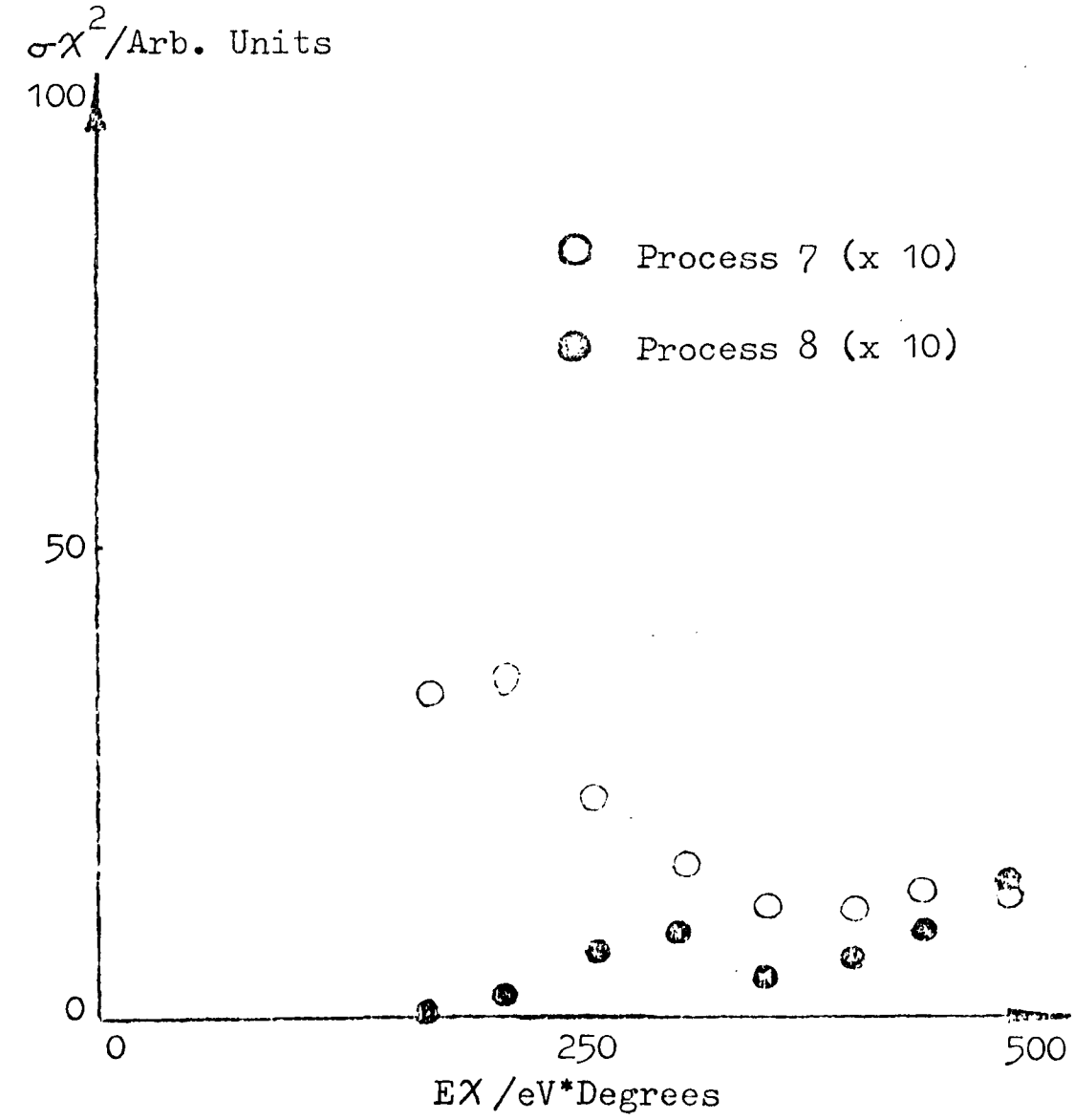

Figure 4.60 : K/CF_3I Differential Cross Sections 170 eV C.M.

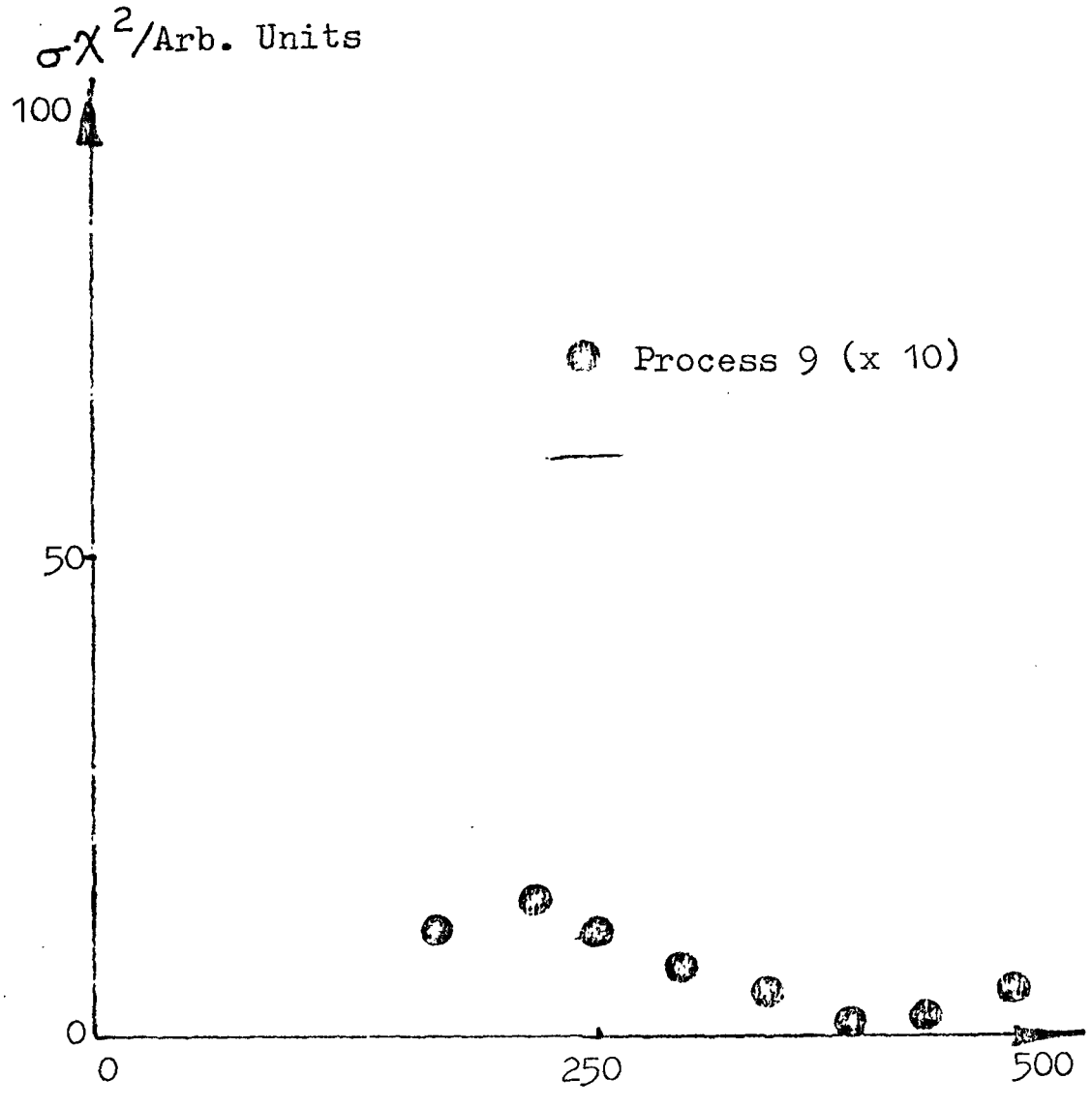

Figure 4.61 : K/CF_3I Differential Cross Sections 170 eV C.M.

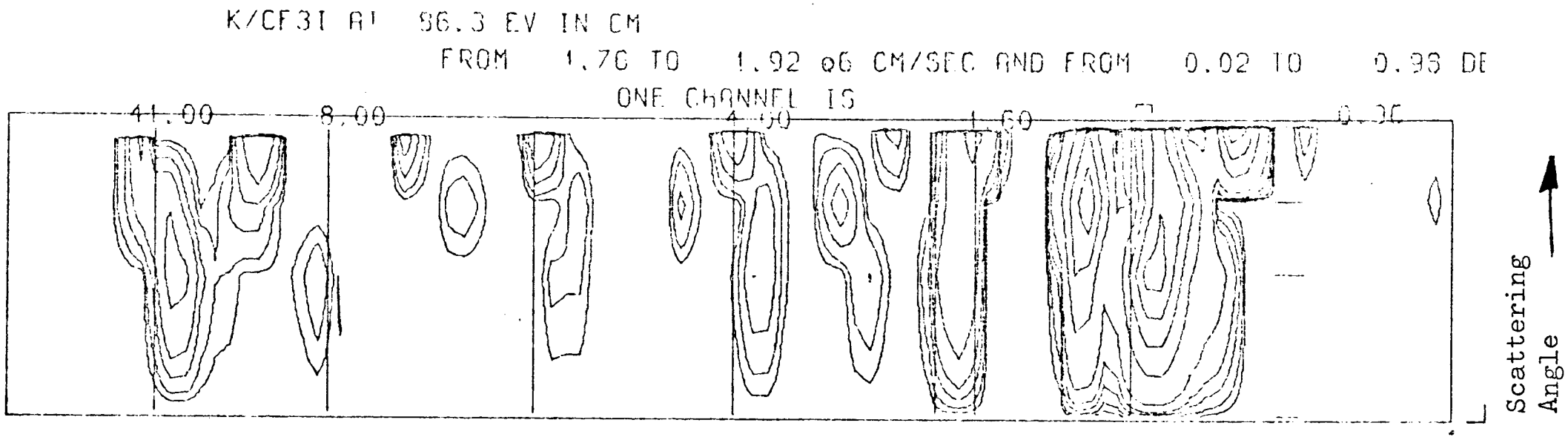

Figure 4.62

Contour map of K/CF_3I at 86 eV C.M.

4.6 K/HI, K/C_3H_7I DATA

The final two sets of data presented involve collisions in which the methyl group is replaced by either a lighter hydrogen atom or the heavier propyl group.

Figure 4.63 shows the contour map for K/HI scattering and Tables 4.6 to 4.8 summarise the energy losses observed.

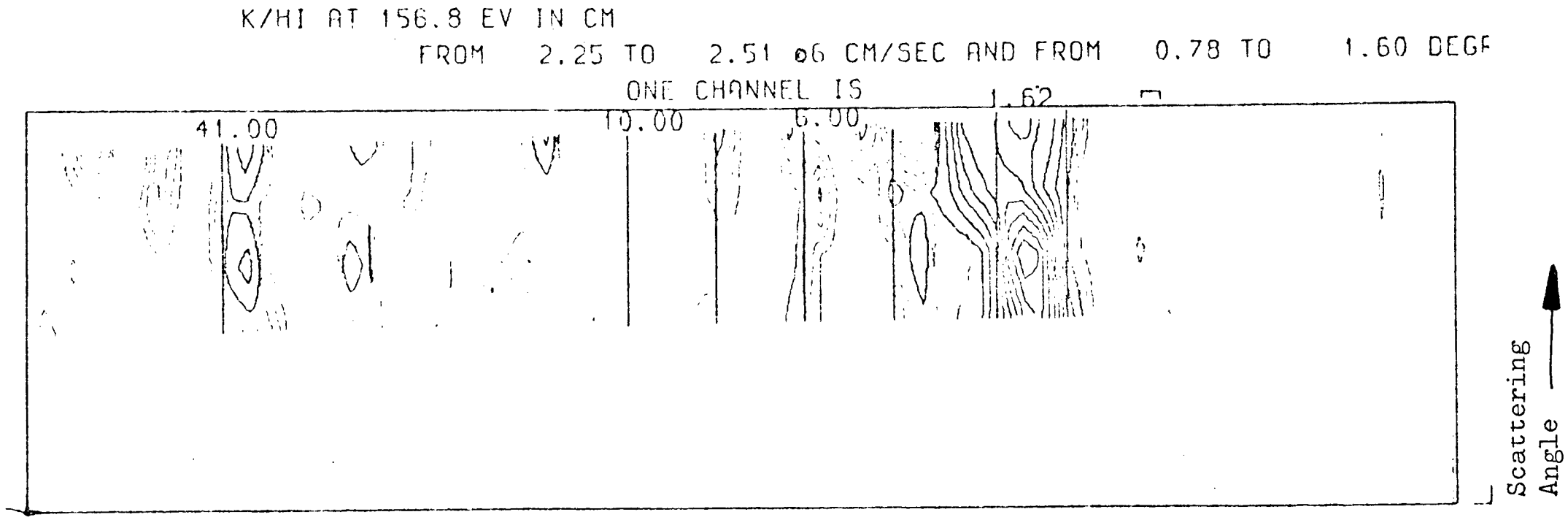

Figure 4.63 : K/HI at 157 eV C.M.

TABLE 4.6

Energy losses in K/CF_3I 86 eV C.M.

1	2	3	4	5	6	7	8
0.0	0.7	2.0	2.6	2.9	3.9	6.2	7.5

TABLE 4.7

Energy losses in K/C_3H_7I 166 eV C.M.

1	2	3	4	5	6	7	8	9	10	11	12
0.0	0.4	1.6	2.2	3.3	4.4	5.1	6.6	8.5	10.8	11.8	13.2

TABLE 4.8

Energy losses in K/HI 156 eV C.M.

1	2	3	4	5	6
0.0	1.6	3.0	5.3	7.4	11.0

CHAPTER 5

DISCUSSION OF THE TIME OF FLIGHT DATA

In discussing the data presented in the last Chapter emphasis has been placed on understanding and explaining the results in terms of as simple a model as possible rather than in developing a sophisticated theoretical treatment. It will be shown that the simplest, "atomic", model whilst partially successful fails to provide an adequate solution and the need for a treatment specifically including the effects of internal motion of the target molecule becomes apparent.

5.1 BACKGROUND

Prior to embarking on the discussion of these results it is worthwhile to pause and consider what may be observed.

The electronically excited states available to the potassium atom fall into the energy range up to 4.3 eV. The lowest lying excited potassium state is the $4^2P_{\frac{1}{2},\frac{3}{2}}$ corresponding to an energy transfer of 1.6 eV. There are a large number of other states extending up to the I.P. at 4.34 eV. The manifold of electronically excited states available in the alkyl halides falls into three classes corresponding to valence transitions in the C-X bond of $n \rightarrow \sigma^*$ type, Rydberg transitions to high nL states similar to those of the halide atom and valence $\sigma \rightarrow \sigma^*$ transitions in the C-H bond. Transitions corresponding to all these three classes are observed in the optical spectra though the C-H transitions are seen only as a continuum background to the other processes (HER 66, BOS 72, WAN 77). Photodissociation of the alkyl halides with radiation

in the region 3.5 - 6 eV occurs via the continuum A state ($n \longrightarrow \sigma^*$) and produces both $X_{\frac{3}{2}}$ and $X_{\frac{1}{2}}$ halide atoms. The same σ^* orbital occupied in the molecular negative ion is responsible for the translational excitation seen in the reaction $K + RI \rightarrow KI + R$ (HER 73), a classic example of electronic harpooning.

In considering the time of flight data it is worth splitting the results into three energy loss regimes corresponding to potassium excitation (0 - 4 eV), A state excitation (4 - 6 eV) and lastly all peaks above 6 eV. Table 5.1 summarises all the energy losses reported in Chapter 4 and compares the optically observed transitions with the collision induced energy losses.

5.2 POTASSIUM EXCITATION AND ELASTIC CHANNEL

Before a model can be developed to explain the inelastic processes observed it is necessary to decide on the mechanism of excitation. If these proceed because of mixing of states the Massey criterion must be satisfied. This states that

$$\Delta E \Delta t \approx \hbar \approx \frac{\Delta E \Delta R}{\text{velocity}} \approx \hbar$$

for mixing of states to take place.

ΔE = Energy difference of states

Δt = Collision lifetime

In the results reported here we observe low angle excitation very far removed from fulfilling the above criterion, leading to the conclusion that some specific process such as curve crossing must be involved.

TABLE 5.1 : TIME OF FLIGHT ENERGY LOSSES

Process Number	TARGET AND C.M. ENERGY				
	HI 157	CH_3Cl 115	CH_3I 81 164	CF_3I 86 171	C_3H_7I 166
1	0.0	0.0	0.0 0.0	0.0 0.0	0.0
2		1.0 2.2	0.6 1.3 1.0	0.7	0.4
3	1.6	2.5	2.0 1.7	2.0 1.7	1.6
4		3.7	3.1 2.8	2.6	2.2
5	3.0		4.0 3.6	2.9 3.7	3.3
6		4.8	4.6 4.8	3.9 4.5	4.4
7	5.3		5.0	5.4	5.1
8		6.0	5.7 5.5	6.2	
9	7.4	7.0	6.2 6.4	7.5 7.8	6.6
10		9.8	8.0 8.4	9.5	8.5
11		11.0	10.4	11.1	10.8
12	11.0		12.4	13	13.2
13				14.8	
14		7.7	6.0 6.4		11.8

OPTICALLY OBSERVED TRANSITIONS

K^* States
1.6 → 4.3 eV

A States
Continuum absorption
onset 3.4 → 4.5 eV.

Assorted Rydberg transitions
$\sim$ 6 eV → I.P.
I.P. $\sim$ 10 eV
C-H transitions

COLLISION INDUCED ENERGY LOSSES

Discrete energy losses

All but one process shows constant energy loss with increasing χ.

Fewer states than optical spectra.

Large energy losses at very small $E\chi$.

The simplest way in which excitation of the K* electronic states can take place involves a transition to the K^+/RX^- ionic potential surface. The vertical electron affinities of these alkyl halides are sufficiently small for the ionic state to intersect all the K* channels (including the ionised continuum) and thus to provide a route for populating these states. The harpoon model, equivalent to adiabatic behaviour at the ionic/covalent potential surface crossing, is well established as the mechanism for reaction in many alkali metal systems at thermal energies. At the collision energies of the present work the reaction channel is essentially closed because the fast K^+ ion cannot accelerate the X^- ion rapidly enough to capture it before leaving the ionic surface. It is proposed that the excitation mechanism involves crossings to the attractive branch of the ionic potential. Crossings on the repulsive wall of the potentials would lead to onset of the inelastic processes at larger $E\chi$ values than those observed.

A number of further assumptions have to be made in order to test the model. As stated in the introduction, the emphasis is placed on developing a simple model to account for the broad features of the observed scattering and, as a first approximation, the collision is assumed to be isotropic and sudden with respect to R-X motion, ie the R-X bond is frozen at its equilibrium value throughout the collision. The diabatic potential surfaces are then solely a function of the K-X co-ordinate. The potentials are shown in Figure 5.1.

The differential cross sections are then obtained by using the small angle scattering formulae (equations 5.1, 5.2) and by evaluating the Landau Zener crossing probability (equation 5.3)

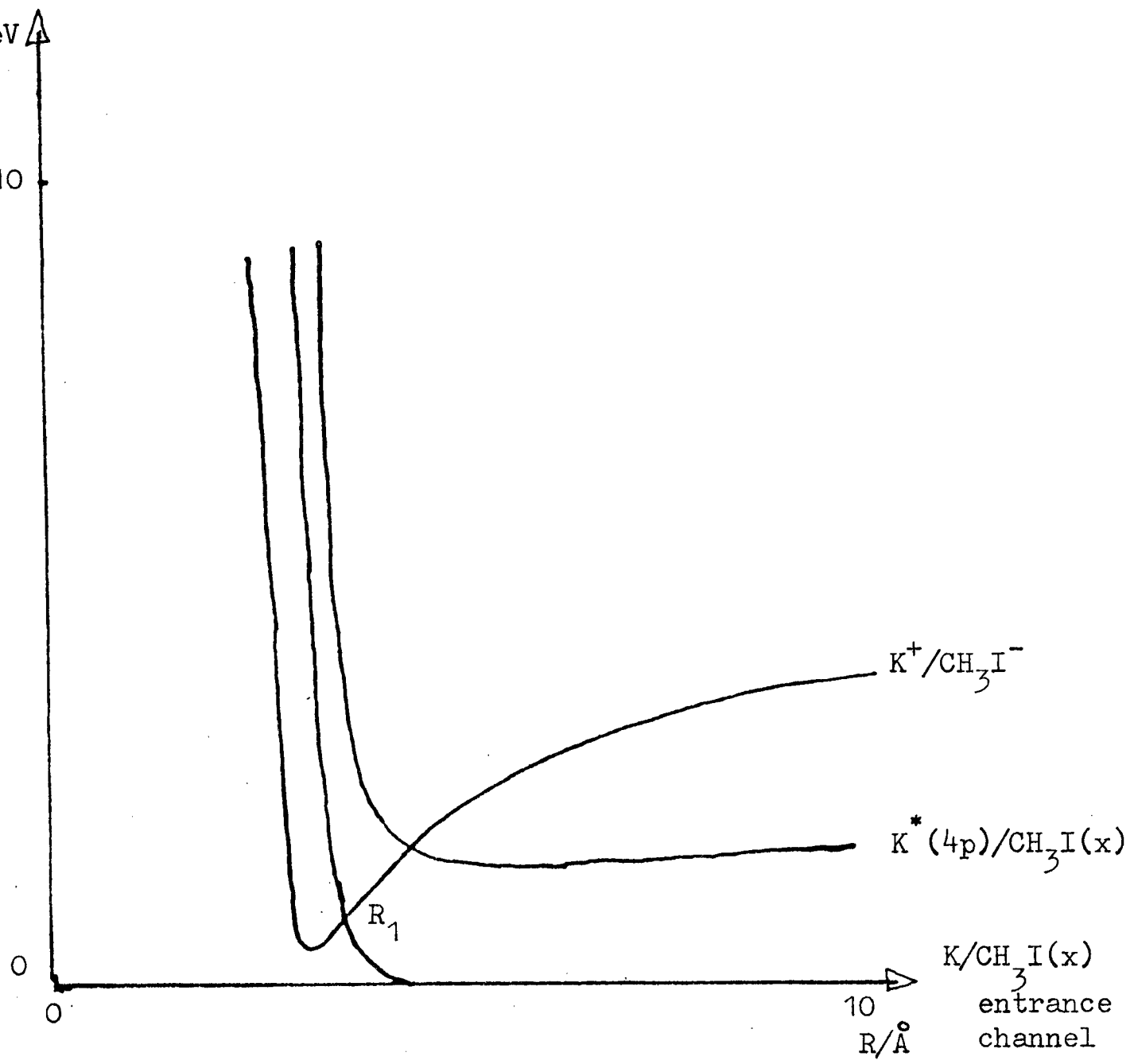

Figure 5.1 : Schematic diagram of potential curves

at each traversal of the crossing regions. It should be noted that any exit channel can be reached via two paths, according to whether or not the electron is transferred on the first passage of the ionic/covalent crossing.

$$\chi = SC\pi^{\frac{1}{2}} \left\{ \frac{\Gamma\left((S+1)/2\right)}{\Gamma\left(\frac{S}{2}+1\right)} \right\} \Big/ \left(2Eb^{S}\right) \qquad 5.1$$

$$\sigma(\chi) = \frac{b}{\operatorname{Sin}\chi \left| \frac{d\chi}{db} \right|} \qquad 5.2$$

$$P = \exp\left(-2\pi^{2}\, \Delta E^{2} \Big/ h\sigma \left| W_{1}' - W_{2}' \right|\right) \qquad 5.3$$

where S = repulsive power of the potential

χ = scattering angle

E = collision energy

b = impact parameter

σ = differential cross section

ΔE = energy gap between adiabatic potentials

W_{1}' = gradient of diabatic potential at the crossing point

σ = radial velocity

h = Planck's constant

P = the probability that there is no change in the electronic state during the passage of the crossing region.

The model is at least partially successful inasmuch as potassium excitation is predicted to onset at very low scattering angles. However the model is less satisfactory in predicting the change in angular onsets of the K* excitation with incident energy observed in the K/CH_3I data. The thresholds are observed to

occur at lower Eχ values in the 81 eV data, whereas the basic model outlined above necessarily predicts constant Eχ values (assuming straight line trajectories). More important are the differences between the predicted and observed energy losses. The model only permits energy losses corresponding to the electronic states of the separated species, the lowest of these being the K(4p) lying 1.62 eV above the ground state. Some of the results show peaks in the spectra at energy losses lower than this. These are clearly not assignable to any electronic excitation and must be associated with vibrational excitation. The most drastic assumption of the basic model is the neglect of the internal motion of the target molecule during the collision. Assuming a vertical transition the electron transfer at the crossing point yields $(RX)^-$ in a strongly repulsive state. During the collision lifetime, typically 10^{-14}S, changes in the C-X bond distance can be expected to occur which will greatly alter the electron affinity and hence the position of the ionic/covalent crossing. Such effects have been discussed by other workers in connection with chemical reaction and chemi-ionisation (ATE 77). The potentials for $CH_3I(x)$, CH_3I^- and $CH_3I(A)$ are shown in Figure 5.2. Stretching of the C-X bond will move the crossing to larger R values (Figure 5.3) and on the return of the electron substantial vibrational excitation can be expected in the C-X bond. The extent of this energy transfer clearly depends on the time spent on the ionic surface, the gradient of the negative molecular ion potential and the reduced mass of the target molecule. For collisions with $b < R_1$ there are two classical paths leading to any angle of deflection, corresponding to diabatic or adiabatic behaviour at the crossing point. This results in each electronic

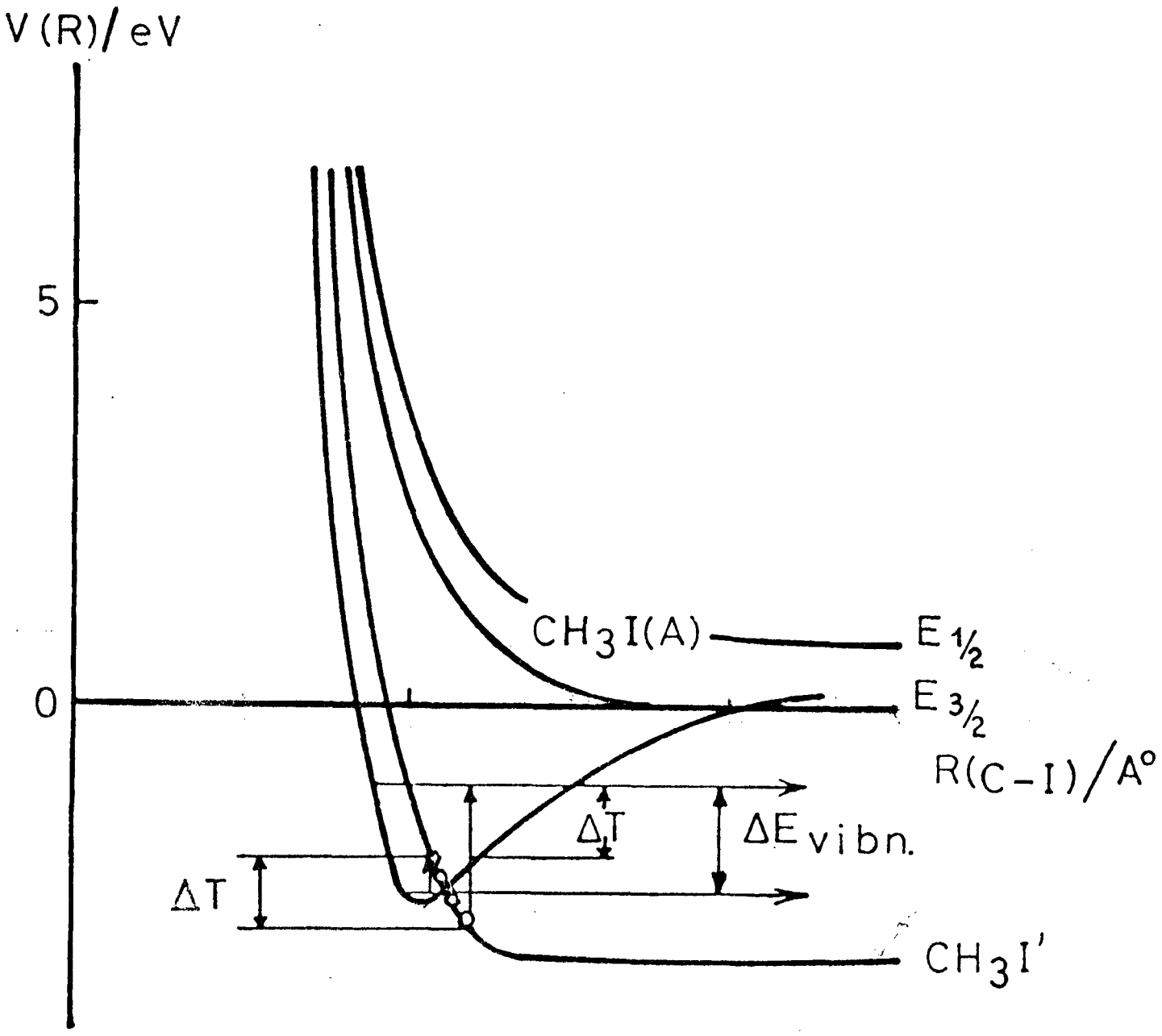

Figure 5.2 : Potentials for CH_3I

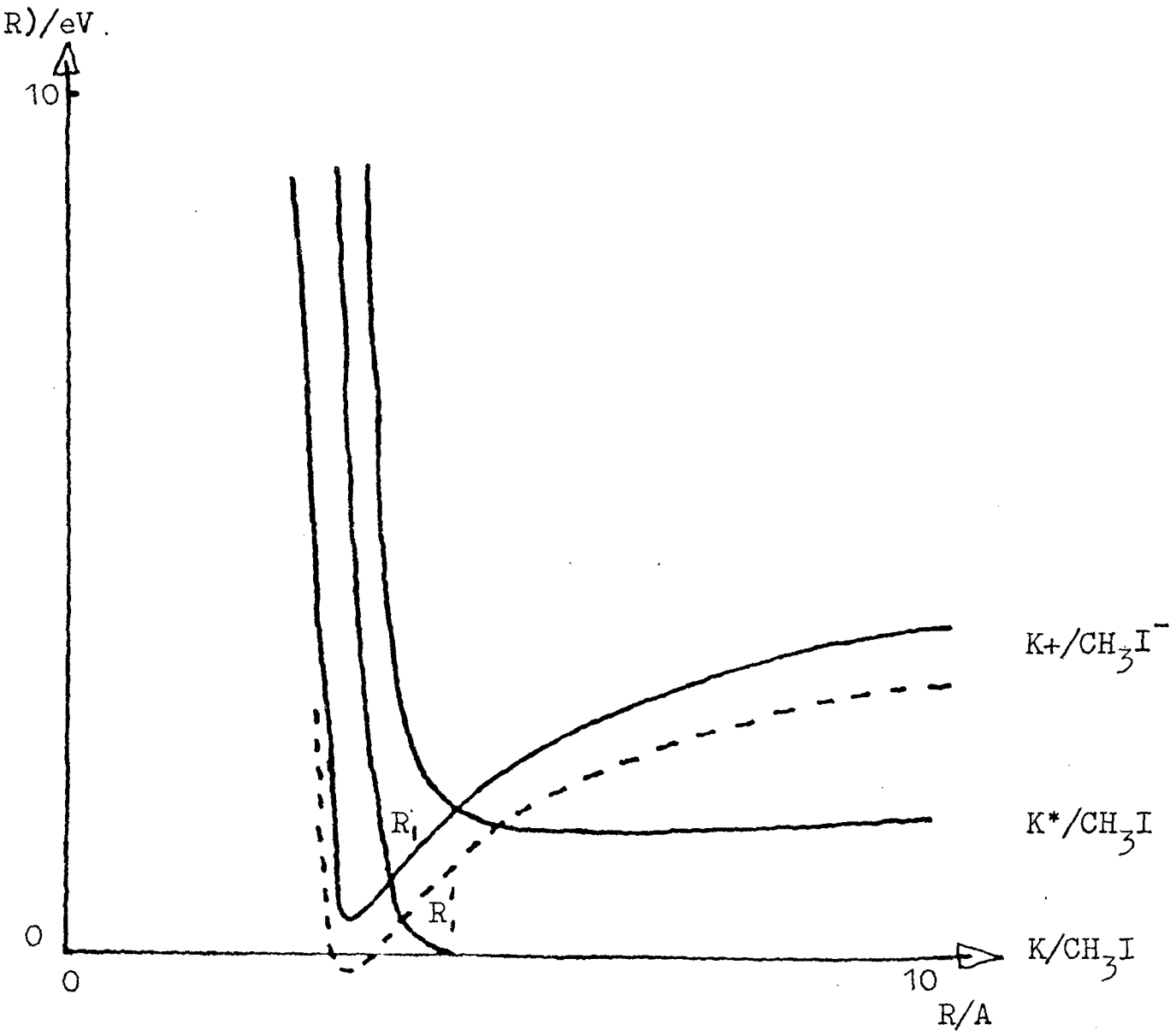

Figure 5.3 : Potential curves for K/RX type system. The solid ionic curve corresponds to C-I in its equilibrium position. Stretching C-I changes the electron affinity and gives the dotted ionic potential with crossing at $R_1' > R_1$

exit channel being accompanied by two peaks in the time of flight spectrum.

Figure 5.4 shows the lower energy losses for each of the data sets, plotted as a function of the collision time, reduced mass of the oscillator and the gradient of the negative ion potential (WEN 69). The losses are observed to be proportional to the collision lifetime and rise with decreasing oscillator mass as predicted by the model.

The model is again tested with the term -

$$V_{ion}\ (R_{R-X}) = A \exp\left\{ - \beta\ (R_{RX} - R(o)_{RX}) \right\} \qquad 5.4$$

introduced into the total potential energy. The potassium-halide atom interaction remains coulombic and there is no K-R interaction.

This model is, however, still inadequate. If the parameters used in $V_{ion}\ (R_{R-X})$ are taken to be those of the isolated ion (WEN 69) too much vibrational excitation is predicted, even in the ground electronic exit state. As the R-X bond stretches the crossing point moves to larger R values leading to a longer time spent on the ionic surface and a runaway situation is obtained with extensive bond dissociation. The data show the vibrational energy gain in the ionic (K(4S) and K(4p) (ionic and covalent)) to be quite small ($\leq$ 1 eV in most cases) and nearly constant with increasing $E\chi$ after threshold.

It thus seems that the RX^- ion is perturbed by the passing K^+

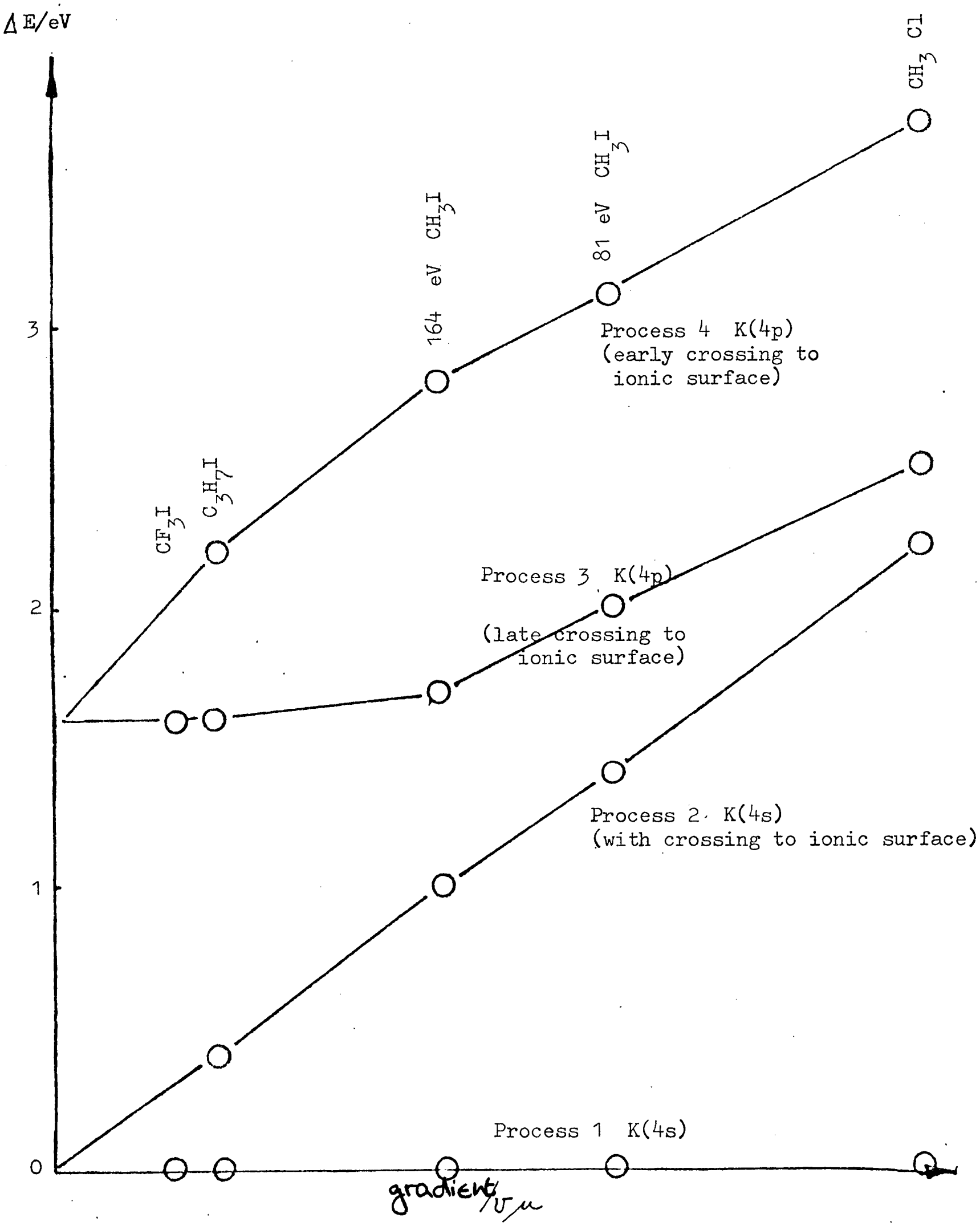

Figure 5.4 : Energy loss plotted against collision time and reduced mass of oscillator and gradient of negative ion potential.

particle. It is not sufficient to adjust the value of β in equation 5.4 since if the vibrational energy gain in the K* (ionic) channel is fitted, too little energy loss is predicted in the K(4S) (ionic) exit channel. The results indicate that the R-X bond distance increases rapidly following electron transfer but that the repulsion soon drops to near zero. This suggests that the form of equation 5.4 is wrong and that V_{ion} also depends on the R-K separation. This is not unreasonable and could be interpreted as repulsion between the departing alkyl group by the K^+ ion hindering the bond stretching, or as a change in the bond order of RX^- due to partial back transfer of the electron to K^+.

The potential surface is changed slightly therefore and an effective potential is used for the RX^- ion (Figure 5.5). The magnitude of the barrier shown on the ionic potential varies with the K/RX separation and is only present at very short separations. This should not be regarded as a physically exact description of the system but as an empirical adjustment made in an attempt to interpret the observations. It is not unreasonable to expect the potential surface in the three-body "close encounter" occurring during the collision to be significantly different from the situation with the isolated RX^- ion and the K^+ particle at infinite separation.

Figure 5.6 shows that this model predicts energy losses in good agreement with observation. The energy losses increase rapidly following onset and thereafter remain constant. Smaller impact parameters, leading to wider scattering angles, result in a

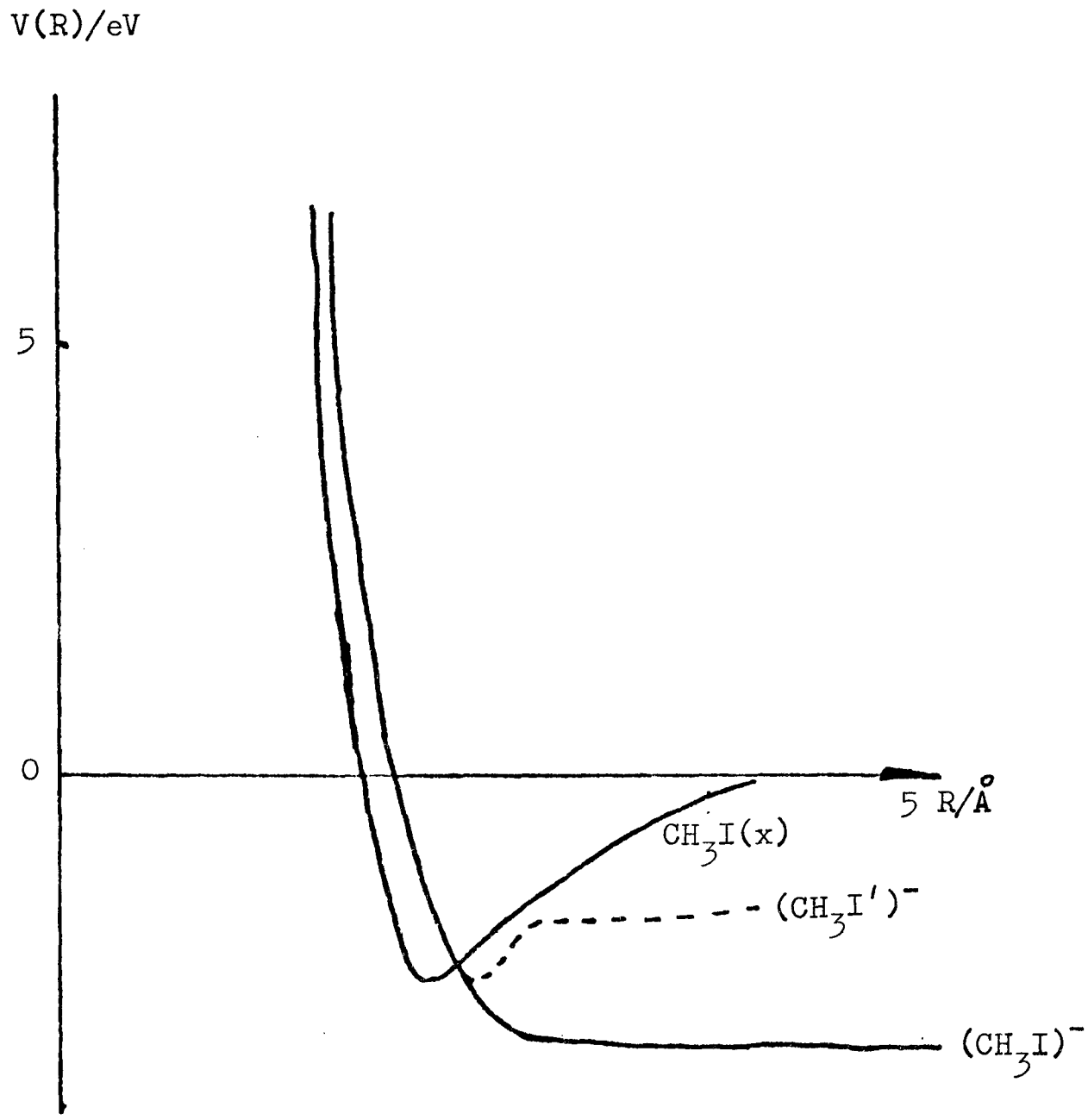

Figure 5.5 : Potentials for RX system. The dotted curve shows the perturbation introduced by the K^+ ion and the form of the effective potential used in these calculations.

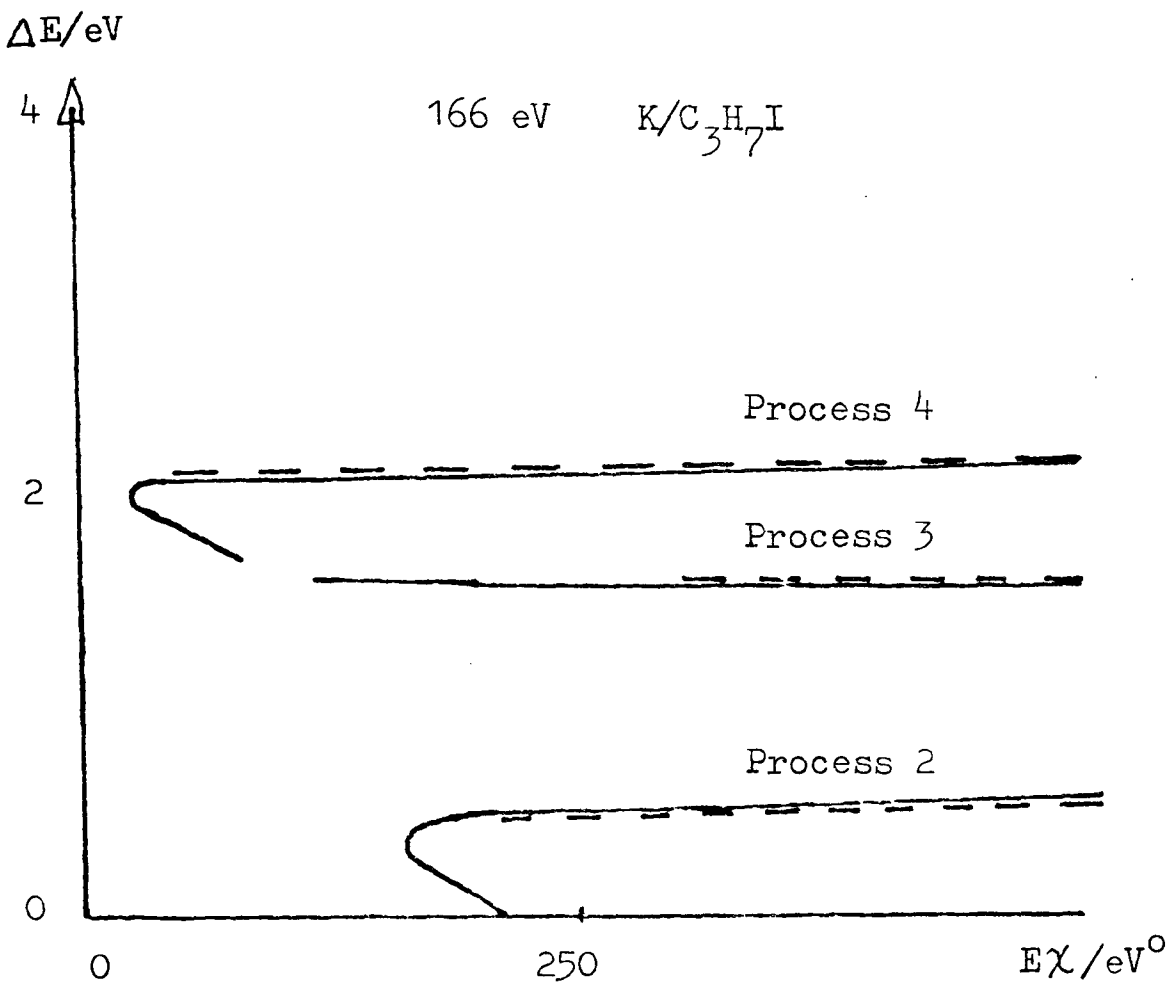

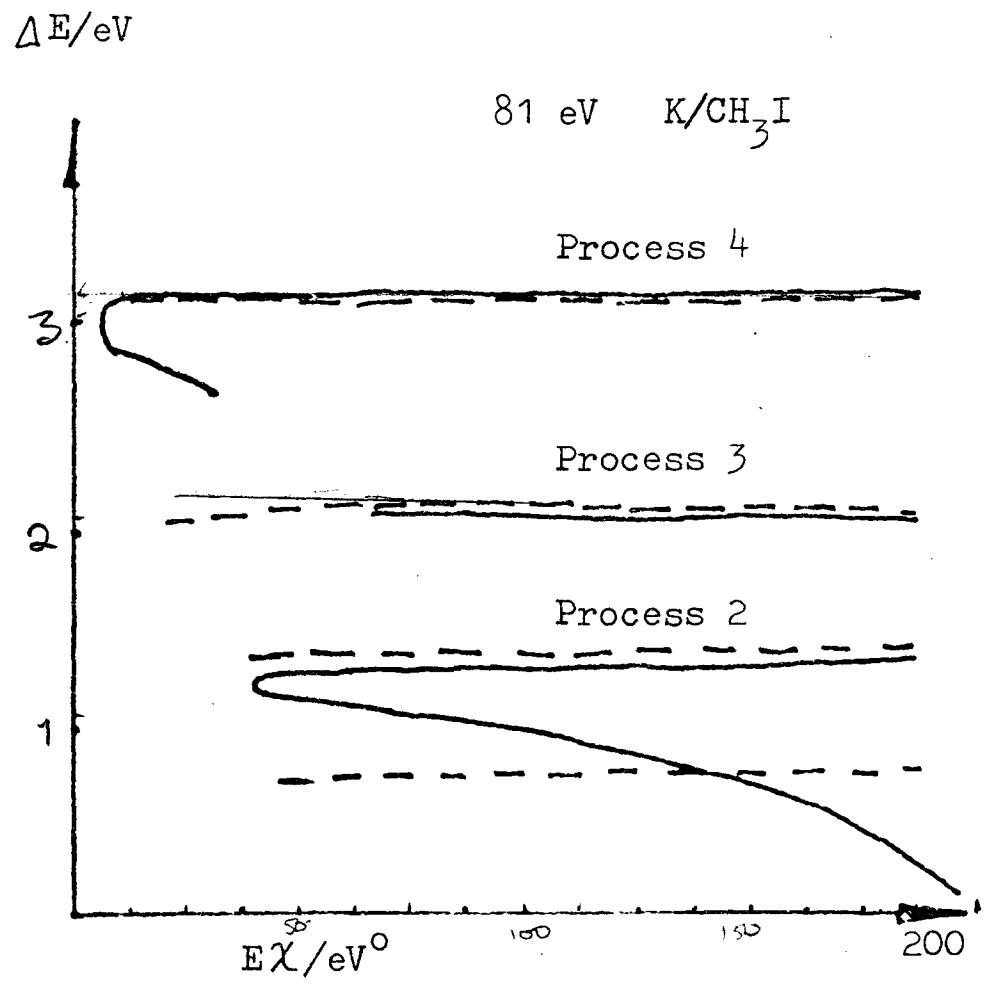

Figure 5.6a : Predicted and observed energy losses. The solid lines are the model predictions, the dotted lines show the average energy losses observed in each channel.

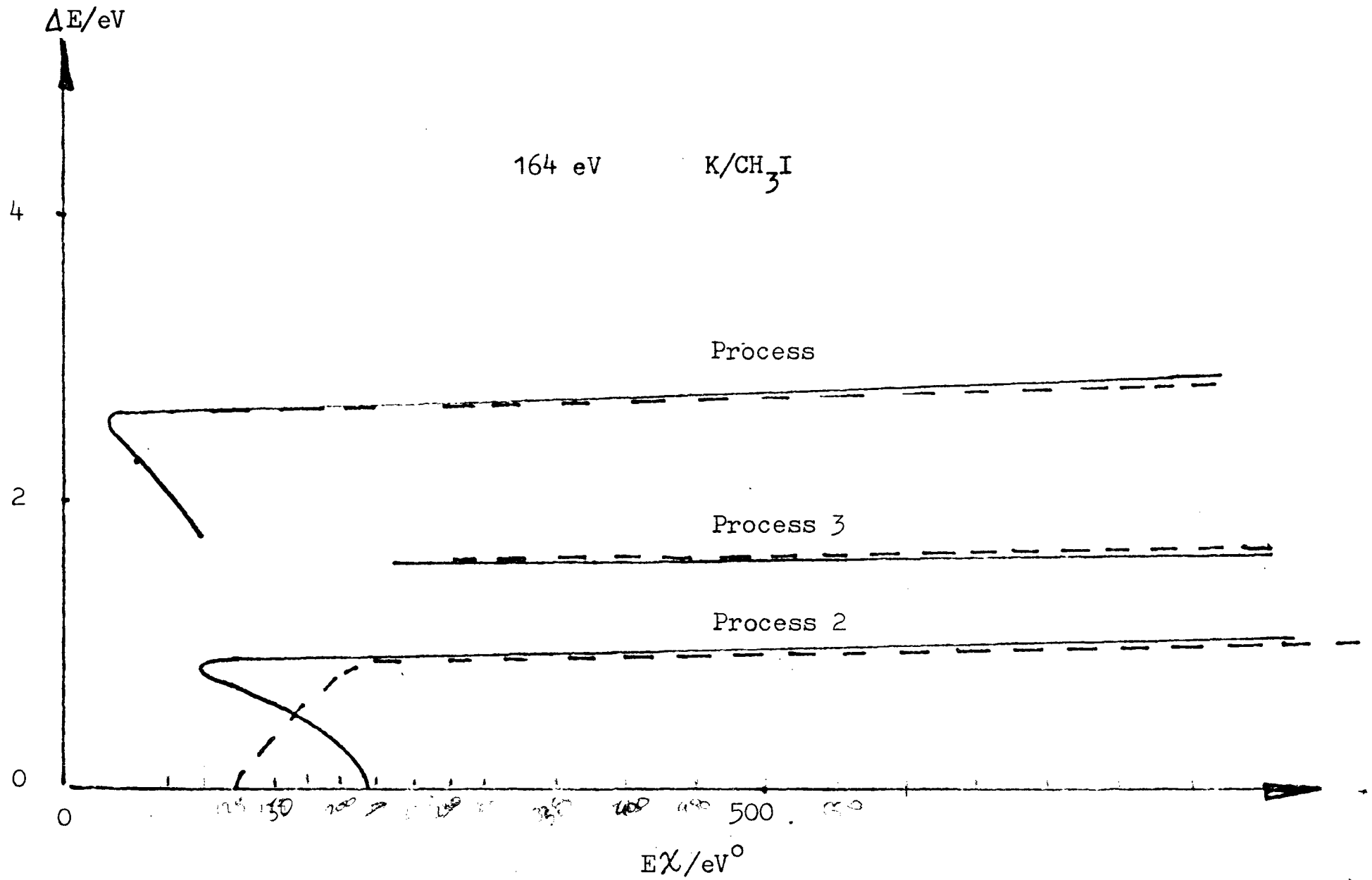

Figure 5.6b : Predicted and observed energy losses. The solid lines are the model predictions, the dotted lines show the average energy losses observed in each channel.

greater barrier being introduced into the RX^- potential, thereby preventing the runaway situation experienced with the unperturbed potentials.

It will be seen that adiabatic behaviour at the crossing point leads to scattering into narrower angles even in the electronic ground state exit channel. This rainbowing is a result of the increase in the crossing radius due to the changing electron affinity which in turn means that more time is spent on the attractive branch of the K^+/RX^- potential (see Figure 5.3). This effect is most pronounced in the 81 eV CH_3I and the 115 eV CH_3Cl data. Smaller impact parameters lead to smaller scattering angles and increased energy losses as the vibrational excitation approaches its maximum value. Thus we note two energy losses are reported for process 2 in these data sets. In the case of the CH_3I this arises because of the longer collision time and with the CH_3Cl it is because of the smaller reduced mass of the oscillator.

A listing of the program is given in Appendix C and its structure is shown below. The ionic surface is accessed at R_1, and, assuming a straight line trajectory, the time spent on the surface, T, can be calculated from b and σ. The acceleration on the system is calculated from $\frac{dV}{dr}$ and the change in the C-X bond length calculated using classical equations of motion.

On return to the main program the crossing radius is recalculated with the electron affinity appropriate to the new C-X bond length. If this is significantly different from the previously calculated

crossing radius then the system will be unable to cross back on to a neutral surface after time T. The trajectory continues on the ionic surface for the extra time ΔT and the changes in the target molecule geometry throughout this period once again have to be evaluated. This iteration takes place until the crossing radius becomes nearly constant, allowing the system access to the neutral surface.

Throughout the collision the separation of the K^+ ion and the $(CH_3I)^-$ has to be calculated in order that the perturbation of the ionic surface by the K^+ can be taken into account in calculating $\frac{dV}{dr}$.

i Input model parameters

ii Output potentials if desired

iii Select initial impact parameter, b

iv Does trajectory involve crossing on to ionic surface?

NO — YES

v Calculate time on ionic potential, T, from b and crossing radii and divide into 50 intervals.

vi Evaluate $\frac{dV}{dr}$ and acceleration of C-I system

vii Find new r at end of T/50 interval.

viii Is time on ionic potential $\lessgtr$ T

YES — NO

ix Return to main program and calculate new crossing radius, R_n'

x Is $|R_n' - R_n| > 0.005\ R_n$?

YES — NO

xi Calculate $\chi(b)$, $\sigma(\chi)$ and Energy loss using small angle formulae for the appropriate portions of each potential curve.

xii Output results and select new b.

The hydrogen iodide data was not plotted on Figure 5.4 due to the enormous difference in the magnitude of the reduced masses. On the basis of the model presented here the HI^- molecule would be expected to rapidly fly apart once the ionic surface is accessed. Figure 5.7 shows the differential cross section data collected for K/HI collisions at 157 eV c.m. and, even allowing for the large error bars, the decrease in scattered intensity expected can be seen. Once on the ionic surface the H-I bond stretching moves the crossings back to the neutral K/HI surfaces to large K-HI separations so rapidly that the K^+ ion becomes trapped on what is simply a K^+/I^- potential curve. The crossing radius for this system is at about 11.3Å and the crossing probability is known to be very small. Thus no neutral flux is observed at scattering angles corresponding to impact parameters smaller than R_1.

Further evidence of the "trapping" is shown in Figure 5.8, the differential cross sections for K/CH_3I at 81 and 164 eV c.m. These show the intensity of all the neutral exit channels summed. Only a small decrease in total intensity is observed in the 164 eV results, whereas a dramatic reduction is seen in the 81 eV data. This suggests that at the lower collision energy dissociation of the CH_3I molecule is taking place, leaving the potassium in its ionic state.

For comparison, the dashed line shows the calculated cross section for single surface scattering from the ground state potential. This curve is not significantly different to the measured cross section for the 164 eV collisions. In contrast, the 81 eV data

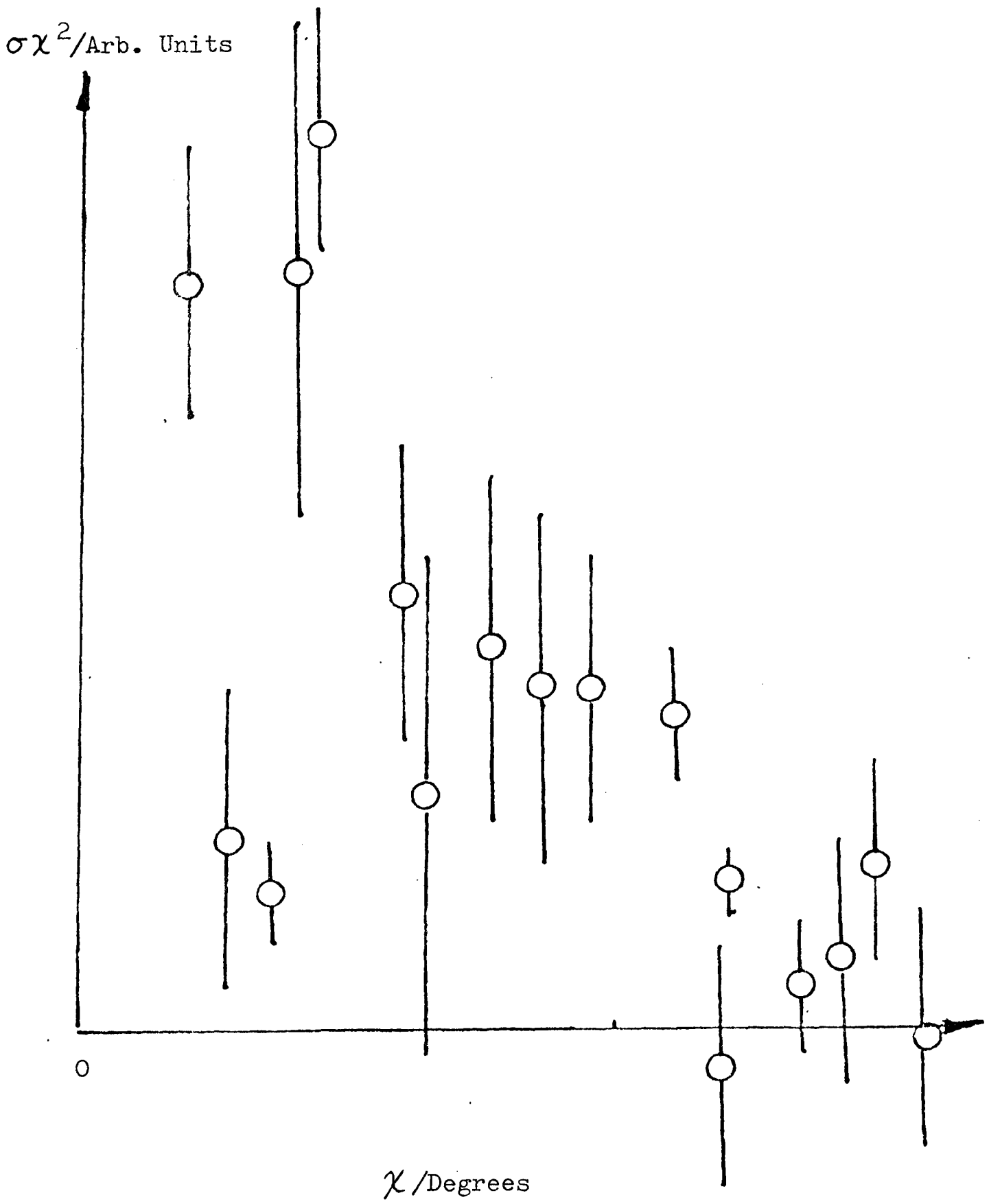

Figure 5.7 : Differential Cross Section for 157 eV K/HI

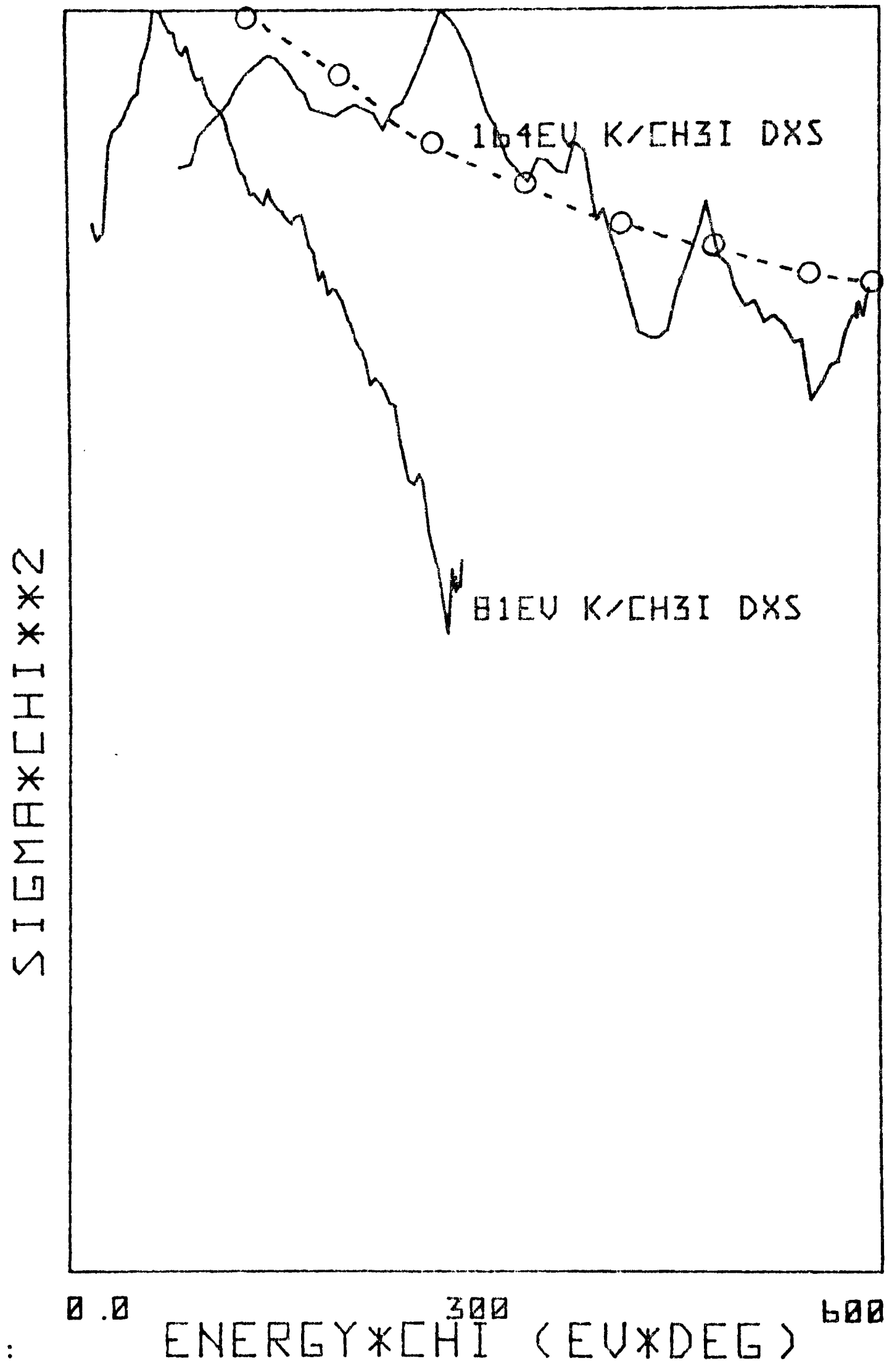

Figure 5.8: K/CH_3I Differential Cross Sections

indicates that substantial ionization is taking place.

Defining -

$$P_{ion}(\chi) = \frac{\sigma calc(\chi) - \sigma obs(\chi)}{\sigma calc(\chi)}$$

where $P_{ion}(\chi)$ is the probability of the system exiting in the ionic state, we can use the deflection function to extract the ionization probability as a function of impact parameter.

b	P_{ion} (b)
3.303	0
3.303	0
3.274	0.3
3.253	0.36
3.232	0.38

This illustrates clearly the effect of longer times being spent on the ionic surface with the target molecule re-arrangement giving rise to trapping on the ionic surface and increased probability of ionization.

Having accounted for the energy losses observed less than 4 eV it is necessary to attempt to fit the intensities observed in these exit channels. Attention is focussed on the CH_3I data since it is only for this collision system that correctly normalised differential cross sections are available. Here too, however, difficulties are encountered in matching the observations with the predictions of the proposed model. The cross sections to be discussed are shown in Figure 4.33. Processes 1 and 2 are

associated with scattering in the electronic ground state with motion at separations less than R_1 taking place on the neutral and ionic surfaces respectively. In the same way processes 3 and 4 correspond to K* (4p) scattering with an early and late crossing. The cross section for 1 seems to show two reductions in intensity. The earlier of these occurs at about 200 eV^{o} and is compatible with a covalent/ionic crossing at about 3.3 Å. There appears to be a further decrease in intensity in the region of 600 eV^{o}, corresponding to smaller impact parameters. Further problems are found in explaining the observed onsets for K(4p) scattering. Process 4, assigned as an early crossing on to the ionic surface, and therefore spending longer on the ionic surface, would be expected to onset at a lower scattering angle than process 3. In contrast the data shows a large increase in the intensity of potassium scattering in channel 3 at 200 eV^{o}, whereas the main onset in channel 4 appears to be at just over 300 eV^{o}. A small peak in the early crossing K(4p) is detected at about 100 eV^{o}.

It is expected that the position of R_1 is dependent on the orientation of the methyl iodide molecule with respect to the incident K atom. It has been shown (BRO 66) that for reaction to take place it is probably necessary for the K to impinge on the I "end" of the CH_3I molecule. See also (BUN 73) for potential surfaces contoured at several different orientations. The existence of two distinct decreases in the intensity of the elastic channel is evidence that the position of R_1 does not vary continuously with the collision angle but varies as shown in Figure 5.9

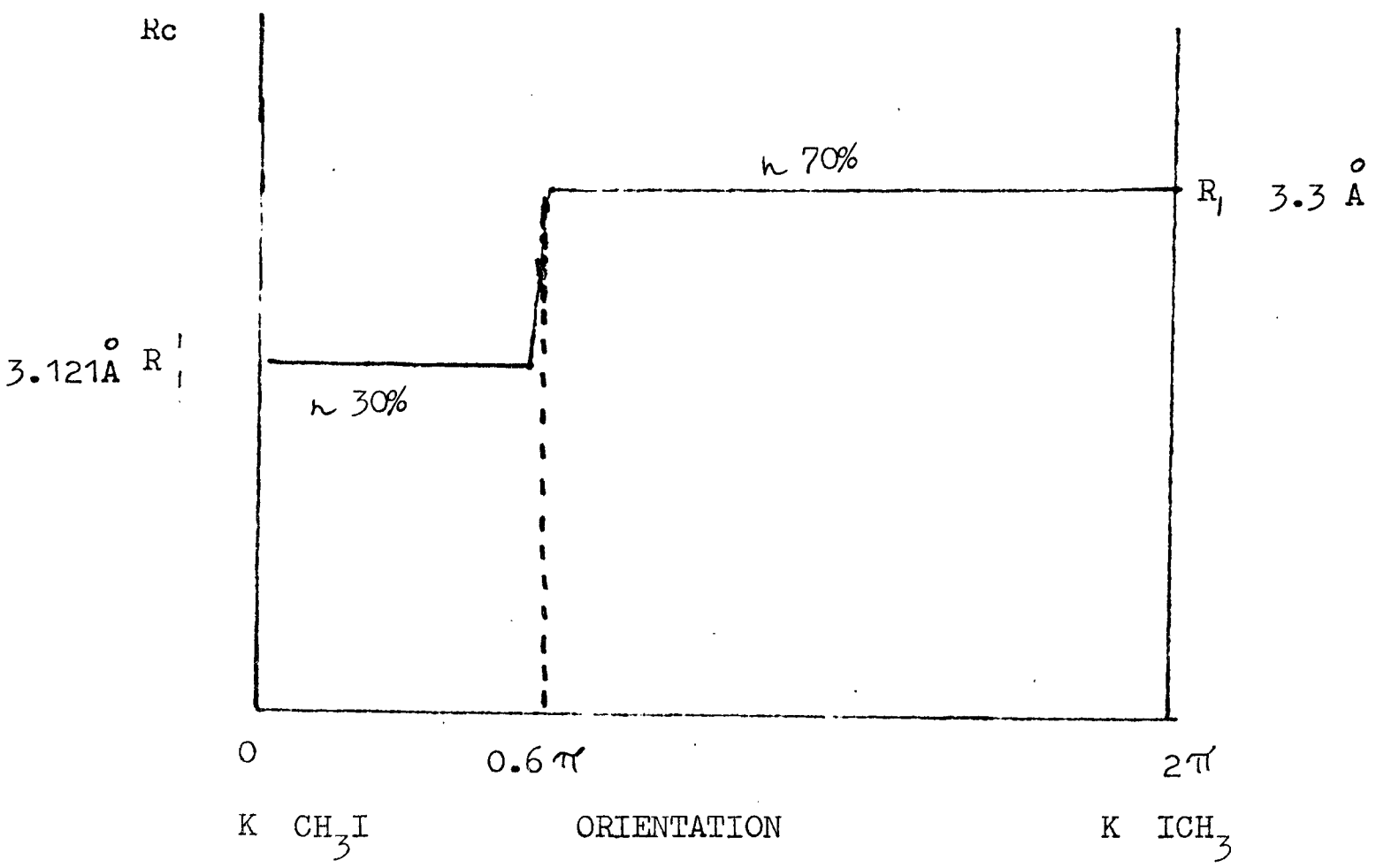

Over most of the angular range Rc does not change. The step change is required to explain the intensity variation with $E\chi$ observed in the Differential Cross Section for this process.

Figure 5.9

If the crossing radius was not constant over most of the angular range the onsets would not be as clear as those observed. From the intensity at different regions in the elastic channel we can estimate that about 70% of the K atoms strike the I end of the CH_3I molecule and 30% impinge on the methyl group. (Remarkably close to Brooks estimate of the ratios of 60:40). One other fact becomes apparent. The second onset observed in channel 4 (corresponding to hitting the CH_3 group) is much more intense than the onset at 100 eV° despite the fact that somewhat less than half as many collisions hit this end as strike the iodine. This can only be explained if the ionic potential involved in this orientation has a large shallow minimum resulting in extensive rainbowing. The potentials used in this final stage of the modelling are shown schematically in Figure 5.10 (and the various values of the parameters summarised below). The results are plotted with the data in Figures 5.11 and 5.12.

Summary of Model Potential Parameters:

Potential 1:

$K(4s)/CH_3I(x)$:

$$V(R) = 0.24 \left\{ \left(\frac{3.8}{R}\right)^{12} - \left(\frac{3.8}{R}\right)^{6} \right\}$$

Potential 2:

$K(4p)/CH_3I(x)$:

$$V(R) = 0.24 \left\{ \left(\frac{3.8}{R}\right)^{12} - \left(\frac{3.8}{R}\right)^{6} \right\} + 1.61$$

Potential 3:

$K^+/(CH_3I)^-$:

(Iodine end) $$V(R) = 0.1 \left(\frac{3.96}{R}\right)^{12} - \frac{120}{R^4} - \frac{14.4}{R} + \text{I.P.} - \text{E.A.}$$

(CH_3 end) $$V(R) = 0.1 \left(\frac{5.4}{R}\right)^{5} - \frac{120}{R^4} - \frac{14.4}{R} + \text{I.P.} - \text{E.A.}$$

$$H_{12} = 0.28 \text{ eV}$$

$$H_{23} = 0.2 \text{ eV}$$

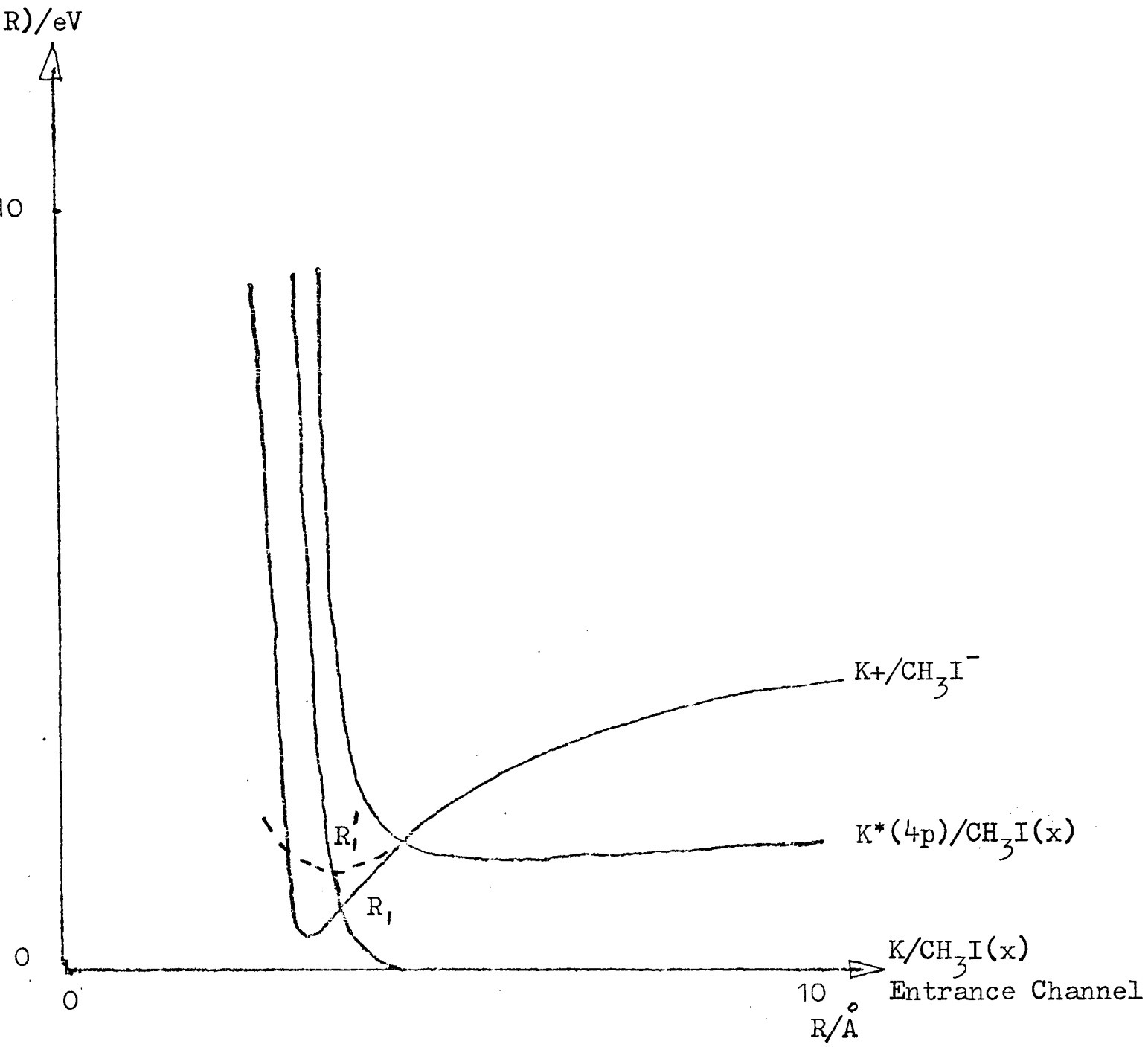

Figure 5.10 : Schematic diagram of potential curves used in the calculations. The solid ionic curve applies if the K atom impinges on the I atom, the dotted potential if the CH_3 group is encountered first.

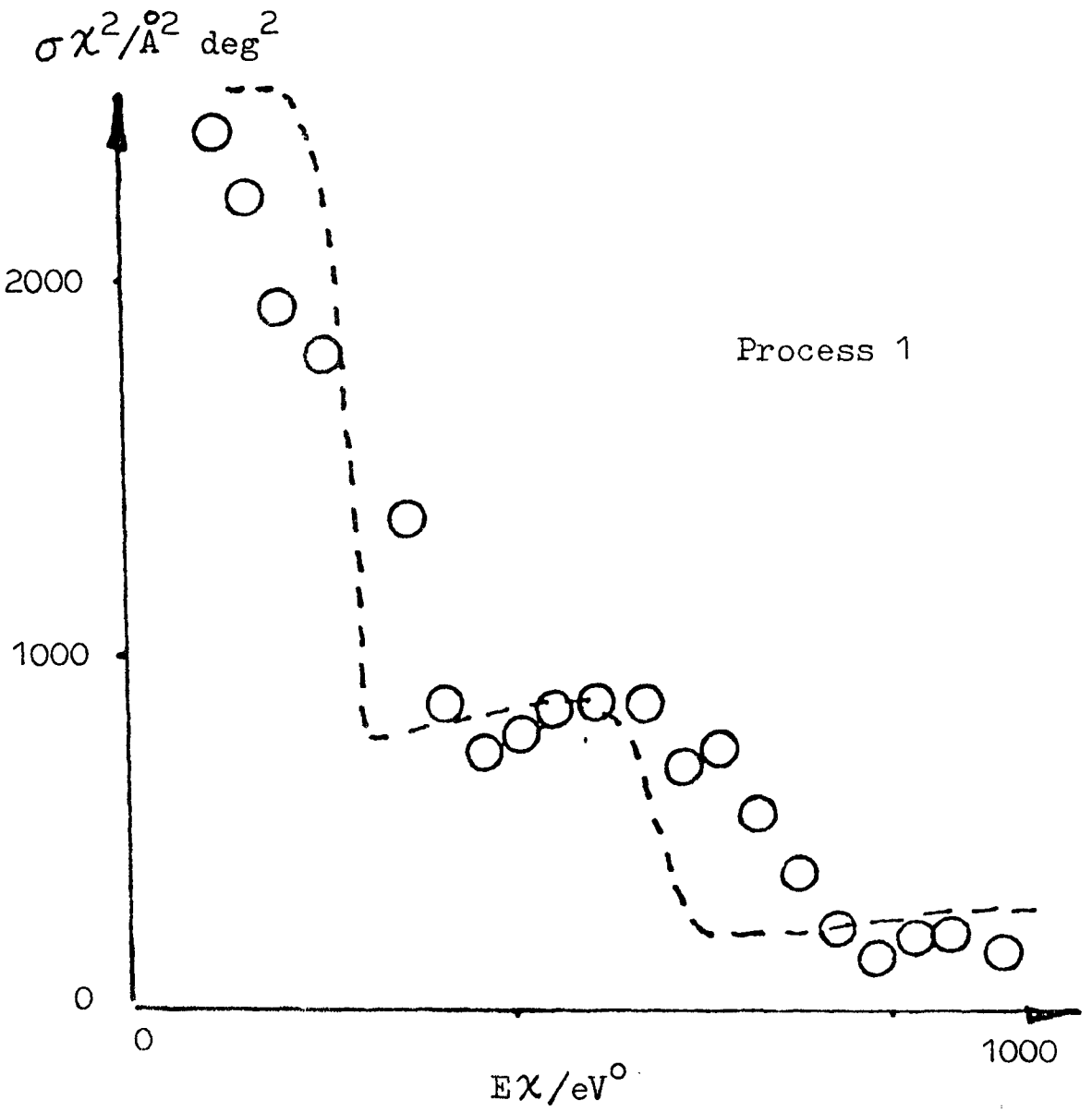

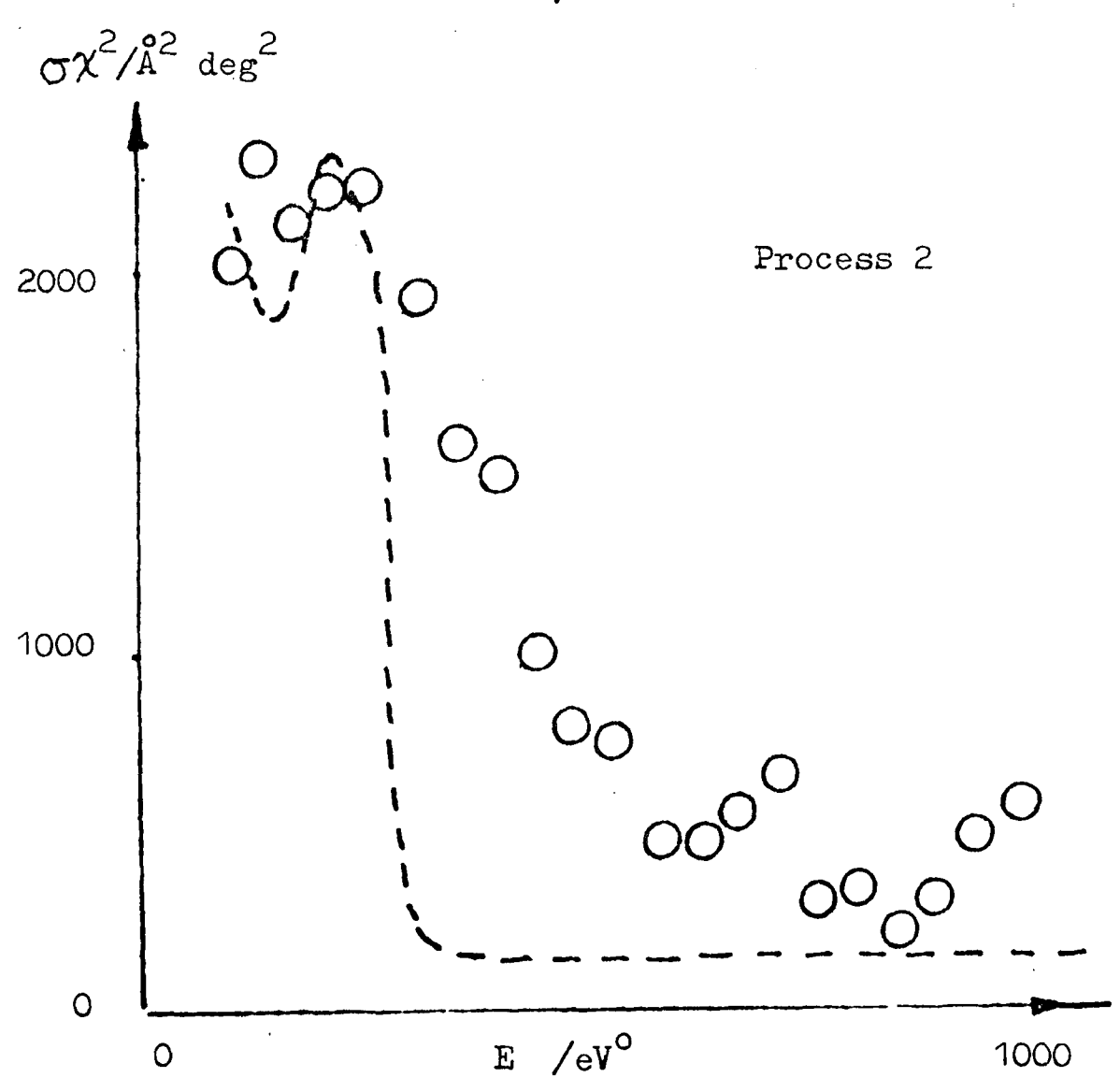

Figure 5.11 : 164 eV K/CH_3I Differential Cross Sections calculation and data.

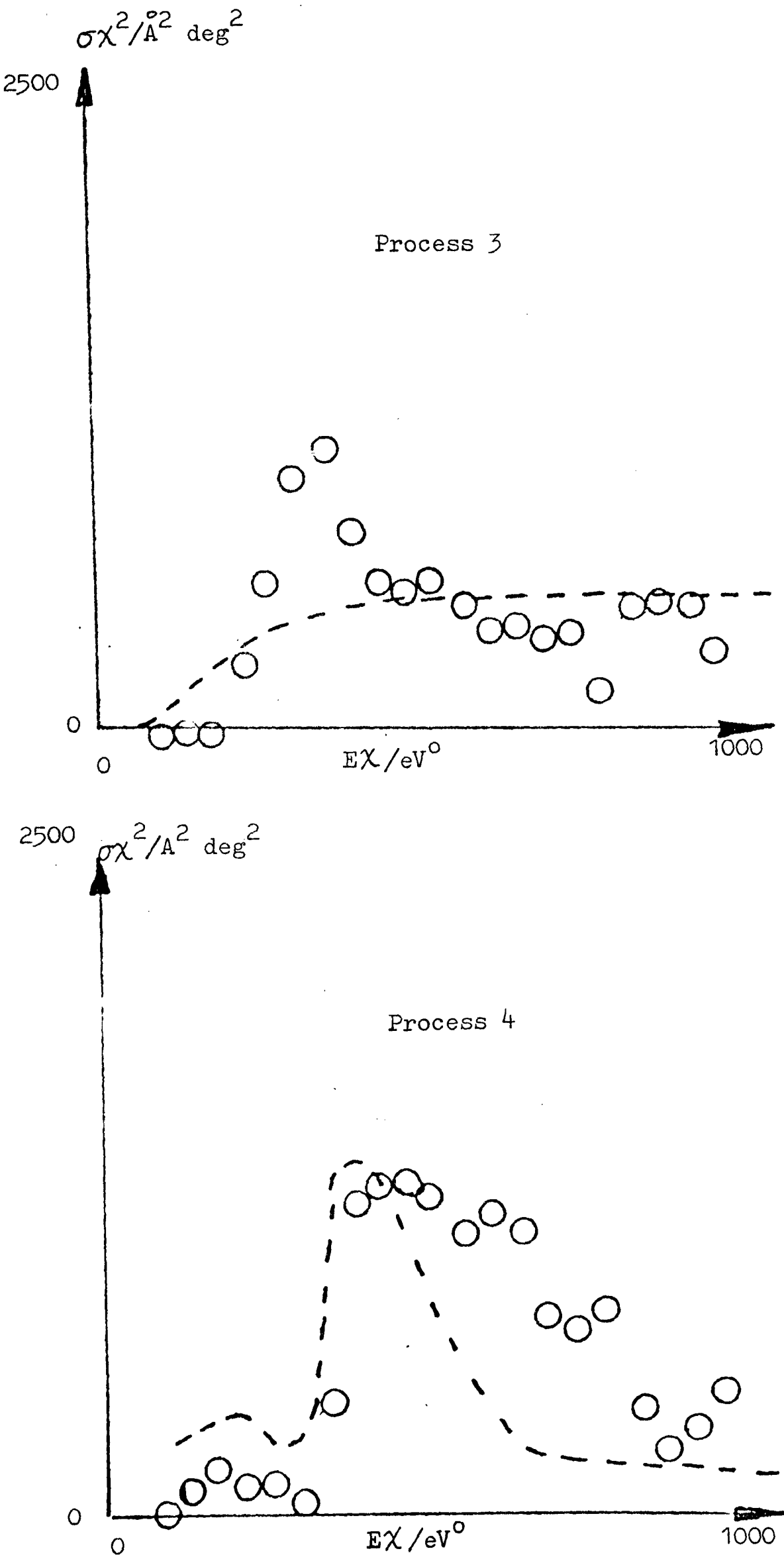

Figure 5.12 : 164 eV K/CH_3I Differential Cross Sections calculation & data

Form of $CH_3I(x)$ Potential:

$$V(R) = Do \left\{ e^{-2\beta (R-Ro)} - 2e^{-\beta (R-Ro)} \right\}$$

$$\beta = \nu o \, (2\pi^2 \mu / D)^{\frac{1}{2}}$$

$(CH_3I)^-$:

$$V(R) = \alpha e^{-\gamma (R-Ro)} - 3.063$$

$$\alpha = 1.65$$

$$\gamma = 4.65$$

5.3 "A" STATE EXCITATION

In section 5.2 processes 1-4 (Table 5.1) were discussed and explained in terms of K excitation involving motion on the K^+/RX^- ionic potential surface. More difficulty is found in understanding the energy losses entered under processes 5-8. Lying above the excited electronic potassium states they must be associated with electronic excitation of the target molecules (possibly accompanied by vibrational energy transfer). The lowest lying Rydberg transitions observed in the optical spectra, corresponding to electron transitions to the (n + 1) Rydberg states (n = 3,Cl; n = 5,I), lie above these energies and so it is concluded that it is the "A" states of the target molecules that are involved. The effective transition is thus $n(X) \rightarrow \sigma^*(C\text{-}X)$. The A states are repulsive (see Figure 5.13 for $CH_3I(A)$) and lead to dissociation of the molecule (HER 66). Optically these are observed to onset in the range 3.5 - 4.5 eV reaching a maximum about 1 eV above onset, corresponding to a vertical transition. The continuum observed involves transitions to several states including those dissociating to $X_{\frac{1}{2}}$ and $X_{\frac{3}{2}}$. Collision induced transitions would be expected to give discrete energy losses resulting from vertical transitions.

The results from the present work show between 2 and 4 processes in this region with energy loss constant with increasing χ and present two problems:- how the energy loss arises and what the population mechanism is.

In the iodides we may expect to observe two peaks in the time of flight spectra arising from dissociation into $I_{\frac{1}{2}}$ and $I_{\frac{3}{2}}$. However this splitting is about 0.9 eV and does not agree well with observed peaks. In the methyl iodide the 81 eV data shows 4 processes at 4, 4.6, 5.0 and 5.7 eV while the 164 eV results show energy losses at 3.6, 4.8 and 5.5 eV. It may be that the observations at 5 and 5.7 eV in the lower energy data are not resolved in the 164 eV collisions and give rise to a single maximum in the spectrum at 5.5 eV. The results would then be interpreted in terms of excitation of the A states (giving rise to two peaks in the spectra at about 4 eV and 5 eV from two states dissociating into $P_{\frac{1}{2}}$ and $P_{\frac{3}{2}}$ iodine atoms). Further splitting of these two branches could be due to different population mechanisms resulting in different degrees of molecular rearrangement, or vibrational excitation, similar to the model proposed for potassium excitation. The problem is not clarified by consulting the CF_3I or C_3H_7I data. In each case the spectra show three peaks in this energy loss region but they are not constant with changing collision energies (see results for K/CF_3I at 86 and 171 eV c.m.). Although some of the peaks have a spacing suggestive of $I_{\frac{1}{2}}$ and $I_{\frac{3}{2}}$ splitting (2.9 and 3.9 eV in 86 eV K/CF_3I, 4.5 and 5.4 eV in 171 eV K/CF_3I, 3.3 and 4.4 eV in C_3H_7I) these are not seen at constant energy loss and no clear pattern emerges.

The K/CH_3Cl data shows two processes at 4.8 and 6.0 eV. This can not be due to the $Cl_{\frac{1}{2}}$ and $Cl_{\frac{3}{2}}$ states which have a spin orbit splitting of only 0.3 eV, however Figure 13 shows that there are a number of states which may be populated. There are clearly enough possibilities but there is not yet enough data to assign the observed energy losses to specific exit channels.

Further difficulties are encountered in formulating a mechanism whereby these states are populated. The most obvious model in which donation of an electron by the K atom into the σ^* (C-X) orbital is followed by recapture of one of the halide lone pair electrons does not seem likely. Although this is the same ionic surface used as an intermediate in the potassium excitation the crossing radii with the K/RX(A) neutral potentials are so large (about 34Å for CH_3I(A)) as to make recapture of an electron by the K^+ ion most unlikely. An alternative mechanism, due to a curve crossing of the ground state entrance channel with the A state potential fails to predict the low angular onsets for these processes.

It is probable that for large extensions of the C-X bond the three-body effects (which play a key role in limiting the vibrational energy transfer associated with potassium excitation) become very important. Thus, these exit channels may only be available to a relatively small subset of the trajectories. Varying the target molecule temperature and measuring the temperature dependence of these processes would possibly provide further insight into this problem.

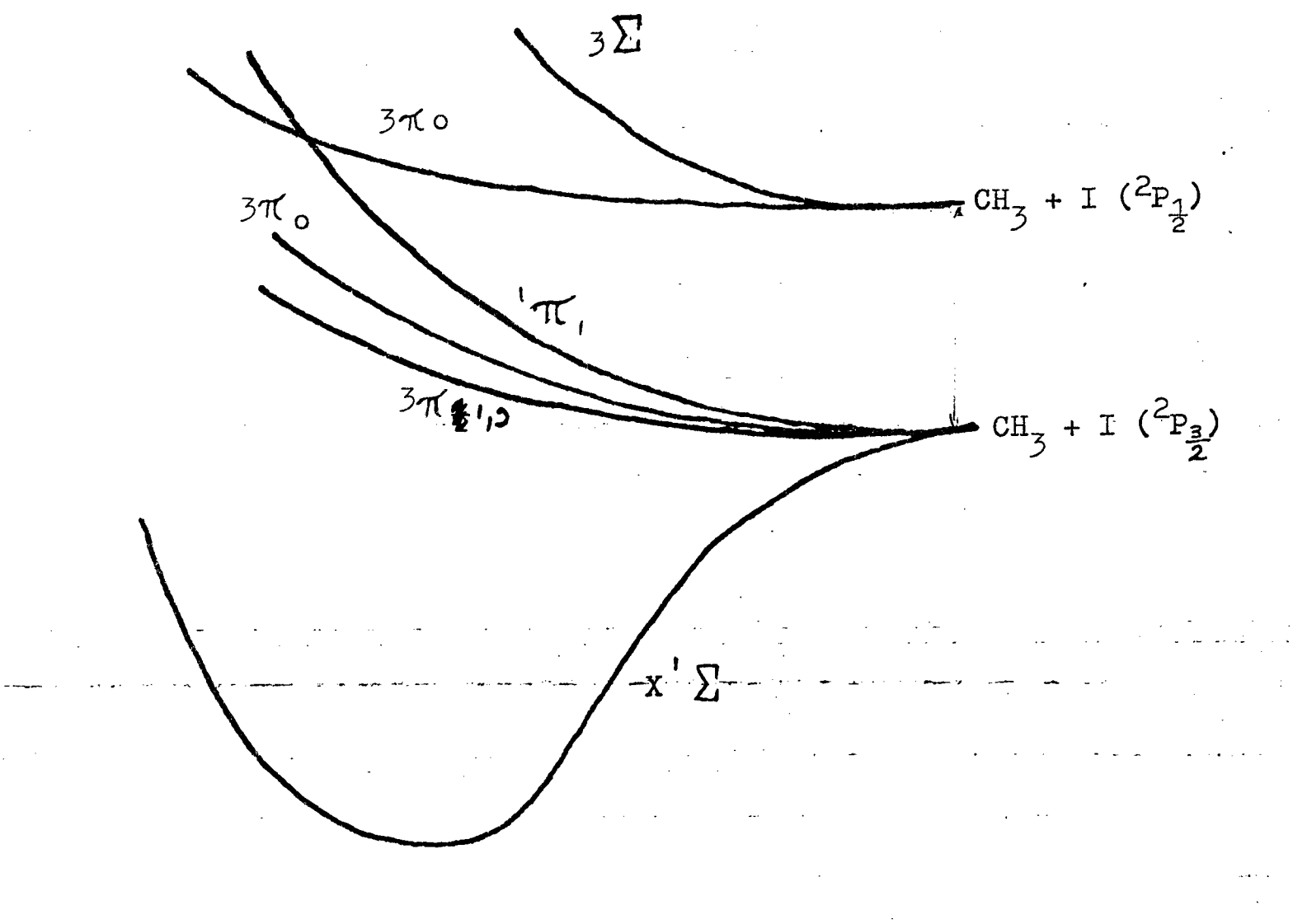

Figure 13 : Schematic of potentials for CH_3I

5.4 ENERGY LOSSES ABOVE 6 eV

Each of the data sets gathered for these systems show a number of peaks in the time of flight spectra in the energy range 6 to 15 eV (processes 9-14 in Table 5.1). With the exception of 14, these processes are observed to be at constant energy loss as the scattering angle is varied. Processes 9 and 10 are seen to occur at the same energy loss in the CH_3I data at 81 and 164 eV c.m. Unfortunately, technical reasons prevent the energy loss spectra being collected for energy losses greater than about 9 eV with experiments conducted at a laboratory collision energy of 100 eV. At this collision energy the spectra are further complicated in this region by the arrival of the ^{41}K isotope atoms.

Perhaps the most remarkable feature of the spectra in the region above 6 eV is low angular onsets for the processes. The combination of substantial energy exchange coupled with small deflections is evidence for the involvement of strong attractive potentials during the collision and suggests that the excitation mechanism may involve a transient negative ion.

Figure 5.14 shows the higher occupied molecular orbitals for some of these systems, along with some of the vacant orbitals. The lowest unoccupied orbitals are the σ^* (C-X) and σ^* (C-H) which are both antibonding in the C-X and C-H respectively. The σ^* (C-X) is the electron acceptor orbital of importance in the reactive and K* excitation process though in principle all the vacant orbitals shown are possible receptor levels.

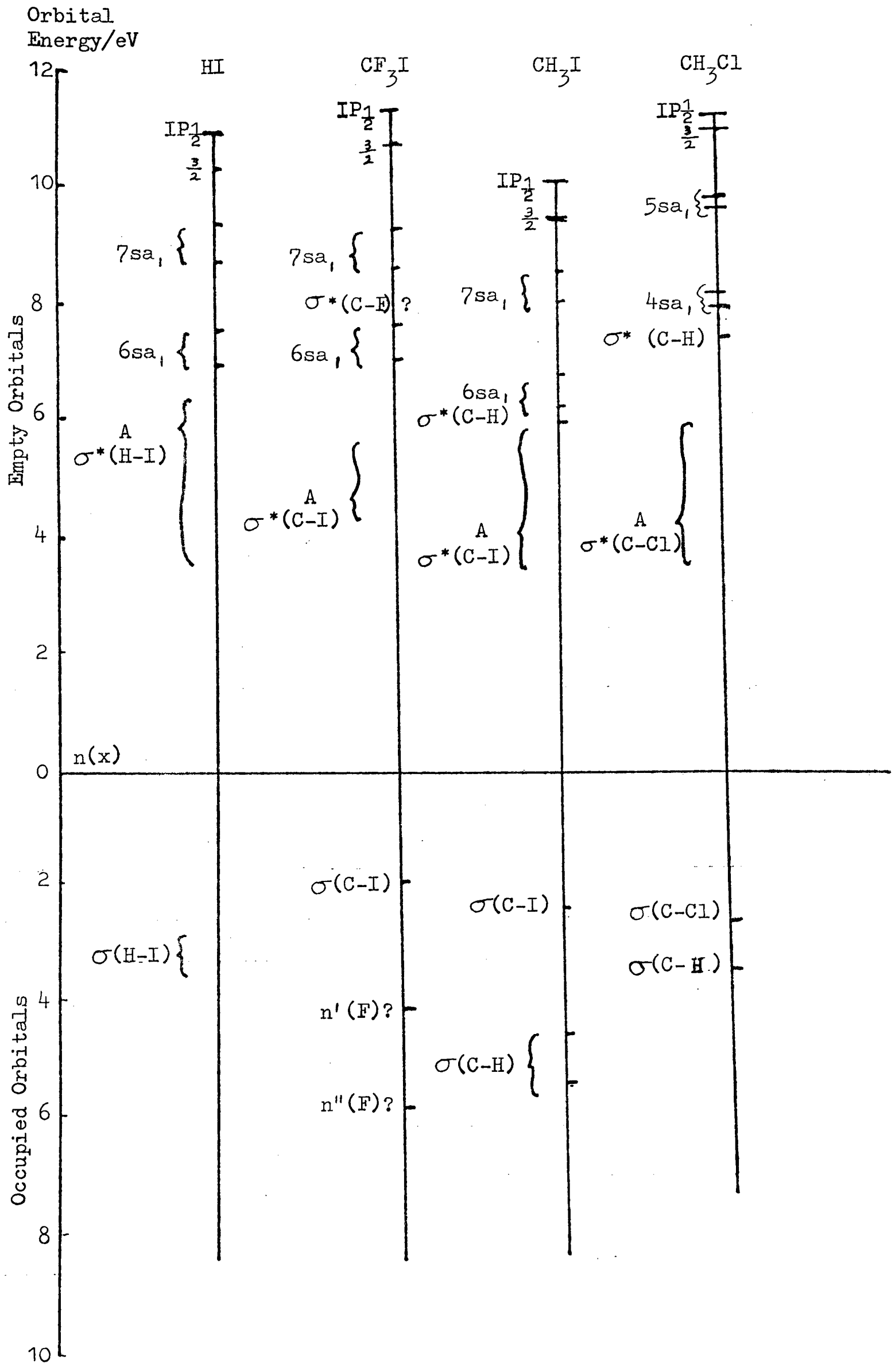
Orbital Energy/eV
HI
CF3I
CH3I
CH3Cl
IP 1/2
3/2
7sa1
6sa1
A σ*(H-I)
σ*(C-I)
σ*(C-F) ?
σ*(C-H)
5sa1
4sa1
σ* (C-H)
A σ*(C-Cl)
Empty Orbitals
12
10
8
6
4
2
0
n(x)
σ(H-I)
σ(C-I)
n'(F)?
n"(F)?
σ(C-H)
σ(C-Cl)
Occupied Orbitals
2
4
6
8
10

Figure 5.14

These measurements are confined to neutral exit channels so electron donation by the K atom must be followed by electron recapture by the K^+ ion on exit. Electronic excitation will take place if an electron is recaptured from a lower, normally filled orbital leaving the receptor orbital occupied and a lower lying vacancy.

From the orbital energies shown in Figure 5.14 it is possible to calculate the possible energy losses arising from this mechanism and to make a tentative assignment of the processes observed experimentally. Table 5.2 shows the energy losses which we might expect for CH_3I and comparison with the results in Table 5.1 suggests the assignment shown in Table 5.3. The 7s and 5d Rydberg states are too close to be resolved and the energy loss given in Table 5.2 represents an average of these. This means that there is some ambiguity about the assignments.

Support for them, however, comes from inspection of the CH_3Cl data. The 5s Rydberg level observed for this molecule (HOC 75) is at 9.83 eV and compares well with the energy loss observed for process 10 of 9.8 eV.

The peaks in the CF_3I time of flight spectrum at 7.7 and 9.5 eV agree with Rydberg transitions at 7.5 eV (6sa, Rydberg) and 9.0 eV (7sa, Rydberg). The photo electron spectrum of CF_3I (BOS 74) though not clearly assigned shows peaks due to the ionisation of the fluorine lone pairs and electrons in the σ(C-F) bonds. Thus analogous to processes 11 and 12 for CH_3I, ($\sigma_{(C-H)} \rightarrow$ 6s, 7s), processes 11 and 12 in CF_3I (at 11.1 and 13.0 eV) correspond to donation into the 6s, 7s Rydberg levels

TABLE 5.2

POSSIBLE ENERGY LOSSES IN CH_3I

ORBITAL FROM WHICH ELECTRON IS RECAPTURED	nI	ORBITAL INTO WHICH ELECTRON IS DONATED			
		* (C-I)	6s Rydberg 6sa	* (C-H)	5d) 7s) Rydberg
	nI	3.5-5.5	6.5	≈6 (onset energy)	8.2
	σ(C-I)	≈7	8.9	8.4	10.6
	σ(C-H)	9.2	11.0	10.7	12.9

TABLE 5.3

TENTATIVE ASSIGNMENT OF ENERGY LOSSES IN CH_3I

OBSERVATION		ASSIGNMENT	
Process Number (Table 5.1)	Energy Loss/eV	Excitation	Predicted Energy Loss
9	6.3	n (I) → 6s	6.5
10	8.2	n (I) → 7s	8.2
11	10.4	σ(C-H) → 6s	11.0
12	12.4	σ(C-H) → 7s	12.9
14	6.2	n (I) → σ*(C-H)	~ 6 *
	ENERGY LOSSES IN CF_3I		
9	7.7	n (I) → 6s	7.5
10	9.5	n (I) → 7s	9.0
11	11.1	n'(F) → 6s	11.5
12	13.0	n'(F) → 7s	13.1
13	14.8	n''(F) → 7s	15.0
	ENERGY LOSSES IN C_3H_7I		
9	6.6	n (I) → 6s	6.5
10	8.5	n (I) → 7s	8.2
11	10.8	σ(C-H) → 6s	11.0
12	13.2	σ(C-H) → 7s	12.9
13	14.8	n (I) → σ*(C-H)	σ*(C-H) orbital in C_3H_7I can not be identified unambiguously *
	ENERGY LOSSES IN HI		
9	7.4	n (I) → 6s	7.4
	Very weak signal in HI due to extensive dissociation prevents detection of other states expected.		
	ENERGY LOSSES IN CH_3Cl		
9	7	n (Cl) → 4s	7.7
10	9.8	n (Cl) → 5s	9.8
11	11.0	σ(C-H) → 4s	~11.3
12	not observed for technical reasons	σ(C-H) → 5s	~13.4
14	7.7	n (Cl) → σ*(C-H)	~ 7.5 *

*States marked with an asterisk in the right hand column are repulsive.

being followed by recapture of one of these fluorine electrons (expected energy losses of 11.5 and 13.1 eV).

Process 14 (assigned as donation into σ^* (C-H) and recapture of one of the halogen lone pairs) is obviously not observed in the CF_3I or HI data. The Rydberg levels used in the other assignments are obtained from optical spectra (HER 66), (BOS 72), (WAN 77), (HOC 75), the occupied orbital energy levels from photo-electron spectra (TUR 70), (BAK 72), (BOS 74) whilst the energy level of σ^* (C-H) is somewhat less certainly derived from the optical spectra of the alkanes (RAY 67). Small angle inelastic scattering of high energy 2.5K eV electrons has been used to study inner shell excitation in methyl halides (HIT 78). Energy losses are observed at 7.5 eV in CH_3Cl and 6.2 eV in CH_3I and these have tentatively been assigned as transitions into the σ^* (C-H) orbital in each of these molecules. This agrees remarkably well with the energy losses observed at onset for the same assignments in the current data (7.7 eV in CH_3Cl, 6.0 eV in CH_3I).

It is notable that this process, which is unique in showing an energy loss increasing with $E\chi$ shown in Figure 5.15, arises from an intermediate ion state which is antibonding and repulsive in the C-H co-ordinate. Since both $E\chi$ and the time spent on this surface are both inversely related to the impact parameter, it can be seen that the increasing energy loss is a result of the substantial changes in molecular geometry which occur during the collision. The small mass of the ejected H atom result in considerable changes in the observed energy loss even over the small $E\chi$ range measured.

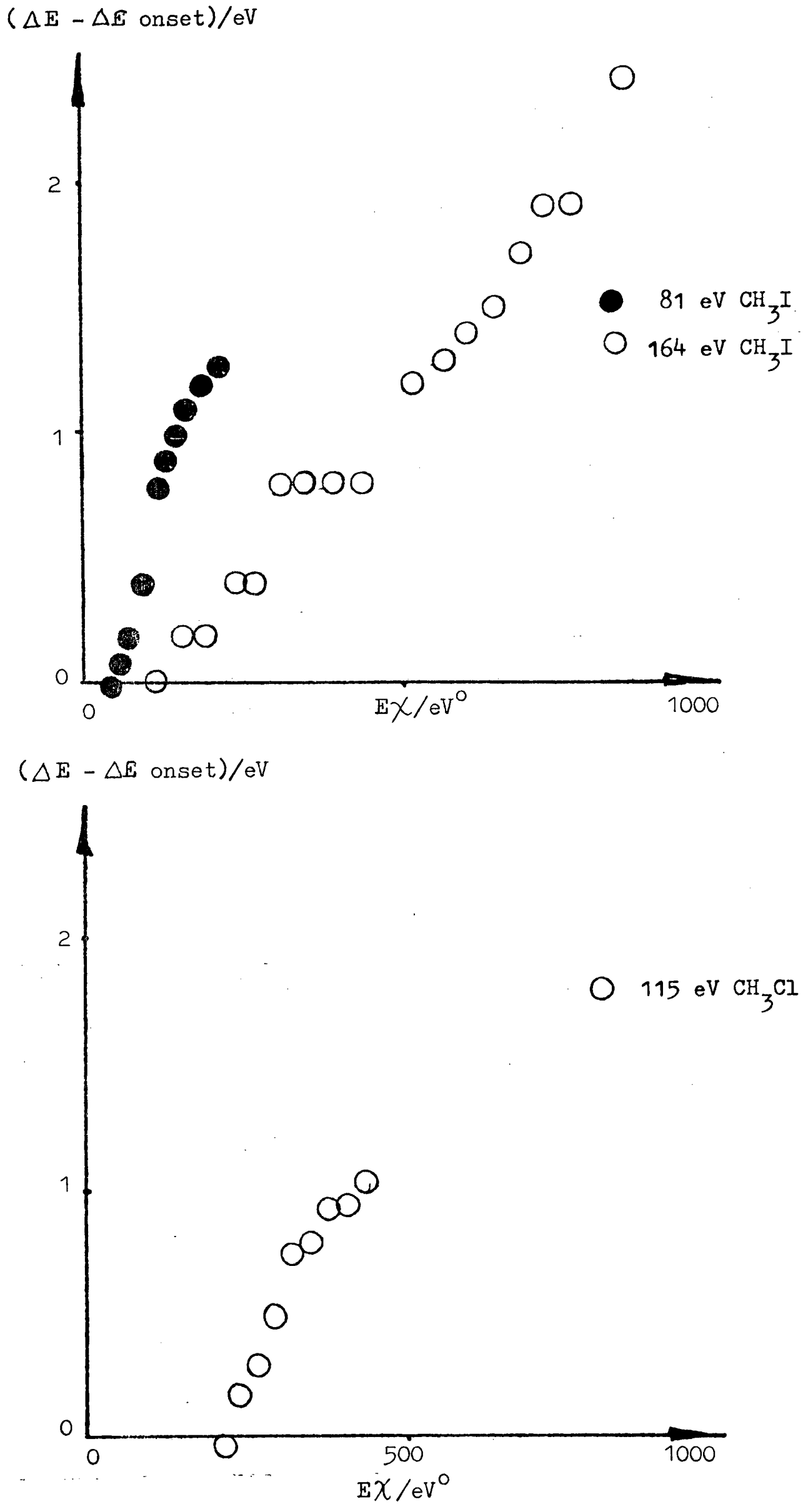

Figure 5.15 : Dependence of energy loss of Process 14 on Eχ.

The energy losses observed can therefore be accounted for on the basis of donation into different vacant orbitals and recapture from lower normally filled orbitals. The tentative assignments that have been made to the various observed energy losses are summarised in Table 5.4.

The C-X force constant is essentially unchanged by population of Rydberg states so transitions to these states would be expected at a fixed energy, as we observe.

A detailed model for the population mechanism of these states was not developed. The proximity of the K+ ion will considerably perturb the various orbitals, leading to extensive mixing. The precise description of the orbital from which recapture occurs is unclear. A simplified diabatic potential scheme for CH_3I is shown in Figure 5.16, the doubly starred curve representing the excited $(CH_3I^*)^-$ state under perturbation by K^+.

The model suggests that the relative probability of excitation is at least partially determined by the RX orientation during the collision. Process 14 ($n(x) \rightarrow \sigma^*$ (C-H)) would presumably be favoured by trajectories in which the K moved first past the alkyl group and then the halide atom. Processes 11 and 12 ($\sigma_{(C-H)} \rightarrow (n+1)S$, $(n+2)S$) would involve trajectories in the opposite direction. Lastly, processes 9 and 10 ($n(I) \rightarrow (n+1)S$, $(n+2)S$) involve only the halide end of the molecule.

TABLE 5.4

Process Number	Assignment	HI	CH_3Cl	CH_3I	CF_3I	C_3H_7I
1	Elastic Scattering	0	0	0	0	0
2	Electronically Elastic + Vibrational Excitation	0	0	0	0 (in 86 eV data only)	0
3	K*(4p) Late Crossing	0	0	0	0	0
4	K*(4p) Early Crossing		0	0	0 (in 86 eV data only)	0
5-8	$n(X) \rightarrow \sigma^*$ (C-X)?	0	0	0	0	0
9	$n(X) \rightarrow (n+1)^{\bullet}_{S}$	0	0	0	0	0
10	$n(X) \rightarrow (n+2)^{\bullet}_{S}$		0	0	0	0
11	σ (C-H) $^{\phi}$ $\rightarrow$ (n + 1)S		0	0	0	0
12	σ (C-H) $^{\phi}$ $\rightarrow$ (n + 2)S		■	0	0	0
14	$n(X) \rightarrow \sigma^*$ (C-H)		0	0	0	0

CODE:

0 Transition observed

■ Not observed for technical reasons

● n = 5 for Iodides : n = 3 for Chlorides

ϕ or σ (C-F) or n(F) for CF_3I

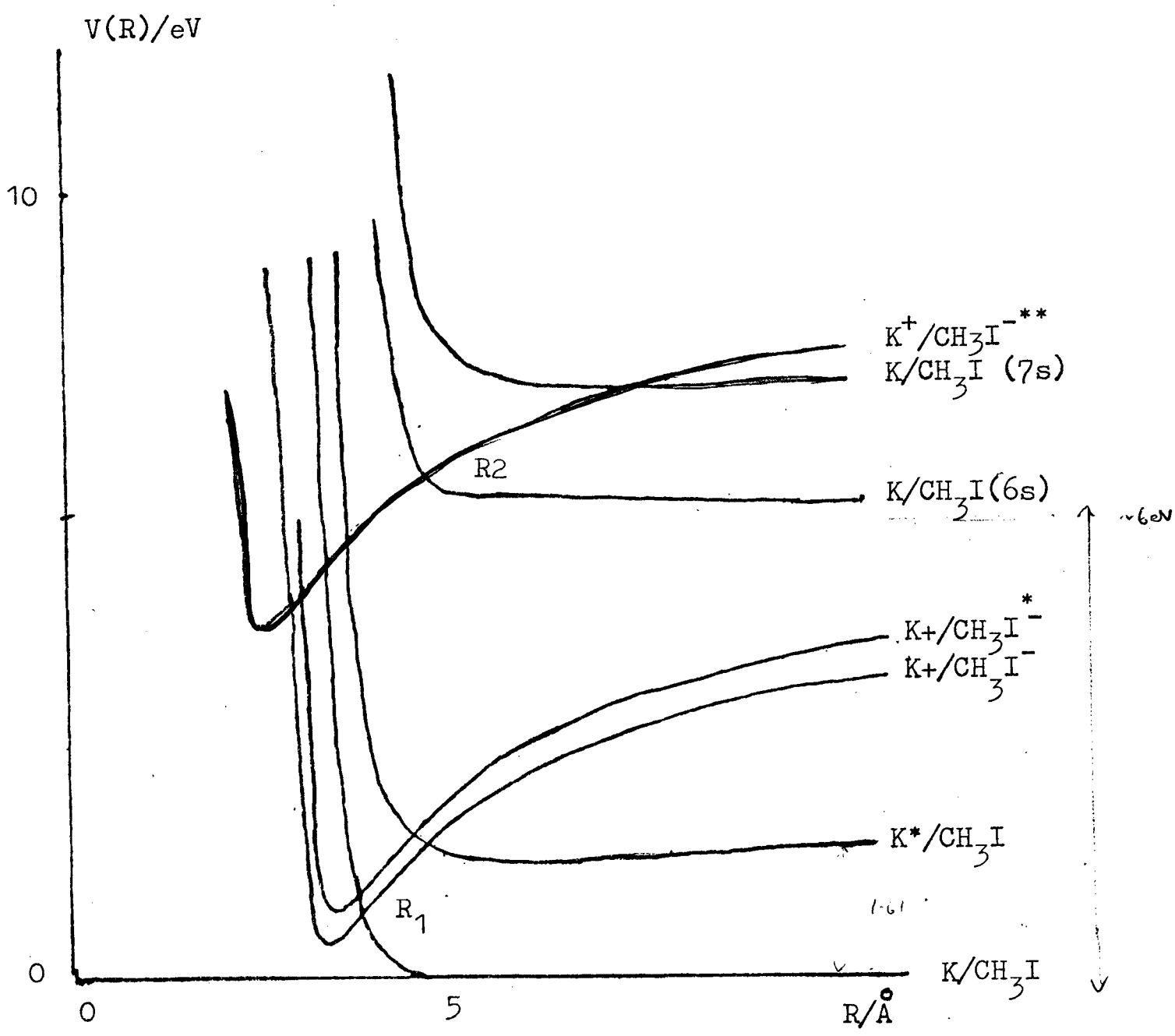

Figure 5.16 : Schematic diagram of K/CH_3I potentials

Finally, it is noted that all the transitions can be assigned to S and σ orbitals (although the assignments are not all unambiguous) suggesting that the electron orbital angular momentum is conserved in these collisions.

5.5 SUMMARY

Time of flight spectra have been collected for a number of alkyl halide like target beams and an attempt has been made to understand and explain the results in as simple a way as possible.

The spectra have been divided into three energy loss regimes and interpreted in terms of potassium excitation, A state excitation and transitions to molecular Rydberg states.

Potassium excitation is accompanied by substantial vibrational excitation, indicating the need to incorporate changes in the internal geometry of the target molecule during the collision into any model. The potential surface on which the system moves during the "3 body" stage in the collision is considerably perturbed by the presence of the K^+ ion and allowance for this has to be made if the observed energy losses are to be fitted. Further complications arise in explaining the observed intensities in the K* channels. The assumption of an isotropic potential is invalid and the crossing radius varies with respect to the orientation of the target molecule and the incident K atom.

Energy losses are observed which can only be assigned to target molecule A states. Neither the mechanism of population of these exit channels nor the energy losses observed can be clearly understood. It is noted that the energy losses detected appear to vary with the incident energy of the K beam.

A number of processes with higher energy losses are observed to onset at very low scattering angles and a model is developed suggesting that electron capture into the lower empty Rydberg or valence levels of the target molecule is possible. All the observed transitions can be assigned to S or σ orbitals suggesting that the electron orbital angular momentum is conserved. The probability of excitation of the different states is dependent on the orientation of the RX molecule and the K atom.

5.6 CONCLUSIONS

The energy losses observed for these collision systems have been interpreted. The lower processes, involving energy transfer of less than 4 eV, are understood in terms of the harpoon model - well established as the mechanism for reaction at lower collison energies.

The energy losses above 6 eV have a more speculative interpretation but they too are interpreted on the basis of electron donation into high lying vacant orbitals followed by recapture from lower lying filled orbitals.

Intermediate energy losses, assigned to A state excitation

presents difficulties of interpretation. An excitation mechanism involving electron donation into the σ^* (C-X) orbital is strongly appealing, paralleling as it does the mechanism described for the higher states.

A number of further experiments would provide further data and clarify some of the more difficult assignments.

Time of flight spectra collected at constant $E\chi$ but with different collision energies would aid the interpretation of processes involving target molecule rearrangement during the collision.

Varying the temperature of the target beam would give the dependence of the results on the C-X bond length - possibly very important in A state excitation.

A photon-particle coincidence experiment would clarify which electronic exit channels are being observed. This would clarify the assignment in those cases in which electronic excitement is accompanied by vibrational excitation.

In both the K* excitation and the Rydberg state excitations the population mechanism depends on the orientation of the target molecule with respect to the potassium atom. Results from experiments conducted with orientated cross beams would verify this interpretation. For example, if the K atom impinged on the alkyl end of the molecule, processes 11 and 12 should no longer take place.

Further experiments, carried out with other target molecules in the same family, would also further verify the proposed interpretation.

CHAPTER 6

FEASIBILITY CALCULATION FOR PHOTON-PARTICLE COINCIDENCE EXPERIMENT

6.1 INTRODUCTION

In the conclusion to the preceding Chapter it was suggested that a photon-particle coincidence experiment would help to resolve the problem of assignment to electronic exit channel in those instances where vibrational energy exchange takes place during the collision. The detection of a photon emitted from the collision zone would gate open the detector (after a suitable delay to allow for the time of flight of the scattered atom) to look for the associated particle. By use of suitable interference filters it should be possible to select the frequency of the photons detected and hence to select the inelastic channel desired. A feasibility calculation was carried out to investigate the viability of modifying the time of flight apparatus to perform this experiment and is presented in this Chapter.

6.2 SIGNAL AND NOISE RATES IN COINCIDENCE EXPERIMENT

The count rate into any exit channel, i, at an angle Θ is $I_i(\Theta)$ where

$$I_i(\Theta) = \left(\frac{I_1}{v_1}\frac{I_2}{v_2}\right)\sigma_i(\Theta)\, V\, v_r\, C\Delta\phi\Delta\Theta \qquad 6.1$$

and

I_1, I_2 = beam fluxes

v_1, v_2 = beam velocities

$\sigma_i(\Theta)$ = differential cross section for scattering at angle Θ in state i.

V = volume of scattering zone

v_r = relative velocity of beams

C = efficiency of particle detector

$\Delta\phi\Delta\Theta$ = angular resolution of detector.

Now let d be the efficiency of the photon collection system. This is given by

$$d = \frac{\eta}{4\pi} W_p \qquad 6.2$$

where η = efficiency of photomultiplier, photon collection and photon transmission system.

W_p = solid angle subtended by the photon collection system.

This gives the signal rate in the coincidence experiment as

$$Sc_i(\theta) = d\ I_i(\theta) \qquad 6.3$$

The number of photons that will be counted in a channel i is

$$Np_i = d\left(\frac{I_1}{\sigma_1}\ \frac{I_2}{\sigma_2}\right) V\ \sigma r\ \sigma i + \text{Dark Count} \qquad 6.4$$

with σi = total cross section for channel, and

Dark Count (DC) = photon dark count rate.

For the processes of interest under investigation DC $\ll$ photons arising from collisions.

Let Δt be the time spread in the coincidence signal arising from the beam velocity spread, the finite size of the collision zone etc then the noise rate, N_c, is given by

$$N_c = Np_i\ \Delta t (N_B + \sum_i I_i(\theta)) \qquad 6.5$$

N_B = the background noise rate of the particle detector.

$\sum_i I_i(\theta)$ = the sum over all exit channels of particles scattered at an angle θ.

$\sum_i I_i(\Theta)$ is highest for an uncorrelated beam in which the probability of an atom entering the collision zone is independent of when the last atom did so. In reality it is likely that there will be some correlation due to space charge effects in the ion beam. If this is the case then the noise due to scattering in other channels will be significantly reduced.

6.3 COMPARISON OF COINCIDENCE EXPERIMENT WITH TIME OF FLIGHT EXPERIMENT

For the time of flight experiment the signal rate, (St, is given by

$$St = Pr\ W\ I_i(\Theta) \qquad 6.6$$

where Pr = beam pulsing rate

W = width of the beam pulse (before compression)

St, of course, refers to the signal rate into channel i only.

The noise rate is simply given by

$$Nt = \sqrt{N_B\ Pr} \qquad 6.7$$

This gives

$$\frac{St}{N_t^{\frac{1}{2}}} = \frac{Pr\ W\ I_i(\Theta)}{(N_B\ Pr)^{\frac{1}{2}}} \qquad 6.8$$

The comparable equation for the coincidence experiment is

$$\frac{Sc_i}{Nc_i^{\frac{1}{2}}} = \frac{dI_i(\Theta)}{\left[Np_i\sqrt{(N_B + \sum_i I_i(\Theta))}\right]^{\frac{1}{2}}} \qquad 6.9$$

Assuming that correlation within the beam reduces $\sum_i I_i(\Theta)$ such that $\sum_i I_i(\Theta) \ll N_B$ equation 6.9 reduces to

$$\frac{Sc_i}{Nc_i^{\frac{1}{2}}} = \frac{dI_i(\Theta)}{\left[Np_i\sqrt{N_B}\right]^{\frac{1}{2}}} \qquad 6.10$$

One method of comparing the coincidence experiment with the time of flight experiment is to evaluate R where R is defined as

$$R = \frac{\frac{S}{N^{\frac{1}{2}}} \text{ (coincidence)}}{\frac{S}{N^{\frac{1}{2}}} \text{ (Time of Flight)}} \qquad 6.11$$

Substituting and expanding equations 6.8 and 6.10 into 6.11 gives

$$R = \frac{dI_i(\theta)/t^{\frac{1}{2}} N_B^{\frac{1}{2}} \left\{ d\left(\frac{I_1 I_2}{\sigma_1 \sigma_2}\right) V \upsilon_r \sigma_i + D.C. \right\}^{\frac{1}{2}}}{Pr\ W\ I_i(\theta)/t^{\frac{1}{2}}\ N_B^{\frac{1}{2}}\ Pr^{\frac{1}{2}}} \qquad 6.12$$

Cancelling through reduces this to

$$R = \frac{d}{Pr^{\frac{1}{2}}\ W\ \left(d\left(\frac{I_1\ I_2}{\sigma_1\ \sigma_2}\right) V\ \upsilon_r \sigma_i + D.C.\right)^{\frac{1}{2}}} \qquad 6.12$$

Recalling the expression for $I_i(\theta)$ given in equation 6.1, we can write

$$R = \frac{d}{Pr^{\frac{1}{2}}\ W\ \left(d\ \frac{I_i(\theta)\sigma_i}{C \Delta\phi \Delta\theta \sigma_i(\theta)} + D.C.\right)} \qquad 6.13$$

The first term in the brackets is the product of the photon detection system efficiency and the total number of collisions taking place in the collision zone. Hopefully this will be very much larger than the dark count allowing equation 6.13 to be written

$$R = \frac{d}{W\ \left(\frac{Pr\ d\ I_i(\theta)\sigma_i}{C \Delta\theta \Delta\phi \sigma_i(\theta)}\right)^{\frac{1}{2}}} \qquad 6.14$$

Assuming detection efficiencies of about 10% and substituting appropriate figures for cross sections, angular resolution and pulse rates and widths gives a value for R of about 5. Thus an improved signal to noise ratio is obtained using the coincidence experiment.

On the other hand, the signal rate will be less in the case of the coincidence experiment since the photon collection efficiency, d, will almost certainly be less than Pr W, the product of the beam pulse rate and pulse width.

The energy resolution of a coincidence experiment would be comparable with that of the time of flight technique currently employed. Since the photon detected can be emitted from a collision occurring anywhere in the collision zone the signal width depends on the time taken for a K atom to traverse the collision zone. This is given by

$$T = {}^{l}/_{\sigma} \qquad 6.15$$

l = length of collision zone ~ 3 mm.

σ = K velocity

For a 200 eV beam $\sigma \sim 3 \times 10^{7}$ mm/sec. Thus $T = 10^{-7}$S = 100 ns. The present FWHH of the beam is about 80 ns.

Reducing the dimensions of the collision zone would increase the resolution but would also reduce the signal.

6.4 PRACTICAL CONSIDERATIONS

The calculations presented in 6.3 show that a photon-particle coincidence experiment is feasible despite the lengthy counting times that may be required. Obviously the most important factor in turning this into a practical experiment is the photon collection system. The two variables governing the efficiency of this are the solid angle around the collision

which the photon gathering apparatus can subtend and the efficiency with which the photons can be transmitted into and through the photomultiplier.

A system utilising fibre optics and mounted on the cross beam monitor currently lying under the collision zone is recommended. A schematic suggested design is shown in Figure 6.1. Photons emitted in the direction away from the fibre optics would be reflected back in the mirror into the fibres. The mirror and fibre optics should be mounted so that their focal points are in the middle of the collision zone. It may be advisable to have the exact position adjustable to allow for different half-lifes of the radiating species (in 10^{-7}S a 200 eV K atom moves approximately 3mm). The need to mount the mirror and fibres as close to the zone is obvious though care should be taken not to obstruct either of the beams.

A concave surface on the fibres is recommended because of the fibres limited acceptance angle. Ideally the photons should strike the fibres normally. Unfortunately it is likely to be impossible to polish the fibre ends and mount them into a hemisphere. A compromise is shown in Figure 6.2 illustrating how a "fly's eye" type mount could be used.

Transmission losses through the optical fibres are low and it is at the various interfaces that the efficiency shall be reduced. The photons will have to be taken out of the vacuum through an optical window and subsequently through a monochrometer into the photomultiplier.

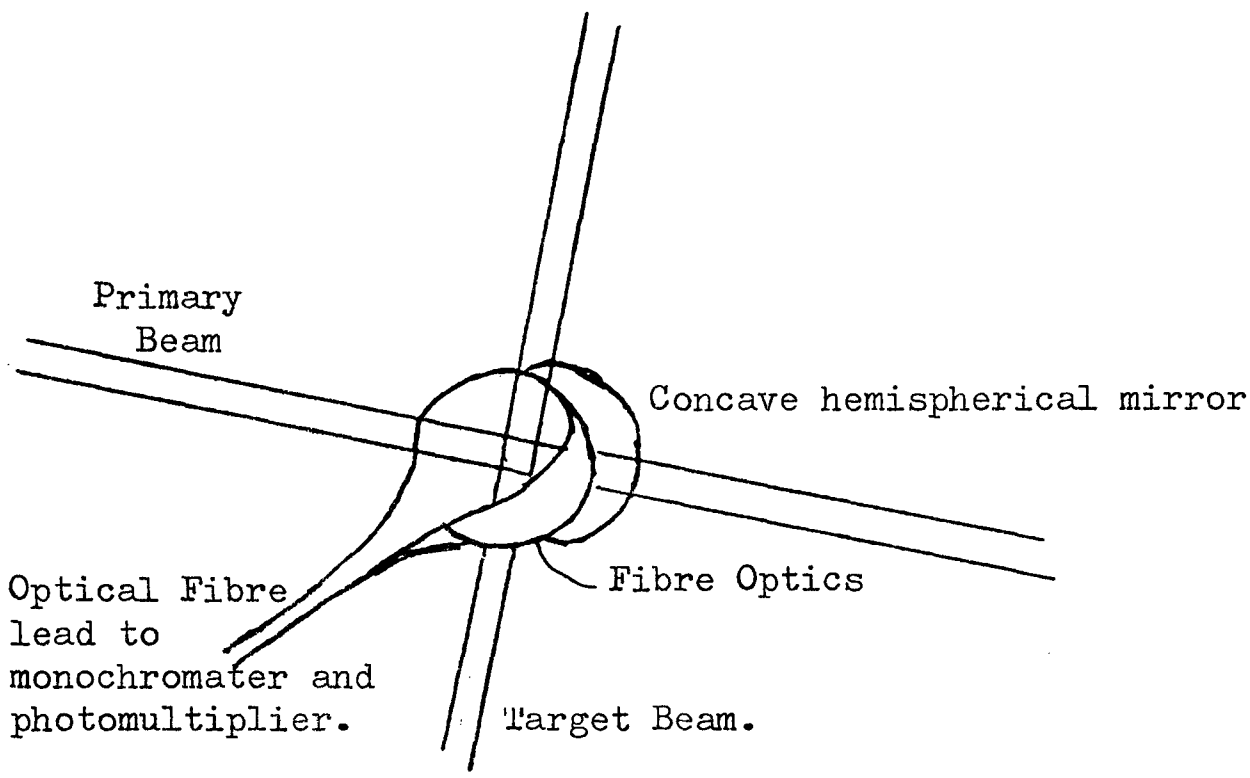

Figure 6.1 : Schematic of photon collection at collision zone.

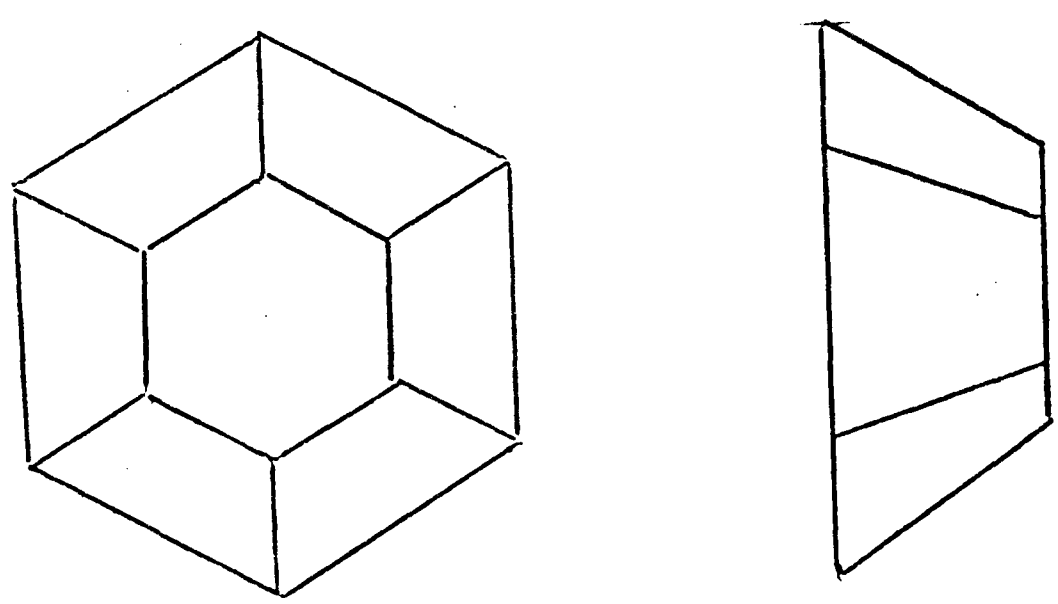

Figure 6.2 :

More practical mount for optical fibres. Fibres are cemented into the 7 flat faces and assembled in the "fly's eye" type configuration shown.

The need to exclude any stray photons is also obvious. The substitution of a stainless steel chamber in place of the present glass collision chamber is probably necessary though it may be possible to conduct trial runs with the present equipment coated with suitable black paint and draped in black cloth.

Photons shall also enter the collision chamber through the same slit as the primary beam. Light baffles shall have to be constructed and again great care shall have to be taken not to obstruct the particle beam.

6.5 CONCLUSIONS

A photon-particle coincidence experiment would be advantageous in interpreting the data and has been shown to be feasible. However, a number of difficulties would be encountered in effecting this modification.

Although it would enable selected inelastic channels to be measured on their own, no improvement in energy resolution would be obtained and very long counting times would be involved for the present apparatus. A multi-angle time of flight machine, with its correspondingly increased data rate, would make the investment of experimental time a practical proposition. In a similar way, if such equipment was designed with this specifically in mind many of the problems which would be encountered in modifying the present equipment would be avoided.

REFERENCES

AQU 72 V. Aquilanti, G. Liuti, F. Veechio-Cattivi and G.G. Volpi, Chem. Phys. Lett., 1972, (15), 305.

ATE 77 J.A. Aten, G.A.H. Lanting and J. Los, Chem. Phys., 1977, (19), 241.

AUE 73 D.J. Auerbach, M.M. Hubers, A.P.M. Baede and J. Los, Chem. Phys., 1973, (2), 107.

BAE 69 A.P.M. Baede, A.M.C. Moutinho, A.E. De Vries and J. Los, Chem. Phys. Lett., 1969, (3), 530.

BAE 71 A.P.M. Baede and J. Los, Physica, 1971, (52), 422.

BAE 75 Charge Transfer Between Neutrals at Hyperthermal Energies, Adv. in Chem. Phys. xxx, 1975, 463.

BAK 72 A.D. Baker and D. Betteridge, Photoelectron Spectroscopy, (Pergamon, Oxford, 1972).

BLA 63 N.C. Blais and D. Bunker, J. Chem. Phys., 1963, (39), 315.

BLA 69 N.C. Blais, J. Chem. Phys., 1969, (51), 856.

BOS 72 R.A. Boschi and D.R. Salahub, Mol. Phys., 1972, (24), 289.

BOS 74 R.A. Boschi and D.R. Salahub, Can. J. Chem., 1974, (52) 1217.

BRO 66 P.R. Brooks and E.M. Jones, J. Chem. Phys., 1969, (50), 5031.

BRO 73 P.R. Brooks and G. Marcelin, J. Amer. Chem. Soc., 1973, (95), 7885.

BUC 68 U. Buck and H. Pauly, Z. Phys., 1968, (208), 309.

BUC 75 U. Buck, Elastic Scattering, Adv. Chem. Phys. xxx, 1975, 313.

BUL 54 T.H. Bull and P.B. Moon, Disc. Faraday Soc., 1954, (17), 54.

BUN 73 D.L. Bunker and E.A. Goring Simpson, Faraday Disc. Chem. Soc., 1973, (55), 95.

DAL 60 N.R. Daly, Rev. Sci. Inst., 1960, (31), 264.

DEL 72 G.A.L. Delvigne and J. Los, Physica, 1972, (59), 61.

DUC 71 B.S. Duchart, Ph.D. Thesis, Edinburgh, 1971.

DUR 73 R. Duren, J. Phys. B, 1973, (6), 1801.

FIR 53 V.G. Firsov, Zh. Eksp. Teor. Fiz., 1953, (24), 279.

FLU 73 M.A.D. Fluendy and K.P. Lawley, Chemical Applications of Molecular Beam Scattering, (Chapman and Hall, London, 1973).

FLU 75 M.A.D. Fluendy, J.H. Kerr, J.M. McCall and D. Munro, On Line Computing in the Laboratory, Ed. R.A. Rosner, B.K. Penney and P.N. Clout, (Advance, London, 1975).

FLU 75a M.A.D. Fluendy, I.H. Kerr, K.P. Lawley and J.M. McCall, J. Phys. B., 1975, (8), L190.

GER 72 M.E. Gersh and R.B. Bernstein, J. Chem. Phys., 1972, (56), 6131.

GRI 75 R. Grice, Reactive Scattering, Adv. Chem. Phys. xxx, 1975, 247.

HAS 64 J.B. Hasted, Physics of Atomic Collisions (Butterworths, London, 1964).

HER 73 D.R. Herschbach, Faraday Disc. Chem. Soc., 1973, (55), 233.

HER 66 G. Herzberg, Electronic Spectra and Electronic Structure of Polyatomic Molecules, (Van Nostrad, New York, 1966).

HIT 78 A.P. Hitchcock and C.E. Brion, J. Electron Spec. and Rel. Phen., 1978, (13), 193.

HOC 75 P. Hochman, P.H. Templet, H. Wang and S.P. McGlynn, J. Chem. Phys., 1975, (62), 2588.

HUB 75 M.M. Hubers and J. Los, Chem. Phys., 1975, (10), 235.

JAN 70 P.A. Jansson et al, J. Opt. Soc. Amer., 1970, (60), 596.

KEM 74 V. Kempter, B. Kubler and W. Mecklenbrauck, J. Phys. B., 1974, (7), 2375.

KEM 75 V. Kempter, Electronic Excitation in Collisions Between Neutrals, Adv. Chem. Phys. xxx, 1975, 417.

KER 75 J.H. Kerr, Ph.D. Thesis, Edinburgh, 1975.

KIN 72 J.L. Kinsey, Molecular Beam Reactions, (M.T.P. Int. Rev. Sci., Physical Chemistry, 1972, Ser. 1, Vol. 9).

KNE 76 T. Kneser, Ph.D. Thesis, Gottingen, 1976.

LAC 70 K. Lacmann and D.R. Herschbach, Chem. Phys. Lett., 1970, (6), 106.

LEE 68 Y.T. Lee, J.D. McDonald, P.R. Le Breton and D.R. Herschbach, J. Chem. Phys, 1968, (49), 2447.

LEE 69 Y.T. Lee, J.D. McDonald, P.R. Le Breton and D.R. Herschbach, Rev. Sci. Instr., 1969, (40), 1402.

MCC 78 J.M. McCall and M.A.D. Fluendy, J. Phys. E., 1978, (11), 631

MAL 70 C.J. Malerich and R. Cross, J. Chem. Phys., 1970, (52), 386

MOU 71 A.M.C. Moutinho, A.P.M. Baede and J. Los, Physica, 1971, (53), 471.

MOU 74 A.M.C. Moutinho, J.A. Aten and J. Los, Chem. Phys., 1974, (5), 84.

PAS 74 J. Pascale and J. Vanderplanque, J. Chem. Phys., 1974, (60), 2278.

RAY 67 J.W. Raymonds and W.T. Simpson, J. Chem. Phys., 1967, (47), 430.

RED 73 J.F. Reddington, Ph.D. Thesis, Edinburgh, 1973.

SCH 72 A. Schutte, D. Bassi, F. Tommasini and G. Scoles, Phys. Rev. Lett., 1972, (29), 979.

STU 32 E.C.G. Stueckelberg, Helv. Phys. Acta, 1932, (5), 369.

TAY 55 E.H. Taylor and S. Datz, J. Chem. Phys., 1955, (23), 1711.

TUL 71 J.C. Tully and R.K. Preston, J. Chem. Phys., 1971, (55), 56.

TUR 70 D.W. Turner, C. Baker, A.D. Baker and C.R. Brindle, Molecular Photoelectron Spectroscopy, (Wiley, New York, 1970).

WAL 58 F.T. Wall, L.A. Hiller and J. Mazur, J. Chem. Phys., 1958, (28), 255.

WAN 77 H.T. Wang, W.S. Felps, G.L. Findley, A.R.P. Rau and S.P. McGlynn, J. Chem. Phys., 1977, (67), 3940.

WEN 69 W.E. Wentworth, R. George and H. Keith, J. Chem. Phys., 1969, (51), 1791.

ZEN 32 C. Zener, Proc. Roy. Soc., 1932, (A137), 697.

ACKNOWLEDGEMENTS

I should like to take this opportunity to express my gratitude to all those people who made this work possible.

My thanks go to Malcolm Fluendy and Kenneth Lawley, whose optimism and "beaming" experience were frequently called upon, and to my parents and wife, who provided encouragement and suffered my pre-occupation with electronic excitation throughout the period of my research. Thanks are due, too, to Geoffrey Black who proved a most helpful co-experimenter, and to Rob Glen, Doug Fernie and Ross Wheeler, whose frequent visits from the neighbouring Lab provided us with light entertainment.

I should also like to acknowledge the technical assistance of Malcolm Fergusson and Jimmy McKemmie, who both served time as the Group's Technician during my stay, and to the electronic wizards of the Chemistry Department electronic workshop.

Finally, I wish to thank the Science Research Council for financial support, The University of Edinburgh for laboratory, computing and workshop facilities, and Nita, whose skill and patience transformed the scribbled manuscript into legible type.

D.P.S.

APPENDIX A

FILE IDENTIFIER : FILTER7 LISTED ON 23/08/79 AT 15.07.14

```
%BEGIN
!
!     THIS PROGRAM TAKES THE RAW DATA AND USES THE REFERENCE TO
!       DECONVOLUTE THE SCATTERED DATA SO THE PEAKS AND VALLEYS AR
!       INTENSIFIED
!
!       ALL CHANNELS ARE SHIFTED +1 RELATIVE TO THE DISPLAY FROM C
!       BECAUSE FILTER5 NUMBERS THE CHANNELS 1 TO NMAX AND CFIT NU
!         THEN CHANNELS 0 TO NMAX
!
!    ST1---RAW DATA
!    ST2---FILE CONTAINING NORMALIZATION DATA
!    ST3---LINE PRINTER LISTING
!    ST4---DATA FOR CONTOURING PROGRAM
!    ST10--I/O FOR COMMANDS
!    ST11--I/O FOR COMMANDS
!
!     FIRST REFBLOCK= REFERENCE SHAPE TO BE USED
!           IF FIRST REFBLOCK IS > SECOND REF THEN SECOND REF IS 1
!     SECOND REF= REFERENCE SHAPE FOLLOWING DATA (=0 IF NO SECOND
!           START BLOCK IS INDEPENDENT OF THE REFERENCE SHAPES AS
!           THE COMPUTER IS CONCERNED, BUT SHOULD BE BETWEEN THE 1
!     START BLOCK=STARTING BLOCK OF DATA
!     NO. BLOCKS=NO. OF DATA BLOCKS TO BE PROCESSED
!     NITS2=MAXIMUM NO. OF ITERATIONS TO BE PERFORMED (200)
!     NFILT=NO. OF FILTER PASSES ON REFERENCE SHAPE
!     NFILT1=NO. OF FILTER PASSES ON DATA SHAPE
!     CENTER= TRUE BEAM CENTER
!     TARGET=TRUE TARGET MASS
!     MIN ITS=MINIMUM NO. OF ITERATIONS BEFORE DECONVOLUTION IS C
!
%INTEGER I,J,K,IK,INDEXX,C,ITS,NITS2,MINITS,REFMAX,RN,PX
%INTEGER REFBLOCK,REFBLOCK2,DATBLOCK,NREF,NDAT,NDAT1,NBLOCKS,BLOC
%INTEGER BLOCKS,JJ,NFILT,NFILT1,ZFLAG,PLAT
%REAL MAX,SUMR,SUM,SUMSQ,X,YE,CENTRE,TARGET,KAPPA
%REAL SAVESQ,NORM,ANGLE,FACTOR
%INTEGERARRAY REFDAT,DATDAT(1:1024),REFCOUNT,DATCOUNT(1:100)
%INTEGERARRAY NPTS,CODE(1:4)
%REALARRAY XNORM,YNORM(0:100)
%REALARRAY XX,YY(1:4,1:256)
%REALARRAY REFVARS,DATVARS(1:120)
%REALARRAY RESID,Y,AF,REF,G,Z(1:256),B,ERRB(-20:20)
%REALARRAY ERR(-1:256,1:3),WORK(-1:258)
%REALARRAY BLX,BLY(1:820)
%REALARRAY POLT,CC(-20:20,1:100)
%REALARRAY DATA(1:100),SHIFT(1:2)
%STRING (1) ST
```

```
'EVENTS','NOISE','ANGLE OF ...','TIME OF ...(SEC)','TARGET FLUX'
'BEAM FLUX','NO. BLOCKS','DATE','BEAM ENERGY','BEAM MASS',
'TARGET TEMP','TARGET MASS','BEAM CENTRE','SEQUENCE NO.',
'CEC SLIT SIZE','POST CEC SLIT','PRE SCAT SLIT','TARGET WIDTH',
'DETECTOR WIDTH','DETECTOR HEIGHT','BEAM HEIGHT','CLOCK PERIOD',
'VAR 16','REF. ANGLE','BLANK','MIN ANGLE','MAX ANGLE',
'STEP SIZE','SCAN FLAG','NO. PULSES','SIGNAL/NOISE','OFFSET',
'MIN PEAK RATE','ENTRY ONE','ENTRY TWO','MB CHECK FREQ','MBM INT
'MBM FLAG','CBM FLAG','REAL START TIME','REAL END TIME',
'FRAC REF CHANNEL'
!
%EXTERNALREALFNSPEC INTERP(%REALARRAYNAME I,W,%REAL AR,%INTEGER
%EXTERNALROUTINESPEC PROMPT(%STRING (15) S)
%EXTERNALROUTINESPEC IMPGRAPH9(%REALARRAYNAME X,Y,%C
%INTEGERARRAYNAME UP,CODE,%INTEGER N,LINES,NPMAX)
%ROUTINESPEC READFROMFILE(%INTEGER BLOCK,%INTEGERARRAYNAME %C
      DATA,COUNT,%REALARRAYNAME VARS)
%ROUTINESPEC SUMMARISE(%INTEGER BLOCK,%REALARRAYNAME VARS)
%ROUTINESPEC ADDUP(%INTEGERARRAYNAME INDAT,%REALARRAYNAME UTDAT,
      ERR,VARS,%INTEGERNAME SIZE)
%ROUTINESPEC OUTPUT
%ROUTINESPEC FILTER(%REALARRAYNAME INDAT,UTDAT,%INTEGER N)
%ROUTINESPEC  ZCALC
%ROUTINESPEC NCALC
%ROUTINESPEC YCALC
%ROUTINESPEC EXPAND(%REALARRAYNAME B,BEX)
%ROUTINESPEC NEWSHAPE(%REALARRAYNAME BEX,BNEW,%INTEGER INDEX)
%ROUTINESPEC COMPRESS(%REALARRAYNAME BNEW,BOUT,%INTEGER N)
%ROUTINESPEC RENORM(%REALARRAYNAME B,C,%INTEGER N)
%REALFNSPEC SPREAD(%INTEGER I)
!
!      INITIALISE
!
CODE(1)='A';CODE(2)='B';CODE(3)='C';CODE(4)='D'
ITS=0
JJ=0
ZFLAG=0 ;! 0 => Z-MOD, 1 => AMP. MOD
SAVESQ=0.
NORM=0.
SELECTINPUT(10)
SELECTOUTPUT(11)
PROMPT('FIRST REFBLOCK:');READ(REFBLOCK)
PROMPT('SECOND REF:');READ(REFBLOCK2)
PROMPT('START BLOCK:');READ(BLOCK)
!
!      CAN ANALYSE MORE THAN ONE DATA BLOCK BUT THE DATA BLOCKS
!      USED MUST BE CONTIGUOUS.
!      SECOND REF MUST BE GREATER THAN FIRST REFBLOCK.
!
PROMPT('NO. BLOCKS:');READ(NBLOCKS);BLOCKS=NBLOCKS
PROMPT('NITS2:');READ(NITS2)
PROMPT('NFILT:');READ(NFILT)
PROMPT('NFILT1:');READ(NFILT1)
PROMPT('CENTRE:');READ(CENTRE)
PROMPT('TARGET:');READ(TARGET)
PROMPT('MIN ITS:');READ(MINITS)
PROMPT('PLATEAU:');READ(PLAT)
KAPPA=10.
NEWLINE
SELECTINPUT(2)
!
!      NORMALISATION DATA
!
    %CYCLE I=0,1,100
    READ(XNORM(I));READ(YNORM(I))
      ----
```

```
SELECT OUTPUT(1)
SETMARGINS(1,1,132)
READFROMFILE(REFBLOCK,REFDAT,REFCOUNT,REFVARS)
%IF REFVARS(9)>200. %THEN ZFLAG=1 ;! E>200EV => AMP. MOD.
ERROR:
     %IF REFVARS(23)#1. %THENSTART
     NEWLINE
     PRINTSTRING(' BLOCK NUMBER');WRITE(REFBLOCK,3)
     PRINTSTRING(' IS NOT A REFERENCE SHAPE');NEWLINE
     %STOP
     %FINISH
    IK=1
ADDUP(REFDAT,WORK,ERR,REFVARS,NREF)
RAW2:
->RAW %IF NFILT=0
     %CYCLE I=1,1,NFILT
     FILTER(WORK,REF,NREF)
         %IF I=NFILT %THEN ->READY1
         %CYCLE J=1,1,NREF
         WORK(J)=REF(J)
         %REPEAT
     %REPEAT
RAW: !  USE RAW REFERENCE SHAPE
!
%CYCLE I=1,1,NREF
REF(I)=WORK(I)
ERR(I,2)=ERR(I,1)
%REPEAT
READY1:
-> IK2 %IF IK=2
MAX=0.
     %CYCLE I=1,1,NREF
     %IF MAX<REF(I) %THENSTART
     !
     !      FIND MAX AND ITS LOCATION
     !
     MAX=REF(I);INDEXX=I
     %FINISH
     %REPEAT
REFMAX=INDEXX ;!  NEED THIS LATER TO ALIGN DATA FOR CONTOURING
IK2:
   X=0.0
   YE=0.0
   %CYCLE I=REFMAX-10,1,REFMAX+10
   %IF REF(I)>=(MAX/2)  %THENSTART
   X=X+REF(I)*I
   YE=YE+REF(I)
   %FINISH
   %REPEAT
   SHIFT(IK)=X/YE-REFMAX
->CONTINUE2 %IF IK=2
REFVARS(42)=SHIFT(IK)
SUMMARISE(REFBLOCK,REFVARS)    ;! JUST PRINTS
!
!
!      SET UP REFERENCE FOR DECONVOLUTION PROCESS
!
%CYCLE I=-20,1,20
K=I+INDEXX
%IF K<1 %THENSTART
ERRB(I)=0.0;B(I)=0.;->OK;%FINISH
B(I)=REF(K)
NORM=NORM+B(I) ;! USED IF AMP MOD ONLY
ERRB(I)=ERR(K,2)
OK:  %REPEAT
```

```
    %REPEAT
->AMP MOD %IF ZFLAG=1
|
|       EXPAND REFERENCE SHAPE
|
EXPAND(B,BEX)
->CONTINUE
AMP MOD:  %CYCLE I=-20,1,20
B(I)=B(I)/NORM ;! UNIT AREA
%REPEAT
CONTINUE:  !
|
|    ******  TREAT SECOND REFERENCE BLOCK  ******
|
%IF REFBLOCK2<REFBLOCK %THEN -> NO REF
DATBLOCK=REFBLOCK2-REFBLOCK
READFROMFILE(DATBLOCK,REFDAT,REFCOUNT,DATVARS)
  %IF  DATVARS(23)#1. %THEN ->ERROR
   ADDUP(REFDAT,WORK,ERR,DATVARS,NREF)
  IK=2
  ->RAW2
CONTINUE2:
DATVARS(42)=SHIFT(IK)
SUMMARISE(REFBLOCK2,DATVARS)
NO REF:
SELECT INPUT(10)
CLOSE STREAM(1)
|
|    ********************************************
|      TREAT SCAT DATA NOW
|    ********************************************
|
SELECT INPUT(1)
SET MARGINS(1,1,123)
DATBLOCK=BLOCK
SUM=1.0@-3
READIN: ! DATA
READFROMFILE(DATBLOCK,DATDAT,DATCOUNT,DATVARS)
|
|       TEMP. PATCH TO CORRECT FAULTY DATA
|
DATVARS(13)=CENTRE
DATVARS(12)=TARGET
DATVARS(42)=SHIFT(1)
%IF REFBLOCK2>REFBLOCK %THEN DATVARS(42)=(BLOCK-REFBLOCK) %C
  *(SHIFT(2)-SHIFT(1))/(REFBLOCK2-REFBLOCK)+SHIFT(1)
%IF DATVARS(23)#0. %THENSTART
NEWLINE
PRINTSTRING(' BLOCK NUMBER');WRITE(BLOCK,3)
PRINTSTRING(' IS NOT SCATTERING DATA');NEWLINE
PRINT STRING(' DO YOU WANT TO FILTER THIS BLOCK?');NEWLINE
SELECT INPUT(10)
2:
PROMPT('Y, N: ')
READ ITEM(ST)
%IF ST='Y' %THEN SELECT INPUT(1) %AND ->4
%IF ST#'N' %THEN ->2
%STOP
%FINISH
4:
SUMMARISE(BLOCK,DATVARS)
ADDUP(DATDAT,WORK,ERR,DATVARS,NDAT1)
|
|    CORRECTION FOR FAULTY DATA (DATA ON A PLATEAU
```

```
  %CYCLE I=1,1,NDAT1
  WORK(I)=WORK(I)-PLAT
  %REPEAT
!
!      NORMALISATION SECTION
!
ANGLE=(DATVARS(3)-CENTRE)*1.E-3
ANGLE=ARCTAN(28.6,ANGLE)*180./£
SUMM=DATVARS(1)-DATVARS(2)
RN=10
%IF DATVARS(9)=100. %THEN RX=30
%IF DATVARS(9)=200. %THEN RX=20
%IF DATVARS(9)>200. %THEN RN=5 %AND RX=10
SUMM=0.
%CYCLE I=REFMAX-RN,1,REFMAX+RX
SUMM=SUMM+WORK(I)
%REPEAT
%IF ANGLE>XNORM(100) %THENSTART
FACTOR=YNORM(100)/(SUMM*ANGLE*ANGLE)
->NORMED
%FINISH
%IF ANGLE=0. %THEN FACTOR=1. %AND ->NORMED
FACTOR=INTERP(XNORM,YNORM,ANGLE,100)/(SUMM*ANGLE*ANGLE)
NORMED: DATVARS(4)=FACTOR
DATVARS(5)=FACTOR
DATVARS(6)=FACTOR
->NOFILT %IF NFILT1=0
     %CYCLE I=1,1,NFILT1
     FILTER(WORK,AF,NDAT1)
       %IF I=NFILT1 %THEN ->READY
       %CYCLE J=1,1,NDAT1
       WORK(J)=AF(J)
       %REPEAT
     %REPEAT
NOFILT: !   USE RAW DATA
%CYCLE I=1,1,NDAT1
AF(I)=WORK(I)
ERR(I,2)=ERR(I,1)
%REPEAT
READY:
!
!      USE FIRST 80 CHANNELS IF NDAT>80
!
NDAT=1024//INTPT(DATVARS(30)) %IF DATVARS(9)>200.
NDAT=100 %IF DATVARS(9)=100.
NDAT=80 %IF DATVARS(9)=200.
%CYCLE I=1,1,NDAT
DATA(I)=0.
K=I+INDEXX-20
%IF K>0 %AND K<=NDAT1 %THEN %START
DATA(I)=AF(K)
ERR(I,1)=ERR(K,2)
%FINISH
%REPEAT
->1 %IF BLOCKS>NBLOCKS ;! ALREADY SET UP
->AMP MOD1 %IF ZFLAG=1
!
!      SET UP NEW REFERENCES SHAPES
!    I.E. CREATE AN ARRAY WITH A REFFRENCE SHAPE FOR EACH DATA C
!
     %CYCLE I=1,1,NDAT
     K=I-20
     NEWSHAPE(BEX,BNEW,K)
     COMPRESS(BNEW,BOUT,I)
     %REPEAT
```

```
->1
AMP MOD1:  %CYCLE I=1,1,NDAT
%CYCLE J=-20,1,20
|
|      REFERENCE SHAPE NOT CHANGING WITH ENERGY LOSS
|
CC(J,I)=B(J)
%REPEAT
%REPEAT
|
| *** START OF ITERATION ***
|
1:
     %CYCLE I=1,1,NDAT
     G(I)=DATA(I)    ;!    INITIALIZE FILTERED ARRAY
     ERR(I,2)=ERR(I,1)
     %REPEAT
ITS=0
SAVESQ=1.
 ->FIN %IF NITS2=0
|
|      ********** TOP OF ITERATION LOOP **********
|
99:
ZCALC
NCALC
ITS=ITS+1
YCALC
SUMSQ=0.
     %CYCLE I=2,1,NDAT-1
     X=Y(I)-DATA(I)
     YE=ERR(I,1)
     %IF YE=0. %THEN YE=(ERR(I-1,1)+ERR(I+1,1))/2.
     %IF YE=0. %THEN YE=100.
     SUMSQ=SUMSQ+X*X/(YE*YE)
     %REPEAT
NEWLINE
PRINTFL(SUMSQ,4)
%IF ITS<MINITS %THEN ->98
%IF MOD((SAVESQ-SUMSQ)/SAVESQ)<SUM %THEN ->100
98:
%IF SUMSQ>SAVESQ %AND SAVESQ#1. %THENSTART
PRINTSTRING(' RESIDUAL INCREASING AFTER');WRITE(ITS,4)
PRINT STRING(' ITERATIONS')
%FINISH
SAVESQ=SUMSQ
->99 %IF ITS<NITS2
|
|      ********** BOTTOM OF ITERATION LOOP **********
|
100:
NEWLINE
PRINTSTRING('DECONVOLUTION COMPLETE AFTER');WRITE(ITS,4)
PRINTSTRING('ITERATIONS')
NEWLINE
FIN:
SELECTOUTPUT(3)
SETMARGINS(3,1,132)
NEWLINE
PRINTSTRING(' ID:  ')
PRINT(DATVARS(14),6,0);WRITE(BLOCK,6);NEWLINES(2)
OUTPUT
|
|      CALCULATE AND PRINT RESIDUE
|
```

```
    %CYCLE I=1,1,NDAT
    RESID(I)=DATA(I)-Y(I)
    XX(1,I)=I;XX(2,I)=I;XX(3,I)=I;XX(4,I)=I
    YY(1,I)=DATA(I);YY(2,I)=Y(I);YY(3,I)=RESID(I);YY(4,I)=G(I)
    %REPEAT
NEWLINE
%CYCLE I=1,1,NDAT
WRITE(I,4);SPACE
PRINT(DATA(I),6,4):SPACES(2);PRINT(Y(I),6,4)
SPACES(2)
%IF DATA(I)#0. %THEN PRINT(RESID(I)/SQRT(MOD(DATA(I))),6,4)
NEWLINE
%REPEAT
NEWLINE
NPTS(1)=NDAT;NPTS(2)=NDAT;NPTS(3)=NDAT;NPTS(4)=NDAT
IMPGRAPH9(XX,YY,NPTS,CODE,4,NDAT,NDAT)
SELECTOUTPUT(4)
!
!      DATA FILE FOR CONTOURING PACKAGE
!
JJ=0
!
!      FIND HOW MANY NON-ZERO CHANNELS
!       G(1)=A(1) AND G(NDAT)=A(NDAT) FOR ALL ITERATIONS
!       THEREFORE  THEY ARE ELIMINATED FROM THE FINAL SPECTRUM
!
    %CYCLE I=2,1,NDAT-1
    JJ=JJ+1 %IF G(I)#0.
    %REPEAT
RN=10
%IF DATVARS(9)=100. %THEN RX=30
%IF DATVARS(9)=200. %THEN RX=20
%IF DATVARS(9)>200. %THEN RN=5 %AND RX=10
SUMM=0.
%CYCLE I=REFMAX-RN,1,REFMAX+RX
K=I-INDEXX+20
SUMM=SUMM+G(K)
%REPEAT
%IF ANGLE>XNORM(100) %THEN %START
FACTOR=YNORM(100)/(SUMM*ANGLE*ANGLE)
-> DAV1
%FINISH
%IF ANGLE=0 %THEN FACTOR=1 %AND -> DAV1
FACTOR=INTERP(XNORM,YNORM,ANGLE,100)/(SUMM*ANGLE*ANGLE)
DAV1:DATVARS(5)=FACTOR
C=0
%CYCLE I=1,1,44
C=C+1
PRINTFL(DATVARS(I),4)
%IF C=4 %THENSTART
C=0;NEWLINE;%FINISH
%REPEAT
NEWLINE
WRITE(REFMAX,6);NEWLINE;!  PEAK POSITION
WRITE(JJ,6);NEWLINE
OUTPUT
C=0
NEWLINE
    %CYCLE I=2,1,NDAT-1
    %IF G(I)#0. %THENSTART
    C=C+1
    WRITE(I-20+INDEXX,4)
    PRINT(ERR(I,2),6,4)
    %IF C=4 %THENSTART
    C=0;NEWLINE;%FINISH
```

```
    %REPEAT
NEWLINE
NBLOCKS=NBLOCKS-1
%IF NBLOCKS=0 %THENSTOP
SELECTOUTPUT(11)
SELECTINPUT(1)
SETMARGINS(1,1,132)
BLOCK=BLOCK+1
DATBLOCK=1
->READIN ;!     FETCH NEXT DATA BLOCK
!
%STOP
%ROUTINE OUTPUT
C=0
%CYCLE I=2,1,NDAT-1
%IF G(I)#0. %THENSTART
C=C+1
!
!      RESTORE TRUE ORIGIN AND PRINT OUT
!
WRITE(I-20+INDEXX,4)
PRINT(G(I),6,4)
%IF C=4 %THENSTART
C=0;NEWLINE;%FINISH
%FINISH
%REPEAT
NEWLINE
%END ;! OUTPUT
!
%ROUTINE FILTER(%REALARRAYNAME INDAT,UTDAT,%INTEGER N)
!
!      FIVE POINT POLYNOMIAL FILTER
!
%INTEGER I
%REAL NSUM
%CYCLE I=-1,1,0
INDAT(I)=INDAT(N+I)
ERR(I,1)=ERR(N+I,1)
%REPEAT
%CYCLE I=N+1,1,N+2
INDAT(I)=INDAT(I-N)
ERR(I,1)=ERR(I-N,1)
%REPEAT
%CYCLE I=1,1,N
NSUM=17.*INDAT(I)+12.*(INDAT(I+1)+INDAT(I-1))-3.*(INDAT(I+2)+INDAT(I-2
UTDAT(I)=NSUM/35.
NSUM=(17.*ERR(I,1))**2+144.*(ERR(I+1,1)**2+ERR(I-1,1)**2)
NSUM=NSUM+9.*(ERR(I+2,1)**2+ERR(I-2,1)**2)
ERR(I,2)=SQRT(NSUM/595.)
%REPEAT
%END ;! FILTER
!
!
%ROUTINE READFROMFILE(%INTEGER BLOCK,%INTEGERARRAYNAME DATA,COUNT,%C
%REALARRAYNAME VARS)
%INTEGER I,J
%REAL X
->GO %IF BLOCK=1
%CYCLE I=1,1,BLOCK-1
%CYCLE J=1,1,1252
READ(X);!   DUMMY PARAM
%REPEAT
%REPEAT
GO:   %CYCLE I=1,1,10.4
READ(DATA(I))
```

```
%CYCLE I=1,1,12
READ(VARS(I))
%REPEAT
%CYCLE I=1,1,100
READ(COUNT(I))
%REPEAT
%END ;! READFROMFILE
!
!
%ROUTINE SUMMARISE(%INTEGER BLOCK,%REALARRAYNAME VARS)
%INTEGER I
NEWLINE
PRINTSTRING(' SUMMARY OF BLOCK NUMBER');WRITE(BLOCK,3)
NEWLINES(2)
%CYCLE I=1,1,42
PRINTSTRING(TITLE(I).': ');PRINT(VARS(I),6,4)
NEWLINE
%REPEAT
%END ;! SUMMARISE
!
!
%ROUTINE ADDUP(%INTEGERARRAYNAME INDAT,%REALARRAYNAME UTDAT,ERR
%INTEGERNAME SIZE)
%INTEGER I,J,N,NPULSE
%REAL SUM,SUMSQ
NPULSE=INTPT(VARS(30)) ;! NO. OF PULSES PER CYCLE
N=1024//NPULSE
SUM=0.
SUMSQ=0.
%CYCLE I=1,1,N
%CYCLE J=0,N,1024-N
!
!      ADD UP CORRESPONDING CHANNELS
!
SUM=SUM+INDAT(I+J)
%REPEAT
UTDAT(I)=SUM
%IF VARS(23)#0 %THEN ERR(I,1)=SQRT(SUM) %AND ->REF
SUM=SUM/NPULSE
%CYCLE J=0,N,1024-N
SUMSQ=SUMSQ+(INDAT(I+J)-SUM)**2
%REPEAT
ERR(I,1)=SQRT(SUMSQ)
SUMSQ=0.
REF:
SUM=0.
%REPEAT
SIZE=N
%END ;! ADDUP
!
%ROUTINE ZCALC
!
!  THIS ROUTINE TOGETHER WITH NCALC CONSTRUCTS THE NEXT
!     APPROXIMATION TO THE DECONVOLUTED SPECTRUM ACCORDING TO
!     EQ(3) P.A. JANSSON ET. AL.,J. OPT. SOC. AMER.,  60,
!     596 (1970),  AND J. OPT. SOC. AMER.,60, 184 (1970)
!     (H. P. VAN CITTERT METHOD)
!
!  THESE TWO ROUTINES ARE NOT AS EFFICIENT AS THE POINT SIMULT/
!     OR POINT SUCCESSIVE OVER-RELAXATION  PROCEDURES, BUT WERE
!     TO BE A MORE STABLE PROCEDURE.
!
%REAL SUM,SUME
%INTEGER K
SUM=0.
```

```
%CYCLE I=1,1,NDAT
%CYCLE J=-20,1,20
K=I+J
%IF K<1 %OR K>NDAT %THEN ->NONE
SUM=SUM+G(K)*CC(J,I)
SUME=SUME+(ERR(K,2)*CC(J,I))**2+(ERRB(J)*G(K))**2
NONE:
%REPEAT
Z(I)=SUM
ERR(I,3)=SUME
SUME=0.
SUM=0.
%REPEAT
%END ;! ZCALC
!
%ROUTINE NCALC
%REAL SUM,SUME
SUM=0.
SUME=0.
!
!      COMPARE SPECTRUM AND FIT OVER 3 CHANNELS
!
!    SUBTRACT FIT FROM DATA AND CREATE A NEW FILE
!
%CYCLE I=2,1,NDAT-1
%CYCLE J=-1,1,1
SUM=SUM+DATA(I+J)-Z(I+J)
SUME=SUME+ERR(I+J,1)**2+ERR(I+J,3)          ;!ERR(I+J,3) IS A
                                             ! VALUE FROM ZCAL
%REPEAT
G(I)=G(I)+SUM/KAPPA
SUM=0.
ERR(I,2)=SQRT(ERR(I,2)**2+SUME/(KAPPA**2))
SUME=0.
%IF G(I)<0. %THEN G(I)=0.
%REPEAT
%END ;! NCALC
!
!
%ROUTINE YCALC
!
!      RECONSTRUCT SPECTRUM
!
%CYCLE I=1,1,NDAT
Y(I)=0.
%REPEAT
%CYCLE I=1,1,NDAT
%CYCLE J=-20,1,20
K=I+J
%IF K<1 %OR K>NDAT %THEN ->NOCON
Y(I)=Y(I)+G(K)*CC(J,I)
NOCON:
%REPEAT
%REPEAT
%END ;! YCALC
!
!
!
!
%ROUTINE EXPAND(%REAL/ARRAYNAME P,BEX)
%INTEGER I,J,K
K=0
!
!      EXPAND REFERENCE SHAPE SO EACH CHANNEL IS EQUIVALENT GO
!
```

```
%CYCLE J=1,1,4
K=K+1
BEX(K)=B(I)
%REPEAT
%REPEAT
%END ;! EXPAND
!
!
%ROUTINE NEWSHAPE(%REALARRAYNAME BEX,BNEW,%INTEGER INDEX)
!
!    CALCULATES REFERENCE BEAM SHAPE FOR DATA CHANNEL INDEX
!
%REAL WIDTH,X,SUM
%INTEGER I,J,IWIDTH,K
WIDTH=SPREAD(INDEX)  ;!  WIDTH OF BEAM IN NS
IWIDTH=INTPT(WIDTH+.5)//5 ;! 5 NS CHANNEL WIDTH
!
!      SET UP THE REQUIRED DELTA FUNCTION (MODIFIED)
!
%CYCLE I=1,1,164
SUM=0.
%CYCLE J=1,1,IWIDTH+1
K=I-J
%IF K<=0 %OR K>164 %THEN X=0. %ELSE X=BEX(K)
SUM=SUM+X
%REPEAT
BNEW(I)=SUM
%REPEAT
%END ;! NEWSHAPE
!
!
%REALFN SPREAD(%INTEGER I)
!
!      CALCULATES SPREAD DUE TO GIVEN ENERGY LOSS
!
%REAL MASSCON,ECHARGE,LSC,ENERGY,MASS,CLOCK
%REAL EX,EP,FACT,SIGMA
!
!      DEFINITIONS
!
MASSCON=1.66043-27 ;! AMU TO KILOS
ECHARGE=1.6021@-19 ;! EV TO JOULES
LSC=.601 ;! SCAT. CENTRE TO DETECTOR (METRES)
CLOCK=DATVARS(22) ;! CLOCK PERIOD (NS)
ENERGY=DATVARS(9) ;! BEAM ENERGY (EV)
MASS=DATVARS(10) ;! BEAM MASS (AMU)
EP=.09*ENERGY ;! APPROX PULSER ENERGY
!
!      CALCULATE ENERGY LOSS CORRESPONDING TO CHANNEL I
!
EX=MOD(CLOCK*I*1.@-9*SQRT(2./(MASS*MASSCON)))
EX=1./(EX/LSC+1./SQRT(ENERGY*ECHARGE))
EX=EX*EX/ECHARGE-ENERGY
EX=MOD(EX) ;! REMOVE SIGN
!
!      CALCULATE SPREAD IN NANOSECONDS
!
FACT=LSC*SQRT(MASS*MASSCON/(2.*ECHARGE))
SIGMA=FACT*(1./SQRT(ENERGY-EX)-1./SQRT(ENERGY) %C
      +1./SQRT(ENERGY+EP)-1./SQRT(ENERGY+EP-EX))
%RESULT=1.@9*SIGMA
%END ;! SPREAD
!
!
%ROUTINE COMPRESS(%REALARRAYNAME BNEW,BOUT,%INTEGER N)
```

```
!          STANDARD ARRAY WITH 20 NS CHANNELS
!
%INTEGER I,J,K
%REAL SUM
K=0
%CYCLE I=-20,1,20
SUM=0.
%CYCLE J=1,1,4
K=K+1
SUM=SUM+BNEW(K)
%REPEAT
BOUT(I,N)=SUM
%REPEAT
%END ;! COMPRESS
!
!
%ROUTINE REWORK(%REALARRAYNAME B,C,%INTEGER N)
!
!      NORMALISE NEW REFERENCE SHAPES TO UNIT AREA
!
%INTEGER I,J,K,INDEX
%REAL MAX,SUM
%CYCLE J=1,1,N
SUM=0.
MAX=0.
%CYCLE I=-20,1,20
%IF MAX<=B(I,J) %THENSTART
INDEX=I;MAX=B(I,J)
%FINISH
SUM=SUM+B(I,J)
%REPEAT
%CYCLE I=-20,1,20
K=I+INDEX
%IF K<-20 %THENSTART
K=K+41
%FINISH
%IF K>20 %THENSTART
K=K-41
%FINISH
C(I,J)=B(K,J)/SUM
%REPEAT
%REPEAT
%END ;! REWORK
!
!
%ENDOFPROGRAM
```

M4305

```
***ERCC 4-75 EMAS***    EDCD06    SUTTON JCMB
***ERCC 4-75 EMAS***    EDCD06    SUTTON JCMB
***ERCC 4-75 EMAS***    EDCD06    SUTTON JCMB
***ERCC 4-75 EMAS***    EDCD06    SUTTON JCMB
***ERCC 4-75 EMAS***    EDCD06    SUTTON JCMB
***ERCC 4-75 EMAS***    EDCD06    SUTTON JCMB
***ERCC 4-75 EMAS***    EDCD06    SUTTON JCMB
***ERCC 4-75 EMAS***    EDCD06    SUTTON JCMB
```

APPENDIX B

FILE IDENTIFIER : DCP5SOUR LISTED ON 23/08/79 AT 15.06.24

```
%BEGIN
%CONTROL 1
%CONTROL 4  ;! NO LINE NUMBERS OR ARR BD CHECK
%REALFN ABS(%REAL B)
B=-B %IF B<0
%RESULT=B
%END  ;! ABS
%ROUTINE SETPOT(%INTEGER X,UNIT)
!
!     X=UNIT => ON, X=0 => OFF
!
!  RELAY1 -- MAIN BEAM MONITOR
!  RELAY2 -- HIGH VOLTAGE ON/OFF
!
*MOV_R1,-(SP)
*MOV_14.(R1),R0  ;! X
*MOV_16.(R1),R1  ;! UNIT
*EMT_352
*MOV_(SP)+,R1
%END  ;! SETPOT
%ROUTINE PRINTCH(%INTEGER I)
LACC(I)
*EMT_305
%END
%ROUTINE SCREEN
PRINTSYMBOL(7)
PRINTCH(27)
PRINTCH(12)
%END ;! SCREEN
%ROUTINE WAIT(%INTEGER X)
!WAITS X/50 SECS AND THEN RETURNS
!X SHOULD NOT EXCEED 32,767
LACC(X)
*EMT_375
%END
%REALFN RTIME
%INTEGER A,B
*MOV_R1,-(SP)
*EMT_321  ;! TIME IN R0,R1
*MOV_R1,R5
*MOV_(SP)+,R1 ;!RESTORE R1
*MOV_R0,34.(R1) ;!HIGH ORDER IN A
*MOV_R5,36.(R1) ;!LOW ORDER IN B
A=A+1 %IF B<0  ;!SIGN BIT?
%RESULT=(A*65536.+B)/3600  ;! MINUTES
%END  ;!OF FILE
%INTEGERFN VOLT(%INTEGER CHAN,GAIN)
```

```
*LIT_0000
%RESULT=ACC
%END  ;! FN VOLT
%REALFN MOD(%REAL X)
*_BIC_#100000,14.(R1)
%RESULT=X
%END  ; ! OF FN MOD
%ROUTINE PRINT(%REAL X,%INTEGER N,M)
%ROUTINESPEC PRINTFL(%REAL X,%INTEGER N)
%OWNINTEGER IMAX=32767 ; !MAX INTEGER IN ONE WORD.
%REAL Y,Z,ROUND
%INTEGER I,J,L,SIGN,DP ;          ! DP =DECIMAL POINT
M=4 %IF M>4 ; DP=0 ;                    ! DEAL WITH STUPID PARAMS
%IF N<=0 %THEN N=1 ;              ! DEAL WITH STUPID PARAMS
Y=MOD(X) ;                        ! ALL WORK DONE WITH Y
ROUND= (1/2)/10**M ;                ! ROUNDING FACTOR
%IF Y>IMAX %THEN %START
PRINTFL(X,M) ; %RETURN ; %FINISH
I=0 ;Z=1 ; Y=Y+ROUND ;
COUNT LEADING PLACES:
I=I+1 ;Z=10*Z ;                    ! NO DANGER OF OVERFLOW HERE
%IF Y>=Z %THEN -> COUNT LEADING PLACES
SPACES(N-I) ;                     ! O.K FOR ZERO OR -VE SPACES
SIGN=' ' ;                        ! '+' IMPLIED
%IF X<0 %THEN SIGN='-'
PRINT SYMBOL(SIGN)
J=I-1 ; Z=10**J
NEXT DIGIT:
L=INTPT(Y/Z) ;                    ! OBTAIN NEXT DIGIT
Y=Y-L*Z ;Z=Z/10 ;                   ! AND REDUCE TOTAL
PRINT SYMBOL(L+'0')
J=J-1
%IF J>=0 %THEN -> NEXT DIGIT
%IF N=0 %THEN %RETURN ;           ! NO DECIMAL PART TO BE O/P
%IF DP=0 %THEN %PRINTTEXT'.'
DP=1 ; J=0 ; Z=1
Y=10*Y ; N=N-1 ; -> NEXT DIGIT
%ROUTINE PRINTFL(%REAL X,%INTEGER N)

%REAL SIGN,ROUND,FACTOR
%INTEGER COUNT,INC
ROUND=.5/10**N
SIGN=1
%IF X=0 %THEN -> ZERO
%IF X < 0 %THENSTART
X=-X ; SIGN=-SIGN ; %FINISH
INC=1 ; COUNT=0 ; FACTOR=1/10
%IF X <= 1 %THENSTART
FACTOR=10 ; INC=-1 ; %FINISH
SCALE: %IF 1<=X+ROUND %AND X+ROUND<10 %THEN -> PRINTOUT
X=X*FACTOR ; COUNT=COUNT+INC
-> SCALE
ZERO: COUNT=-99
PRINTOUT: PRINT(SIGN*X,1,N)
%PRINTTEXT'e'
WRITE(COUNT,2)
%END
%END
%ROUTINE READF(%REAL.%IL XX)
%INTEGER ADR
  *_MOV_14.(R1),36.(R1) ;   ! ADR=ADDR(XX)
!
!
%ROUTINESPEC READ(%INTEGER ADR,PARM)
%ROUTINESPEC SKIP SYMBOL
```

```
%INTEGER CH,P,PT,DIG,STATE
%INTEGERARRAY L(1:72)
%OWNINTEGERARRAY A(0:48)=  %C
  2, -1, -1,  5, -1, -1, -1,
  2,  2,  3,  5,  6, -1, -1,
  1,  0,  0,  4,  0,  0,  0,
  1,  0,  0, -1,  0,  0,  0,
 -1, -1,  4, -1, -1, -1, -1,
  3,  3, -1, -1, -1, -1, -1,
 -1, -1, -1, -1, -1, -1, -1
%INTEGER ROW
!VAR
!
!
  -> FIRST
RESET:
  %PRINTTEXT'WRONG
'
FIRST:
  P=0
  STATE=1
INSCH:
  READ SYMBOL(CH)
  P=P+1
  L(P)=CH
  ROW=0
  %IF CH='+' %OR CH='-' %THEN -> OUT
  ROW=ROW+1
  %IF '0'<=CH %AND CH<='9' %THEN -> OUT
  ROW=ROW+1
  %IF CH=' ' %THEN -> OUT
  ROW=ROW+1
  %IF CH=10 %THEN -> OUT
  ROW=ROW+1
  %IF CH='@' %THEN -> OUT
  ROW=ROW+1
  %IF CH='.' %THEN -> OUT
  ROW=ROW+1
OUT:
  STATE=A(7*ROW+STATE-1)
  -> INSCH %IF STATE>0
  -> RESET %IF STATE<0
  PT=1
  READ(ADR,1)
!
!
!
%ROUTINE READ(%INTEGER ADR,PARM)
%INTEGER FLAG,CURSYM ; ! FLAG= 0FOR'-',1 FOR '+'
%INTEGER IVALUE,J
%REAL RWORK,SCALE,WK2
%OWNREAL IMAX=327e7.0
         FLAG=1
         -> TEST SIGN
IGNORE LEADING SPACES:
         SKIP SYMBOL
TEST SIGN:CURSYM=NEXT SYMBOL ;                  ! CARE NOT TO READ TERM
         -> IGNORE LEADING SPACES %IF CURSYM=' ' %OR CURSYM=10
         -> PASS SIGN %IF CURSYM='+'
         -> DIGIT %UNLESS CURSYM='-'
MINUS:   FLAG=0 ;                               ! RECORD INITIAL MINUS
PASS SIGN: SKIP SYMBOL ;                        ! MOVE OVER SIGN ONCE I
         CURSYM=NEXT SYMBOL ;                   ! BEEN RECORDED IN FLAG
DIGIT:   -> DIGIT NOT FIRST %UNLESS '0'<=CURSYM %AND CURSYM<='9'
```

```
LOOP:     SKIP SYMBOL
          CURSYM=NEXT SYMBOL
          -> NOT DIG %UNLESS '0'<=CURSYM %AND CURSYM<='9'
          RWORK=10*RWORK+(CURSYM-'0') ;  ! CONTINUE EVALUATING
          -> LOOP
NOT DIG:  -> TRY AT %UNLESS CURSYM='.'
          SCALE=10
FPART:    SKIP SYMBOL
          CURSYM=NEXT SYMBOL
          -> TRY AT %UNLESS '0'<=CURSYM %AND CURSYM<='9'
          RWORK=RWORK+(CURSYM-'0')/SCALE
          SCALE=10*SCALE ; -> FPART
TRY AT:
! THE VALUE HAS NOW BEEN READ INTO RWORK. THERE MIGHT BE AN EXPO
! E.G. '1.7@ 10'  IS VALID DATA FOR READ
          -> FIX %UNLESS CURSYM='@'
          SKIP SYMBOL ;                    ! MOVE PAST THE '@'
          READ( ADDR(IVALUE),0) ; ! RECURSIVE CALL TO FIND EXPONE
          %IF IVALUE<=-99 %THENSTART
             RWORK=0
             -> FIX
             %FINISH
          WK2=10.0
          %IF IVALUE<0 %THENSTART
             IVALUE=-IVALUE
             WK2=-0.1
             %FINISH
          -> FIX %IF IVALUE=0
          %CYCLE J=1,1,IVALUE
          RWORK=RWORK*WK2
          %REPEAT
FIX:
! KNOCK NUMBER INTO RIGHT FORM
          -> INT READ %IF PARM=0
          %IF FLAG=0 %THEN RWORK=-RWORK
          !REAL(ADR)=RWORK
          !J=ADDR(RWORK)
          !!INTEGER(ADR)=INTEGER(J)
          !!INTEGER(ADR+2)=INTEGER(J+2)
*_MOV_#46.,R0
*_ADD_R1,R0     ; ! R0=ADDR(RWORK)
  *_MOV_14.(R1),R3
  *_MOV_(R0)+,(R3)+
  *_MOV_(R0)+,(R3)+
          %RETURN
INT READ:
          !IVALUE= INT(RWORK)
          WK2=0.5
          %IF RWORK<0 %THEN WK2=-0.5
          IVALUE=INTPT(RWORK+WK2)
          %IF FLAG=0 %THEN IVALUE=-IVALUE
          !INTEGER(ADR)=IVALUE
          *_MOV_42.(R1),@14.(R1)
%RETURN
DIGIT NOT FIRST:
! CAN HAVE  .73 AS VALID IMP NO
          SKIP SYMBOL
          CURSYM=NEXT SYMBOL
          RWORK=(CURSYM-'0')/10
          SCALE=100 ; -> FPART
          %END ; ! READ
%ROUTINE SKIPSYMBOL
  PT=PT+1
  %END ; ! SKIP SYMBOL
%INTEGERFN NEXT SYMBOL
```

```
        %END ; ! NEXT SYMBOL
        %END ; ! READF
%ROUTINE READ(%INTEGERNAME I)
%REAL X
! USE READF FOR INTEGERS SINCE IT IS IMMUNE TO SYMBOL IN DATA
READF(X)
%IF X>30000. %THENSTART  ; ! INTPT FAILS FOR X>2**15
I=30000 ;%RETURN ;%FINISH
I=INTPT(X+.001)
%END
!
! DIRECT ACCESS FILE ROUTINES
!
%ROUTINE CREATE(%INTEGERARRAYNAME FILE)
LACC(ADDR(FILE(2)))
*MOV_R1,-(SP)
*MOV_(R0),R2
*MOV_-(R0),R1
*MOV_-(R0),R0
*EMT_345  ;! CREATE
*MOV_(SP)+,R1  ;! RESTORE R1
%END  ;! CREATE
%INTEGERFN FIRSTBLOCK(%INTEGERARRAYNAME FILE)
LACC(ADDR(FILE(2)))
*MOV_R1,-(SP)
*MOV_(R0),R2
*MOV_-(R0),R1
*MOV_-(R0),R0
*EMT_344  ;! UDEX
*MOV_(SP)+,R1  ;! RESTORE R1
%RESULT=ACC
%END  ;! FIRSTBLOCK
%INTEGERFN NEXTBLOCK(%INTEGER BLOCK)
LACC(BLOCK)
*MOV_R1,R5
*EMT_340
*MOV_R5,R1
%RESULT=ACC
%END  ;! NEXTBLOCK
%INTEGERFN FILESIZE(%INTEGERARRAYNAME FILE)
%INTEGER I,J
I=0
J=FIRSTBLOCK(FILE)
1: %RESULT=I %IF J=0 %OR I=4000
I=I+1
J=NEXTBLOCK(J)
->1
%END  ;! FILESIZE
!
%INTEGERFN BLOCKNOF(%INTEGER FIRST,N)
%INTEGER I
%RESULT=0 %IF N<1 %OR N>4000
I=FIRST
1:%IF N=1 %OR I=0 %THEN %RESULT=I
I=NEXTBLOCK(I)
N=N-1
->1
%END  ;! BLOCKNOF
!
!
%OWNINTEGER DABLOCK
%OWNINTEGER DAPROTEC
%ROUTINE OPENDA(%INTEGERARRAYNAME FILE)
! OPEN FOR READ OR WRITE
1:LACC(ADDR(FILE(2)))
```

```
*MOV_(R0),R1
*MOV_-(R0),R1
*MOV_-(R0),R0
*EMT_344   ;! UDEX
*MOV_R1,-(SP)
*MOV_R5,R1   ;! RESTORE R1
DABLOCK=ACC
*MOV_(SP)+,R0
DAPROTEC=ACC
%RETURNIF DABLOCK#0
CREATE(FILE)
->1
%END ;! OPENDA
%ROUTINE WRITEDA(%INTEGER BLOCK,X)
! X IS ADDRESS OF START OF 512 BYTE BLOCK
%INTEGER DWBLOCK,I,J
%IF BLOCK<0 %OR BLOCK>200 %THENSTART
%PRINTTEXT' BAD BLOCK NUMBER
'
*EMT_372
%STOP ;%FINISH
%IF DABLOCK=0 %THENSTART
%PRINTTEXT' DAFILE NOT OPEN
'
*EMT_372
%STOP ;%FINISH
2:DWBLOCK=BLOCKNOF(DABLOCK,BLOCK)
%IF DWBLOCK=0 %THENSTART ;!FILE TOO SMALL
LACC(DAPROTEC)
*MOV_R0,-(SP)
LACC(DABLOCK)
*MOV_R1,R5
*MOV_(SP)+,R1
*EMT_341   ;! APPEND
*MOV_R5,R1
->2
%FINISH
LACC(X)
!ADDRESS
*MOV_R0,-(SP)
LACC(DAPROTEC) ;! PROTEC
*MOV_R0,-(SP)
LACC(DWBLOCK) ;! BLOCK NUMBER
*MOV_R1,R5
*MOV_(SP)+,R3
*MOV_#-400,R2
*MOV_(SP)+,R1
*EMT_330 ;! WRITE
*MOV_R5,R1
%END   ;! WRITEDA
!
%REAL MAXH1,STOST,NOW7,ETA,NOW8,NOW9
%INTEGER FIXUP
%ROUTINESPEC MEANANDSD(%REALARRAYNAME D1,%REAL M1,I IM,%C
%REALNAME MEAN,SIGMA,%INTEGERNAME N1)
%ROUTINESPEC MBMONITOR
%ROUTINESPEC GETVARS
%ROUTINESPEC RINGBELL(%INTEGER I)
%REALFNSPEC SQRT(%REAL X)
%INTEGERFNSPEC READBIT
%ROUTINESPEC READIN
%ROUTINESPEC DECODE
%ROUTINESPEC PASSVECTOR
%ROUTINESPEC SETOUTPUT
%ROUTINESPEC WRITETODISC
```

```
%ROUTINESPEC PROCESSDATA
%ROUTINESPEC DRIVESTEPPER
%ROUTINESPEC DRIVEMOTOR(%INTEGER UNIT,STEPS)
%ROUTINESPEC STOPPROG
%ROUTINESPEC CHECKFAULT
%ROUTINESPEC INITIALISE
%ROUTINESPEC TESTOFLO
%ROUTINESPEC CALIBRATE
%ROUTINESPEC MBCENT1
%ROUTINESPEC MBCENTRE
%ROUTINESPEC UPDATE
%ROUTINESPEC QUALITY
%ROUTINESPEC FETCHBLOCK
%ROUTINESPEC CHOOSEANGLE
%ROUTINESPEC MBEAMCH
%ROUTINESPEC RESETCLOCKS
%ROUTINESPEC FLASHFILAMENT
!
!
%INTEGER TIMEM,ANCH,MEMOR,STATE,XBFLAG
%INTEGER I,I1,K,ANGLE,OLDANG,FLAG,OLDFLAG,I1,I2,STEPS
%INTEGER J,A,XBEAM,MODE,RTE,NEWANGLE,BASE
%INTEGER COUNT,N2,MRTE,NBLOCKS,C,L,DATA,DISPC
%INTEGER MBCHK,MBCHK1
%INTEGER NUM,SEQNO,MODFLAG,MODOUT,BLOCK
%INTEGER STBLOCK,MAXANG,MINANG,MESH,DRIVEFLAG
%INTEGER DUMK,MBFLAG,QFLAG,CFLAG
%INTEGER ERROR,ENTRY,IB,JB,MBCHECK,ANGLECOUNT
!
%REAL WC,MM,LL,DS,MS,XMEAN,ERR,OLDXMEAN,TIME,XBID,XBMID
%REAL NOISE,EVENTS,THEN,SOFAR,EXPTIME,NPOW,NPOW1
%REAL MPRESS,PRESERR,OLDMPRESS,NOW1,NOW2,NOW3,NOW4
%REAL PKRAT,TAUPUL,PROB,DELTAT,MARK,XBEAMAREA,NOW5
%REAL OLDMBEAM,MBEAMAREA,MBZERO,MBMAX,MMBEAM
%REAL ARR,CALTIME,MBFACTOR,AVCOUNT,WAITMARK,MAXH
%REAL SOVERU,PEAK,PEAK1,TALLY,TALLY1,STALLY,STALLY1,STIME,C3,C4
!
%INTEGERARRAY D(0:15)
%INTEGERARRAY S(1:4)
%INTEGERARRAY SS(1:4)
%INTEGERARRAY P(1:4)
%INTEGERARRAY ARRIVE(0:1023)
%INTEGERARRAY FNAME(0:2)
%INTEGERARRAY INDEX(1:50)
%INTEGERARRAY MULT(1:50)
%INTEGERARRAY NADD(0:5)
!
%REALARRAY MAINBEAMON(1:20)
%REALARRAY MAINBEAMOFF(1:20)
%REALARRAY CROSSBEAM(1:200)
%REALARRAY EXPVAR(1:32)
%REALARRAY PRESS(1:200)
%SWITCH RTESET(1:6)
!
!INITIALISATION
!
SETPOT(0,2)  ;! ENABLE NORMAL CONDITION FOR MODULATIO
SETPOT(4,4)
! X BEAM RELAY
XBFLAG=0
! X BEAM CONTROL FLAG
%CYCLE I=1,1,32
EXPVAR(I)=0  ;! SET EXP. VARIABLES TO ZERO
%REPEAT
```

```
OLDANG=0  ;  ANGLE CHECK YEAR
OLDMBEAM=-1.  ;! MAIN BEAM MONITOR SIGNAL
              ;! ON FIRST PASS ONLY
MMBEAM=0
STBLOCK=1  ;! DAFILE START BLOCK
INITIALISE
!
ENTRY=2  ;! READ FROM THE DISC
GETVARS
RTE=4
MBFLAG=2  ;! MAKE SURE WE MEASURE ONLY ONE REFERENCE SHAPE AT S
FLASH FILAMENT  ;! NICE AND CLEAN FOR START
SEQNO=INTPT(EXPVAR(7))-1  ;! EXPVAR(7) IS TITLING PARAM
SETOUTPUT
TIMEM=0
STATE=0
MAXH1=0
MEMOR=0
MBCHK1=0
MINANG=INTPT(EXPVAR(19))
MAXANG=INTPT(EXPVAR(20))
MESH=INTPT(EXPVAR(21))
DRIVEFLAG=INTPT(EXPVAR(22))
MBCHECK=INTPT(EXPVAR(29))
%IF EXPVAR(25)=1 %THEN %START
DL69:
%PRINTTEXT 'IDEAL CROSS BEAM: '
READF(XBID)
NEWLINE
XBMID=XBID*27.3
%IF XBID<0 %OR XBID>150 %THEN -> DL69
%FINISH
ANGLECOUNT=MBCHECK-1  ;! START WITH MONITOR CALIBRATION
IB=INTPT(EXPVAR(27))  ;! ENTRY POINT IN ANGLE TABLE
JB=INTPT(EXPVAR(28))  ;! ENTRY POINT IN ANGLE TABLE
%IF MINANG<3100 %THENSTART
RINGBELL(40)
NEWLINE
%PRINTTEXT' INPUT ERROR  ; MINANGLE SET TO 3100'
NEWLINE
MINANG=3100
%FINISH
%IF MAXANG <MINANG %OR MAXANG>8100 %THENSTART
RINGBELL(40)
NEWLINE
%PRINTTEXT' INPUT ERROR  ; MAXANGLE SET TO 8100'
NEWLINE
MAXANG=8100
%FINISH
%IF MESH<1 %OR MESH>500 %THENSTART
RINGBELL(40)
%PRINTTEXT' INPUT ERROR  ; MESH SIZE SET TO 100'
NEWLINE
MESH=100
%FINISH
NEWLINE
NEWLINE
K=0
!
!********** MAIN PROGRAM STARTS HERE **********
!
1: FETCHBLOCK
ERROR=0
DECODE
%IF ERROR#0 %THEN ->1
```

```
69:
->RTESET(RTE)
|
|********** PROCEDURE TABLE **********
|
RTESET(1):MBMONITOR
|
|MONITORS MAIN BEAM
->1
|
|
|
RTESET(2): | DATA COLLECTION
PROCESSDATA
RTESET(3): | CHECK DATA ONLY
->1
RTESET(5): | RESTART DATA COLLECTION AFTER AUTO ANGLE CHANGE
FIXUP=0
RTE=2
->1
RTESET(6):| WAIT FOR BEAM OFF
%IF (RTIME-WAITMARK)>.02 %THEN RTE=2
->1
RTESET(4): CHOOSEANGLE  ;|ENTRIES SET TO CALIBRATE MAIN BEAM MOI
RTE=5  ;| RESTART DATA COLLECTION
->1
|
|********** MAIN PROGRAM ENDS **********
|
%ROUTINE FETCHBLOCK
|
|      FILLS D(0:15) WITH GOOD SENTENCE
|
1: READIN
%RETURNIF D(0)=426 %AND D(15)&504=336  ;| START AND END CODES
| SEARCH FOR START CODE
%CYCLE I=1,1,15
%IF D(I)=426 %THENSTART
|
|      FOUND IT
|
%CYCLE II=I,1,15
| II POINTS TO ELEMENTS WHICH ARE OK
| SHIFT THEM ALONG
D(II-1)=D(II)
%REPEAT
K=15-I+1  ;| K HAS NO. OF ELEMENTS TO BE FILLED
->1  ;| FILL THEM
%FINISH
%REPEAT
->1  ;| WHOLE NEW SENTENCE REQUIRED
%END  ;| FETCHBLOCK
%ROUTINE DECODE
| *** MANUAL FLAG SEMAPHORE ***
| FLAG=7 ->NEWANGLE
| FLAG=6 ->COLLECT DATA
| FLAG=5 ->WAIT
| FLAG=4 ->LIST EXPVARS
| FLAG=3 ->STOP
| FLAG=2 ->FEEDBACK
| FLAG=1 ->CHANGE EXPERIMENTAL VARIABLES
|
| *** BRANCHING SEMAPHORE ***
| RTE=1 -- NOT USED AT PRESENT
```

```
! RTE=3 -- COLLECT DATA ONLY, NO PROCESSING
! RTE=4 -- CALIBRATE MAIN BEAM MONITOR
! RTE=5 -- RESTART DATA COLLECTION AFTER AUTO ANGLE CHANGE
! RTE=6 -- WAIT 1 SECOND FOR MAIN BEAM TURN OFF
!          AFTER MAIN BEAM MONITOR READINGS
J=(D(10)&128)>>7+(D(12)&64)>>6
! J SHOULD BE ZERO FOR TOF MODE
%IF J#0 %THENSTART
RINGBELL(40)
NEWLINE
%PRINTTEXT' FUNCTION IDENTIFIERS WRONG ' ;WRITE(J,4)
ERROR=1
NEWLINE
%RETURN
%FINISH
J=0
%CYCLE I1=1,8,9
%CYCLE I2=0,2,2
J=J+1
I=I1+I2  ;!D(I) HAS 8 LEAST SIG BITS OF SCALER J
! OTHER 2 BITS ARE IN 2 LEAST SIG BITS OF D(I+1)
S(J)=1023-D(I)-(D(I+1)&3)<<8 ;! JTH SCALER (INVERTED)
SS(J)=3-(D(I+1)&12)>>2  ;! JTH STORE (INVERTED)
P(J)=1-(D(I+1)&16)>>4  ;! JTH ARRIVAL FLAG (INVERTED)
%REPEAT
%REPEAT
XBEAM=D(5)+(D(6)&240)<<4  ; ! CROSS BEAM SIGNAL (INVERTED)
ANGLE=0
%CYCLE I=8,-1,7
A=15-D(I)>>4
ANGLE=ANGLE*10+A
A=15-D(I)&15  ;! ANGLE ENCODER IS INVERTED BCD
ANGLE=ANGLE*10+A
%REPEAT
%IF OLDANG#0 %THEN CHECKFAULT
FLAG=(D(6)&14)>>1  ;! MANUAL FLAG
MODE=D(6)&1
MODFLAG=(D(10)&64)>>6
WC=D(14)*256.+D(13)
WC=65535.-WC
%END  ;! DECODE
%ROUTINE FEEDBACK
SELECTOUTPUT(0)
SCREEN
WAIT(75)  ;! TEMP WAIT FOR 4010 TO GET READY
SOFAR=RTIME-THEN
ENTRY=1 ;QUALITY
EXPTIME=TIME
NEWLINE
!
!      NEVER MIND THE QUALITY - FEEL THE WIDTH!
!
%PRINTTEXT' SEQUENCE NUMBER ' ;WRITE(SEQNO,3) ;NEWLINE
%PRINTTEXT'    BLOCK NUMBER ' ;WRITE(STBLOCK//6+1,3) ;NEWLINES(2
%PRINTTEXT' ENERGY ' ;PRINT(EXPVAR(2),4,0) ;NEWLINE
%PRINTTEXT' ANGLE ' ;WRITE(ANGLE,5) ;SPACE
%PRINTTEXT'(' ;WRITE(I6,3) ;WRITE(J6,3) ;%PRINTTEXT')' ;NEWLINE
%PRINTTEXT' XBEAM ' ;PRINT(XBEAM/27.3,6,2) ;NEWLINE
%PRINTTEXT' MBEAM ' ;PRINT(AMBEAM,6,4) ;NEWLINES(2)
%PRINTTEXT' EVENTS ' ;PRINT(EVENTS,10,3) ;NEWLINE
%PRINTTEXT' NOISE COUNTS ' ;PRINT(NOISE,10,3) ;NEWLINE
%PRINTTEXT' PEAK RATE ' ;PRINT(PEAK,6,4) ;NEWLINE
%PRINTTEXT' PEAK RATE(JUST) ' ;PRINT(PEAK1,6,4) ;NEWLINE
%PRINTTEXT' NOISE RATE ' ;PRINT(NPOW1,6,4) ;NEWLINE
%PRINTTEXT' ESTIMATED S/N '
```

```
%IF EXPVAR(30)=0. %THEN %PRINTTEXT' 9999.0000' %ELSE %C
%IF NPOW=0 %THEN %PRINTTEXT' 9999.0000' %ELSE %C
PRINT(TALLY/SQRT(NPOW),6,4)
%FINISH
NEWLINES(2)
%PRINTTEXT' EXPERIMENTAL TIME (SECS)' ;PRINT(EXPTIME,6,4)
NEWLINE
%PRINTTEXT' ELAPSED TIME (MINS) ' ;PRINT(SOFAR,6,2) ;NEWLINE
NEWLINE
NEWLINE
%IF PEAK<0.000001 %THEN PEAK=0.00001
ETA=EXPVAR(24)/PEAK
%IF EXPTIME <0.00001 %THEN -> AEVV
ETA=ETA/(EXPTIME/SOFAR)
ETA=ETA-SOFAR
%PRINTTEXT ' ETA = ' ;PRINT(ETA,6,2)
NEWLINE
AEVV:
%IF RTE#3 %THEN %PRINTTEXT' COLLECTING DATA' %ELSE %C
%PRINTTEXT' DATA BEING CHECKED BUT NOT COLLECTED' ;NEWLINE
%RETURN
%END ;! OF FEEDBACK
%ROUTINE TESTOFLO
%RETURN  ;! TEMP UNTIL TESTED
%END
%ROUTINE CHOOSEANGLE
!
!      CHOOSES NEXT ANGLE
!      ALSO DETERMINES WHEN MB CHECKS ARE DUE
!
!      THREE MODES OF OPERATION ARE AVAILABLE
!      1 MANUAL INPUT OF NEXT ANGLE
!        IN THIS CASE AUTOMATIC RETURNS TO THE MAIN BEAM
!        ARE CARRIED OUT BUT DETECTION OF 'RESOLVED' SPECTRUM
!        IS NOT SO THIS MUST BE DONE BY THE OPERATOR
!
!      2 INCREMENTAL STEPPING OF ANGLE
!        STEP SIZE IS SET AT INITIALISATION
!
!      3 PSEUDO-RANDOM SELECTION OF ANGLE
!        ENTRY POINTS IN THE TABLE ARE SET AT
!        INITIALISATION
!        IT IS POSSIBLE TO START WHERE ONE LEFT OFF
!        IN A PREVIOUS RUN BY SETTING THE POINTS TO
!        THE VALUES OUTPUT AT THE END OF THE RUN
!      STEP SIZE IN TABLE MAY BE DOUBLED BY SETTING
!      EXPVAR 22 TO 3
!
%OWNINTEGERARRAY A(1:41)=0,1,2,3,4,5,6,7,8,9,10,11,12,13,14,15,
19,20,21,22,23,24,25,26,27,28,29,30,31,32,33,34,35,36,37,38,39,
%OWNINTEGERARRAY B(1:25)=84,80,60,0,72,40,8,88,28,44,4,68,76,3
96,12,52,24,92,16,20,64,48
%OWNREAL RANGE
%OWNINTEGER D=1
%SWITCH DRIVE(0:3)
RANGE=(MAXANG-MINANG)/4100.
->START %IF MBFLAG=2
ANGLECOUNT=ANGLECOUNT+1
%IF ANGLECOUNT#MBCHEC! %THEN ->SKIP
MBFLAG=1 %IF MBFLAG=0
START:ANGLECOUNT=0
EXPVAR(16)=1.  ;! MEASURE REFERENCE SHAPE
CALIBRATE  ;! CALIBRATE THE MAIN BEAM MONITOR
FIRST:
%RETURN
```

```
!*********** ANGLE CHANGE SECTION STARTS HERE
!
SKIP: !NOT TIME FOR MSCHECK
->DRIVE(DRIVEFLAG)
DRIVE(0):SELECTOUTPUT(0)
SELECTINPUT(20)
! MANUAL ANGLE INPUT
RINGBELL(20)  ;! ALERT OPERATOR
1: %PRINTTEXT' NEW ANGLE:' ;READ(NEWANGLE) ;NEWLINE
%RETURNIF NEWANGLE=ANGLE
->1 %IF NEWANGLE<MINANG %OR NEWANGLE>MAXANG
->3
DRIVE(1): ! SIMPLE STEPWISE ANGLE CHANGE
NEWANGLE=ANGLE+MESH
%IF OLDANG=0 %THEN NEWANGLE=MINANG
->3
DRIVE(3): D=2*D %IF MOD(D)=1  ;! CHANGE STEP SIZE
DRIVE(2): ! PSEUDO-RANDOM SCAN
IB=IB+D
%IF IB>41 %OR IB<1 %THENSTART
D=-D ;IB=IB+D  ;! CHANGE DIRECTION
JB=JB+1-D  ;! AND SHIFT B BY ONE
%FINISH
JB=JB+D
JB=1 %IF JB>25
JB=25 %IF JB<1
II=100*A(IB)+B(JB)
NEWANGLE=MINANG+INTPT(RANGE*II)
3: SELECTOUTPUT(0)
MEMOR=0
RINGBELL(2)
%PRINTTEXT' ANGLE CHANGE' ;NEWLINE
DRIVESTEPPER
FIXUP=1
OLDANG=NEWANGLE
MAXH1=0
FETCHBLOCK ;DECODE  ;! THIS CHECKS ANGLE AND
                    ;! PATCHES UP ANY ERRORS
FIXUP=0
%END  ;! CHOOSEANGLE
%ROUTINE MBCENT1
NEWANGLE=INTPT(EXPVAR(6))
DRIVESTEPPER
%RETURN
%END ; !MBCENT1
%ROUTINE MBCENTRE
NEWANGLE=INTPT(EXPVAR(17))
DRIVESTEPPER
%RETURN
%END  ;! MBCENTRE
%ROUTINE DRIVE STEPPER
%IF NEWANGLE>8100 %OR NEWANGLE<3000 %THENSTART
RINGBELL(40)
%PRINTTEXT' ANGLE OUT OF RANGE '
WRITE(NEWANGLE,6) ;NEWLINE
NEWANGLE=8100
%FINISH
STEPS=NEWANGLE-ANGLE
DRIVE MOTOR(4,STEPS)
%END ;!OF DRIVE STEPPER
%ROUTINE DRIVE MOTOR(%INTEGER UNIT,STEPS)
%RETURN %IF STEPS=0
*MOV_R1,-(SP) ;! SAVE R1
*MOV_14.(R1),R0 ;! UNIT NUMBER
*MOV_16.(R1),R1 ;! NUMBER OF STEPS
```

```
*MOV_(SP)+,R1   ;!RESTORE R1
%END ;! OF DRIVE MOTOR
%ROUTINE PROCESSDATA
%INTEGER I
SELECTOUTPUT(0)
%IF MODFLAG=1 %THENSTART
MODOUT=MODOUT+1
%IF MODOUT>5 %THENSTART
RINGBELL(40) ;NEWLINE
%PRINTTEXT' MODULATION FAULT  ; DATA COLLECTION STOPPED'
NEWLINE ;RTE=3 ;MODOUT=0 ;NOW5=RTIME ;%RETURN
%FINISH
%RETURN
%FINISH
MODOUT=0
%CYCLE J=1,1,4
%IF P(J)#1 %THEN ->NO
! TRUE ARRIVAL FOUND
%IF STATE=1 %THEN %START
%IF SS(J)=3 %THEN %START
C3=C3+1
%FINISH
%FINISH
AVCOUNT=AVCOUNT+1
%IF SS(J)=1   %THENSTART
! CROSS BEAM ON
ARRIVE(S(J))=ARRIVE(S(J))+1  ;! SIGNAL
%IF ARRIVE(S(J))=32000 %THENSTART
! PREVENT INTEGER OVERFLOW
ARRIVE(S(J))=0 ;UPDATE ;%FINISH
EVENTS=EVENTS+1
%FINISH
%IF SS(J)=2 %THENSTART
%IF EXPVAR(16)=1. %THEN ->SQR
ARRIVE(S(J))=ARRIVE(S(J))-1  ;! NOISE
->CONT
SQR:ARRIVE(S(J))=ARRIVE(S(J))+1  ;! PULSE TUNING
CONT:NOISE=NOISE+1
%FINISH
NO:
%REPEAT
%IF ANGLE>10000 %THENSTART
RINGBELL(40)
%PRINTTEXT' TELETRAK FAULT ' ;WRITE(ANGLE,6)
NEWLINE
%PRINTTEXT' DATA COLLECTION STOPPED
'
RTE=3  ;! STOP DATA COLLECTION
NOW5=RTIME  ;! SET UP TO ADJUST CLOCKS
%RETURN
%FINISH
COUNT=COUNT+1
%IF WC=1 %THEN %START
C4=S(4)*EXPVAR(15)/1000000
TIME=TIME+C4/1000
->D1
%FINISH
TIME=TIME+WC*1.024*EXPVAR(15)/1000000.  ;! REAL TIME FROM WORD C
!     TIME IN SECONDS
D1:
TESTOFLO
%IF RTIME-NOW1>15. %THENSTART
NOW1=RTIME
ENTRY=2  ;! CALCULATE ALL THE FACTORS
QUALITY
```

```
AVCOUNT=AVCOUNT/10.
%IF AVCOUNT<1. %THENSTART
RINGBELL(40) ;SCREEN ;WAIT(75) ;NEWLINE
%PRINTTEXT' COUNT RATE VERY LOW  ; DATA COLLECTION STOPPED'
NEWLINE
RTE=3  ;! STOP DATA COLLECTION
NOW5=RTIME
%RETURN
%FINISH
AVCOUNT=0.
%FINISH
%IF RTIME-NOW2>2. %THENSTART  ;! QUALITY MONITOR SECTION
QFLAG=QFLAG+1  ;! FOR ANGLE CHANGE SECTION
NOW2=RTIME
ENTRY=2
QUALITY
->NOTUNE %IF EXPVAR(16)#1.
%PRINTTEXT'C ' ;PRINT(PEAK1,6,4) ;SPACES(2)
%PRINTTEXT'S/N ' ;PRINT(SOVERN,6,4) ;NEWLINE
NOTUNE: ! NO REPORT IN SCATTERING EXPT
%FINISH
%IF COUNT=1 %THEN MARK=TIME
CROSSBEAM(COUNT)=XBEAM
PRESS(COUNT)=VOLT(0,1)
! PRESSURE ON CHANNEL ZERO
%IF COUNT#200 %THENRETURN
! 200 TRANSFERS
DELTAT=TIME-MARK  ;! TIME FOR 200 SENTENCES
XMEAN=1000
NUM=COUNT
->NOCBM %IF INTPT(EXPVAR(32))=0  ;! NO CROSS BEAM MONITOR
MRTE=1
MM=0
LL=100000
! NO REJECTION ON FIRST PASS
MEANANDSD(CROSSBEAM,MM,LL,MS,DS,N2)
DS=2.*DS
MRTE=2
MEANANDSD(CROSSBEAM,MS,DS,XMEAN,ERR,N2)
ERR=ERR/SQRT(N2)
NOCBM: ! NO CROSS BEAM MONITOR
MM=0
LL=100000
MRTE=1
MEANANDSD(PRESS,MM,LL,MS,DS,N2)
DS=2.*DS
MRTE=2
MEANANDSD(PRESS,MS,DS,MPRESS,PRESERR,N2)
PRESERR=PRESERR/SQRT(.2)
COUNT=0
!
!      READ MAIN BEAM MONITOR
!
%IF STATE=1 %THENSTART
RTE=1
%IF RTIME-NOW6>2. %THENSTART
!
!    TIME UP
!
MBEAMCH
%RETURN
%FINISH
%FINISH
%IF EXPVAR(31)=0. %THEN ->NOMBM  ;! NO MAIN BEAM MONITOR
%IF RTIME-NOW3<EXPVAR(30) %THEN ->NOMBM
```

```
TIMEM=1
RTE=1
%RETURN
NOMBM: ! NO MAIN BEAM MONITOR
NBLOCKS=NBLOCKS+1
PASSVLCTOR
! LOAD DISPLAY AREA
! USED BY CFIT AND REAL TIME DISP
ENTRY=1  ;! LEVEL ONE FOR WRITETODISC
%IF RTIME-NOW4>10. %THENSTART
! DISC WRITE IF WE HAVE BEEN GOING FOR 10 MINUTES
ENTRY=2
NOW4=RTIME
%FINISH
WRITETODISC
%RETURNIF RTE=3  ;! DIV BY ZERO IN MEANANDSD
%RETURN %IF STATE=1
!
! NO POINT IN CHECKING PEAK RATE WHILE MONITORING
!
->REFTEST %IF MBFLAG#0
->NOTEST %IF CFLAG=QFLAG
CFLAG=QFLAG  ;! RESET FLAG
             ;! TEST EVERY TWO MINUTES - MORE OFTEN WASTES TIME
MAXH=0.
!
!     ESTIMATE INTENSITY IN PEAK
!
%CYCLE I=0,1,1023
%IF MAXH<ARRIVE(I) %THEN MAXH=ARRIVE(I)
%REPEAT
%IF MEMOR=1 %THENSTART
MAXH=EXPVAR(23)*MAXH+MAXH1
%FINISH
%IF MEMOR=0 %THENSTART
MAXH=EXPVAR(23)*MAXH
%FINISH
%IF MAXH>EXPVAR(24) %THENSTART
!
!     TIME TO CHANGE ANGLE
!
ENTRY=2  ;! WRITE DATA TO DISC
WRITETODISC
NOW3=RTIME
TIMEM=0
RTE=1
%RETURN
%FINISH
->NOTEST %IF EXPVAR(16)#1.  ;! NOT MAIN BEAM
REFTEST: ! MUST BE MEASURING REFERENCE SHAPE
%IF (EVENTS+NOISE)>15000 %THENSTART
! 15000 SEEMS REASONABLE FOR THE PRESENT
! MAY BE CHANGED IN THE FUTURE
ENTRY=2  ;! WRITE DATA
WRITETODISC
!
!     HAVE WE FLASHED THE FILAMENT YET
!
%IF MBFLAG=1 %THENSTART
MBFLAG=2 ;FLASHFILAMENT
NOW3=RTIME
TIMEM=0
RTE=1
%RETURN
%FINISH
```

```
!*** END OF FILE - FLASH SECTION
!
MBFLAG=0 ;EXPVAR(1,)=0.   ;! SCATTERING FROM NOR OR
NOW3=RTIME
TIMEM=0
RTE=1
%RETURN
%FINISH
NOTEST: ! CONTINUE
!
!      CHECK PEAK COUNTING RATE
!      IF TOO LOW THEN STOP DATA COLLECTION
!
%IF PEAK1<EXPVAR(26) %THENSTART
RINGBELL(40) ;SCREEN ;WAIT(75)  ;! WAIT FOR 4010
%PRINTTEXT' PEAK RATE VERY LOW  ; CHECK BEAMS'
NEWLINE
%PRINTTEXT' DATA COLLECTION STOPPED' ;NEWLINE
RTE=3
NOW5=RTIME
%FINISH
%RETURN
%END ;! OF PROCESSDATA
%ROUTINE WRITETODISC
!
!      CHECKS BEAMS AND PRESSURES
!      WRITES DATA TO DISCFILE IF ENTRY=2
!
%REALARRAY DUMMY(0:127)
%INTEGERARRAY DUMMY1(0:255)
%CYCLE L=0,1,127
DUMMY(L)=0.
%REPEAT
%CYCLE L=0,1,255
DUMMY1(L)=0
%REPEAT
SELECTOUTPUT(0)
%IF XMEAN>4000 %THEN %PRINTTEXT' CROSS BEAM OUTPUT CLOSE TO SATU
'
%IF NBLOCKS=1 %THENSTART
OLDXMEAN=XMEAN
OLDMPRESS=MPRESS
%FINISH
%LONGJUMP
%IF EXPVAR(25)=1 %THEN %START
%IF XMEAN>1.05*XBMID %AND XBFLAG=0 %THEN %START
%PRINTTEXT 'SWITCHING ON XBEAM RELAY'
NEWLINE
NOW8=RTIME
SETPOT(0,4)
XBFLAG=1
%FINISH
%IF XMEAN<XBMID %AND XBFLAG=1 %THEN %START
NOW9=RTIME
SETPOT(4,4)
%PRINTTEXT 'SWITCHING OFF XBEAM RELAY'
NEWLINE
XBFLAG=0
%FINISH
%IF XMEAN>1.1*XBMID %AND XBFLAG=1 %THEN %START
%IF RTIME-NOW8>10 %THEN %START
%PRINTTEXT 'TURN UP BAROSTAT CONTROL OR NEEDLE VALVE'
NEWLINE
NOW8=RTIME-5
%FINISH
```

```
%IF [illegible]
%IF RTIME-NOW9>15 %THEN %START
%PRINTTEXT 'TURN DOWN BAROSTAT CONTROL OR NEEDLE VALVE'
NEWLINE
NOW9=RTIME-5
%FINISH
%FINISH
%FINISH
XBEAMAREA=XBEAMAREA+0.5*(OLDXMEAN+XMEAN)*DELTAT
%IF ABS(OLDXMEAN-XMEAN)>.1*OLDXMEAN %THENSTART
RINGBELL(40)
%PRINTTEXT' CROSS BEAM INTENSITY CHANGED FROM '
PRINT(OLDXMEAN/27.3,6,1)
%PRINTTEXT' TO ' ;PRINT(XMEAN/27.3,6,1)
NEWLINE
OLDXMEAN=XMEAN
%IF INTPT(EXPVAR(32))=2 %THENSTART
%PRINTTEXT' DATA COLLECTION STOPPED' ;NEWLINE
RTE=3
NOW5=RTIME
%FINISH
%FINISH
%IF ABS(OLDMPRESS-MPRESS)>30 %THENSTART
NEWLINE
RINGBELL(40)
%PRINTTEXT'PRESSURE CHANGED FROM ' ;PRINT(OLDMPRESS,6,1)
%PRINTTEXT ' TO ' ;PRINT(MPRESS,6,1)
NEWLINE
OLDMPRESS=MPRESS
%FINISH
%RETURNIF ENTRY=1
BLOCK=STBLOCK
DUMMY(0)=EVENTS ;DUMMY(1)=NOISE ;DUMMY(2)=ANGLE
DUMMY(3)=TIME ;DUMMY(4)=XBEAMAREA
DUMMY(5)=MMBEAM
DUMMY(6)=NBLOCKS
%CYCLE L=1,1,32
DUMMY(L+6)=EXPVAR(L)
%REPEAT
%CYCLE L=1,1,50
DUMMY1(L-1)=INDEX(L)
DUMMY1(L+49)=MULT(L)
%REPEAT
WRITEDA(BLOCK,ADDR(ARRIVE(0)))
BLOCK=BLOCK+1
WRITEDA(BLOCK,ADDR(ARRIVE(256)))
BLOCK=BLOCK+1
WRITEDA(BLOCK,ADDR(ARRIVE(512)))
BLOCK=BLOCK+1
WRITEDA(BLOCK,ADDR(ARRIVE(768)))
BLOCK=BLOCK+1
WRITEDA(BLOCK,ADDR(DUMMY(0)))
BLOCK=BLOCK+1
WRITEDA(BLOCK,ADDR(DUMMY1(0)))
%END ;! OF WRITETODISC
%ROUTINE PASSVECTOR
BASE=-8192
! AREA IN SEG 7
%CYCLE I=0,1,1023
INTEGER(BASE)=ARRIVE(I)
BASE=BASE+2
! TWO BYTES PER INTEGER
%REPEAT
%END ;! OF PASSVECTOR
%ROUTINE CHECKFLAG(%INTEGERNAME F)
[illegible]
```

```
%IF F=OLDFLAG %THEN %RETURN
->S(F)
S(0):! FLAG RESET OR NOT SET
! NO CHANGE TO RTE
OLDFLAG=0
%RETURN
S(1):! CHANGE EXPERIMENTAL VARIABLES
%IF RTE#3 %THEN %RETURN
ENTRY=1   ;! READ FROM KEYBOARD
GETVARS
MESH=INTPT(EXPVAR(21))
MINANG=INTPT(EXPVAR(19))
MAXANG=INTPT(EXPVAR(20))
DRIVEFLAG=INTPT(EXPVAR(22))
MBCHECK=INTPT(EXPVAR(29))
OLDFLAG=1
%RETURN
S(2):! FEEDBACK REQUESTED
%PRINTTEXT' FEEDBACK
'
OLDFLAG=2
ENTRY=1   ;! SUPPRESS CALCULATION OF 'INST' VALUES
FEEDBACK
%RETURN
S(3):! CONTROLLED EXIT
OLDFLAG=3
%IF RTE#3 %THEN %RETURN   ; ! STOP VIA FLAG=5 ONLY
STOPPROG
%RETURN
S(4):! LIST OF EXPVARS REQUESTED
SCREEN ;WAIT(75)
%PRINTTEXT 'L=LIST EXP VAR, R=MEAS REF, F=FIL FLASH, X=ALTER XBE
'
NEWLINE
%PRINTTEXT ':'
READSYMBOL(I)
NEWLINE
%IF I='L' %THEN %START
%PRINTTEXT' EXPERIMENTAL VARIABLES
'
%CYCLE I=1,1,32
WRITE(I,4) ;SPACES(2) ;PRINT(EXPVAR(I),6,3) ;NEWLINE
%REPEAT
%FINISH
%IF I='R' %THENSTART
MBFLAG=2
ENTRY=2
WRITETODISC
STBLOCK=STBLOCK+6
INITIALISE
CHOOSEANGLE
RTE=3
%PRINTTEXT 'DATA NOT BEING COLLECTED
'
%FINISH
%IF I='F' %THENSTART
%PRINTTEXT '60 SECOND FILAMENT FLASH
'
NEWLINE
SETPOT(1,1)
WAIT(3000)
SETPOT(0,1)
WAIT(250)
%FINISH
```

```
DL70:
%PRINTTEXT  'NEW XBEAM IDEAL'
READF(XBID)
NEWLINE
%IF XBID<0 %OR XBID>150 %THEN ->DL70
XBMID=27.3*XBID
%FINISH
OLDFLAG=4
%RETURN
S(5):! WAIT DATA COLLECTION
%PRINTTEXT' DATA BEING CHECKED BUT NOT COLLECTED
'
RTE=3
NOW5=RTIME
OLDFLAG=5
%RETURN
S(6): ! START DATA COLLECTION
%PRINTTEXT' COLLECTING DATA
'
RTE=2
FIXUP=0
OLDFLAG=6
RESETCLOCKS  ;! GMT OR BST??
%RETURN
S(7):! NEW ANGLE REQUESTED
%IF RTE#3 %THEN %RETURN
! ANGLE FIXED IF DATA BEING COLLECTED
OLDFLAG=7
ENTRY=2
WRITETODISC
STBLOCK=STBLOCK+6  ;! NEW SECTION OF DAFILE
INITIALISE
CHOOSLANGLE
RTE=3  ;! OVERWRITE MUM CALIBRATE
%RETURN
%END ; ! OF CHECKFLAG
%ROUTINE STOPPROG
ENTRY=2
WRITETODISC
SELECTOUTPUT(0)
NEWLINE
%PRINTTEXT' WHEN RESTARTING PROGRAM SET 7TH PARAMETER TO'
WRITE(SEQNO+1,4)
NEWLINE
%PRINTTEXT' ALTERNATIVELY COPY THE ACCUMULATED DATA FILES ONTO'
NEWLINE
%PRINTTEXT' MAGNETIC TAPE.' ;NEWLINE
%PRINTTEXT' NOTE THAT THIS MUST BE DONE IN ANY CASE WHEN THE NU
NEWLINE
%PRINTTEXT' OF FILES ON THE DISC REACHES 51' ;NEWLINES(2)
%PRINTTEXT' POSITION IN ANGLE SCAN IS ' ;WRITE(IB,6) ;WRITE(JB,
NEWLINE
*EMT_372
%STOP
%END
%ROUTINE GETVARS
%INTEGER K
SELECTOUTPUT(0)
->3 %IF ENTRY=2  ;! READ FROM DISC FILE CHEMDA
1:%PRINTTEXT' EXPERIMENTAL VARIABLES
 NUMBER TO BE READ?
'
READ(I)
%IF I<1 %THEN %RETURN
%IF I>32 %THEN ->1
```

```
NEWLINE
%CYCLE J=1,1,I
2:READ(K)
%IF K<1 %OR K>32 %THENSTART
%PRINTTEXT' WRONG
'
->2
%FINISH
READF(EXPVAR(K))
%REPEAT
->4
3: SELECTINPUT(21)
%CYCLE I=1,1,32
READ(K) ;READF(EXPVAR(K))
%REPEAT
SELECTINPUT(20)
4:
%IF EXPVAR(23)<1 %THENSTART  ;! CHECK NO. PULSES SET
RINGBELL(40) ;NEWLINE
%PRINTTEXT' NO. PULSES NOT SET (PARAM 23) ' ;NEWLINE
->1
%FINISH
RTC=3
%RETURN
%END ;! OF GETVARS
%ROUTINE READIN
%CYCLE I=K,1,15
D(I)=READBIN
%REPEAT
K=0
%END ;! OF READIN
%INTEGERFN READBIN
*EMT_337
*MOV_12.(R1),R1
*RTS_PC
%END ;! OF FN READBIN
%ROUTINE SETOUTPUT
%INTEGER I,A,B,LENGTH
SELECTOUTPUT(0)
SEQNO=SEQNO+1
%PRINTTEXT' OUTPUT FILE IS CHLM'
A='C' ;B='H'
FNAME(0)=B<<8+A
A='E' ;B='M'
FNAME(1)=B<<8+A
A=INTPT(SEQNO/10)
B=INTPT(SEQNO-10*A+48) ;A=A+48
FNAME(2)=B<<8+A
PRINTSYMBOL(A)
PRINTSYMBOL(B)
NEWLINE
!
!      CHECK IF FILE EXISTS
!      IF IT DOES THEN ADJUST POINTER
!      TO APPEND NEW DATA
!
OPENDA(FNAME)
LENGTH=FILESIZE(FNAME)
%IF LENGTH>5 %THEN ->1
%PRINTTEXT' THIS IS A NEW FILE
' ;NEWLINE ;->2
!
1: %PRINTTEXT' THIS FILE CONTAINS ' ;WRITE(LENGTH//6,6)
%PRINTTEXT' BLOCKS' ;NEWLINE
```

```
WRITE(STBLOCK//6+1,6) ;NEWLINE
2:
%END ;! OF SETOUTPUT
%REALFN SQRT(%REAL X)
%REAL Y,Z
%IF X<=0 %THENSTART
%IF X=0 %THEN %RESULT=0
%PRINTTEXT' NEG ARG IN SQRT
'
RTE=3  ;%PRINTTEXT' DATA COLLECTION STOPPED' ;NEWLINE
NOW5=RTIME
%RESULT=1.
%FINISH
Y=(1+X)/2
1:Z=(Y+X/Y)/2
%IF Z>=Y %THEN %RESULT=Y
Y=Z
->1
%END ;! OF FN SQRT
%ROUTINE CHECKFAULT
%IF ABS(ANGLE-OLDANG)>20 %AND FIXUP=0 %THENSTART
RINGBELL(40)
%PRINTTEXT' TELETRAK/MOTOR FAULT  ; DATA COLLECTION STOPPED'
WRITE(OLDANG,6) ;NEWLINE
RTE=3
NOW5=RTIME
OLDANG=ANGLE  ;! RING BELL ONCE ONLY
%RETURN
%FINISH
%IF MOD(ANGLE-OLDANG)>1 %AND FIXUP=1 %THENSTART
DRIVESTEPPER
OLDANG=ANGLE
%FINISH
%RETURN
%END
%ROUTINE RINGBELL(%INTEGER I)
%INTEGER K
%CYCLE K=1,1,I
PRINT SYMBOL(7)
! BELL IS CTRL G ON TT
%REPEAT
%END ;! OF RINGBELL
%ROUTINE MEANANDSD(%REALARRAYNAME D1,%REAL M1,LIM,%REALNAME MEAN,
          SIGMA,%INTEGERNAME N1)
%INTEGER NA,NB,IMIN,IMAX,C
%REAL E,MIN,MAX,M2,SD
NA=1
NB=NUM
->NO REJECTION %IF MODE=2 %OR NUM<=20
C=0
! SORT ELEMENTS
AGAIN: MIN=D1(NA)
MAX=MIN
IMIN=NA
IMAX=NA
%CYCLE I=NA,1,NB
E=D1(I)
%IF E<MIN %THENSTART
MIN=E
IMIN=I
%FINISH
%IF E>MAX %THENSTART
MAX=E
IMAX=I
```

```
%REPEAT
D1(IMIN)=D1(NA)
D1(NA)=MIN
D1(IMAX)=D1(NB)
D1(NB)=IMAX
NA=NA+1
NB=NB-1
C=C+1
->AGAIN %IF C<NUM//20
NO REJECTION: M2=0.
SD=0.
C=0
%IF LIM<=0. %THEN LIM=.0001  ;! SMALL PERTURBATION
%CYCLE I=NA,1,NB
E=D1(I)
%IF ABS(E-M1)<LIM %THENSTART
M2=M2+E
C=C+1  ;! ACCEPTED ELEMENTS
%FINISH
%REPEAT
->OK %UNLESS C<2
RINGBELL(40)
%PRINTTEXT' DIVISION BY ZERO IN MEAN AND SD' ;NEWLINE
WRITE(C,4) ;WRITE(RPTE,4) ;WRITE(NUM,4) ;WRITE(NA,4) ;WRITE(NB,4
NEWLINE
PRINT(M1,6,4) ;PRINT(LIM,6,4) ;PRINT(E,6,4) ;PRINT(MAX,6,4)
PRINT(MIN,6,4) ;NEWLINE
MEAN=1 ;SIGMA=1
%PRINTTEXT' DATA COLLECTION STOPPED' ;NEWLINE
RINGBELL(40) ;RTE=3
*EMT_301  ;! PUT PROGRAM IN WAIT QUEUE
NOW5=RTIME
NEWLINE ;%RETURN
OK;M2=M2/C  ;! NEW ESTIMATE OF MEAN
%CYCLE I=NA,1,NB
E=D1(I)  ;! SUBTRACT MEAN TO AVOID LOSS OF PRECISION
%IF ABS(E-M1)<LIM %THEN SD=SD+(E-M2)*(E-M2)
%REPEAT
 N1=C
MEAN=M2
SIGMA=SQRT(SD/(C-1))  ;! STANDARD ERROR
%END ;! OF MEANANDSD
%ROUTINE CALIBRATE
!
!      CALIBRATE MONITOR
!
MBCENTRE ;OLDANG=INTPT(EXPVAR(17)) ;FIXUP=1
FETCHBLOCK ;DECODE ;! SEE WHERE WE ARE
FIXUP=0
FETCHBLOCK ;DECODE
%IF ABS(ANGLE-EXPVAR(17))>5. %THENSTART
RINGBELL(40)
%PRINTTEXT' TELETRAK/MOTOR FAULT IN CALIBRATE' ;NEWLINE
PRINT(ANGLE,6,2) ;SPACES(5) ;PRINT(EXPVAR(17),6,2) ;NEWLINE
*EMT_301  ;! PROGRAM TO WAIT QUEUE
          ;! INSERT BY CTRL C IN
NOW5=RTIME
%FINISH
%END  ; !OF CALIBRATION
%ROUTINE MBMONITOR
%LONGJUMP
%IF MBCHK1=1 %THEN->99
MBCHK1=1
MEMOR=0
%IF TIMEM=1 %THENSTART
```

```
ENTRY=2
NOW5=RTIME
WRITETODISC
%CYCLE I=0,1,1023
ARRIVE(I)=0
%REPEAT
PASSVECTOR
MAXH1=MAXH ;ANCH=ANGLE ;MLMOR=1
%FINISH
STOST=EXPVAR(16) ;EXPVAR(16)=1
INITIALISE
RTE=1
MBCENT1;OLDANG=INTPT(EXPVAR(6));FIXUP=1
FETCHBLOCK;DECODE
WC=0
FIXUP=0
STATE=1
!   MONITORING ONLY => DO NOT WRITE TO DISC
NOW6=RTIME ;NOW1=RTIME ;NOW2=RTIME ;NOW4=RTIME
MBCHK=0
99:PROCESSDATA
100:%IF MBCHK=0 %THEN %RETURN
MBCHK1=0
STBLOCK=STBLOCK+6
INITIALISE
%LONGJUMP
%IF TIMEM=1 %THENSTART
MAXH=0
NEWANGLE=ANCH
SELECTOUTPUT(0)
RINGBELL(2)
%PRINTTEXT  'WAGONS ROLL!!!!'
NEWLINE
DRIVESTEPPER
FIXUP=1
OLDANG=NEWANGLE
FETCHBLOCK ;DECODE
FIXUP=0
RTE=5
EXPVAR(16)=STOST;TIMEM=0  ;STATE=0
%RETURN
%FINISH
%IF TIMEM=0 %THENSTART
EXPVAR(16)=STOST
CHOOSLANGLE
%FINISH
TIMEM=0 ;STATE=0
RTE=5
%END ; ! OF MBMONITOR

%ROUTINE MBEAMCH
MBCHK=1
PASSVECTOR
MMBEAM=0
%CYCLE I=0,1,1023
MMBEAM = MMBEAM+ARRIVE(I)
%REPEAT
MMBEAM=MMBEAM+C3
MMBEAM=MMBEAM/TIME
C3=0
%IF OLDMBEAM=-1 %THENSTART
OLDMBEAM=MMBEAM
->NTC
%FINISH
!     NO WARNINGS FIRST  PASS
```

```
%IF ABS(OLDMBEAM-MMBEAM)>0.1*OLDMBEAM %THENSTART
%PRINTTEXT 'MAIN BEAM CHANGED FROM '
PRINT(OLDMBEAM,6,4) ; %PRINTTEXT ' TO '
PRINT(MMBEAM,6,4) ;NEWLINE
OLDMBEAM=MMBEAM
%IF INTPT(EXPVAR(31))=2 %THENSTART
RTE=3
%PRINTTEXT '
DATA COLLECTION STOPPED ' ;NEWLINE
%FINISH
DUNK=1
%FINISH
%IF DUNK=1 %THEN ->SON1
%PRINTTEXT 'MAIN BEAM CHANGED FROM '
PRINT(OLDMBEAM,6,4) ;%PRINTTEXT ' TO '
PRINT(MMBEAM,6,4) ;NEWLINE
SELECTINPUT(20)
SON1:DUNK=0
%FINISH
NTU:
%END ;! OF MBEAMCH
%ROUTINE FLASH FILAMENT
!
!      FLASHES FILAMENT FOR TWO MINUTES
!      HT IS TURNED OFF FIRST
!
SETPOT(1,1)   ;! HT OFF, FILAMENT ON
RINGBELL(40)
%PRINTTEXT' FILAMENT BEING FLASHED NOW' ;NEWLINE
WAIT(6000)   ;! TWO MINUTES
SETPOT(0,1)   ;! FILAMENT OFF, HT ON
WAIT(250)   ;! WAIT FOR FIVE SECONDS TO LET HT SETTLE
%END   ;! FLASH FILAMENT
%ROUTINE QUALITY
%INTEGER I,J,K,MAX,L,M
J=0
MAX=0
NPOW=0.
TALLY=0.
TALLY1=0.
%CYCLE I=0,1,5
NADD(I)=0
%REPEAT
%CYCLE I=0,1,1023
%IF MAX<ARRIVE(I) %THENSTART
MAX=ARRIVE(I) ;J=I ;%FINISH
%REPEAT
I=INTPT(EXPVAR(23))   ;! NO. OF PULSES
%CYCLE K=1,1,I
L=(K-1)*1024//I+J   ;! ADD UP I PEAKS
%IF L>1023 %THEN L=L-1024
MAX=L+25   ;! SAFE OFFSET FOR NOISE POWER ESTIMATE
!
!      ESTIMATE NOISE POWER
!
%CYCLE M=0,1,5
MAX=MAX+M
%IF MAX>1023 %THEN MAX=MAX-1024
NADD(M)=NADD(M)+ARRIVE(MAX)
%REPEAT
TALLY=TALLY+ARRIVE(L)
L=L+10
%IF L>1023 %THEN L=L-1024
%IF L<0 %THEN L=L+1024
```

```
%REPEAT
%CYCLE M=0,1,5
NPOW=NPOW+NADD(M)*NADD(M)
%REPEAT
NPOW=NPOW/6.
%IF TIME>.0001 %THEN NPOW1=SQRT(NPOW)/TIME %ELSE NPOW1=999.
!
PEAK=9999.
%IF TIME>.0001 %THEN PEAK=TALLY/TIME
%RETURNIF ENTRY=1
%IF TALLY1-STALLY1>.0001 %THEN %C
SOVERN=(TALLY-STALLY)/SQRT(TALLY1-STALLY1)
%IF TIME-STIME>.0001 %THEN %C
PEAK1=(TALLY-STALLY)/(TIME-STIME)
STALLY=TALLY
STALLY1=TALLY1
STIME=TIME
%END  ;! QUALITY
%ROUTINE RESETCLOCKS
!
!     RESETS ALL REALTIME CLOCKS
!     TO COMPENSATE FOR TIME THAT
!     DATA COLLECTION WAS WAITED
!
%REAL X
X=RTIME-NOW5  ;! REQUIRED OFFSET
THEN=THEN+X
NOW1=NOW1+X
NOW2=NOW2+X
NOW3=NOW3+X
NOW4=NOW4+X
NOW5=RTIME
%END  ;! RESETCLOCKS
%ROUTINE UPDATE
%INTEGER I
!
! PREVENT INTEGER OVERFLOW BY CLEARING CHANNELS WHICH REACH
! 32000 AND NOTING HOW MANY TIMES THEY ARE CLEARED SO THAT THE
! TRUE SPECTRUM CAN BE RECONSTRUCTED
!
%CYCLE I=1,1,50
%IF INDEX(I)=J %THENSTART
MULT(I)=MULT(I)+1
%RETURN
%FINISH
%IF INDEX(I)=-1 %THENSTART
INDEX(I)=J
MULT(I)=MULT(I)+1
%RETURN
%FINISH
%REPEAT
%RETURN
%END  ;! UPDATE
%ROUTINE INITIALISE
%CYCLE I=0,1,1023
ARRIVE(I)=0
%REPEAT
%CYCLE I=1,1,50
MULT(I)=0
INDEX(I)=-1
%REPEAT
DISPC=-1
PASSVECTOR  ; ! INITIALISE COMMON AREAS TO ZEROES
C3=0 ; ! NUMBER OF ARRIVALS WITH CODE 3
EVENTS=0  ; ! NUMBER OF EVENTS
```

```
AVCOUNT=0.  ;I AVERAGE COUNT RATE
NOISE=0   ; I NOISE COUNTS
COUNT=0   ;I CYCLING SENTENCE COUNTER
TIME=0   ;I REAL TIME FROM WORD COUNT
CALTIME=0.   ;I REAL TIME FROM WORD COUNTER
NBLOCKS=0   ;I NUMBER OF BLOCKS OF DATA
DATA=0   ;I BLOCK COUNTER
DISPC=0   ;I DISPLAY COUNTER
FIXUP=0   ;I STEADY ANGLE FLAG
OLDFLAG=7   ;I FLAG RECORD - SET TO 7 TO STOP ANGLE DRIVE ON NEW
THEN=RTIME   ;I INITIALISE REAL TIME COUNTER -- USED TO TIME EXP
NOW1=RTIME   ;I ANOTHER REAL TIME COUNTER -- TIMES EXPERIMENTAL
NOW2=RTIME   ;I YET ANOTHER REAL TIME COUNTER -- TIMES QUALITY F
NOW3=RTIME   ;I TIMES INTERVALS BETWEEN MAIN BEAM MONITOR READIN
NOW4=RTIME   ;I TIMES DISC TRANSFERS
NOW5=RTIME   ;I TIMES CHECKING MODE -- OTHERS  RESET BY THIS ON
NOW8=RTIME   ;I TIMING FOR COMPUTER CONTROL OF CROSS BEAM
NOW9=RTIME   ;I TIMING FOR COMPUTER CONTROL OF CROSS BEAM
MODOUT=0   ;I MODULATION ERROR COUNT
PKRAT=0   ;I BEAM COUNT RATE
PROB=0   ;I BIAS PROBABILITY
BLOCK=STBLOCK   ;I DA BLOCK COUNTER
XBEAMAREA=0.   ;I XBEAM NORMALISATION
MBEAMAREA=0.   ;I MBEAM NORMALISATION
RTC=4   ;I CALIBRATE MAIN BEAM MONITOR
TALLY=0.   ;I COUNTERS FOR QUALITY ESTIMATES
TALLY1=0.
STALLY=0.
STIME=0.
SOVERN=9999.   ;I S/N ESTIMATE
PEAK1=9999.   ;I PEAK RATE BASED ON LIMITED SAMPLE
QFLAG=0
CFLAG=0
%END ;I OF INITIALISE
%ENDOFPROGRAM


    W#3901

***ERCC  4-75  EMAS***          EDCD06          SUTTON JCMB
***ERCC  4-75  EMAS***          EDCD06          SUTTON JCMB
***ERCC  4-75  EMAS***          EDCD06          SUTTON JCMB
***ERCC  4-75  EMAS***          EDCD06          SUTTON JCMB
***ERCC  4-75  EMAS***          EDCD06          SUTTON JCMB
***ERCC  4-75  EMAS***          EDCD06          SUTTON JCMB
***ERCC  4-75  EMAS***          EDCD06          SUTTON JCMB
***ERCC  4-75  EMAS***          EDCD06          SUTTON JCMB
```

APPENDIX C

```
#LIST*
 EDCD04.SARPATCH1          Compiled: 25/09/79    18.06.53
 CORPATCH1

et: OPT


      E.R.C.C. NRIMPS COMPILER RELEASE  8 VERSION 29AUG79


 1533
   %REALSLONG
   %BEGIN
       %REALARRAY SCS(1:1000)
       %REAL EPS1,EPS2,EPS3,SIG1,SIG2,SIG3,E12,E13,H12,H23,E13P
       %REAL B,RIKE,RELVEL,PCL,RCDUM,R13,R133,R13D,R23,R23D,R34,R34D,SIGP
       %REAL GA1,GA2,GA3,GA4,GA5,GA6,GA7,GA8,GA10,GA11,GA12,GA13
       %REAL MU,MU1,V0,ROCH,DCH,PI,BETA,KIP,AL,AL1,D,PCH,STRETCH
       %REAL DFP1,DFP2,DFP3,DFP4,DFP5,DFP6,KEETA,CRETA,R13ADD
       %REAL GDFP1,GDFP2,GDFP3,GDFP4
       %REAL EL1,EL2,EL3,EL4
       %REAL DEMT,TF,T,VCI,DT,ACC,DRCH,P1,P2,SP,MORS0,ROCH1
       %REAL MORS03,ROCH3,E133
       %REAL VAR,V1,V2,V3
       %REAL DION,BETAION
       %REAL PKE1,KM,PKTM,BDUM,DUMV,RON,ROFF,BARR
       %INTEGER FLAGE2,FLAGE1,FLAGE,IRP1,IRP,PATH,I,FLAG1,CHNG,SCSI
       %STRING(63) STRING
       %ROUTINESPEC OUTPUT(%REALNAME B,DFP,EL,SIGMA,RCH %INTEGER PATH)
       %ROUTINESPEC READFILENAME(%STRINGNAME NAME)
       %EXTERNALROUTINESPEC DEFINE(%STRING(63) S)
       %EXTERNALROUTINESPEC CLEAR(%STRING(255) S)
       %EXTERNALROUTINESPEC RUN(%STRING(255) S)
       %EXTERNALROUTINESPEC PROMPT(%STRING(255) S)
       %REALFNSPEC TANH(%REAL X)
       %EXTERNALREALFNSPEC GAMMAFN(%REAL X)
       %REALFNSPEC MTCR(%REALNAME P1,E,R2,RSTART %INTEGER PATH)
       %REALFNSPEC MORSION(%REALNAME R)
       %REALFNSPEC MORSPOT(%REALNAME R,AL)
       %REALFNSPEC CROSPT(%REALNAME E,EPS1,SIG1,EPS2,SIG2, %REALFN %C
       POT1,POT2, %INTEGER FLAGS)
       %REALFNSPEC LANZEN (%REALNAME P, %INTEGER PATH)
       %REALFNSPEC IONPOT(%REALNAME R,SIG,EPS)
       %REALFNSPEC POWPOT(%REALNAME R,SIG,EPS)
       %REALFNSPEC DEFION(%REAL B)
       %REALFNSPEC DEFPOW(%REAL EPS,SIG,B)
       %REALFNSPEC GDEFION(%REAL B)
       %REALFNSPEC GDEFPOW(%REAL EPS,SIG,B)
       %CYCLE I=1,1,1000
       SCS(I)=0.0D0-99
       %REPEAT
```

```
SP=SQRT(PI)
L15:
FLAGE=0
FLAGE1=0
FLAGE2=0
PROMPT("Input ?:")
READFILENAME(STRING)
%IF STRING="TT" %OR STRING="LOCAL" %THEN SELECTINPUT(0) %AND ->L1
DEFINE("ST1,".STRING)
SELECTINPUT(1)
L16:
PROMPT("Output ?:")
READFILENAME(STRING)
%IF STRING="TT" %OR STRING="LOCAL" %THEN STRING=".OUT"
DEFINE("ST2,".STRING)
PROMPT("Eps1:")
READ(EPS1)
PROMPT("Eps2:")
READ(EPS2)
PROMPT("Eps3:")
READ(EPS3)
PROMPT("Sig1:")
READ(SIG1)
PROMPT("Sig2:")
READ(SIG2)
PROMPT("Sig3:")
READ(SIG3)
STRETCH=0
KIP=4.3
E12=1.62
!  ASSYMPTOTIC LIMIT OF 1ST EXCITED STATE
PROMPT("Ion rep pow:")
READ(IRP)
IRP1=IRP//2
PROMPT("H12:")
READ(H12)
PROMPT("H23:")
READ(H23)
GA1=GAMMAFN(6.5)
GA2=GAMMAFN(7)
GA3=GAMMAFN(5.5)
GA4=GAMMAFN(4)
GA5=GAMMAFN(2.5)
GA6=GAMMAFN(3)
GA7=GAMMAFN(1)
GA8=GAMMAFN(1.5)
GA10=GAMMAFN((IRP+1)/2)
GA11=GAMMAFN(IRP/2+1)
GA12=GAMMAFN((IRP1+1)/2)
GA13=GAMMAFN(IRP1/2+1)
PROMPT("Red mass:")
READ(MU)
MU=MU*1.67258-27
PROMPT("RIKE:")
READ(RIKE)
RELVEL=2*RIKE*1.60210-19/MU
RELVEL=SQRT(RELVEL)
PRINTSTRING("                PARAMETERS RELEVANT TO TARGET MOLECULE
NEWLINE
PROMPT("Red mass:")
READ(MU1)
MU1=MU1*1.67252-27
PROMPT("R?:")
READ(ROCH)
ROCH3=(ROCH+STRETCH)*1.-1
```

```
ROCH=ROCH*1@-10
ROCH1=ROCH
PROMPT("V0:")
READ(V0)
PROMPT("D0:")
READ(DCH)
%IF DCH>1@-10 %THEN DCH=DCH*1.60210@-19
PROMPT("DION:")
READ(DION)
%IF DION>1@-10 %THEN DION=DION*1.602@-19
PROMPT("BETAION:")
READ(BETAION)
%IF BETAION<1@5 %THEN BETAION=BETAION*1@10
PRINTSTRING("TARGET MOLECULE ION POTENTIAL HAS THE FORM
V(R)=D*EXP(-BETA*(R-R0))+K*(TANH(R-RON)-TANH(R-ROFF))")
NEWLINE
PRINTSTRING("K CONTROLS THE BEHAVIOUR OF V(R) W.R.T. THE K+/T
SEPARATION AND THE HEIGHT OF THE BARRIER INTRODUCED.")
NEWLINE
PRINTSTRING("INPUT RON AND ROFF. ")
NEWLINE
PROMPT("RON:")
READ(RON)
PROMPT("ROFF:")
READ(ROFF)
PRINTSTRING("MAXIMUM HEIGHT OF TANH BARRIER")
NEWLINE
PROMPT("BARRIER:")
READ(BARR)
BARR=BARR*1.60210@-19
PROMPT("K BETA:")
READ(KBETA)
PROMPT("CBETA:")
READ(CBETA)
PROMPT("TEMP FIX:")
READ(R13ADD)
BETA=V0*SQRT(2*PI*PI*MU1/DCH)
PRINTSTRING("ASSYMPTOTIC LIMITS")
NEWLINE
PROMPT("GSN A.L.:")
READ(AL)
PROMPT("ION A.L.:")
READ(AL1)
%IF AL1>1@-10 %OR AL1<-1@-10 %THEN AL1=AL1*1.60210@-19
PROMPT("PCL:")
READ(PCL)
BDUM=TANH(KBETA*R13ADD)*BARR
MORS03=MORSPOT(ROCH3,AL)
MORS0=MORSPOT(ROCH,AL)
E133=KIP-(MORS03-MORSION(ROCH3))
E13=KIP-(MORS0-MORSION(ROCH))
PRINTSTRING("E13 = ")
PRINT(E13,4,2)
NEWLINE
FLAG1=1
RCH=ROCH
PROMPT("R13:")
READ(R13R)
SIG3=EPS1*(SIG1/R13R)**6*((SIG1/R13R)**6-1)+[illegible]/R13 **[illegible]
SIG3=SIG3+14.394/R13R-[illegible]
SIG3=1[illegible]*SIG3*R13R**IRP
SIG3=EXP(LOG(SIG3)/IRP)
PRINTSTRING("SIG3 = ")
PRINT(SIG3,3,3)
NEWLINE
RI33=C[illegible]SPT([illegible]
```

```
R13=CROSPT(E13,EPS3,SIG2,EPS1,SIG1,IONPOT,POWPOT,FLAG1
NEWLINE
PRINTSTRING("       R13 = ")
PRINT(R13,6,4)
NEWLINE
D=E13-E12
FLAG1=3
R23=CROSPT(D,EPS3,SIG3,EPS2,SIG2,IONPOT,POWPOT,FLAG1)
PRINTSTRING("       R23 = ")
PRINT(R23,5,3)
NEWLINE
!
!
!    START OF CALCULATION
!
!
PROMPT("Output pots?:")
SKIPSYMBOL %UNTIL NEXTSYMBOL='Y' %OR NEXTSYMBOL='N'
READSYMBOL(I)
%IF I='Y' %THEN %START
PROMPT("Pot1 output:")
READFILENAME(STRING)
%IF STRING="TT" %OR STRING="LOCAL" %THEN STRING=".OUT"
DEFINE("ST12,".STRING)
PROMPT("Pot2 output:")
READFILENAME(STRING)
%IF STRING="TT" %OR STRING="LOCAL" %THEN STRING=".OUT"
DEFINE("ST13,".STRING)
PROMPT("Pot3 output:")
READFILENAME(STRING)
%IF STRING="TT" %OR STRING="LOCAL" %THEN STRING=".OUT"
DEFINE("ST14,".STRING)
VAR=R13-1.5
%CYCLE I=1,1,100
VAR=VAR+.05
V1=POWPOT(VAR,SIG1,EPS1)
%IF V1>10 %THEN ->PL1
SELECTOUTPUT(12)
PRINT(VAR,5,3)
SPACES(2)
PRINT(V1,5,3)
NEWLINE
PL1:
V2=POWPOT(VAR,SIG2,EPS2)+E12
%IF V2>10 %THEN ->PL2
SELECTOUTPUT(13)
PRINT(VAR,5,3)
SPACES(2)
PRINT(V2,5,3)
NEWLINE
PL2:
V3=IONPOT(VAR,SIG3,EPS3)+E13
%IF V3>10 %THEN ->PL3
SELECTOUTPUT(14)
PRINT(VAR,5,3)
SPACES(2)
PRINT(V3,5,3)
NEWLINE
PL3:
%REPEAT
SELECTOUTPUT(0)
PROMPT("Continue:")
SKIPSYMBOL %UNTIL NEXTSYMBOL='Y' %OR NEXTSYMBOL='N'
READSYMBOL(I)
%IF I='N' %THEN %OUTP
%FINISH
```

```
L6:
PROMPT("IMPACT PARM:")
READ(B)
%IF B<-90 %THEN ->L15
PROMPT("WHICH CHANNEL:")
READ(CHNO)
R23D=R23
R13D=R13
%IF CHNO=1 %THEN %START
RCDUM=R13
L9:
DFP1=DEFPOW(EPS1,SIG1,B)
EL1=0.000
GDFP1=MOD(GDEFPOW(EPS1,SIG1,B))
DFP1=MOD(DFP1)
PATH=1
%IF B<R13 %THEN SIGMA=LANZEN(B,PATH)*B/(GDFP1*SIN(DFP1))
%IF B>R13 %THEN SIGMA=B/(GDFP1*SIN(DFP1))
OUTPUT(B,DFP1,EL1,SIGMA,RCH,PATH)
%IF DFP1*180/PI>6 %THEN ->L8
B=B-0.003
->L9
%FINISH
%IF CHNO=2 %THEN %START
L10:
%IF B>R13 %THEN ->L8
VCI=0
DEMT=MTCR(R13,B,R13,ROCH1,2)
D=KIP-(MORSPOT(RCH,AL)-MORSION(RCH))
D=D-(MORSPOT(RCH,AL)-MORS0)
FLAG1=1
RCDUM=CROSPT(D,EPS3,SIG3,EPS1,SIG1,IONPOT,POWPOT,FLAG1)
R13D=R13
%IF FLAGE=0 %THEN %START
L1:
FLAGE2=1
%IF RCDUM-R13D>0.005*R13D %THEN %START
DEMT=MTCR(R13D,B,RCDUM,RCH,3)
D=KIP-(MORSPOT(RCH,AL)-MORSION(RCH))
D=D-(MORSPOT(RCH,AL)-MORS0)
FLAG1=1
R13D=RCDUM
RCDUM=CROSPT(D,EPS3,SIG3,EPS1,SIG1,IONPOT,POWPOT,FLAG1)
%IF FLAGE=0 %THEN ->L1
R13D=RCDUM
%FINISH
%FINISH
DFP2=DEFPOW(EPS1,SIG1,R13)/2+DEFPOW(EPS1,SIG1,R13D)/2
DFP2=DFP2+DEFION(B)-(DEFION(R13)+DEFION(R13D))/2
DFP2=MOD(DFP2)
GDFP2=GDEFPOW(EPS1,SIG1,R13)/2+GDEFPOW(EPS1,SIG1,R13D)/2
GDFP2=GDFP2+GDEFION(B)-(GDEFION(R13)+DEFION(R13D))/2
GDFP2=MOD(GDFP2)
EL2=DEMT+MORSPOT(RCH,AL)-MORS0
PATH=2
SIGMA=LANZEN(B,PATH)*B/(DFP2*SIN(GDFP2))
OUTPUT(B,DFP2,EL2,SIGMA,RCH,PATH)
%IF DFP2*180/PI>6 %THEN ->L8
B=B-0.003
FLAGE1=0
FLAGE=1
FLAGE8=0
->L10
%FINISH
%IF CHNO=3 %THEN %START
L11:
```

```
VCI=0
DEMT=MTCR(R133,B,R23,RCH3,3)
D=KIP-(MORSPOT(RCH,AL)-MORSION(RCH))-E12
D=D-(MORSPOT(RCH,AL)-MORS0)
FLAG1=3
RCDUM=CROSPT(D,EPS3,SIG3,EPS2,SIG2,IONPOT,POWPOT,FLAG1)
R23D=R23
%IF FLAGE=0 %THEN %START
L2:
%IF RKTM>10 %THEN %START
PRINTSTRING("B = ")
PRINT(B,5,3)
PRINTSTRING(" TARGET OPENED UP. ABANDONED !")
NEWLINE
->BL1
%FINISH
%IF RCDUM-R23D>0.025*R23D %THEN %START
FLAGE2=1
DEMT=MTCR(R23D,B,RCDUM,RCH,3)
R23D=RCDUM
D=KIP-(MORSPOT(RCH,AL)-MORSION(RCH))-E12
D=D-(MORSPOT(RCH,AL)-MORS0)
RCDUM=CROSPT(D,EPS3,SIG3,EPS2,SIG2,IONPOT,POWPOT,FLAG1)
%IF FLAGE=0 %THEN ->L2
R23D=RCDUM
%FINISH
%FINISH
EL3=DEMT+E12+MORSPOT(RCH,AL)-MORS0
DFP3=DEFPOW(EPS1,SIG1,B)-DEFPOW(EPS1,SIG1,R133)/2
DFP3=DFP3+DEFION(R133)/2-DEFION(R23D)/2+DEFPOW(EPS2,SIG2,R23D)/2
DFP3=MOD(DFP3)
GDFP3=GDEFPOW(EPS1,SIG1,B)-GDEFPOW(EPS1,SIG1,R13)/2
GDFP3=GDFP3+GDEFION(R13)/2-GDEFION(R23D)/2+GDEFPOW(EPS2,SIG2,R23D)/2
GDFP3=MOD(GDFP3)
PATH=3
SIGMA=LAMZEN(B,PATH)*B/(GDFP3*SIN(DFP3))
OUTPUT(B,DFP3,EL3,SIGMA,RCH,PATH)
%IF DFP3*180/PI>6 %THEN ->L8
BL1:
B=R-0.003
FLAGE1=0
FLAGE=0
->L11
%FINISH
!
!
%IF CHNO=4 %THEN %START
L12:
FLAGE2=0
VCI=0
DEMT=MTCR(R13,B,R23,RCH1,4)
D=KIP-(MORSPOT(RCH,AL)-MORSION(RCH))
D=D-E12-(MORSPOT(RCH,AL)-MORS0)
FLAG1=3
RCDUM=CROSPT(D,EPS3,SIG3,EPS2,SIG2,IONPOT,POWPOT,FLAG1)
R23D=R23
L3:
%IF FLAGE=0 %THEN %START
%IF RCDUM-R23D>0.025*R23D %THEN %START
FLAGE2=1
DEMT=MTCR(R23D,B,RCDUM,RCH,3)
R23D=RCDUM
D=KIP-(MORSPOT(RCH,AL)-MORSION(RCH))
D=D-E12-(MORSPOT(RCH,AL)-MORS0)
RCDUM=CROSPT(D,EPS3,SIG3,EPS2,SIG2,IONPOT,POWPOT,FLAG1)
```

```
%IF FLAGE=0 %THEN ->L3
R23D=RCOUM
%FINISH
%FINISH
EL4=DEMT+E12+MORSPOT(RCH,AL)-MORS0
DFP4=DEFPOW(EPS1,SIG1,R13)/2
DFP4=DFP4+DEFION(B)-DEFION(R13)/2-DEFION(R23D)/2
DFP4=MOD(DFP4+DEFPOW(EPS2,SIG2,R23D)/2)
GDFP4=GDEFPOW(EPS1,SIG1,R13)/2
GDFP4=GDFP4+GDEFION(B)-GDEFION(R13)/2-GDEFION(R23D)/2
GDFP4=MOD(GDFP4+GDEFPOW(EPS2,SIG2,R23D)/2)
PATH=4
SIGMA=LANZEN(B,PATH)*B/(GDFP4*SIN(DFP4))
OUTPUT(B,DFP4,EL4,SIGMA,RCH,PATH)
%IF DFP4*180/PI>6 %THEN ->L8
B=B-0.003
FLAGE=0
FLAGE1=0
->L12
%FINISH
!
!
L8:
R13D=R13
R23D=R23
PROMPT("OUTPUT DXS:")
SKIPSYMBOL %UNTIL NEXTSYMBOL='Y' %OR NEXTSYMBOL='N'
READSYMBOL(I)
%IF I='Y' %THEN %START
PROMPT("OUTPUT:")
READFILENAME(STRING)
%IF STRING="TT" %OR STRING="LOCAL" %THEN STRING=".OUT"
DEFINE("ST11,",STRING)
SELECTOUTPUT(11)
%CYCLE SCSI=1,1,1200
%IF SCS(SCSI)>10-6 %THEN %START
WRITE(SCSI,4)
SPACE
PRINTFL(SCS(SCSI),3)
NEWLINE
%FINISH
%REPEAT
SELECTOUTPUT(0)
CLOSESTREAM(11)
CLEAR("11")
PROMPT("GRAPH THEM:")
SKIPSYMBOL %UNTIL NEXTSYMBOL='Y' %OR NEXTSYMBOL='N'
READSYMBOL(I)
%IF I='Y' %THEN %START
%EXTERNALINTEGERSPEC EXIST(%STRING(63) FILE)
%EXTERNALROUTINESPEC DRAW TEXT(%STRING(63) S)
%EXTERNALROUTINESPEC NLINE
%EXTERNALROUTINESPEC STORE ON
%EXTERNALROUTINESPEC STORE OFF
%EXTERNALROUTINESPEC VIEWON
%EXTERNALROUTINESPEC VIEWOFF
%EXTERNALROUTINESPEC NEWPIC
%EXTERNALROUTINESPEC ERASE
%EXTERNALROUTINESPEC WINDOW(INTEGER A,B,C,D)
%EXTERNALROUTINESPEC SWINDOW(%INTEGER A,B,C,D)
%EXTERNALROUTINESPEC FRAME
%EXTERNALROUTINESPEC DRAW(INTEGER X,Y)
%EXTERNALROUTINESPEC MOVE(INTEGER X,Y)
%EXTERNALROUTINESPEC POINT(INTEGER X,Y)
%EXTERNALROUTINESPEC PLOT(INTEGER X,Y)
%EXTERNALROUTINESPEC
```

```
%EXTERNALROUTINESPEC POINT(%INTEGER X,Y)
%EXTERNALROUTINESPEC DEFSUB(%INTEGER NAME)
%EXTERNALROUTINESPEC ENDSUB
%EXTERNALROUTINESPEC CHAR(%INTEGER CVAL)
%EXTERNALROUTINESPEC INSTAN(%INTEGER NAME,SIZE,ORIENT,XREF,YREF)
%EXTERNALROUTINESPEC REVU
%EXTERNALROUTINESPEC TEKTYP(%INTEGER TYPE)
%EXTERNALROUTINESPEC SNAPSHOT(%STRING(20) FILE)
%EXTERNALROUTINESPEC CURSOR(%INTEGERNAME CVAL, X, Y)
%EXTERNALROUTINESPEC DEFHEAD(%STRING(230) T)
%EXTERNALROUTINESPEC DEFMENU(%STRING(9) T, %INTEGER LINE)
%EXTERNALROUTINESPEC DRAWMENU
%EXTERNALROUTINESPEC TPRINT(%REAL NO,%INTEGER DIGITS, DECPL)
%EXTERNALROUTINESPEC TWRITE(%INTEGER NO, DIGITS)
%EXTERNALROUTINESPEC BIGSTRING(%STRING(255) S, %INTEGER ROT, SCALE)
%BEGIN
    %ROUTINESPEC AXES(%STRING(63) L)
    %EXTERNALROUTINESPEC DEFINE(%STRING (63) T)
    %ROUTINESPEC EXTREMA(%REALARRAYNAME X,Y %REALNAME MINX,MAXX,MINY,
    MAXY %INTEGERNAME N)
    %ROUTINESPEC DISPLAYPOINTS(%INTEGERNAME N,FLAG %REALARRAYNAME X,Y
    %REALNAME MINX,MAXX,MINY,MAXY)
    %ROUTINESPEC FREEZE
    %ROUTINESPEC LABEL
    %ROUTINESPEC CLEAR
    %ROUTINESPEC READFILENAME(%STRINGNAME S)
    %REAL MINX,MAXX,MINY,MAXY,SCALEX,SCALEY
    %INTEGER I,N,FLAG,XX,YY,X1,Y1,DX1,DY1,DX,DY,POSN,JJ,KK,FLAG2,FLAG3
    %INTEGER FLAG4,PSD
    %STRING (12) BC,NEXT
    %REALARRAY X,SD(1:1000),Y(1:1000)
    %ON %EVENT 9 %START
    ->INDA
    %FINISH
    FLAG2=0
    FLAG3=0
    PRINTSTRING("
    SET GRAPH MODE
    ")
    PROMPT("TEKTRONIX NO:")
    READ(I) %UNTIL I=4002 %OR I=4006 %OR I=4010 %OR I=4012 %OR I=4014
    TEKTYP(I)
    NEWPIC
    ERASE
    JJ=0
    POSN=0
    L2:
    PROMPT("PLOT S.D:")
    SKIPSYMBOL %WHILE NEXTSYMBOL#'Y' %AND NEXTSYMBOL#'N'
    READSYMBOL(I)
    FLAG4=0
    %IF I='Y' %THEN FLAG4=1
    PROMPT("INPUT FILE:")
    READFILENAME(BC) %UNTIL EXIST(BC)=1
    POSN=POSN+25
    DEFINE("ST1,",BC)
    JJ=JJ+1
    SELECTINPUT(1)
    N=0
    %CYCLE I=1,1,1000
    READ(X(I))
    READ(Y(I))
    READ(SD(I)) %IF FLAG4=1
    N=N+1
    %REPEAT
    INDA:SELECTINPUT(0)
```

```
CLOSE STREAM(1)
PROMPT("PLOT SYMBOLS:")
SKIPSYMBOL %WHILE NEXTSYMBOL # 'Y' %AND NEXTSYMBOL # 'N'
READSYMBOL(I)
FLAG=0
%IF I='Y' %THEN %START
PROMPT("SYM:")
SKIPSYMBOL %WHILE NEXTSYMBOL = NL
READSYMBOL(KK)
FLAG=1
%FINISH
PROMPT("PLOT LINE:")
SKIPSYMBOL %WHILE NEXTSYMBOL =NL
READSYMBOL(I)
FLAG2=1
%IF I='N' %THEN FLAG2=0
%IF FLAG3=1 %THEN ->L4
EXTREMA(X,Y,MINX,MAXX,MINY,MAXY,N)
L4:DISPLAYPOINTS(N,FLAG,X,Y,MINX,MAXX,MINY,MAXY)
L1:MOVEA(0,775-POSN)
PROMPT(":")
READFILENAME(NEXT)
POSN=POSN+25
%IF NEXT="F" %THEN FREEZE %AND ->L1
%IF NEXT="L" %THEN LABEL %AND ->L1
%IF NEXT="STOP" %THEN ERASE %AND ->JIMBO
%IF NEXT="C" %THEN ERASE %AND ->L1
%IF NEXT="A" %THEN %START
PROMPT("SAME SCALE:")
SKIPSYMBOL %WHILE NEXTSYMBOL # 'Y' %AND NEXTSYMBOL # 'N'
READSYMBOL(I)
%IF I='Y' %THEN FLAG3=1
%IF I='N' %THEN FLAG3=0
->L2
%FINISH
->L1
%ROUTINE EXTREMA(%REALARRAYNAME X,Y %REALNAME MINX,MAXX,MINY, %C
MAXY %INTEGERNAME N)
    MINX=0
    MAXX=0
    MINY=2.139
    MAXY=0
    %CYCLE I=1,1,N
    %IF MINX>X(I) %THEN MINX=X(I)
    %IF MINY>Y(I) %THEN MINY=Y(I)
    %IF MAXX<X(I) %THEN MAXX=X(I)
    %IF MAXY<Y(I) %THEN MAXY=Y(I)
    %REPEAT
    %END ; ! END OF EXTREMA
%ROUTINE DISPLAYPOINTS(%INTEGERNAME N,FLAG %REALARRAYNAME X,Y %C
%REALNAME MINX,MAXX,MINY,MAXY)
    DEFSUB(JJ)
    DX=577
    DY=720
    SCALEX=(MAXX-MINX)/DX
    SCALEY=(MAXY-MINY)/DY
    %CYCLE I=1,1,N
    XX=INTPT((X(I)-MINX)/SCALEX)
    YY=INTPT((Y(I)-MINY)/SCALEY)
    %IF FLAG4=1 %THEN PSC=INTPT(SP(I)/SCALEY).
    %IF I=1 %THEN %START
    MOVEA(XX+100,YY+95)
    X1=XX
    Y1=YY
    %FINISH
    DX1=XX-X1
```

```
    DY1=YY-Y1
    %IF FLAG2=0 %THEN %START
    MOVER(DX1,DY1)
    %IF FLAG4=1 %THEN %START
    MOVER(0,PSD)
    DRAWR(0,-2*PSD)
    MOVER(0,PSD)
    %FINISH
    ->L3
    %FINISH
    DRAWR(DX1,DY1) %IF I#0
    %IF FLAG4=1 %THEN %START
    MOVER(0,PSD)
    DRAWR(0,-2*PSD)
    MOVER(0,PSD)
    %FINISH
    L3:
    %IF FLAG=1 %THEN %START
    MOVER(-3,-5)
    CHAR(KK)
    MOVER(-9,5)
    %FINISH
    X1=XX
    Y1=YY
    %REPEAT
    ENDSUB
    INSTAN(JJ,128,0,0,0)
    %END ; ! END OF DISPLAYPOINTS
%ROUTINE FREEZE
    %STRING(12) FILE
    PROMPT("Tekfile:")
    READ FILE NAME(FILE)
    SNAPSHOT(FILE)
    %END  ;! FREEZE
%ROUTINE CLEAR
    ERASE;                                          ! Clear screen
    NEWPIC;                                         ! Clear picture definition
    %END  ;! CLEAR
%ROUTINE READ FILE NAME(%STRINGNAME NAME)
        %INTEGER I
        NAME = ""
        SKIP SYMBOL %WHILE NEXT SYMBOL = '''' %OR NEXT SYMBOL = ' ' %C
                          %OR NEXT SYMBOL = NL
        %CYCLE
           READ SYMBOL(I)
           NAME = NAME.TO STRING(I)
           %EXIT %IF NEXT SYMBOL = NL %OR NEXT SYMBOL = ''''
        %REPEAT
        SKIP SYMBOL %WHILE NEXT SYMBOL = NL
        SKIP SYMBOL
    %END  ;! READ FILE NAME
%ROUTINE LABEL
    %STRING(63) LABEL
    PROMPT("LABEL:")
    READFILENAME(LABEL)
    AXES(LABEL)
    %END ; ! END OF LABEL
%ROUTINE AXES(%STRING(63) LABEL)
    DEFSUB(5)
    MOVE(100,35)
    DRAWR(0,INTPT(DY/4));DRAWR(0,INTPT(DY/4))
    DRAWR(0,INTPT(DY/4));DRAWR(0,INTPT(DY/4))
    DRAWR(INTPT(DX/4),0);DRAWR(INTPT(DX/4),0)
    DRAWR(INTPT(DX/4),0);DRAWR(INTPT(DX/4),0)
    DRAWR(0,-INTPT(DY/2))
    DRAWR(0,-INTPT(DY/2))
```

```
        DRAWR(-INTPT(DX/2),0)
        DRAWR(-INTPT(DX/2),0)
        MOVEA(200,700)
        DRAWTEXT(LABEL)
        ENDSUB
        INSTAN(5,128,0,0,0)
        %END
    JIMBO:
    %END
%FINISH
%FINISH
%CYCLE I=1,1,1000
SCS(I)=0.00@-99
%REPEAT
PROMPT("CONTINUE?:")
SKIPSYMBOL %UNTIL NEXTSYMBOL='Y' %OR NEXTSYMBOL='N'
READSYMBOL(I)
%IF I='Y' %THEN ->L6
%REALFN MTCR(%REALNAME R1,B,R2,RSTART %INTEGER PATH)
    %REAL RCH1
    %IF B>R13 %THEN %RESULT=-999
    %IF PATH=2 %THEN %START
    TF=2*(SQRT(R1*R1-B*B)*1@-10/RELVEL)
    RKE1=SQRT(R1*R1-B*B)
    %FINISH
    %IF PATH=3 %OR PATH=5 %THEN %START
    !   CROSSING TO IONIC CURVE ON WAY OUT
    TF=(SQRT(R2*R2-B*B)*1@-10-SQRT(R1*R1-B*B)*1@-10)/RELVEL
    RKE1=SQRT(R1*R1-B*B)
    %FINISH
    %IF PATH=4 %OR PATH=6 %THEN %START
    !   CROSSING TO IONIC CURVE ON WAY IN
    TF=(SQRT(R1*R1-B*B)*1@-10+SQRT(R2*R2-B*B)*1@-10)/RELVEL
    RKE1=SQRT(R1*R1-B*B)
    %FINISH
    T=0
    RCH1=RSTART
    !   EQUILIBRIUM C-I BOND DISTANCE
    DT=TF/50
    !   STEP LENGH FOR CALCULATION OF INCREASE IN C-I BOND
    KM=0
    !   PATCH TO ALLOW FOR THE INFLUENCE OF THE K+ ION ON THE TM- KEPULSIO
    L30:
    %IF PATH=3 %OR PATH=5 %THEN %START
    RKTM=SQRT((RKE1+KM)*(RKE1+KM)+B*B)
    %FINISH
    %IF PATH=2 %OR PATH=4 %OR PATH=6 %THEN %START
    RKTM=SQRT((RKE1-KM)*(RKE1-KM)+B*B)
    %FINISH
    %IF RKTM>15 %THEN ->M1
    !   CROSSING POINT MOVED TO BEYOND 15 ANGSTROMS.  LITTLE
    !   POINT IN PROCEEDING FURTHER WITH CALCULATIONS AT THIS IMPACT
    !   PARAMETER.  IT ALSO SIDESTEPS THE PROBLEMS CAUSED BY
    !   THE EXP ARGUMENT.
    BDUM=TANH(KBETA*(R13+R13ADD-RKTM))*BARR
    %IF BDUM<0 %THEN BDUM=0
    ACC=-BETAION*DION*EXP(-BETAION*(RCH1-RCH0))
    ACC=ACC+4@10*BDUM*((TANH(CBETA*(RCH1*1@10-RCFF))))**2- DC
    (TANH(CBETA*(RCH1*1@10-RCN))))**2)
    ACC=-ACC/MU1
    DRCH=VCI*DT+0.5*ACC*DT*DT
    VCI=VCI+ACC*DT
    RCH1=RCH1+DRCH
    T=T+DT
    KM=RELVEL*T*1@10
    %IF KM>=RKE1 %THEN FLAG1=1
```

```
%IF FLAGE1=1 %AND CHNO=4 %THEN %START
DUMV=IONPOT(RKTM,SIG3,EPS3)+KIP-E12-POWPOT(RKTM,SIG2,EPS2)
DUMV=DUMV-MORSPOT(RCH1,AL)+MORSION(RCH1)
%IF DUMV<0 %THEN DUMV=-DUMV
%IF DUMV<0.05 %THEN FLAGE=1 %AND FLAGE1=0 %AND ->M1
%FINISH
%IF CHNO=4 %AND FLAGE2=1 %THEN %START
DUMV=IONPOT(RKTM,SIG3,EPS3)+KIP-E12-POWPOT(RKTM,SIG2,EPS2)
DUMV=DUMV-MORSPOT(RCH1,AL)+MORSION(RCH1)
%IF DUMV<0 %THEN DUMV=-DUMV
%IF DUMV<0.05 %THEN FLAGE=1 %AND ->M1
%FINISH
%IF FLAGE1=1 %AND CHNO=2 %THEN %START
DUMV=IONPOT(RKTM,SIG3,EPS3)+KIP-POWPOT(RKTM,SIG1,EPS1)
DUMV=DUMV-MORSPOT(RCH1,AL)+MORSION(RCH1)
%IF DUMV<0 %THEN DUMV=-DUMV
%IF DUMV<0.05 %THEN FLAGE=1 %AND FLAGE1=0 %AND ->M1
%FINISH
%IF CHNO=2 %AND FLAGE2=1 %THEN %START
DUMV=IONPOT(RKTM,SIG3,EPS3)+KIP-POWPOT(RKTM,SIG1,EPS1)
DUMV=DUMV-MORSPOT(RCH1,AL)+MORSION(RCH1)
%IF DUMV<0 %THEN DUMV=-DUMV
%IF DUMV<0.05 %THEN FLAGE=1 %AND ->M1
%FINISH
%IF CHNO=3 %AND FLAGE2=1 %THEN %START
DUMV=IONPOT(RKTM,SIG3,EPS3)+KIP-E12-POWPOT(RKTM,SIG2,EPS2)
DUMV=DUMV-MORSPOT(RCH1,AL)+MORSION(RCH1)
%IF DUMV<0 %THEN DUMV=-DUMV
%IF DUMV<0.05 %THEN FLAGE=1 %AND ->M1
%FINISH
%IF T<TF %THEN ->L30
!    MOTION DOWN (CH3I)- CURVE FINISHED
!    NOW CALCULATE CHANGE IN K+/CH3I- CURVE
     M1:
     RCH=RCH1
     P1=MORSION(ROCH1)
     P2=MORSION(RCH)
     %RESULT=P1-P2
     %END
%REALFN TANH(%REAL X)
     %RESULT=(EXP(X)-EXP(-X))/(EXP(X)+EXP(-X))
     %END
%REALFN IONPOT(%REALNAME R,SIG,EPS)
     %RESULT=EPS*(SIG/R)**IRP-POL/R**4-14.394/R
     %END
%REALFN POWPOT(%REALNAME R,SIG,EPS)
     %RESULT=EPS*(SIG/R)**6*((SIG/R)**6-1)
     %END
%REALFN CROSPT(%REALNAME E,EPS1,SIG1,EPS2 ,SIG2,%REALFN POT1,POT2  %C
%INTEGER FLAGS)
          %SPEC POT1(%REALNAME R,SIG,EPS)
          %SPEC POT2(%REALNAME R,SIG,EPS)
     %REAL R,V1,V2,W1,W2,G,X,Y,EE,HH
     %INTEGER FLAG
     !    THIS FUNCTION EVALUATES THE CROSSING RADII FOR THE
     !    THREE NEUTRAL CURVES AND THE IONIC CURVE.
     FLAG = 
     HH =.05
     %IF E<0 %THEN%START
          EE = -E/14.394
          W1 = 0; W2 = 1
          R = 2
          ->L1
          %FINISH
     EE = E/14.394
     W1 = 0; W2 = 1
```

```
    %IF FLAGS = 1 %THEN R = 2.6
    %IF FLAGS = 2 %THEN R=4
    %IF FLAGS = 3 %THEN R = 3
    L1:     V1 = EE*POT1(R,SIG1,EPS1)/14.394
        V2 =POT2(R,SIG2,EPS2)/14.394
    %IF V1>=V2%OR FLAG = 1 %THEN ->L2
        W1 = V1
        W2 = V2
        R = R+HH
    ->L1 %UNLESS R>1000
    ->L3
    L2:     X = W1-W2
        Y = V1-V2
        G = -(X-Y)/HH
    R = R-HH-X/G
        W1 = V1; W2 = V2
        HH = -(HH+X/G)
        FLAG = 1
    ->L1 %UNLESS ABS(V1-V2)<10-5
    %RESULT = R
    L3:     %RESULT = -10
    %END
%REALFN GDEFICN(%REAL B)
    %REAL X,Y,Z
    !   THIS FUNCTION EVALUATES THE GRADIENT OF CP1(B) VS. B AT B
    X=IRP*EPS3*SIG3**IRP*SP*(GA10/GA11)/(2*RIKE*B**IRP)
    X=-IRP*X/B
    Y=-PCL*SP*4*(GA5/GA6)/(2*RIKE*B**4)
    Y=-4*Y/B
    Z=-14.394*SP*(GA7/GA8)/(2*RIKE*B)
    Z=-Z/B
    %RESULT=X+Y+Z
    %END
%REALFN DEFPOW(%REAL EPS,SIG,B)
    %REAL X,Y
    !   THIS FUNCTION EVALUATES THE CONTRIBUTION TO THE DEFLECTION
    !   FUNCTION FROM ANY OF THE NEUTRAL L-J POTENTIALS. THE POTENTIAL
    !   IS DEFINED BY THE VALUES FED IN TO SIG AND EPS.
    X=12*EPS*(SIG/B)**12*SP*(GA1/GA2)/(2*RIKE)
    Y=-6*EPS*SIG**6*SP*(GA3/GA4)/(2*RIKE*B**6)
    %RESULT=X+Y
    %END
%REALFN GDEFPOW(%REAL EPS,SIG,B)
    %REAL X,Y
    !   THIS FUNCTION CALCULATES D/DB(CHI(B)) AT B FOR
    !   NEUTRAL POTENTIALS
    X=12*EPS*SP*(GA1/GA2)*(SIG/B)**12/(2*RIKE)
    X=-12*X/B
    Y=-6*EPS*SIG**6*SP*(GA3/GA4)/(2*RIKE*B**6)
    Y=-6*Y/B
    %RESULT=X+Y
    %END
%REALFN LAMZEN(%REALNAME B, %INTEGER PATH)
    %REAL P1DD,P1,P1D,P2D,VP1,P2,VP2
    !   THIS ROUTINE CALCULATES THE PROBABILITY OF EXITING VIA
    !   A GIVEN PATH. H12,H23 AND H34 ARE REDUCED COUPLING PARAMETERS
    !   (UNITS ARE 10**9 CM/S)
    %IF B>R13 %THEN %START
    P1D=1
    P2D=1
    P1=1
    P2=1
    ->L1
    !   NO CHANCE OF INELASTIC BEHAVIOUR
    %FINISH
    VP1=RELVEL*10-4*SQRT(1-(B/R13)**2)
```

```
    P1D=EXP(-H12*EXP(2*(R13-R13D))/VR1)
    P1DD=EXP(-H12*EXP(2*(R23-R23D))/VR1)
    P1=EXP(-H12/VR1)
    VR2=1E-4*RELVEL*SQRT(1-B*B/(R23D*R23D))
    P2D=EXP(-H23*EXP(R23-R23D)/VR2)
    P2=EXP(-H23/VR2)
    L1:
    %IF PATH=2 %THEN %RESULT=(1-P1D)*(1-P1)
    %IF PATH=1 %THEN %RESULT=P1*P1
    %IF PATH=3 %THEN %RESULT=P1*(1-P1)*(1-P2D)
    %IF PATH=4 %THEN %RESULT=(1-P1)*P1DD*(1-P2D)
    %END
%REALFN DEFTON(%REAL B)
    %REAL X,Y,Z
    !   THIS FUNCTION EVALUATES THE CONTRIBUTION TO THE DEFLECTION
    !   FUNCTION FROM THE IONIC K+/CH3I- CURVE
    X=IRP*EPS3*SIG3**IRP*SP*(GA10/GA11)
    X=X/(2*PIKE*B**IRP)
    Y=-POL*SP**4*(GA5/GA6)/(2*PIKE*B**4)
    Z=-14.394*SP*(GA7/GA8)/(2*PIKE*B)
    %RESULT=X+Y+Z
    %END
%REALFN MORSION(%REALNAME R)
    %RESULT=(DION*EXP(-BETAION*(R-ROCH1))+EDUP*(TANH(CBETA*(1E10*R-ROE
    -TANH(CBETA*(1E10*R-ROFF)))+AL1)/1.60218E-19
    %END
%REALFN MORSPOT(%REALNAME R,AL)
    %REAL V,R1
    R1=R
    !
    !   SI UNITS
    !
    V=DCH*(EXP(-2*BETA*(R1-ROCH))-2*EXP(-BETA*(R1-ROCH)))
    %RESULT=(V+AL)/1.6021E-19
    %END
%ROUTINE OUTPUT(%REALNAME B,DFP,EL,SIGMA,RCH,%INTEGER PATH)
    %REAL DFPD
    SELECTOUTPUT(10)
    WRITE(PATH,2)
    SPACE
    PRINT(B,5,3)
    SPACE
    DFPD=DFP*180/PI
    PRINT(PIKE*DFPD,4,2)
    SCSI=INTPT(PIKE*DFPD+0.5)
    SPACE
    PRINT(EL,3,2)
    SPACE
    PRINTFL(SIGMA*DFP*DFP,2)
    %IF SCSI<1000 %AND SCSI>=1 %THEN %START
    SCS(SCSI)=SCS(SCSI)+SIGMA*DFP*DFP
    %FINISH
    SPACE
    PRINT(RCH*1E10,5,3)
    SPACE
    PRINTFL(RCDUM,3)
    NEWLINE
    SELECTOUTPUT(0)
    %END
%ROUTINE READFILENAME(%STRINGNAME NAME)
    %INTEGER I
    NAME = ""
    SKIP SYMBOL %WHILE NEXT SYMBOL = "" %OR NEXT SYMBOL = " "
    %OR NEXT SYMBOL = /
    %CYCLE
```

```
            READSYMBOL(I)
            NAME = NAME.TO STRING(I)
            %EXIT %IF NEXT SYMBOL = NL %OR NEXT SYMBOL = "."
            %REPEAT
            SKIP SYMBOL %WHILE NEXT SYMBOL # NL
            SKIP SYMBOL
            %END  ;! READ FILE NAME
        %ENDOFPROGRAM

LINES ANALYSED IN  5694 MSECS  -  SIZE= 36206
```

PUBLICATIONS

67/2

Electronic Excitation in Potentially Reactive Atom–Molecule Collisions

By Malcolm A. D. Fluendy, Kenneth P. Lawley, John McCall, Charlotte Sholeen and David Sutton

Department of Chemistry, University of Edinburgh, Edinburgh EH9 3JJ

Received 11*th December*, 1978

Inelastic differential scattering cross sections for the system potassium + alkyl halide have been measured in the small angle region for $E\chi$ between 20-1000 eV°. Electronic excitation of both collision partners is seen together with vibrational excitation of the alkyl halide.

Evidence is adduced suggesting that excitation occurs by either of two paths corresponding to the preliminary transfer of an electron in the entrance channel or as the colliding pair recedes. A harpooning model incorporating bond stretching in the negative molecular ion is developed that agrees well with most of the observations.

A large number of exit channels are open in the collision system alkali atom + alkyl halide at higher energies. They include:

$M + RX \rightarrow M + RX(RX^{\dagger})$	elastic (inelastic)	(i)
$\rightarrow MX + R$	reaction	(ii)
$\rightarrow M^{+} + RX^{-}$	chemi-ionisation	(iii)
$\rightarrow M^{*} + RX$ $\quad M + RX^{*}$	electronic excitation	(iv)
$\rightarrow M + R + X$	dissociation.	(v)

The first two processes have been extensively investigated at thermal collision energies [1,2] and are well known examples of the electronic harpooning mechanism, subsequent chemical reaction occurring at thermal energies by ionic combination.

The chemi-ionisation channel is less well explored [3] but provides direct evidence for non-adiabatic behaviour at the ionic/covalent surface crossing. The importance of an ionic surface in coupling ground and excited electronic states of the atom is confirmed by collision-induced fluorescence studies.[4]

In the work described here continuing the programme outlined in a previous Faraday Discussion,[5] we have eliminated the reaction channel by working at high relative kinetic energies and choosing a heavy halogen atom, iodine. Equally important from the point of view of analysis, by confining scattering observations to very small angles ($\lesssim 5°$) the K atom trajectories are essentially rectilinear and of constant velocity. Nevertheless, because the forward momentum is high, interesting regions of the potential inside the harpooning radius can be probed by these small deflections. Electronic excitation of several eV is readily observed.

EXPERIMENTAL

APPARATUS

The apparatus used in this work is shown schematically in fig. 1. The beam of fast alkali atoms was produced initially as ions by surface ionization and electrostatic focusing. The ion beam was then pulse modulated, using a velocity compression technique described elsewhere,[6] so that the energy loss resulting from a collision could be recorded by measurement of the flight time of the scattered atom and hence the post-collision states of the atom and molecule inferred. After modulation the ion beam was neutralised in a vapour cell and any remaining ions deflected away.

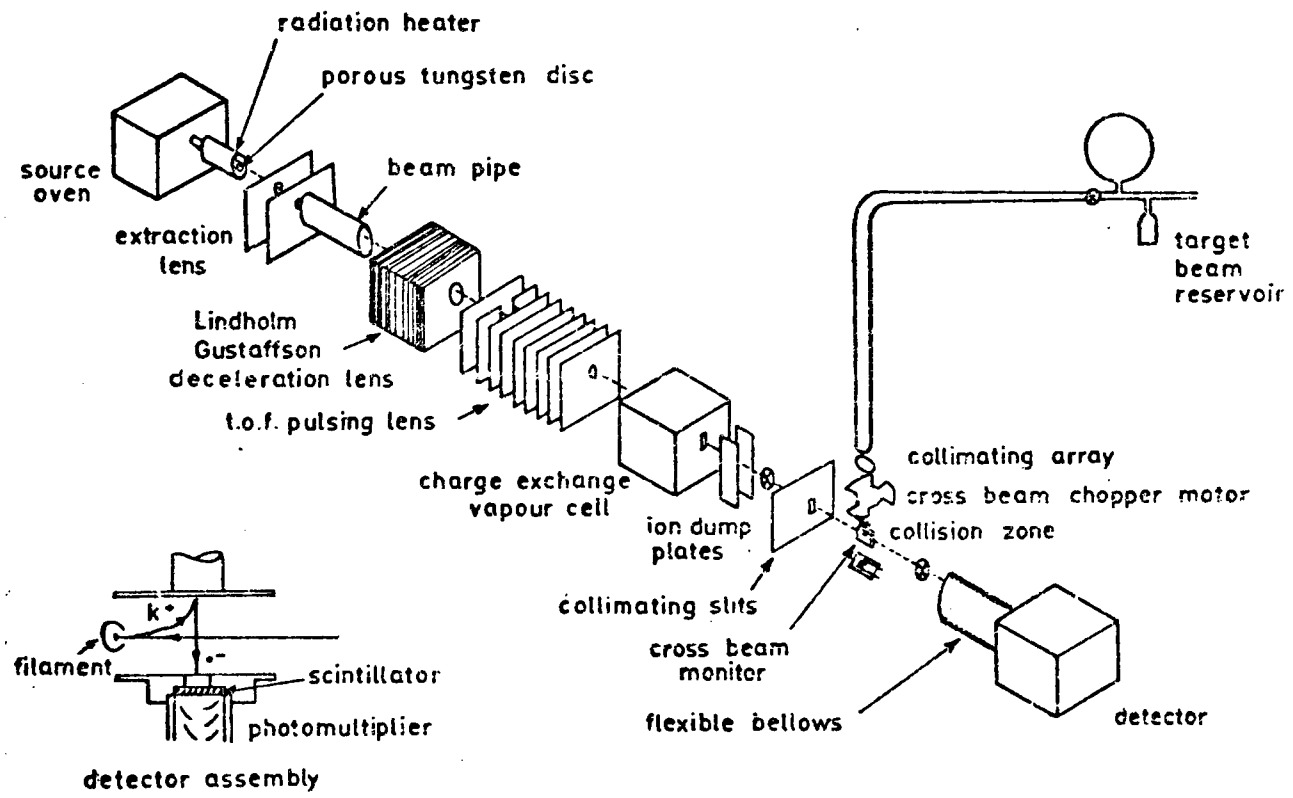

FIG. 1.—Schematic representation of apparatus.

The fast neutral beam then intercepted a slow target beam of molecules formed by effusion from a capillary array in a well defined collision zone. This beam was also modulated (at 47 Hz) and the target flux continuously monitored by a gauge placed directly below the collision zone.

Potassium atoms scattered from this region were ionized on a cool W wire and detected *via* a scintillator and photomultiplier. The detector could be varied in angle with a precision of $\pm 0.002°$. Atom arrivals located in angle by the detector position were arranged to stop a 50 MHz clock running in synchronism with the pulse modulation so that the flight time could be recorded.

The collection of data and the operation of the experiment were controlled by an on-line computer.[7] The signal collection and experimental control arrangement are shown schematically in fig. 2. Hard copy log and graphical output facilities were provided to allow operator intervention.

DATA COLLECTION AND ANALYSIS

Count rates are very low in this experiment (<0.01 counts s^{-1}) and periods of ≈ 12 h were required to collect sufficient counts at the widest angles. Data collection thus took place over periods of about five days. During this time the main beam arrival time profile was checked at intervals under program control and data collection suspended and the operator

M. A. D. FLUENDY, K. P. LAWLEY, J. MCCALL, C. HOLEEN AND D. SUTTON 111

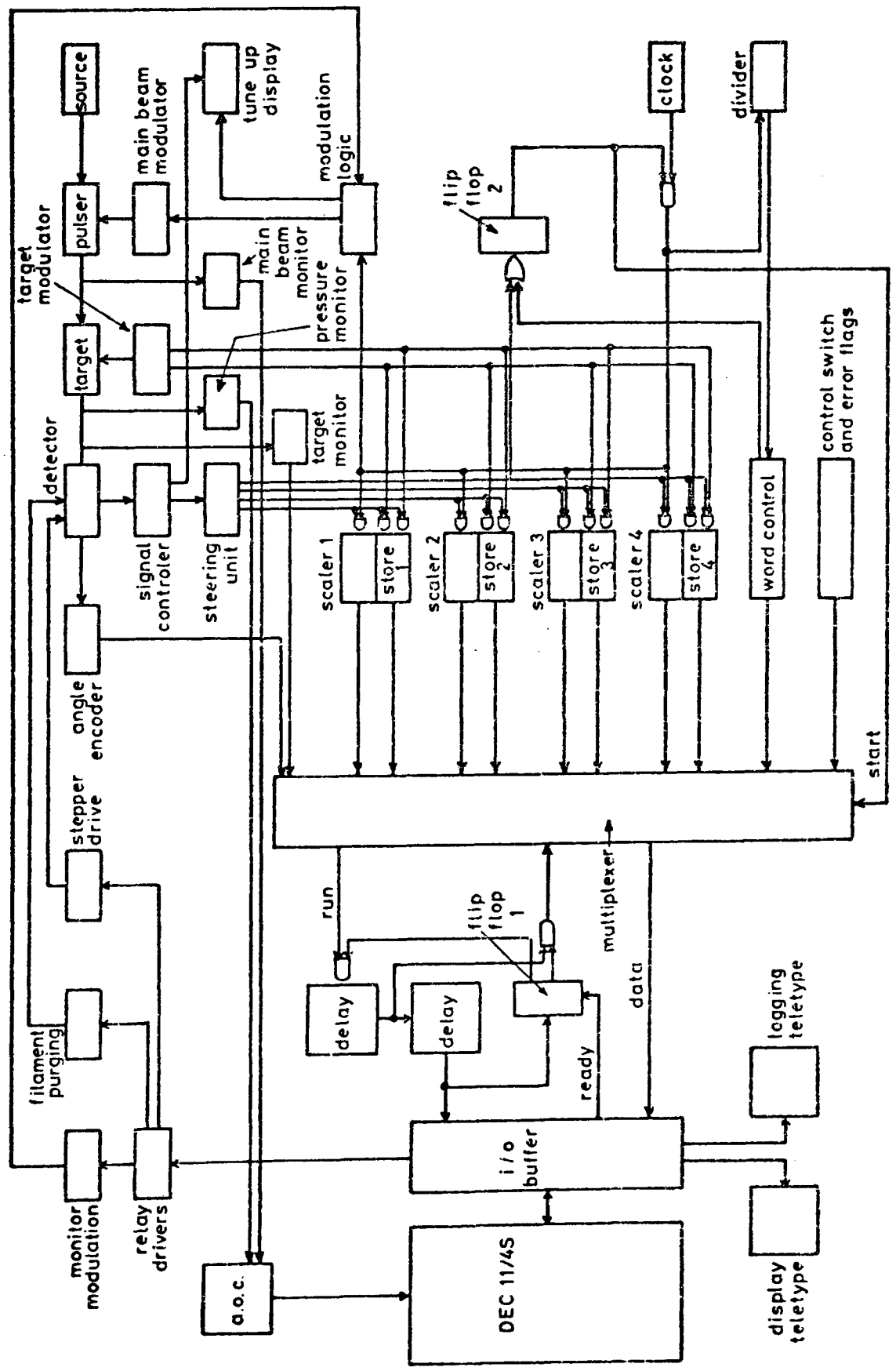

FIG. 2.—Schematic representation of data collection.

alerted if any significant changes in the beam fluxes or other operating conditions took place. The angular scan was made automatically to a predetermined sequence, angle changes being initiated automatically when a set precision had been reached.

The data reported in this paper were accumulated over a period of about eighteen months during which time the equipment was removed from one building to another and a number of small changes made. Partly as a result the time location of the primary beam pulse varied by as much as 30 ns between different experiments. The data were therefore adjusted in time so as to be relative to the unscattered beam arrival as measured in each experiment. Any accompanying variation in the pulse width was corrected by a process of deconvolution and reconvolution to a standard pulse width, the stability of these operations being checked by trials with synthesised noisy data. Inconsistencies of this type between different experimental runs rather than counting statistics account for most of the noise seen in the results.

After these adjustments had been made in the laboratory frame the data were transformed into the c.m. frame using the most probable laboratory velocities.

RESULTS

These results are most compactly presented as c.m. contour maps showing the variation in the product of the scattered intensity and the square of the scattering angle, $I(\chi)\chi^2$, as a function of the variable $\tau(\tau =$ collision energy $\times$ scattering angle, $E\chi)$ and the post-collision velocity.

The contour map in fig. 3 shows such a plot for K + Ar and illustrates the energy

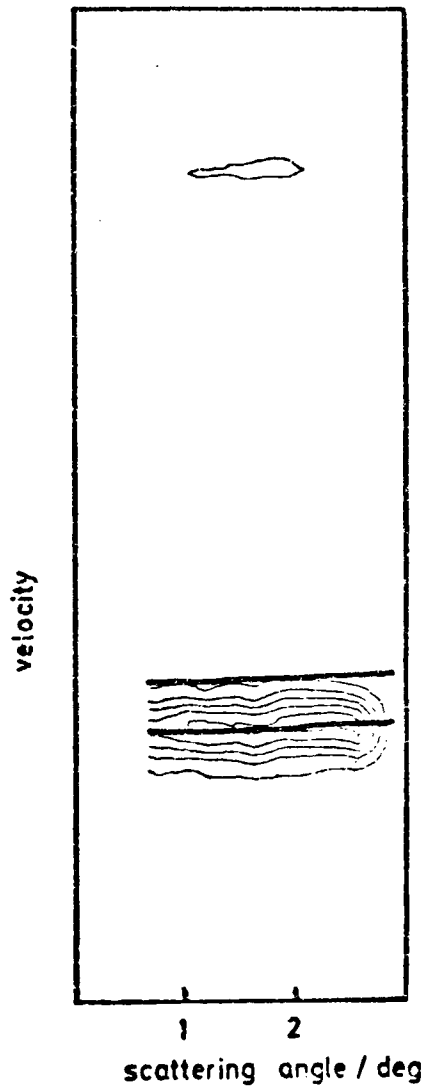

FIG. 3.—K + Ar scattering at 108 eV c.m. collision energy. The thick lines indicate energy losses of 0.0 and 1.6 eV (centre of mass frame).

resolution since in this E region the scattering is at least 98 % elastic. The island of intensity at slow exit velocities is due to the K^{41} isotope present at ≈6 % abundance. The other contour maps in fig. 4-6 show similar plots for methyl and propyl iodide at various initial collision energies. In comparison with the K + Ar data considerable inelasticity, particularly at the wider angles, is immediately apparent and can be seen to onset at specific $E\chi$.

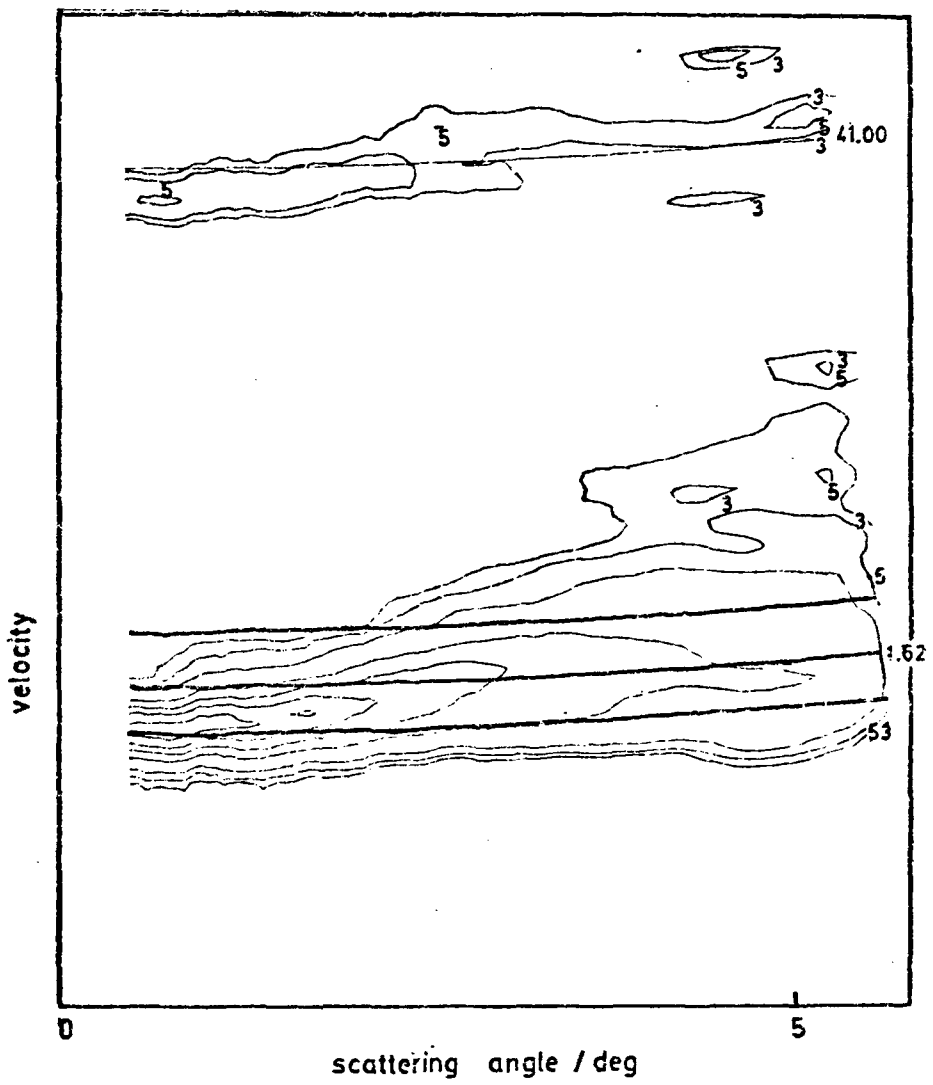

FIG. 4.—K + CH_3I scattering at 164 eV collision energy. The thick lines indicate energy losses of 0.0 1.6 and 3.47 eV (centre of mass frame).

Cuts through the surface show the intensity of scattered K atoms as a function of the energy lost by them in collision are perhaps more suggestive. A number of examples computed by averaging together several sets of independent observations in a narrow range of angle are shown in fig. 7 and 8. The solid curves on these figures show the results of a deconvolution procedure using the 0° profile as a reference profile. The peaks are sharpened by this process but can already be distinguished in the unprocessed data; moreover, independent angular scans yield peaks which move smoothly with angle as in fig. 9-11. The enhanced scattering profiles prepared in this way are combined to yield similarly sharpened contour maps as shown in fig. 12 and 13.

Time of flight data of this type are of limited value in molecular systems because it is not possible to associate a given velocity change in the K atom with a specific exit channel, owing to the number of closely spaced energy states. Thus, in the K + RI system the K ionisation continuum starts at 4.34 eV and there is a near con-

tinuum of vibration–rotation states in each electronic level of RI. Table 1 summarises the relevant information for K and CH_3I (C_3H_7I is similar).

In view of this continuum of vibronic levels, it is remarkable that discrete energy losses are observed at least up to 10 eV at the largest angles of scattering.

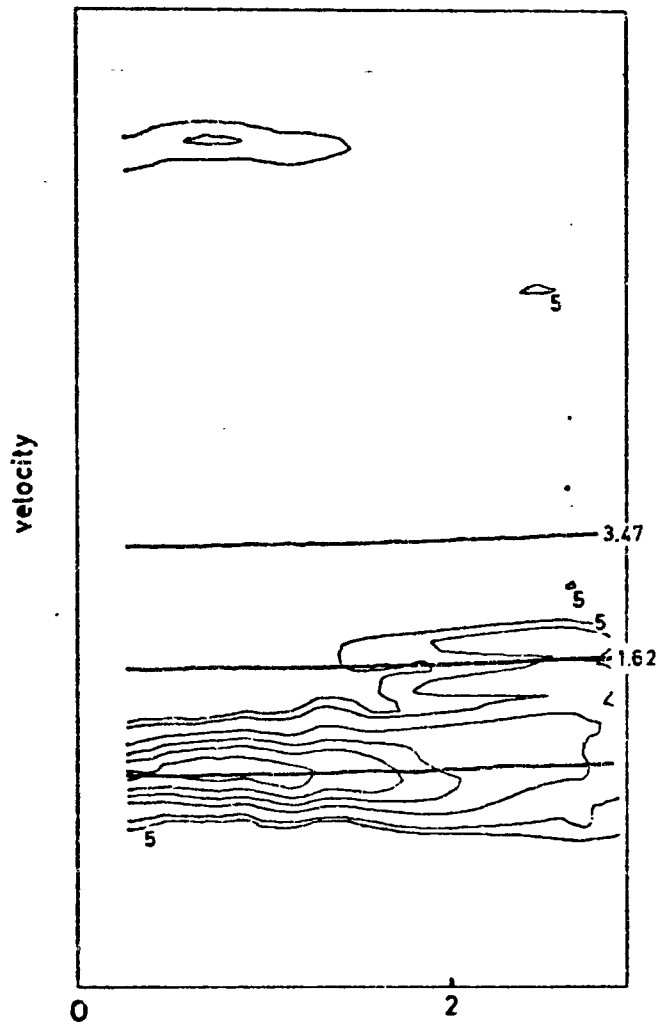

FIG. 5.—K + CH_3I scattering at 81 eV collision. The thick lines indicate energy losses of 0.0, 1.6 and 3.47 eV (centre of mass frame).

DISCUSSION

At scattering angles $\chi \lesssim 5°$, the momentum transfer perpendicular to the incident velocity is small (χ = final transverse momentum/incident forward momentum).

The various small-angle approximations are valid and the momentum changes in the forward direction cancel on the incoming and outgoing halves of the trajectory. Under these conditions the maximum energy transferable to vibration/rotation of the molecular partner is

$$\Delta E = \left(\frac{M_R M_I}{M_R + M_I}\right)\left(\frac{M_K}{M_X^2}\right) E_l \chi^2 \qquad (1)$$

where X = I or R, the end struck, and a " forceless " oscillator has been assumed. The maximum energy thus transferred at the angles of observation will be <0.5 eV, far smaller than most of the observed energy loss channels. The extensive vibronic energy transfer that is observed can only occur if the potential energy surfaces are

profoundly modified in the course of the collision. The source of this alteration is clearly the crossing onto the ionic state.

The harpoon model, equivalent to adiabatic behaviour at the ionic/covalent crossing, is well established as the mechanism for chemical reaction in many alkali metal systems at thermal energies. At the collision energies of the present experiments the reactive channel is essentially closed because the fast K^+ ion cannot accelerate the

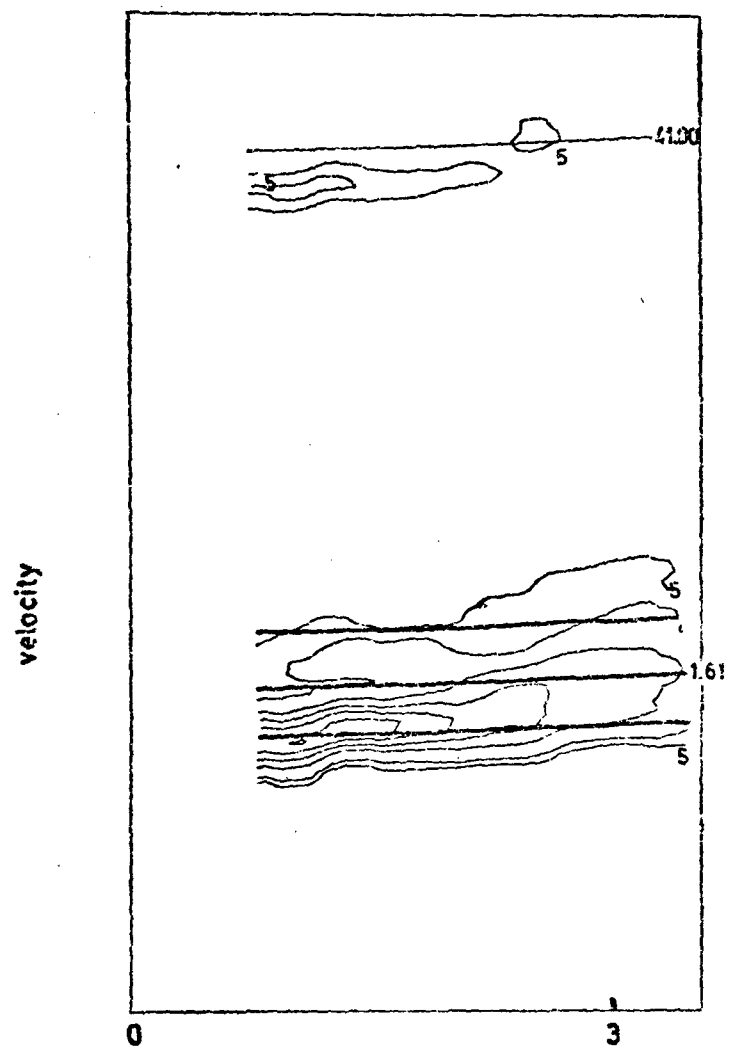

FIG. 6.—K + C_3H_7I scattering at 166 eV collision. The thick lines indicate energy losses of 0.0, 1.6 and 3.47 eV (centre of mass frame).

I^- ion sufficiently rapidly to capture it before leaving the ionic surface. The residual electronic excitation is like the grin on the face of the Cheshire Cat, the aftermath of a much more profound electronic rearrangement.

We develop a model to account for the broad features of the observed scattering in two stages. As a first approximation, the collision is assumed to be isotropic and sudden with respect to the R–I motion, *i.e.*, the R–I bond is clamped at its equilibrium value throughout the collision. The behaviour of the various diabatic potential surfaces can then be displayed solely as a function of the K–I coordinate, fig. 14(*a*). The vertical electron affinity of the alkyl iodides is sufficiently small (−0.9 eV) for the ionic state to intersect all the K* channels (including the ionised continuum) and thus to provide a route for populating these states. Excited electronic states of RI, except the *A* state, lie above the dissociation limit of K^+RI^- (5 eV) and must then be populated

by a different mechanism. We speculate that an excited charge transfer state is involved but the mechanism will not be discussed here.

The only important adjustable parameter in these potentials is the short range repulsion behaviour of the ionic state and the coupling matrix elements at the various crossings. Whatever the values of the parameters, some simple consequences arise because any exit channel can be reached *via* two paths, according to whether or not the electron is transferred on the first passage of the ionic/covalent crossing.

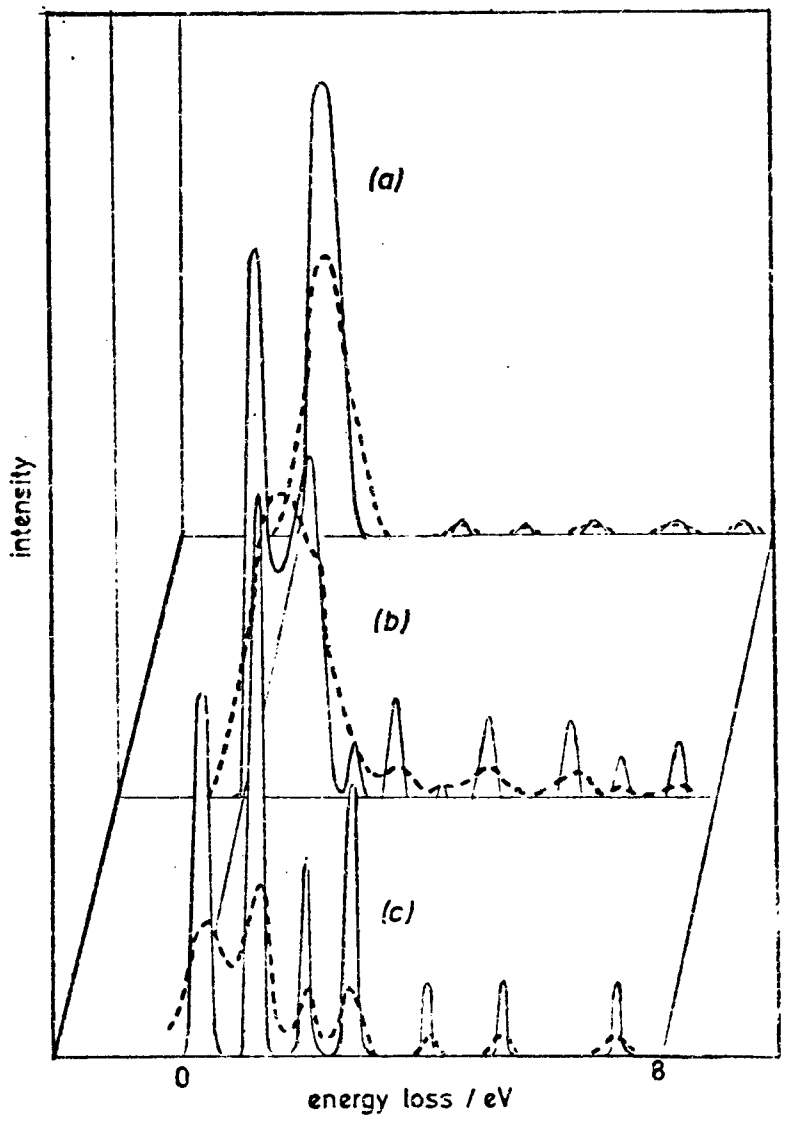

FIG. 7.—Energy loss profiles observed at various scattering angles for K + CH_3I at 81 eV collision energy. The dashed curves are observed values and the solid lines their deconvolution. (*a*) 61, (*b*) 122 and 203 eV°.

The predictions of this model (using the potentials shown, the Landau–Zener approximation and the classical small-angle formúlae to evaluate the cross sections) are compared with experiment at 164 eV in fig. 15, the energy loss data being partitioned in accord with the asymptotic energy losses assuming only electronic excitation.

The model is partially successful, especially in predicting the narrow angle thresholds of K* and CH_3I^* (*A*) state onsets. If the route to these states involved a crossing on the respulsive wall of the potential, the angular threshold would appear at much larger angles and the intervention of a strongly attractive surface is unambiguous.

The model is less satisfactory in predicting the change in angular onsets of the various channels with incident energy. These thresholds are seen to occur at lower E values in the 81 eV data, whereas the basic model necessarily predicts constant $E\chi$ values (assuming straight line trajectories). More important differences are seen in

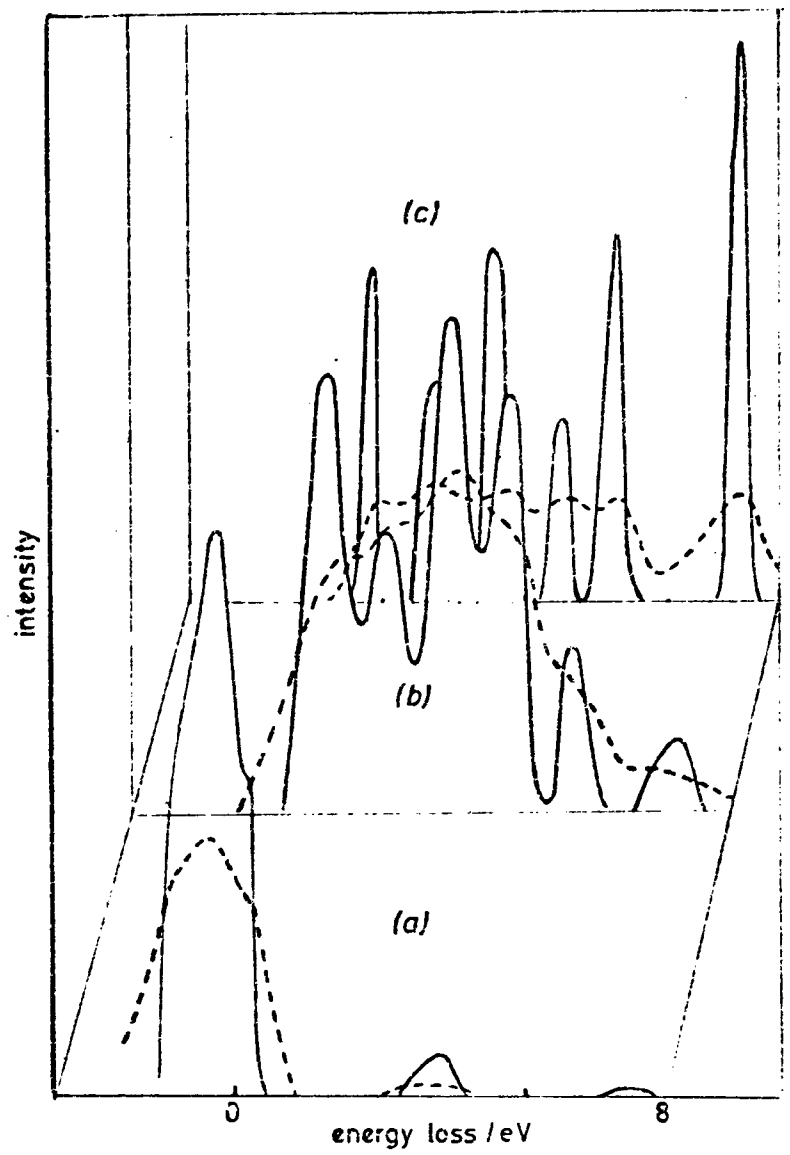

FIG. 8.—Energy loss profiles observed at various scattering angles for K + CH_3I at 164 eV collision energy. The dashed curves are observed values and the solid line their deconvolution. (*a*) 75, (*b*) 450 and (*c*) 900 eV°.

the energy loss spectrum where the model only permits energy losses corresponding to the electronic states of the separated species. The observations (*e.g.*, fig. 7 and 8) show a much larger number of discrete energy loss processes, some of them (those <1.6 eV) not being assignable at all to electronic excitation. The most serious assumption of the basic model lies in the neglect of the internal motion of the target molecule. During the collision lifetime, typically 10^{-14} s, changes in the C–I bond distance can occur which greatly alter the vertical electron affinity and hence the position of the ionic/covalent crossing. Such effects have been discussed by other workers[8] in connection with chemical reaction and chemi-ionisation. The initial crossing at R_1 yields CH_3I^- in a strongly repulsive state [fig. 14(*b*)], assuming a vertical transition. As the C–I bond stretches on the ionic surface, the ionic/covalent crossing moves to larger R values (fig. 16) and on the return of the electron a large amount of energy can be dumped in the Me–I vibration. The extent of such energy transfer clearly depends on the time spent on the ionic surface and ranges from zero if the motion at R_1 is diabatic (electron not transferred) to actual dissociation of the Me–I bond if the MeI^- surface is sufficiently repulsive. Since there are in general two classical paths leading to a particular angle of deflection (if $b < R_1$), corresponding to diabatic or adiabatic motion at R_1, each electronic exit channel should be accompanied by two distinct peaks in the time of arrival spectrum.

Our second model, then, is to permit relaxation of the C–I bond in the ionic state by introducing a term

$$V^{\text{ion}}(R_{\text{R–I}}) = A \exp\left[-\alpha(R_{\text{RI}} - R_{\text{RI}}^{(0)})\right] \qquad (2)$$

into the total potential energy. The I–K interaction remains coulombic and there is no K–R interaction. One result emerges immediately from this model. If the parameters in $V^{\text{ion}}(R_{\text{RI}})$ are taken to be those of the isolated ion,[9] far too much vibrational excitation is predicted even in the ground electronic exit state. In fact, we would have a runaway situation with extensive bond dissociation (and probably chemi-ionisation). In practice (fig. 9-11) the vibrational energy gain in both the ionic K and K* channels is quite small ($\approx$1 eV) and almost constant with $E\chi$ after the threshold.

The CH_3I^- ion is thus perturbed by the passing K^+ ion and we can very crudely incorporate this effect in the model by making α adjustable. However, even this degree of freedom is not sufficient for the data to be fitted; if the vibrational energy gain in the K* (ionic) channel is fitted, too little energy loss occurs in the ground state channel. In qualitative terms, the initial acceleration of the methyl group after

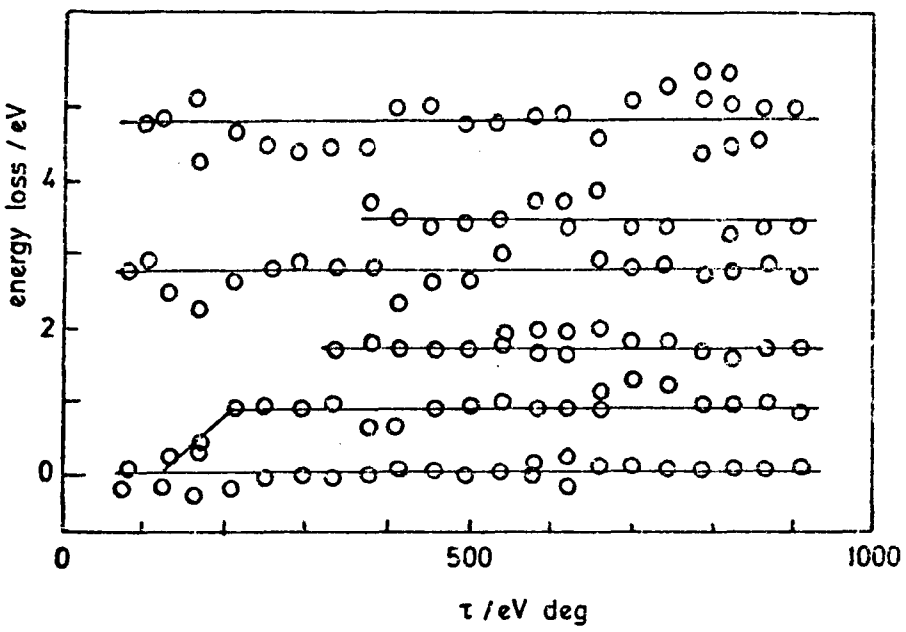

FIG. 9.—Plot showing the location of the peaks observed in the energy loss measurements as a function of the reduced scattering angle, τ. CH_3I + K 164 eV collision energy.

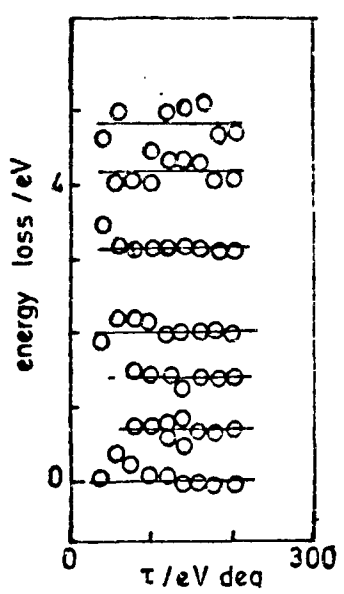

FIG. 10.—Plot showing the location of peaks observed in the energy loss measurements. CH_3I + K at 81 eV collision energy.

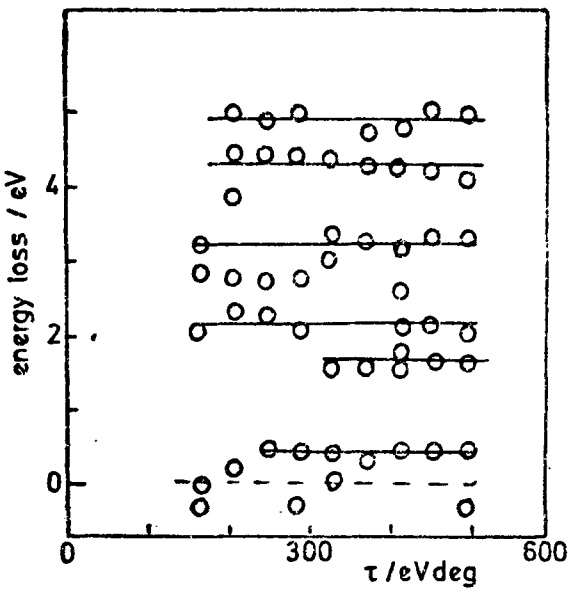

FIG. 11.—Plot showing the location of peaks observed in the energy loss measurements. C_3H_7I + K at 166 eV collision energy.

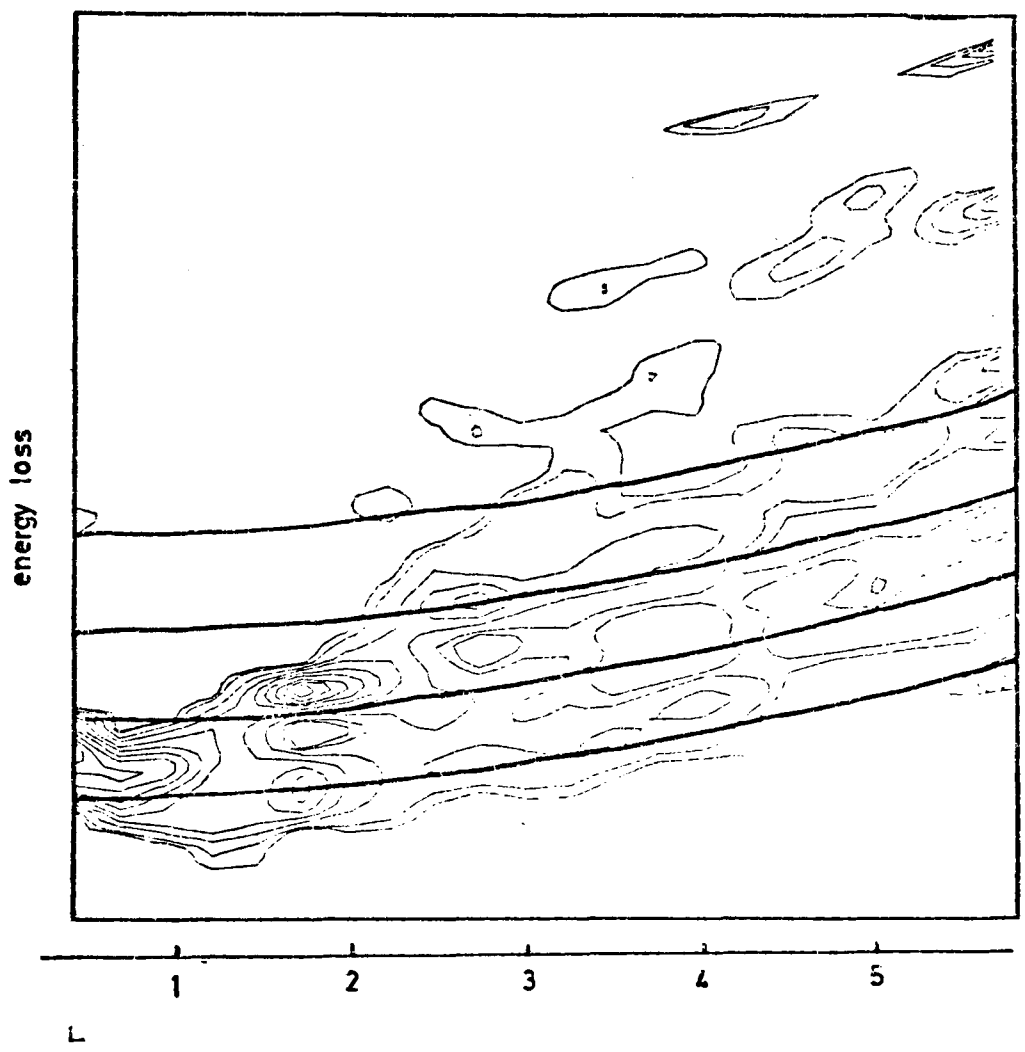

FIG. 12.—Contour plot showing CH_3I + K scattering as a function of energy loss and c.m. scattering angle at a collision energy of 164 eV and after enhancement by deconvolution. Thick lines are drawn at energy losses of 0.0, 0.86, 1.6 and 2.8 eV.

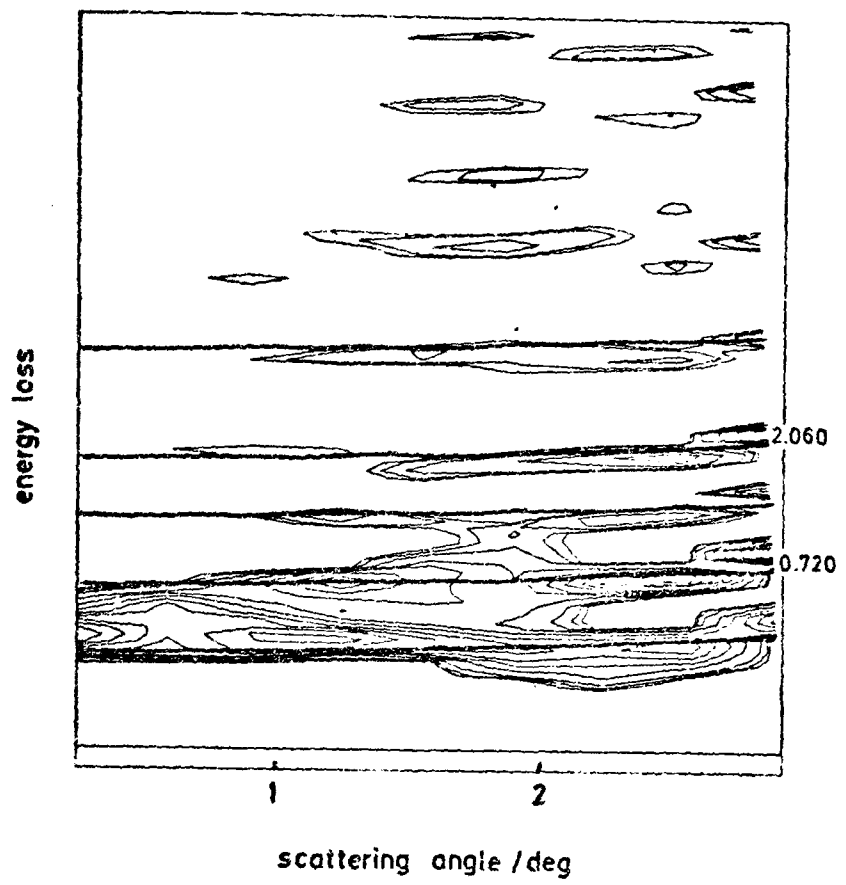

FIG. 13.—Contour plot showing CH_3I + K scattering as a function of energy loss and scattering angle at a collision energy of 81 eV and after enhancement by deconvolution. Thick lines are drawn at energy losses of 0.0, 0.72, 1.4, 2.0 and 3.2 eV.

electron transfer seems to be rapid, but the repulsion soon drops almost to zero. The functional form of eqn (2) must be wrong and the dependence of V^{ion} on R_{MeK} should be introduced. This could be interpreted as due to the repulsion of the departing Me group by the K^+ ion, or the change in bond order of MeI^- due to partial back transfer of the electron to K^+.

Nevertheless, relaxation of the Me–I bond on the ionic surface is a key step in the collision process. Besides leading to extensive vibrational excitation, the deflection of trajectories sampling the ionic surface will depend on the extent of R–I relaxation during the collision. The angular thresholds for all electronic processes fed by the ionic surface will not thus scale with $E\chi$, and will also depend upon the reduced mass of RI. These effects can be seen in fig. 17 where the energy losses calculated from this

TABLE 1

K state	energy	CH_3I	energy/eV
$4^2S_{\frac{1}{2}}$	0.0	$X(^1A_1)$	0.0
$4^2P_{\frac{1}{2},\frac{3}{2}}$	1.62	A^*	3.47*
$5^2S_{\frac{1}{2}}$	2.61	B, $C(E)$	6.10, 6.16
$3^2D_{\frac{3}{2},\frac{5}{2}}$	2.67	D, (E)	6.77
$5^2P_{\frac{1}{2},\frac{3}{2}}$	3.06	E,	7.30
Rydberg states		F, G	9.4, 9.8
I.P.	4.34	Rydberg states	
		I.P.	9.54

* Onset of continuous adsorption; peak at 4.5 eV.

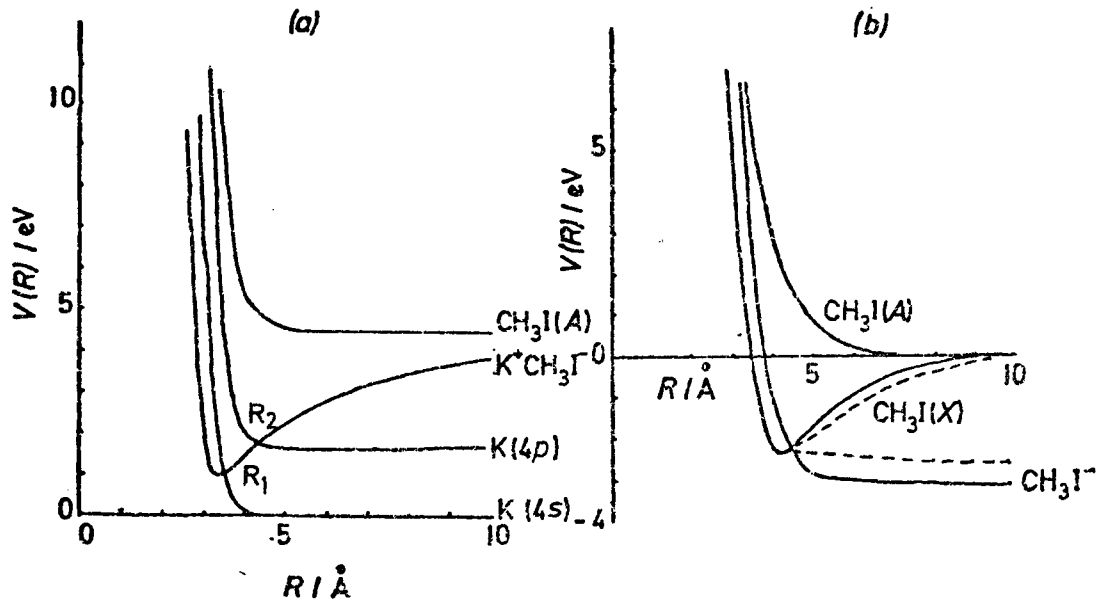

FIG. 14.—(*a*) Isotropic diabatic potential model for K + RI interaction. (*b*) CN_3I and CN_3I^* potentials. Dashed curves show the perturbation used to obtain the approximate fit described.

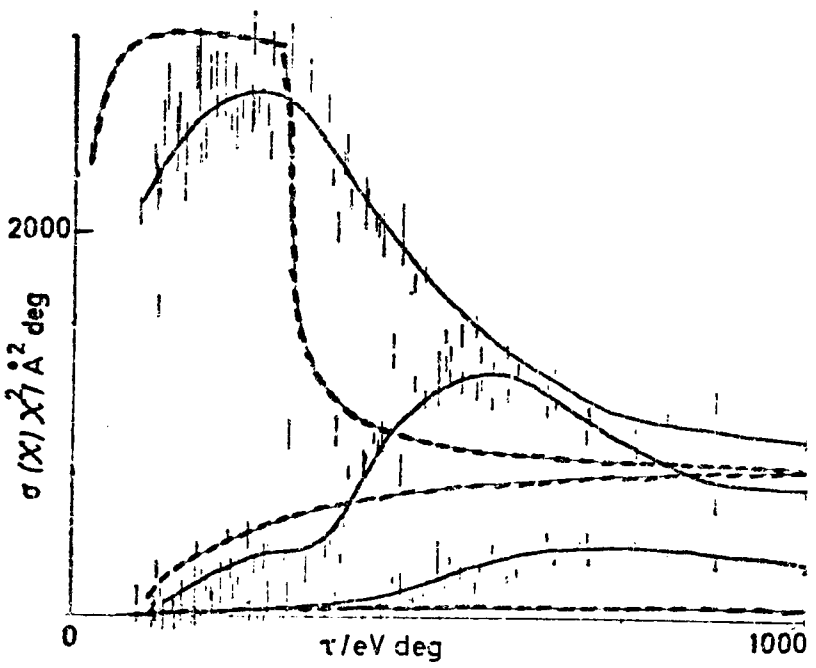

FIG. 15.—Isotropic sudden model; comparison with observations for CH_3I + K at 164 eV.

model are displayed against the corresponding scattering angle. In the $E\chi$ region around 150 eV[6], particularly at 81 eV collision energy, a rainbow feature can be seen where two branches for the ionic ground state scattering coalesce.

The invariance of vibrational excitation with angle of scattering is a remarkable feature of all the plots and again points to relatively small shift of the ionic/covalent seam with changing transit time over the surface.

Finally, the differential cross sections for the channels identified are displayed, together with the model predictions, in fig. 18 and 19.

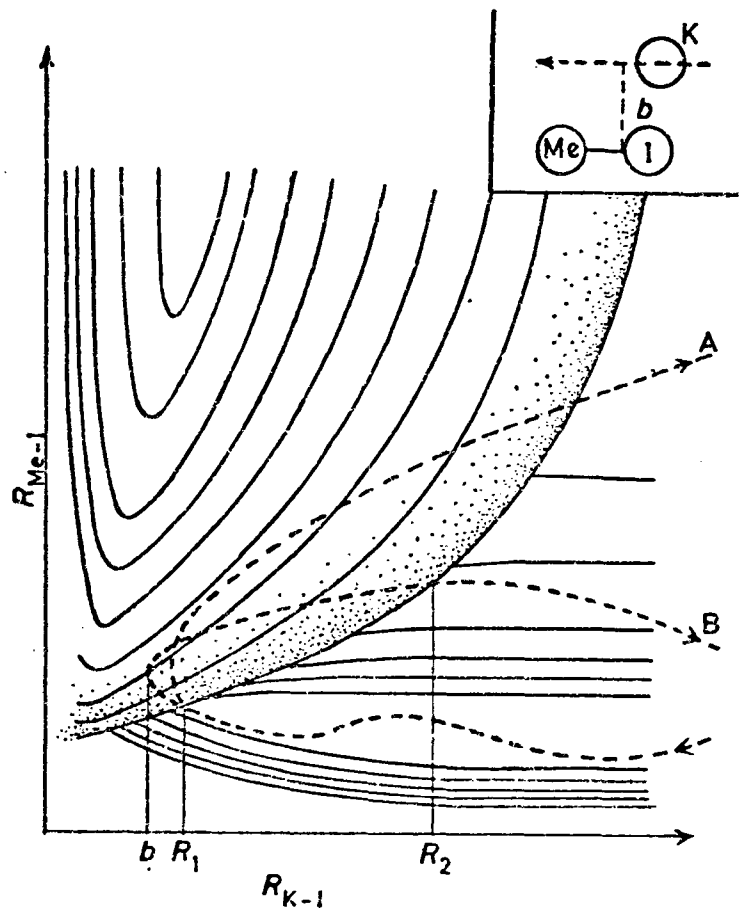

FIG. 16.—High energy trajectories on an ionic/covalent surface. Two trajectories are shown, corresponding to different initial kinetic energies ($E_A > E_B$). The crossing point on the outward path (R_2) is very sensitive to E. In case B, R_2 is so large that dissociation or ionisation would result. The K trajectory in real space is inset.

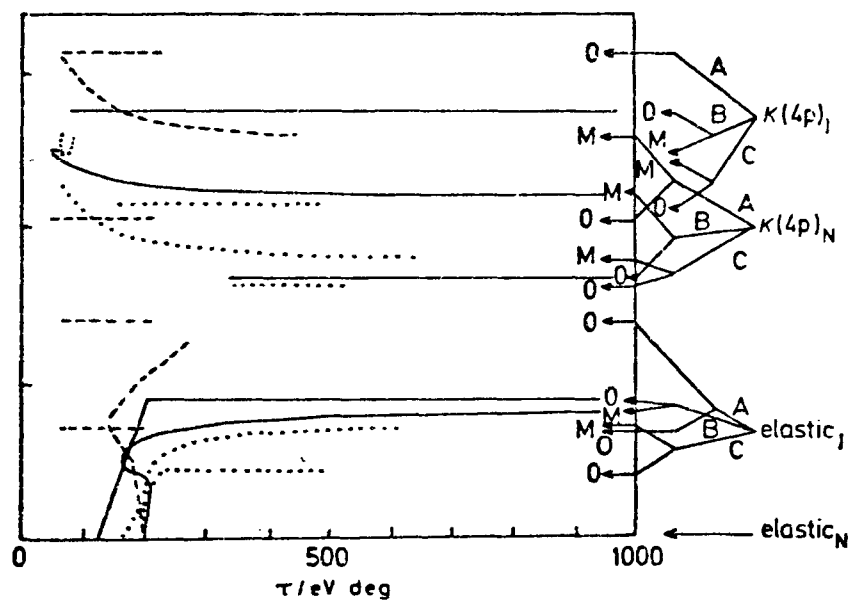

FIG. 17.—Comparison of observed (O) and bond stretching model predictions(M) for the energy loss as a function of reduced scattering angle. The subscript I indicates motion on the neutral surface. Model and experiment are in accord in predicting an increasing energy loss as the mass of R decreases and as the collision lifetime increases.

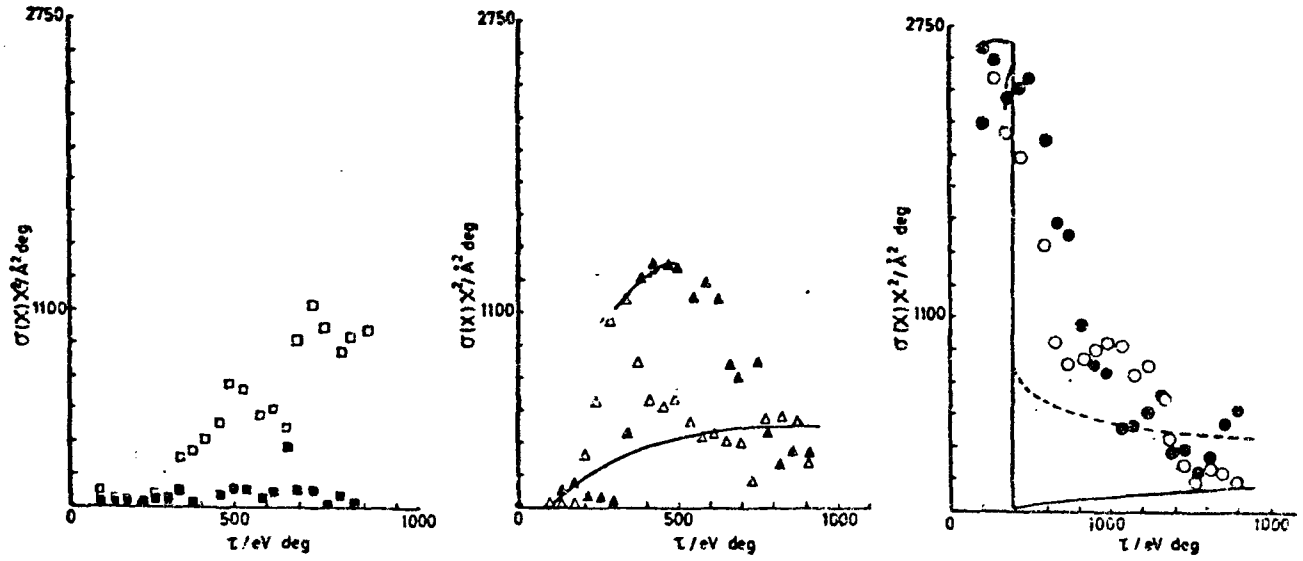

FIG. 18.—Differential cross sections for K + CH_3I at 164 eV. (○, ●) ground state N, I, (△, ▲) K* (4*p*) N, I. □, ▩ CH_3I^* (*A*) N, I. Lines are the model fit (——) N and (- - - -) I.

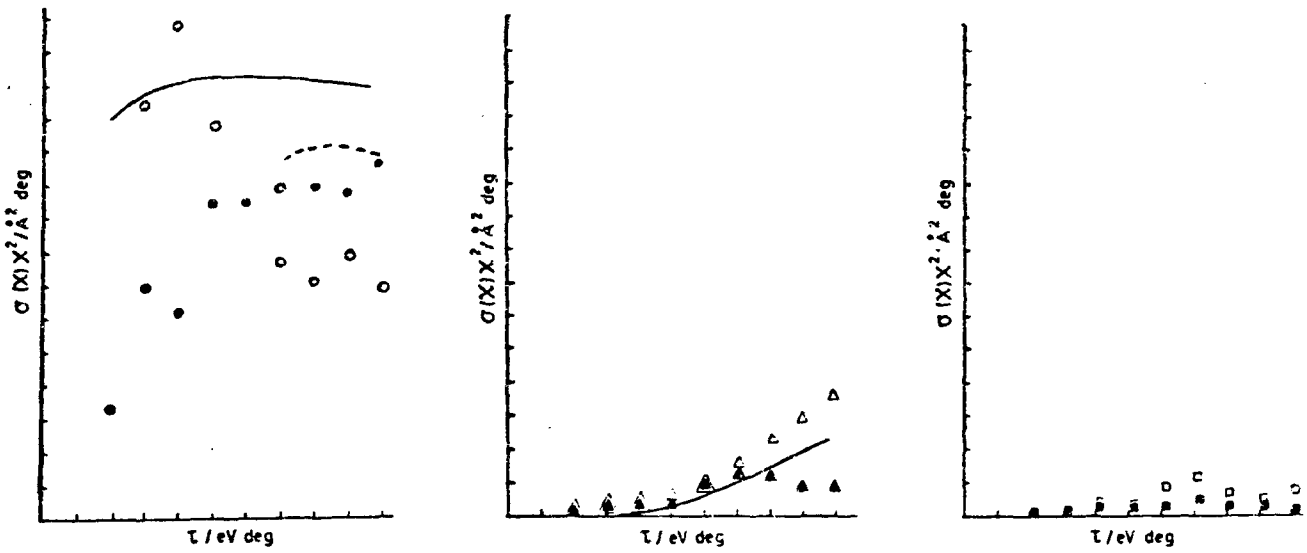

FIG. 19.—As for fig. 18, but at 81 eV.

CONCLUSIONS

Our conclusions as to the processes involved may be summarised with reference to fig. 14(*a*) as follows:

(*a*) Each electronic exit channel is accompanied by two vibrational channels, one with small or zero internal energy change, the other with substantial vibrational excitation. These two channels correspond to, respectively, diabatic or adiabatic (harpooning) behaviour at the first crossing R_1. Both channels are important in the experimental energy range.

(*b*) The negative ion state involved is a repulsive state, but with rather different characteristics from the isolated RI^- ion. In particular, the amount of bond stretching is less than expected (at least in the configuration probed in the bound state exit channels) and points to some containment of the alkyl group.

(*c*) The differential cross section summed over all discrete exit channels (ground plus excited states) is approximately constant over the χ range from 0.5 to 5° (LAB). This strongly suggests that continuum processes (bond dissociation and ionisation), unless they onset at very small angles of deflection, play a negligible role at impact parameters $\lesssim \sigma_{<J}$.

(*d*) The excitation of the *A* state of CH_3I is observed to have two energy loss contributions and angular thresholds, but these have less intensity than in the K* channel. An ionic surface again probably intervenes because of the small angular thresholds. But even without bond stretching, the ground state $K^+CH_3I^-$ surface would lead to a crossing at ≈ 50 Å on the outward branch, at which point the coupling matrix element between the two states would be essentially zero. Some electronic excitation of the negative ion may be involved, *i.e.*, harpooning to a different empty orbital.

(*e*) Discrete energy losses >5 eV are observed and these must correspond to electronic excitation of the alkyl iodide. Since these energy levels are above the energy of the separated K^+RI^- ion pair, the ground state ionic surface cannot be involved in their coupling.

[1] J. L. Kinsey, *Molecular Beam Reactions* (M.T.P. Int. Rev. Sci., Physical Chemistry, 1972 ser. 1, vol. 9.
[2] M. E. Gersh and R. B. Bernstein, *J. Chem. Phys.*, 1972, **56**, 6131.
[3] A. P. M. Baede, *Charge Transfer between Neutrals at Hyperthermal Energies, Adv. Chem. Phys.*, 1975, **30**.
[4] V. Kempter, *Electronic Excitation in Collisions between Neutrals, Adv. Chem. Phys.*, 1975, **30**.
[5] M. A. D. Fluendy, K. P. Lawley, J. M. McCall and C. Sholeen, *Faraday Disc. Chem. Soc.*, 1977, **62**, 149.
[6] J. M. McCall and M. A. D. Fluendy, *J. Phys. E*, 1978, **11**, 631.
[7] M. A. D. Fluendy, J. H. Kerr, J. M. McCall and D. Munro, *On-line Computing in the Laboratory*, ed. R. A. Rosner, B. K. Penney and P. N. Clout (Advance, London, 1975).
[8] J. A. Aten, G. A. H. Lanting and J. Los, *Chem. Phys.*, 1977, **19**, 241.
[9] W. E. Wentworth, R. George and H. Keith, *J. Chem. Phys.*, 1969, **51**, 1791.

ELECTRONIC EXCITATION IN POTASSIUM ALKYL IODIDE COLLISIONS

F. CASTANO ‡, M.A.D. FLUENDY, K.P. LAWLEY, C. SHOLEEN ‡ and D. SUTTON
Department of Chemistry, University of Edinburgh, Edinburgh EH9 3JJ, UK

Received 23 April 1979; in final form 7 June 1979

The production of highly excited states of the alkyl iodides by collision with fast potassium atoms has been studied by a time of flight molecular beam technique. A simple electron capture and recapture mechanism is advanced to account for the observations.

The manifold of electronically excited states available in the alkyl iodides falls into three classes corresponding to valence transitions in the C–I band of $n \rightarrow \sigma^*$ type, Rydberg transitions to high nl states similar to those of the iodine atom and valence $\sigma \rightarrow \sigma^*$ transitions in the C–H bond. Transitions corresponding to all these three classes are observed in the optical spectrum though the C–H transitions are seen only as a continuum background to the other processes [1–3]. Photodissociation of the alkyl iodides with radiation in the 3.5–5.5 eV region occurs via the continuum A state ($n \rightarrow \sigma^*$) and produces both ground, $I_{3/2}$, and excited, $I_{1/2}$ atoms [4] while the same σ^* orbital occupied in the molecular negative ion is responsible for the substantial translational excitation seen in the reaction [5]

$$K + RI \rightarrow KI + R, \qquad (1)$$

which are classic examples of electron harpooning.

In this work inelastic differential scattering cross sections have been measured for this system in the high energy (50–200 eV) small angle (0–5°) region in which the collision trajectory is approximately rectilinear and explores the potential surfaces inside the harpooning radius. The reaction channel itself is closed in this regime due to momentum constraints on the I capture so that the electronic transitions can be studied in isolation from the capture dynamics.

The measurements described were made by a time of flight method in which the potassium atom beam was pulse modulated and the energy loss in the collision inferred from the change in the measured flight time. In this way a contour map was built up showing the scattered K atom flux versus scattering angle and energy loss at various initial collision energies [6,7].

Very considerable inelasticity is observed in these measurements with energy losses ranging from 0.5 to ≈12 eV. The lower energy processes, <5 eV which include the electronically elastic, K(4p) and CH_3I (A) state as exit channels have been discussed elsewhere [8] and shown to involve an ionic intermediate repulsive in the C–I bond. This paper discusses the higher energy loss processes corresponding to Rydberg and C–H transitions, which are also seen, though with smaller cross sections.

Typical energy loss profiles are shown in fig. 1 for several reduced scattering angles ($E\chi$, eV°). The optical spectrum in the same energy region shows a very large number of discrete features associated with transitions from n(I) to various Rydberg states (n, l) having $n > 5$, l = s, d, p and core terms of $E_{1/2}$ and $E_{3/2}$. Continuum absorption from C–H transitions is seen as a background to these discrete features. In comparison, the relative sparsity of the collision induced transitions is immediately apparent and at each angle of scattering or impact parameter only discrete energy losses are seen. The observed features occur systemati-

‡ Present address: Departamento de Quimica Fisica, Facultad de Ciencas, University de Bilbao, Bilbao, Spain.
‡ Present address: Argonne National Laboratory, Argonne, Illinois, USA.

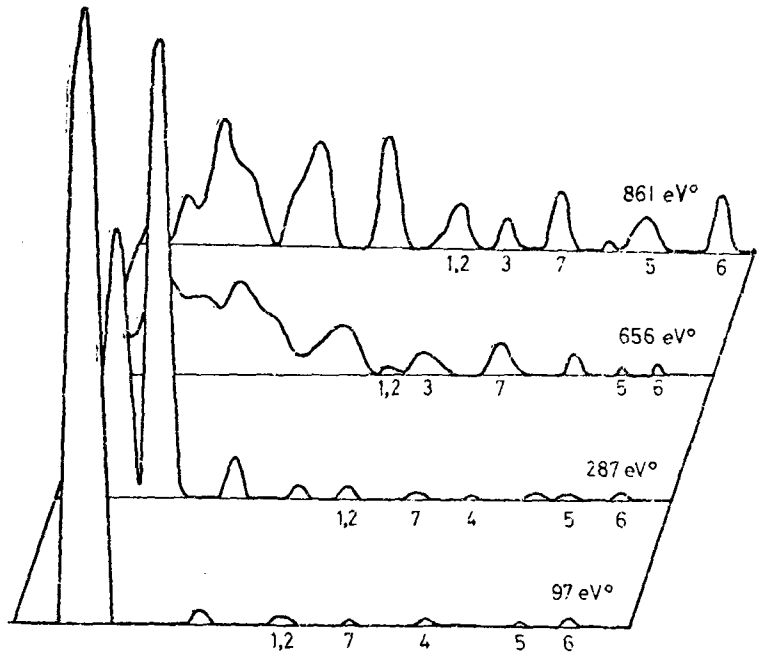

Fig. 1. Observed energy loss profiles K/CH_3I at centre of mass collision energy of 164 eV, $E\chi$ in eV°. Peak numbers refer to table 1.

cally as the scattering angle is varied, though the intensity varies considerably; their behaviour is summarised in table 1. The observed energy losses are independent of reduced scattering angle with one exception, process 7 for which the energy loss observed increases approximately linearly with $E\chi$. The angular dependence of the differential cross sections is illustrated in fig. 2 where the results have been approximately scaled by normalising the very small angle elastic scattering (arising from outside the harpooning radius) to model potentials for this region developed in molecular dynamic studies [12].

The energy loss processes reported are seen in fig. 2 to onset at small $E\chi$ values, This combination of a substantial energy exchange coupled with a small reduced deflection is good evidence for the involvement of strong attractive potentials during the collision and suggests that processes of interest may also occur via a transient negative ion.

Table 1
Observed energy losses

Process number	Observed energy loss (eV)			Proposed assignment (see table 2)	
	MeI		PrI		
	c.m. collision energy = 81 eV	c.m. collision energy = 164 eV	c.m. collision energy = 166 eV	effective transition	predicted energy loss (eV)
1	5.2	5.5	6	$n(I) \rightarrow \sigma^*_{(C-I)}$	3.5 a)
2	5.7				5.5
3	6.4	6.4	6.6	n(I) → 6s Rydberg	6.5
4	8	8.4	8.5	n(I) → 7s Rydberg	8.2
5	higher energy loss process	10.4	10.8	$\sigma_{p(C-H)} \rightarrow$ 6s Rydberg	11.0
6	obscured by ^{41}K isotope	12.4	13.2	$\sigma_{p(C-H)} \rightarrow$ 7s Rydberg	12.9
7	6–7.2 in $E\chi$ range 40–220 eV°	6.4–9.0 in $E\chi$ range 60–900 eV°	11–12.8 in E_χ range 160–550 eV°	$n(I) \rightarrow \sigma^*_{(C-H)}$	internal energy internal energy b)

a) This transition is to the dissociative A state of CH_3I.
b) The equivalent $\sigma^*_{(C-H)}$ orbital in propyl iodide cannot be identified unambiguously but is likely to be considerably higher in energy.

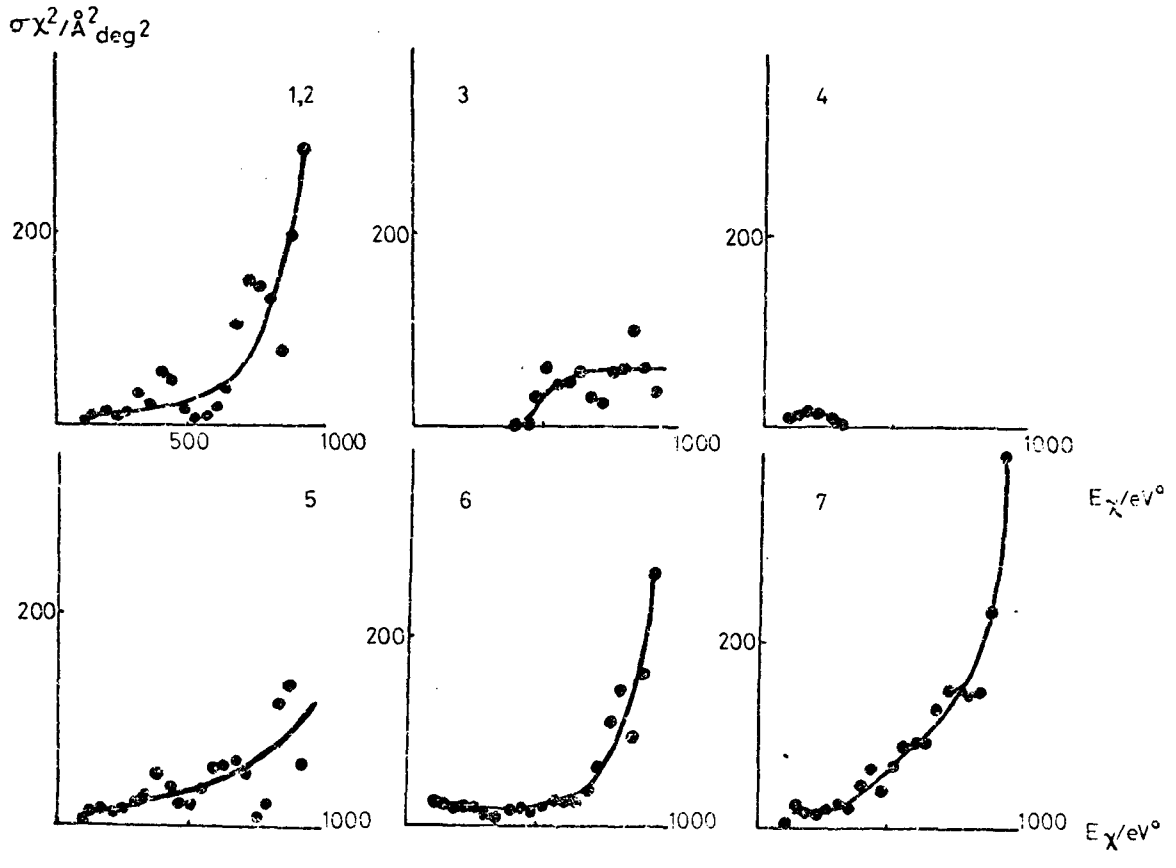

Fig. 2. Differential scattering cross sections for K/CH_3I at 164 eV (c.m.). The processes are identified in table 1.

A schematic energy diagram showing the location of the lower orbitals in CH_3I is drawn in fig. 3. The lowest unoccupied orbitals include the $\sigma^*_{(C-I)}$ (the electron receptor orbital of importance in the reactive and smaller energy loss processes) and the $\sigma^*_{(C-H)}$, which are both antibonding in the C–I and C–H respectively, together with the Rydberg levels 6sa, 7sa and $5da_1$ + 2e. These are all possible receptor levels – higher Rydberg states though available in principle will have considerably smaller coupling matrix elements due to the large size of these orbitals and are thus unlikely to be important.

Since these measurements are confined to the neutral exit channel, electron capture must be followed by the recapture of an electron by the K^+ ion on exit from the collision. Electronic excitation will now take place if an electron is recaptured from a lower, normally filled orbital leaving the receptor orbital occupied and a lower lying vacancy. Possible energy losses arising from this mechanism are shown in table 2; the spin orbit splitting is comparable to the energy resolution of the measurements at the 164 eV collision energy while the 7s and 5d Rydberg states are also too close to be resolved and the energies of these states are averaged together in table 2. Comparison with the observa-

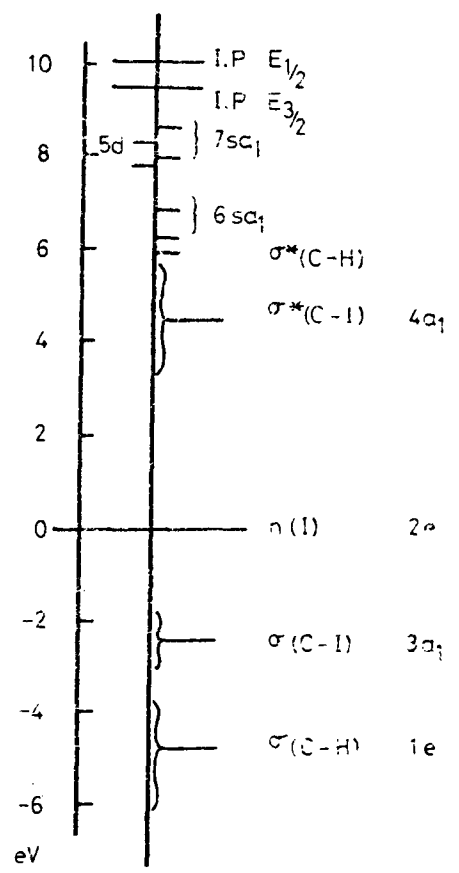

Fig. 3. Schematic orbital energy diagram for CH_3I. The orbitals n(I), $\sigma_{(C-I)}$ and $\sigma_{(C-H)}$ are located from photoelectron spectra [9,10]. The $\sigma^*_{(C-I)}$ and Rydberg levels form optical spectra [1–3]. The $\sigma^*_{(C-H)}$ is derived with rather less certainty from the optical spectra of the alkanes [11].

Table 2
Transitions and energy losses expected from electron harpooning and subsequent recapture in CH_3I

Exit process: Orbitals from which electron is recaptured	Incident process: Lowest unoccupied orbital	Orbital into which electron is captured: $\sigma^*_{(C-I)}$ $4a_1$	6s Rydberg $6sa_1$	$\sigma^*_{(C-H)}$	5d, 7s } Rydberg $7sa_1$ $5da_2$ + 2e	Energy losses in eV
Highest occupied orbital						
n(I) 2e		3.5–5.5	6.18 and 6.77 6.5	≈6.0	7.84 8.30 8.03 8.65 8.2	
σ(C–I) $3a_1$		≈7	8.6 and 9.2 8.9	8.4		
σ_p(C–H) 1e		9.2	10.9 and 11.1 11.0	10.7	12.5 13.0 12.7 13.4 12.9	

tions in table 1 is immediately suggestive and leads to the tentative assignment shown in table 1. The model thus suggests that electron capture into the lower empty Rydberg or valence levels is possible. The relative probability being at least partly determined by the orientation of the CH_3I during the collision. Thus process 7, $n(I) \rightarrow \sigma^*_{(C-H)}$, involving capture into the $\sigma^*_{(C-H)}$ followed by recapture of an electron from the iodine lone pairs would presumably be favourable for trajectories in which the K moves first past the CH_3 and then the I groups. Similarly processes 5 and 6, $\sigma_{(C-H)} \rightarrow$ 6s and 7s, would involve trajectories moving in the reverse direction while the other transitions occur at the iodine atom only. It is notable that with this model process 7 which was unique in showing an energy loss increasing with $E\chi$, is seen to arise from an intermediate ion state which is antibonding and repulsive in the C–H coordinate. Since $E\chi$ is inversely related to the impact parameter, itself inversely related to the time between the capture and recapture episodes on the trajectory, the time spent in this repulsive state increases with $E\chi$. The increasing energy loss can now arise as a result of the substantial changes in geometry which occur during the collision.

Similar effects as a result of populating the $\sigma^*_{(C-I)}$ orbital can be distinguished in the lower energy losses but because of the much greater mass of the ejected group (CH_3 as compared to H in the case of the $\sigma^*_{(C-H)}$ orbital) the effect is much smaller and cannot be distinguished in the $E\chi$ range discussed here. The dynamics leading to this dissociative state are further complicated since it may be accessed on either the inward or outward branches of the trajectory [8]. It is possible that the two channels observed at 81 eV, where the resolution is better (≈ 0.25 eV), correspond to dissociative states leading to either the $I_{1/2}$ or $I_{3/2}$ states of iodine with considerable translational energy; the spin orbit splitting is not resolved experimentally at the higher collision energies.

The C–I force constant is essentially unchanged by population of Rydberg states so that transitions to these states would be expected at a fixed energy in accordance with these observations. Finally it is worth noting that all the capture transitions can be assigned to s or σ orbitals (though the 5d and 6p $E_{1/2}$ levels at 8.30 and 7.99 eV could not be distinguished from the 7s levels) suggesting that electron orbital angular momentum is conserved in these collisions.

Considerable mixing of the various orbitals will take place under the time dependent perturbation of the K^+ ion and the precise description of the orbital from which recapture finally occurs is unclear. A simplified diabatic potential scheme illustrating a possible mechanism is shown in fig. 4 where the doubly starred

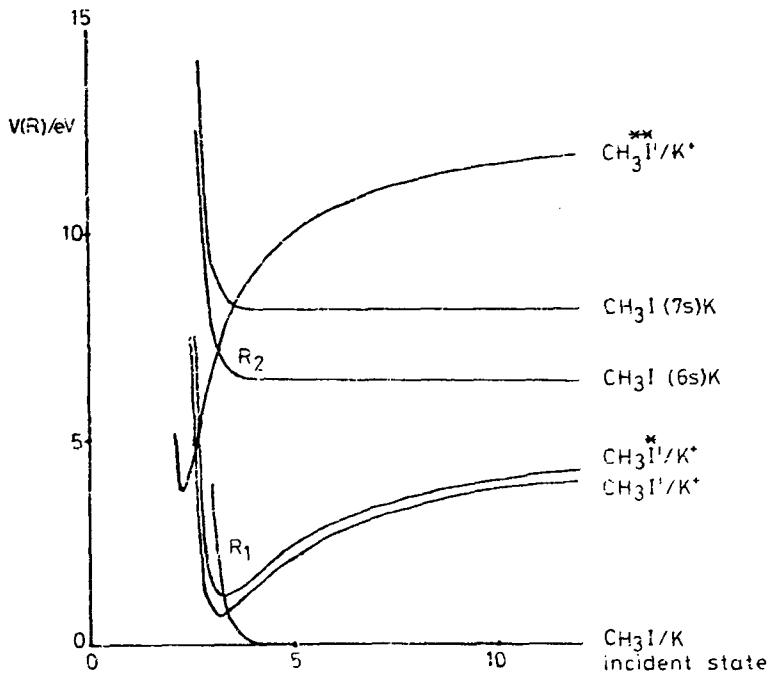

Fig. 4. Diabatic potentials illustrating the incident channel and the electron capture and recapture processes at R_1 and R_2 leading to excited RI states.

curve represents the state of the CH_3I under perturbation by K^+. The most significant features of this model are the two electron transfers at R_1 and R_2 on entry and exit and the strong attractive exit potential which will produce scattering at small $E\chi$.

The authors are glad to acknowledge helpful discussions with Dr. Stephen Cradock.

References

[1] G. Herzberg, Electronic spectra and electronic structure of polyatomic molecules (Van Nostrand, Princeton, 1966).
[2] R.A. Boschi and D.R. Salahub, Mol. Phys. 24 (1972) 289.
[3] H.T. Wang, W.S. Felps, G.L. Findley, A.R.P. Rau and S.P. McGlynn, J. Chem. Phys. 67 (1977) 3940.
[4] S.J. Riley and K.R. Wilson, Faraday Discussions Chem. Soc. 53 (1972) 132.
[5] D.R. Herschbach, Faraday Discussions 55 (1973) 233.
[6] M.A.D. Fluendy, J.H. Kerr, J.M. McCall and D. Munro, in: On-line computing in the laboratory, eds. A. Rosner, B.K. Penney and P.N. Clout (Advance, London, 1975).
[7] J.M. McCall and M.A.D. Fluendy, J. Phys. E 11 (1978) 631.
[8] M.A.D. Fluendy, K.P. Lawley, J.M. McCall, C. Sholeen and D. Sutton, Faraday Discussions 67 (1979), to be published.
[9] D.W. Turner, C. Baker, A.D. Baker and C.R. Brundle, Molecular photoelectron spectroscopy (Wiley, New York, 1970).
[10] A.D. Baker and D. Betteridge, Photoelectron spectroscopy (Pergamon, Oxford, 1972).
[11] J.W. Raymonda and W.T. Simpson, J. Chem. Phys. 47 (1967) 430.
[12] L.M. Raff and M. Karplus, J. Chem. Phys. 44 (1966) 1212.

ELECTRONIC EXCITATION AND ENERGY TRANSFER IN K–N_2 COLLISIONS

G.W. BLACK, M.A.D. FLUENDY and D. SUTTON
Department of Chemistry, University of Edinburgh, Edinburgh EH9 3JJ, UK

Received 15 October 1979; in final form 1 November 1979 .

Inelastic differential scattering cross sections for the system K/N_2 have been measured in the small-angle regime for E_X in the range 80–600 eV deg. A cross beam time-of-flight technique was used to measure energy transfer effects occurring in the collision. The dominant inelastic process in the region explored was production of the $K(4\,^2P)$ state together with simultaneous vibrational excitation of the N_2 molecule. The observations are in excellent agreement with published potentials and a simple classical model involving an intermediate with considerable negative-ion character.

1. Introduction

The quenching of alkali atoms as a result of collisions with diatomic molecules has been of interest for a considerable time [1]; the system Na/N_2 has been of particular interest both experimentally [2] and theoretically [3,4]. The inverse process, atomic excitation as a result of energetic collisions with diatomic molecules, has also been studied [5]. More recently the system of interest here, K/N_2, has been studied by a novel coincidence technique [6] in which the differential cross section for the process $K(4\,^2S) + N_2 \rightarrow K(4\,^2P) + N_2$ was determined, the final state of the molecule not being measured in this experiment. All this work is consistent with an early suggestion that an ion-pair (K^+/N_2') state is an important intermediate.

In the present experiments the time-of-flight technique provides additional information on the excitation of other states, vibrational excitation of N_2 and elastic scattering. The combination of this data with Kempter's observations is consistent with significant ionic character in the description of the collision system both in the angular distributions and now in the vibrational excitation of the N_2.

2. Experimental

2.1. Apparatus

A schematic of the apparatus is shown in fig. 1. The beam of fast alkali atoms is produced initially as ions by surface ionisation on a porous tungsten disc heated radiatively to ≈1500 K. The ions are accelerated to the required collision energy and electrostatically focused. The beam is then pulse-modulated, using a velocity compression technique [7], so that the time-of-flight analysis of the scattered atoms may be carried out. After modulation, the ion beam is neutralised by charge exchange in a vapour cell, and any residual ions are deflected away.

The fast neutral beam enters the collision zone where it intercepts the orthogonally introduced slow target beam, formed by effusion through a capillary array, and modulated at 47 Hz. The scattered potassium atoms are ionised on a cool tungsten wire at the detector, and arrivals are counted via a scintillator and a photomultiplier. The detector can be varied in angle with a precision of ±0.002 deg. The arrivals at the detector stop a 50 MHz crystal clock running in synchronism with the pulse modulation, and so their flight time is recorded. The data collection and experimental operation are controlled by an on-line computer [8], which also monitors important experimental conditions, such as beam fluxes, throughout the run. Due to

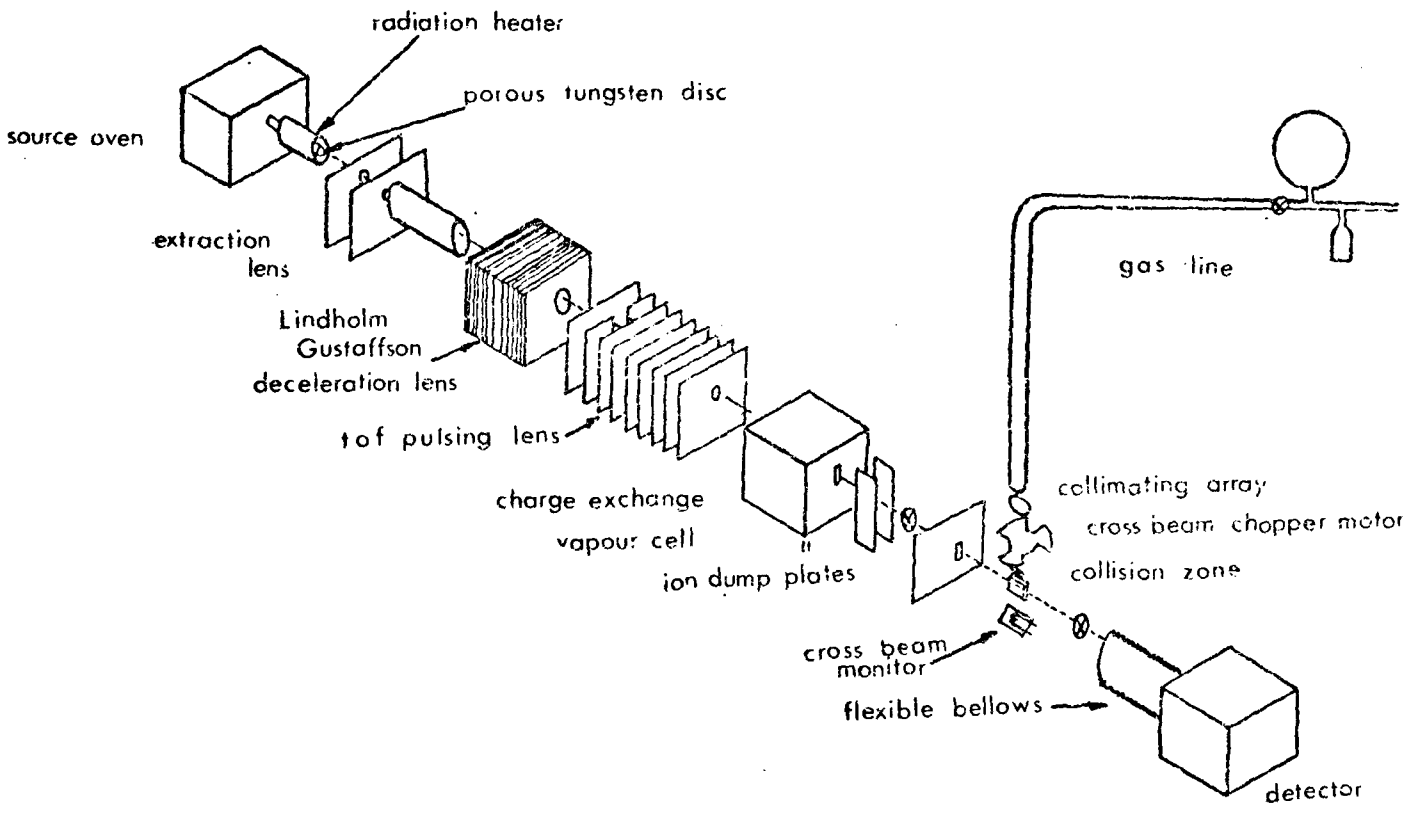

Fig. 1. Schematic of the apparatus.

the very low count rates associated with experiments of this type, less than 0.01 s^{-1} at wide angles, an experiment takes about five days. In these experiments the resolution in $E\chi$, the reduced scattering angle, was ≈35 eV deg and the energy loss could be determined to ±0.15 eV.

2.2. Results

The results were collected over two separate experimental runs, and are presented after transformation to the c.m. reference frame. A c.m. contour map showing the variation in the product of the scattered intensity and the square of the scattering angle, $I(\chi)\chi^2$, as a function of scattering angle and post-collision velocity, is presented in fig. 2.

Such contour plots are highly information-intensive but the grosser features are more easily displayed in a time-of-flight profile. Fig. 3 shows such a profile averaged over all the angles of observation. It is immediately apparent that the elastic channel dominates the collision while an inelastic process with a most probable energy loss of 2.8 eV arises in ≈16% of collisions. A number of very much smaller processes are seen at greater energy losses. The ^{41}K isotope with 6% abundance provides a useful marker.

Measurements of this type do not unambiguously identify the exit channel; however, the lowest excited state of N_2, $A\,^3\Sigma_u^+$, is 6.2 eV above the incident channel, while fluorescence measurements [10] on this system revealed predominantly K(4 ^{2}P) excitation, the K(5 ^{2}P) and (6 ^{2}S), states being populated to ≈2% and 0.6% in comparison. The inelastic channel observed in this experiment onsetting at 1.6 eV and having a maximum at 2.8 eV is therefore assigned to K(4 ^{2}P) excitation with, by elimination, concurrent vibrational excitation of the N_2. A very weak inelastic peak with an energy loss of 4.7 eV and ≈10% of the intensity of the K(4 ^{2}P) scattering can also be seen. This may be associated with similar excitation of the K atom to K(5 ^{2}S) or (5 ^{2}P) states and again concurrent vibrational excitation of the N_2, but will not be further discussed here. The proposed assignment is supported by the success of the model based upon this interpretation of the energy loss data.

Previous time-of-flight measurements by Gersing et al. [11] on this system show similar loss profiles to those observed in this work but were interpreted solely as K excitation and led to the conclusion that production of K (5s) and (3d) states was the main inelastic channel – an unsafe conclusion in view of the fluorescence experiments [10].

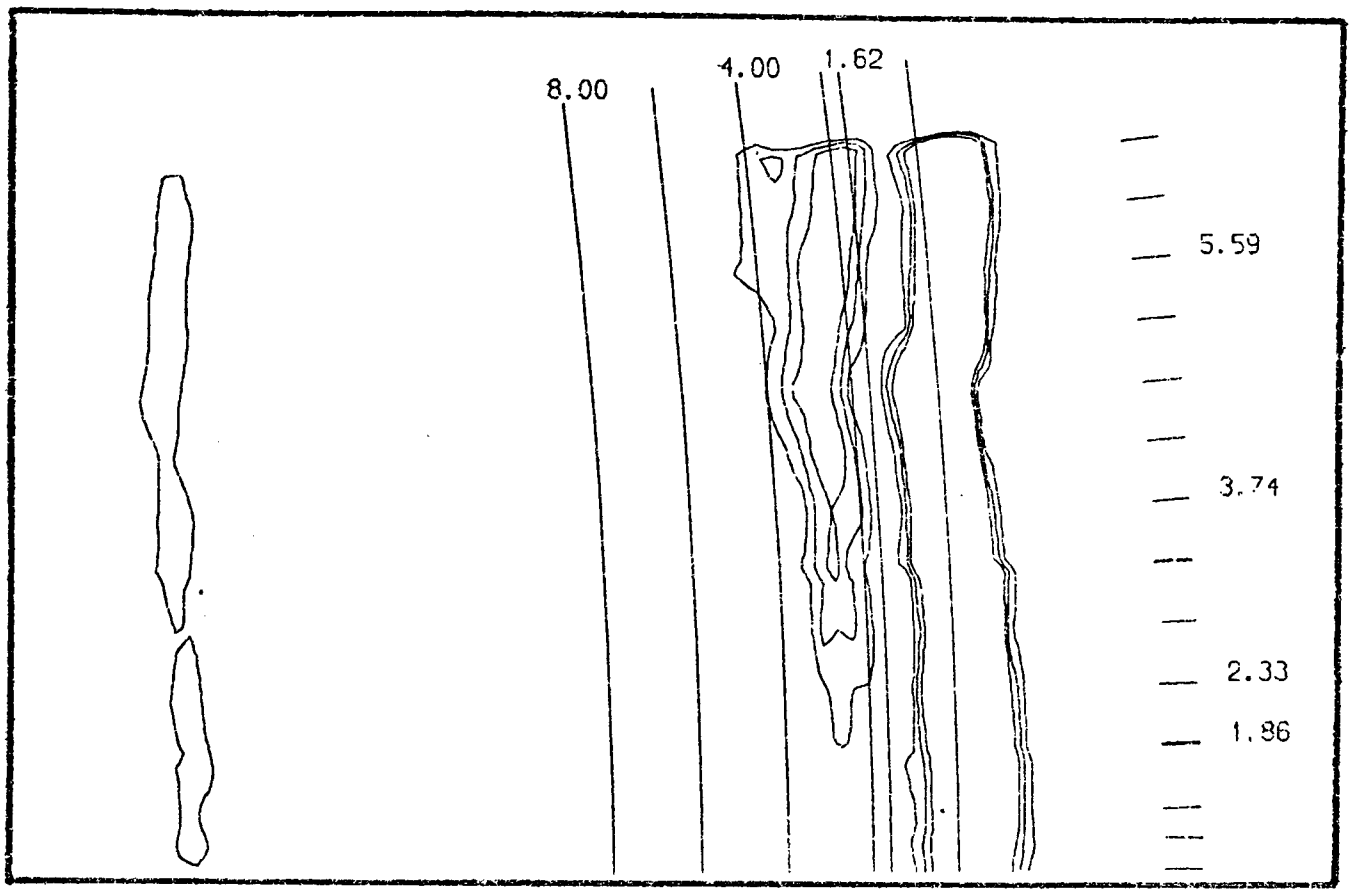

Fig. 2. Polar contour plot showing $I(\chi)\chi^2$ as a function of c.m. scattering angle, χ, and energy loss. The K/N_2 collision energy was 85.5 eV (c.m.). Contours are drawn at 5, 10 and 15%. The angles at which observations were taken are indicated together with an energy-loss graticule. Two distinct peaks can be seen; the lowest shows an energy loss < 0.6 eV, the higher (a rather weaker one) a loss ≈ 2.8 eV. The feature at the top of the figure arises from the ^{41}K isotope.

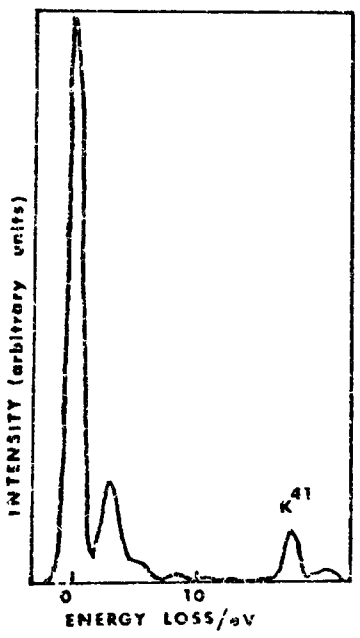

Fig. 3. Energy-loss profile averaged over all angles of observation (0.9–7.5 c.m.). Collision energy 85.5 eV.

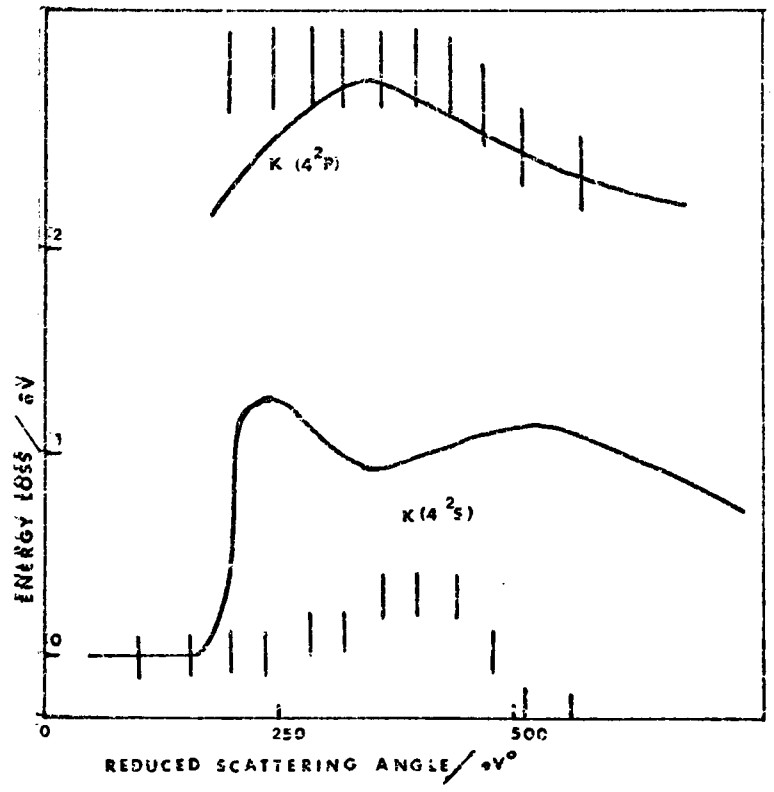

Fig. 4. Most-probable energy loss associated with $K(4\,^2S)$ and $K(4\,^2P)$ scattering. Experimental observations are shown as bars, two standard deviations long. Continuous curve is model prediction. Collision energy 85.5 eV.

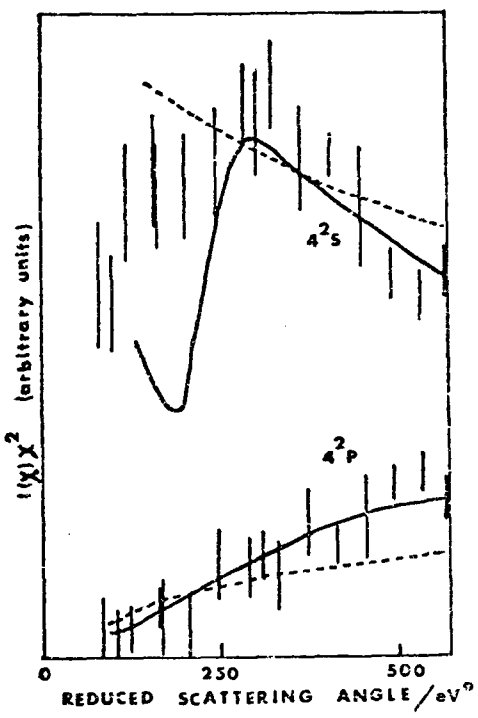

Fig. 5. Differential scattering cross sections, $I(\chi)\chi^2$, in arbitrary units for K(4 ^{2}S) and K(4 ^{2}P) scattering. Model predictions using the Kempter potentials are dashed, approximately adjusted potentials solid line. Collision energy 85.5 eV.

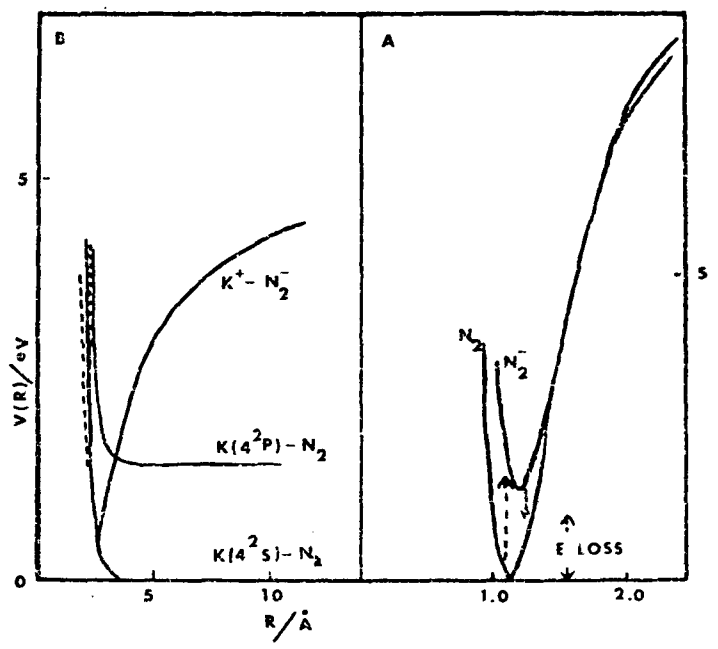

Fig. 6. (a) Potentials [10] for N_2 and N_2'; vertical electron transitions are shown arrowed. (b) Diabatic potentials for K/N_2. The potentials adjusted to accord with the results are shown in solid line, the Kempter potentials are dashed.

In the coincidence experiments of Kempter et al. [6], only K(4 ^{2}P) excitation was reported. However the flight-time resolution of their experiment, as estimated from the reported apparatus dimensions, was insufficient to distinguish the additional energy loss associated with N_2 vibrational excitation and the two experiments are thus not in contention.

The differential cross sections for the electronically elastic and inelastic channels, calculated by summing appropriate regions of the individual energy loss profiles are plotted in fig. 5. They are similar to those reported by Kempter et al. In fig. 4, the most probable loss for these two channels is plotted against scattering angle.

3. Discussion

The measurements reported are confined to the narrow angle region in which the trajectories are approximately rectilinear and of constant velocity so that the deflection angle, collision lifetime and impact parameter can be simply related by small-angle formulae [12]. The collision lifetime is dependent upon the impact parameter but is of the order 10^{-14} s and so is comparable to the vibrational period of N_2 and N_2'.

The potentials relevant to this system are displayed in fig. 6, 6a illustrating the potentials for N_2 and N_2' derived by Gilmore [13], while 6b shows a very simplified set of diabatic potentials for the K–N_2 interaction. It can be seen that both the ground and excited K atom scattering can arise by two routes according to whether the crossing to the surface with ionic character occurs on the ingoing or outgoing phases of the collision. The electron transfer corresponding, in this simple picture, to the formation of the negative ion and the subsequent recapture of an electron to reform neutral potassium in either a ground or excited state are illustrated in fig. 6a. The transitions are assumed vertical in position and to conserve momentum. Since the potential curves for N_2 and N_2' are mutually displaced, the period spent as a negative ion results in vibrational excitation of the N_2 molecule on exit from the collision.

A simple classical model based on this picture using the Landau–Zener approximation to compute the crossing probability and assuming independent motion in the N–N and (N_2)–K dimensions was developed. (The model is very similar to that successfully used to describe similar processes in systems of the type K–RI [14].) In this model the only interaction permitted between these separate motions was via vertical electron transitions and changes in R_c occurring as a result

of the variation in electron affinity as the N–N bond stretched. The model calculations were performed in a simple iterative fashion; the initial estimates of cross section, scattering angle and lifetime on the ionic surface (and hence N_2 vibrational excitation) were computed using the small-angle formulae based on the $v = 0$ N_2 electron affinity. Numerical computation of the N_2' motion during the collision lifetime produced a revised vertical electron affinity and R_c that were used to update the small-angle scattering calculation. Iteration of this process yielded very rapid convergence.

The potentials used in this model for N_2 and N_2' were of Morse form fitted to the well-established Gilmore potentials [13] in their bowl region of importance in the calculation:

$$V_{N_2} = D_1\{1 - \exp[-\beta_1(R - R_{01})]\}^2 - D_1, \qquad (1)$$

where

$$D_1 = 9.8\ \text{eV},\quad \beta_1 = 2.5,\quad R_{01} = 1.10\ \text{Å};$$

$$V_{N_2'} = D_2\{1 - \exp[-\beta_2(R - R_{02})]\}^2 - D_2 + 0.3, \qquad (2)$$

where

$$D_2 = 8.5\ \text{eV},\quad \beta_2 = 2.2,\quad R_{02} = 1.185\ \text{Å}$$

corresponding to a vertical electron affinity of 1.9 eV at the N_2 equilibrium distance.

The K/N_2 potentials were initially chosen to be identical to those used by Kempter et al. to fit the $K(4\,^2P)$ scattering. These were later modified to provide better agreement particularly with the angular distribution of $K(4\,^2S)$ scattering observed here, and the forms finally chosen are

$$V_{K/N_2} = \epsilon(\sigma/R)^s, \qquad (3)$$

where

$$s = 6.4 \quad (R > R_c),$$
$$= 9.0 \quad (R < R_c),$$
$$\epsilon = 0.05\ \text{eV},\quad \sigma = 4.03\ \text{Å},$$

$$V_{K/N_2'} = V_{K/N_2} - 62.2/R^4$$
$$- 14.394/R + 6.25\ \text{eV} \quad (R > R_c),$$
$$= V_{K/N_2} \quad (R < R_c).$$

The crossing probability was of the usual Landau–Zener form with $V_{12} = 0.7$ eV.

The vibrational excitation predicted by this model is largely determined by, and is rather sensitive to, the difference in the N_2 and N_2' potentials, while the angular dependence is similarly primarily a function of the K/N_2 potential. This separation results from the bounded motion of the N_2' ion and the limited changes in R_c which occur as the N_2' vibrates.

The predictions for energy loss are shown in fig. 4. The agreement in the $K(4\,^2P)$ channel is particularly satisfying and is certainly well within the available precision of the N_2' potential. The observed energy loss for $K(4\,^2S)$ scattering is in less satisfactory agreement – possibly as a result of changes in V_{12} with the N–N distance which are not included in the present model. Increasingly diabatic behaviour can be expected as R_{N_2} increases, diminishing the contribution of the ionic surface, with its attendant vibrational excitation, to scattering in the $K(4\,^2S)$ state, and so decreasing the average energy loss actually observed. Incorporation of such a V_{12} dependence in the model would improve agreement with the observations but observations over a wider collision energy range would be required to establish its validity.

Interestingly, the model predicts that the vibrational excitation oscillates with scattering angle (i.e. collision lifetime) as the N_2' ion itself oscillates. A similar mechanism has been advanced to account for maxima in the total ionization cross section observed in Cs/O_2 collisions [15]. In the present experiments, since the early and late crossing contributions to the scattering are in an approximately random phase relation, this oscillation would be difficult to resolve. Experiments at lower collision velocities, where the energy loss resolution is substantially improved and probably adequate to resolve the predicted separate early and late crossing contributions, will be particularly interesting in testing the detailed success of this primitive classical model.

Finally, in distinction to systems of the K/RI type where the RI negative ion was found to be substantially perturbed by the K^+ ion, the N_2' pair potential (within the limited precision with which it is known) accounts for the present results rather well.

The differential cross sections computed from the model are compared with experiment in fig. 5. The agreement is satisfactory considering the simple analytic forms used to represent the K/N_2 potentials. The maxima and minima calculated in the $K(4\,^2S)$ channel,

which is the sum of early and late crossing contributions, arises from the operation of the LZ terms in the model.

References

[1] H.S.W. Massey and E.H.S. Burhop, Electronic and ionic impact phenomena, Vol. 3 (Oxford Univ. Press, London, 1973).
[2] I.V. Hertel, H. Hofmann and K.A. Rost, Chem. Phys. Letters 47 (1977) 163.
[3] C. Bottcher, Chem. Phys. Letters 35 (1975) 367.
[4] E. Bauer, E.R. Fisher and F.R. Gilmore, J. Chem. Phys. 51 (1969) 4173.
[5] V. Kempter, Advan. Chem. Phys. 80 (1975) 417.
[6] P.J. Martin, E. Clemens, L. Zehnle and V. Kempter, Z. Physik A289 (1979) 373.
[7] J.M. McCall and M.A.D. Fluendy, J. Phys. E11 (1978) 631.
[8] M.A.D. Fluendy, J.H. Kerr, J.M. McCall and D. Munro, in: On line computing in the laboratory, eds. A. Rosner, B.K. Penney and P.N. Clout (Adv., London, 1975).
[9] K. Lacmann and D.R. Herschbach, Chem. Phys. Letters 6 (1970) 106.
[10] V. Kempter, B. Kübler, P. LeBreton, J. Lorek and W. Mecklenbrauck, Chem. Phys. Letters 21 (1973) 164.
[11] E. Gersing, H. Pauly, E. Schadlich and M. Vonderschen, Faraday Discussions Chem. Soc. 55 (1973) 211.
[12] M.A.D. Fluendy and K.P. Lawley, Chemical applications of molecular beams (Chapman and Hall, London, 1973).
[13] F.R. Gilmore, J. Quant. Spectry. Radiative Transfer 5 (1965) 369.
[14] M.A.D. Fluendy, K.P. Lawley, J. McCall, C. Sholeen and D. Sutton, Faraday Discussions Chem. Soc. 67 (1979), to be published.
[15] A.W. Kleyn, M.M. Hubers and J. Los, Chem. Phys. 34 (1978) 55.